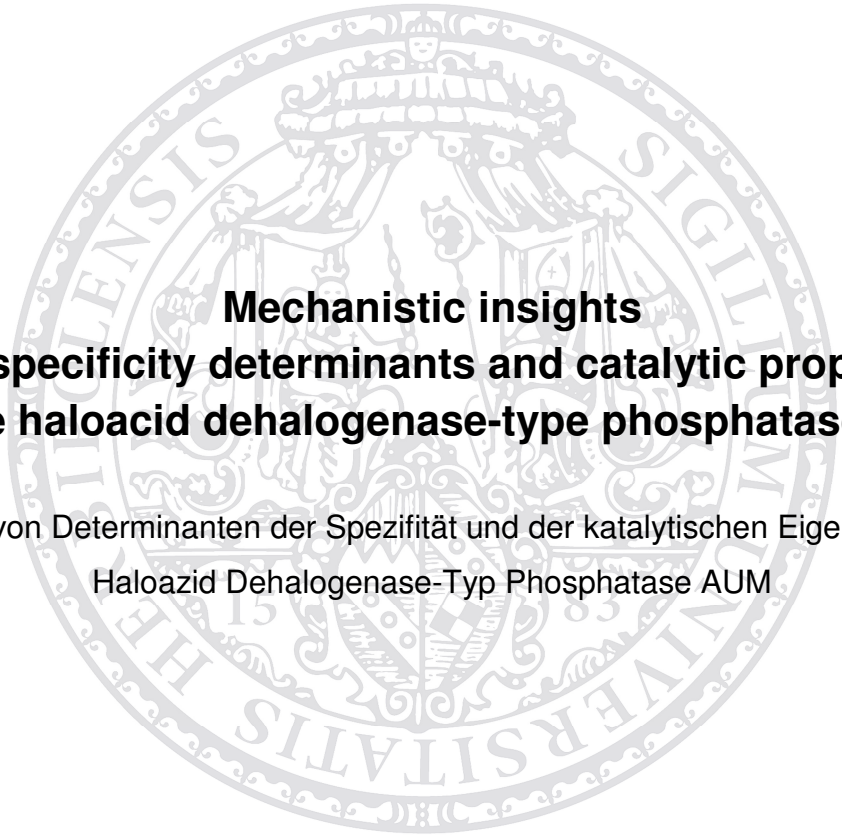

Mechanistic insights into specificity determinants and catalytic properties of the haloacid dehalogenase-type phosphatase AUM

Aufklärung von Determinanten der Spezifität und der katalytischen Eigenschaften der Haloazid Dehalogenase-Typ Phosphatase AUM

Dissertation

for a doctoral degree at the Graduate School of Life Sciences,

Julius-Maximilians-Universität Würzburg,

Section Biomedicine

submitted by

Annegrit Seifried

from Aschaffenburg

Würzburg, April 2014

Submitted on: ……..

Members of the *Promotionskomitee*:

Chairperson: Prof. Dr. Manfred Gessler

Primary Supervisor: Prof. Dr. Antje Gohla

Supervisor (Second): Prof. Dr. Hermann Schindelin

Supervisor (Third): Prof. Dr. Martin J. Lohse

Date of Public Defence: ……..…

Date of Receipt of Certificates: ……..

dedicated to Dr. med. vet. Günter Schäfer (1927 - 2014)

Table of Contents

1 Introduction

Reversible protein phosphorylation is the most widespread and fundamental mechanism by which cellular processes can be regulated (Krebs and Beavo, 1979). It represents a major control mechanism in signaling processes as diverse as cell growth and proliferation, metabolism and migration. The principle of phosphorylation-dephosphorylation as a reversible, covalent protein modification was first elucidated for the glycogen phosphorylase (Fischer and Krebs, 1955). Protein phosphorylation is of ancient origin, representing a universal covalent modification among organisms (Cohen, 2002; Hunter, 2007). The phosphorylation of proteins on specific residues is exquisitely regulated and highly dynamic, resulting in changes of protein conformation and thereby affecting protein function (Cohen, 1992). Abnormal regulation of protein phosphorylation can lead to a variety of diseases.

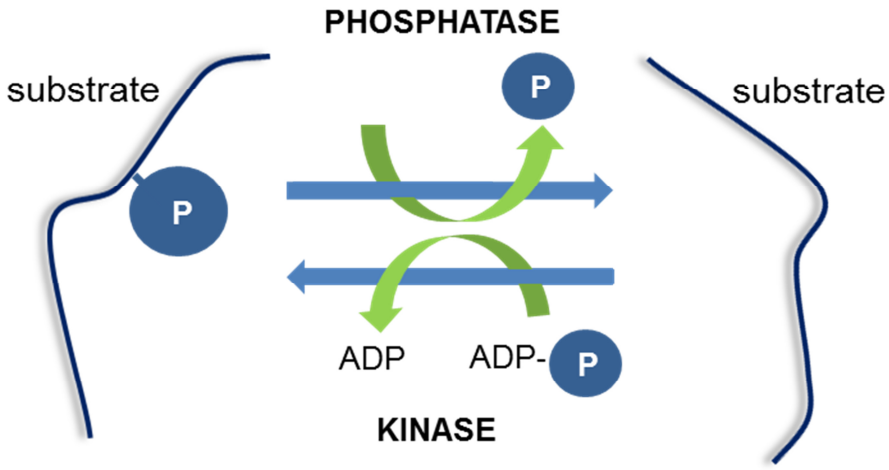

Figure 1: Schematic representation of the mode of the antagonistic action of protein kinase and protein phosphatase towards a phosphorylated substrate.

Protein phosphorylation events can occur on nine different amino acids (histidine, glutamate, aspartate, lysine, arginine, cysteine, threonine, serine, tyrosine). In eukaryotes, the phosphorylation on serine, threonine and tyrosine residues is predominantly found. For example, in humans, the phosphorylation on tyrosine, serine and threonine residues is found with a distribution of 1.8%, 86.5% or 11.8%, respectively (Olsen *et al.*, 2006). These types of modifications are also observed in bacteria (Macek *et al.*, 2008; Soufi *et al.*, 2008; Macek *et al.*, 2007). The phosphorylation of proteins is controlled by the family of protein kinases and by the family of protein phosphatases. Protein phosphatases and kinases form 2-4% of the genes in a typical eukaryotic genome (Cohen, 2000; Manning *et al.*, 2002). Phosphatases

determine the cellular response to a physiological stimulus in a strictly coordinated interplay with their functionally antagonistic partners, the kinases (figure 1). Therefore, it is important to understand how specificity and function of both phosphatases and kinases are regulated.

1.1 The families of mammalian protein phosphatases

In contrast to the protein kinases, which are derived from a common ancestor, protein phosphatases (PPs) evolved in separate families, resulting in structurally and mechanistically distinct enzymes. The families of PPs evolved independently several times. A series of gene duplication events then took place, and novel modules or domains were additionally fused to the catalytic core (Moorhead *et al.*, 2009). Due to these events, three classes of protein phosphatases (figure 2) are observed in the mammalian phosphatome controlling the phosphorylation state of serine, threonine and tyrosine residues (Pils and Schultz, 2004). The serine/threonine- (Ser/Thr) directed class of protein phosphatases is subdivided into the family of phosphoprotein phosphatases (PPPs) and metal-dependent protein phosphatases (PPMs). Diversity is achieved by the combination of regulatory and catalytic subunits. The family of protein tyrosine phosphatases (PTPs) is split in the class of transmembrane or cytosolic PTPs, the dual specificity PTPs (DUSPs), the low-molecular-mass PTPs (LMPTPs) and Cdc25 isoforms. The most recently classified group is the family of aspartate-based phosphatases, the haloacid dehalogenase-type (HAD) phosphatases.

In contrast to protein kinases, protein phosphatases are notoriously regarded as unspecific. This notion is based on their often promiscuous activity *in vitro* and on a lack of information about the regulation of phosphatase substrate specificity. In the following paragraphs, the diverse mechanisms of catalysis and the different regulatory mechanisms of substrate selectivity/specificity known till date are highlighted for the family of PSPs, PTPs and HAD phosphatases.

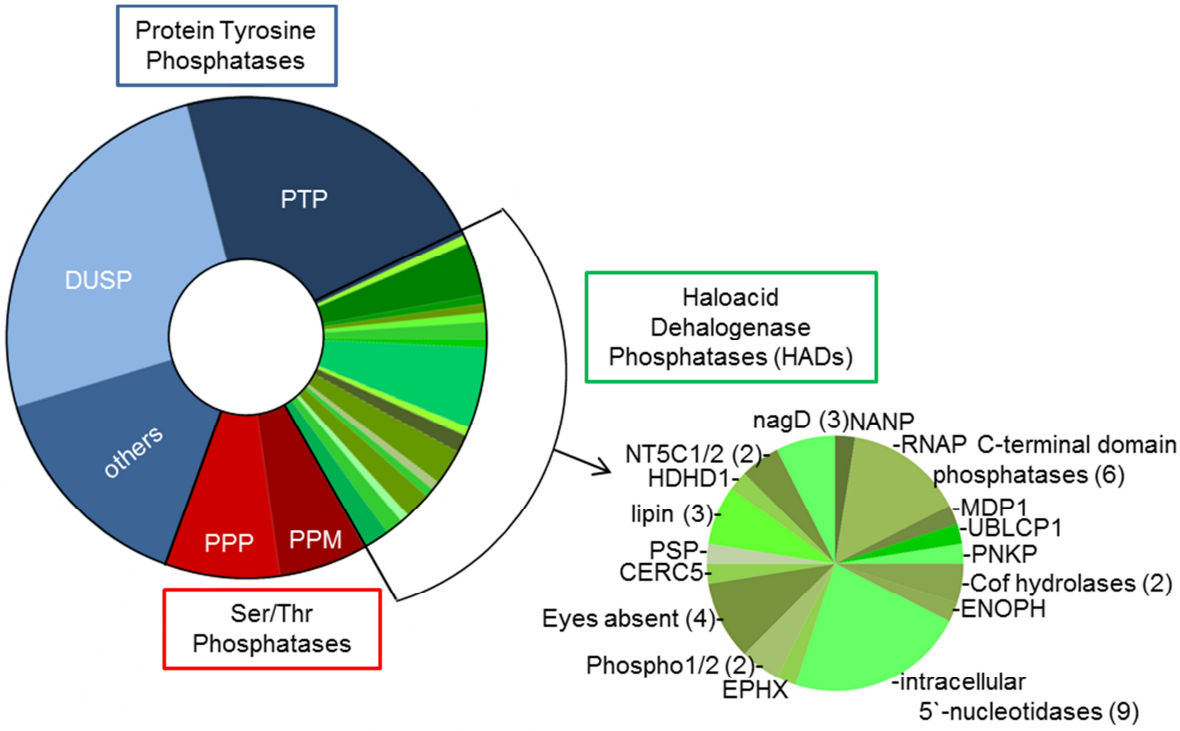

Figure 2: Human protein phosphatases in signal transduction.
The protein phosphatase families that have been implicated in the regulation of signal transduction are shown on the left circular chart. They are represented by the structurally and mechanistically distinct families of protein tyrosine phosphatases (PTPs), protein Ser/Thr phosphatases and haloacid dehalogenase-type phosphatases. The major categories are subdivided into the indicated subassemblies. The family of PTPs is subdivided into "classical" PTPs (receptor-like and non-transmembrane PTPs), the dual specificity PTPs (DUSPs) and others (low molecular weight protein tyrosine phosphatases, Cdc25 isoforms). The family of protein Ser/Thr phosphatases is presented by the phosphoprotein phosphatases (PPPs) and the metal-dependent protein phosphatases (PPMs). The breakdown of the HADs into individual categories is shown on the right circular chart in green hue (based on Seifried *et al.*, 2013). The figure is generated on the basis of (Tonks, 2013).

1.2 The Family of protein serine/threonine phosphatases

The family of protein Ser/Thr phosphatases (PSPs) dephosphorylates phosphoserine (pSer) and phosphothreonine (pThr) residues. The PSPs are divided in two subfamilies, the phosphoprotein phosphatases (PPPs) and the metal-dependent protein phosphatases (PPMs). The PPPs are represented by PP1, PP2A, PP2B (calcineurin), PP4, PP5, PP6 and PP7. PP1 and PP2A are the most abundant phosphatases in most cell types. PP2C and the pyruvate dehydrogenase phosphatase belong to the PPM family (Shi, 2009).

The mechanism of catalysis

The PPP family is composed of a catalytic core (~30 kDa) that comprises three conserved sequence motifs: GDxHG, GDxVDRG and GNHE (G, glycine; D, aspartate; H, histidine; V, valine; R, arginine; N, asparagine, E, glutamic acid; x, any amino acid). The highly identical core structure is based on a central β-sandwich, inserted between two α-helical domains.

The interface of two β-sheets creates a shallow catalytic site (PDB: 1FJM, 2PKG, 1U32). The three conserved motifs form the connecting loops of the β-strands and α-helices (Terrak *et al.*, 2004).

Catalysis is metal ion dependent. For PP1, Mn^{2+} and Fe^{2+} and for PP2A and PP2B, Zn^{2+} and Fe^{2+} are described (Chu *et al.*, 1996; Zhang *et al.*, 1992; Shi, 2009). The PPM family is manganese/magnesium dependent (Jackson *et al.*, 2003). Three histidines, two aspartates and one asparagine residue coordinate the metal ions in the active cleft (Swingle *et al.*, 2004). An aspartate and a water molecule bridge both metal ions to form a binuclear metal center. A metal-bound water molecule acts as a nucleophile to attack the phosphate group in an S_N2 mechanism (Goldberg *et al.*, 1995). The residues mediating the metal-induced catalysis are highly conserved in the PPP family, suggesting a general mechanism. The replacement of any of the metal-coordinating residues leads to a reduction of activity (Mertz *et al.*, 1997). Many PPPs can be potently inhibited by small molecular weight toxins, targeting the active site. Inhibition through microcystin, nodularin, calyculin A, tautomycin and okadaic acid has been described (Pereira *et al.*, 2011). The fungal metabolite cyclosporine A inactivates PP2B (Swanson *et al.*, 1992).

Substrate selectivity

The human genome encodes for 428 Ser/Thr kinases but only for ~30 PSPs (Shi, 2009). The low number of catalytic subunits (C subunits) of PSPs indicates a broad substrate range for each subunit mismatching with the described high specificity of the PSPs. This discrepancy can be explained with a large number of regulatory subunits (R subunits) adding specificity to the catalytic subunits of the PSPs. Binding of R subunits to the C subunits enhances substrate specificity by introducing an additional recognition site to the overall complex.

The catalytic domain that is common to all PP1-type phosphatases can bind to more than 200 biochemically confirmed regulators, forming hundreds of highly specific holoenzymes (Hendrickx *et al.*, 2009). Most R subunits and some substrates contain the binding motif RVxF/W to interact with PP1. The first holoenzyme structure of PSPs presented the complex of PP1 and MYPT (PDB: IS70) visualizing the anchor points between catalytic and regulatory subunits (Terrak *et al.*, 2004).

Like PP1-enzymes, the PP2A holoenzyme also displays exquisite substrate specificity. A scaffold subunit (A subunit) and the C subunit build a heterodimeric phosphatase core (Grinthal *et al.*, 2010). Both A and C subunits exist in two isoforms. As for PP1, the PP2A core enzyme interacts with a variety of regulatory subunits. They are divided into four families (B, B´, B´´, B´´´). In addition, isoforms and multiple splice variants of the regulatory subunits are described. The subfamilies of regulatory subunits share little sequence similarity and are expressed in a tissue-specific manner (Virshup and Shenolikar, 2009).

Finally, PP2B (calcineurin) consists of a C subunit (calcineurin A) and an R subunit (calcineurin B). Calcineurin A contains an R subunit binding domain, a Ca^{2+}-calmodulin-binding motif and an autoinhibitory domain. The C subunit gets activated upon association with Ca^{2+} and calmodulin (Klee *et al.*, 1979).

The PPM family does not have regulatory subunits, but harbors additional domains determining substrate specificity.

1.3 The protein tyrosine phosphatase superfamily

The PTP catalytic subunits have evolved independently, giving rise to three classes of this phosphatase family. Class I includes the dual specificity PTPs (DUSPs, 61 members), the receptor-type PTPs (21 members) and non-receptor PTPs (17 members). These phosphatases are referred to as "classical" PTPs. Class II is represented by the low molecular weight protein tyrosine phosphatase (LMWPTP, one member) and class III comprises the Cdc25 isoforms (three members). Together, the human genome encodes for 107 PTPs, of which 105 have a mouse ortholog (Alonso *et al.*, 2004; Andersen *et al.*, 2004).

Signature motifs

The catalytic domain is build up out of ~280 residues and consists of an α/β structure (Barford *et al.*, 1994). The catalytic domain harbors the PTP signature motif HCX_5R, the mobile Trp-Pro-Asp (WPD) loop, the phosphotyrosine recognition (pTyr-) loop and the Q loop. The structural elements harbor additional residues important for catalysis (Barford *et al.*, 1995): The WPD loop closes the entrance to the active site, thereby shielding the nucleophile-substrate intermediate from water molecules, and promoting hydrolysis (Yang *et al.*, 1998; Barr *et al.*, 2009). The Q loop coordinates water molecules in the active site and the correct positioning of the aspartate residue of the WPD loop. The pTyr-loop is located at the active cleft surface, determining the depth of the active center. This residue is missing in the DUSPs, resulting in a shallower active center, allowing the binding of pTyr, pSer, pThr residues, sugars and lipids (Myers *et al.*, 1997; Maehama and Dixon, 1998).

The mechanism of catalysis

Catalysis occurs in a two-step mechanism. Upon substrate binding, the phosphoryl group of the substrate undergoes nucleophilic attack by the thiolate side chain of the conserved cysteine of the catalytic motif. Due to substrate binding, a conformational change of the active center occurs. The WPD loop closes around the side chain of the pTyr residue of the substrate. In accordance with the "induced-fit" concept, the conformational change upon substrate binding ("fit") induces catalysis. The conserved aspartate residue of the WPD loop protonates the tyrosyl residue of the substrate. In the second part of the reaction, the cysteinyl-phosphate intermediate gets hydrolyzed. Hydrolysis is mediated via the glutamate residue of the Q-loop. It functions as a general base, coordinating a water molecule and the

aspartate of the WPD loop, releasing the phosphate in the second part of the reaction (Zhang *et al.*, 1994b).

Regulation of substrate specificity

PTPs exhibit exceptional substrate specificity *in vivo*. Residues flanking the targeted pTyr of the substrate, and non-catalytic residues lining the surface of the active cleft determine substrate specificity. The residues exposed on the surfaces of the active clefts are highly variable between the members of the PTPs, resulting in a different surface electrostatic potential. This makes the substrate docking site unique, yielding high specificity of the phosphatase (Barr *et al.*, 2009). In addition, PTPs gain specificity by the fusion of regulatory domains like the kinase interaction domain (KIM) of PTP-SL (Pulido *et al.*, 1998), the SH2 domains of SHP-1 and SHP-2 (Tiganis and Bennett, 2007) or a FERM domain found in PTPH1 and PTPD1/D2 (Mohi and Neel, 2007). Further, mechanisms like restricted subcellular localization, and specific tissue distribution contribute to phosphatase specificity.

Regulation of catalysis

PTP function can be regulated by oligomerization. RPTP dimerization is observed in living cells, affecting RPTP phosphatase activity (Lee *et al.*, 2007). The crystal structure of the intracellular catalytic domain D1 of RPTPα shows symmetrical dimers (PDB: 1YFO). The N-terminal segment of each monomer occludes the active site of the opposing monomer (Bilwes *et al.*, 1996). This structural arrangement suggested dimer-induced inactivation (Majeti *et al.*, 1998).

Besides oligomerization, posttranslational modifications regulate PTP activity (proteolysis, phosphorylation, sumoylation, oxidation). The phosphatase activity of PTP-1B, PTP-MEG and SHP-1 is regulated by protease cleavage. Calpain dependent cleavage activates the phosphatase (Frangioni *et al.*, 1993; Gu and Majerus, 1996; Falet *et al.*, 1998). Next to proteolysis, phosphorylation is a key regulator of PTP activity. Tyrosyl phosphorylation of PTP-1B results in increased activity (Dadke *et al.*, 2001), whereas the phosphatase activity of PTP-PEST is stimulated by phosphorylation of a specific serine residue (Garton and Tonks, 1994). Besides the regulation of activity, phosphorylation creates docking sites for interaction partners (Bennett *et al.*, 1994). In addition, the posttranslational modification with small ubiquitin-related modifier proteins (SUMO) is known to modulate phosphatase function. Upon sumoylation, PTP-1B gets inactivated in response to insulin (Dadke *et al.*, 2007).

Reversible oxidation

The cellular redox state plays a crucial role in mechanisms regulating tyrosine phosphorylation-dependent events. The majority of classical PTPs are regulated by reversible oxidation. For PTPs like PTP-1B (Lee *et al.*, 1998; Mahadev *et al.*, 2001), TCPTP (Meng *et al.*, 2004), SHP-2, SHP-1 (Meng *et al.*, 2002; Kwon *et al.*, 2005), CD45 (Singh *et*

al., 2005), PTP-PEST (Wu *et al*., 2005), mitogen activated protein kinase phosphatase (Levinthal and Defranco, 2005), PTEN (Kwon *et al*., 2004) and LMWPTP (Caselli *et al*., 1998) the mechanism of reversible oxidation has been described.

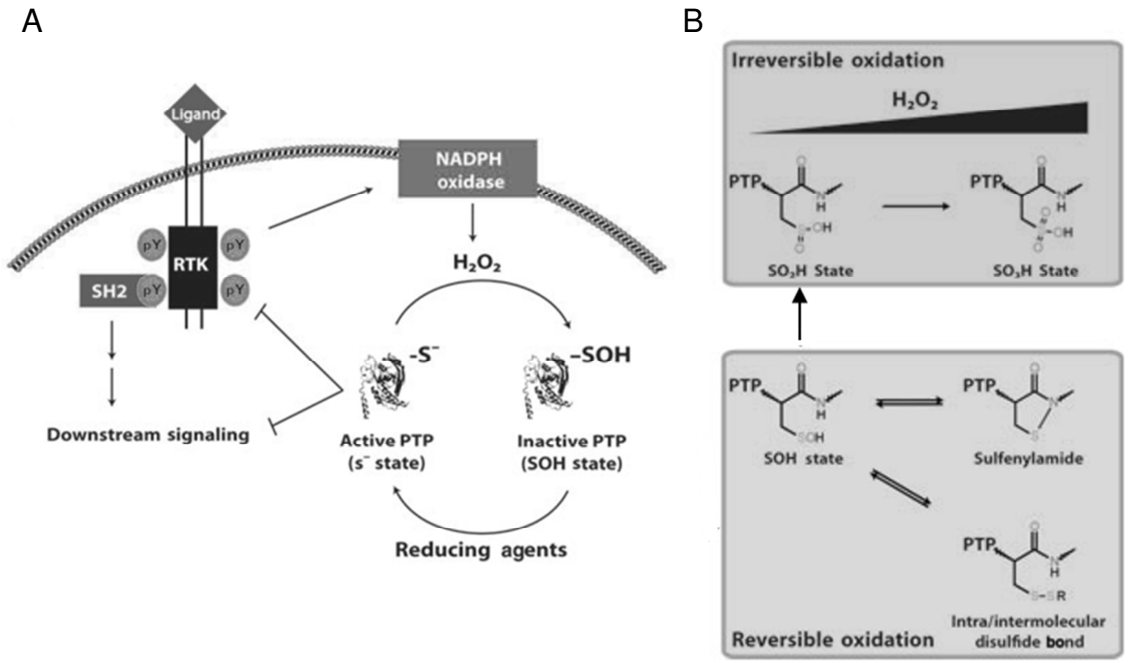

Figure 3: Redox regulation of protein tyrosine phosphatases (PTPs). (A) Receptor tyrosine kinase (RTK) activation results in a transient and local production of hydrogen peroxide (H_2O_2) by the NADPH oxidase (NOX) enzyme family. H_2O_2 causes a reversible oxidation of the catalytic cysteinyl residue of PTPs to the sulfenic acid state (PTP-SOH). The resulting inactivation leads to increased tyrosyl phosphorylation of PTP substrates and induces downstream signaling events. H_2O_2 levels decrease as a consequence of the inactivation of the NOX enzymes, leading to a PTP re-activation (PTP-S^-) by reducing agents (i.e. glutathione peroxidases). **(B)** The sulfenic acid state (PTP-SOH) is labile and spontaneously re-arranges to form an intramolecular sulfenylamide or a disulfide bond with a nearby cysteine residue (lower panel). This re-arrangement prevents hyper-oxidation and makes PTP re-activation possible. Upon hyper-oxidation, the PTP gets irreversible inactivated. The catalytic cysteinyl residue gets oxidized to the biologically irreversible sulfinic (PTP-SO_2H) and sulfonic (PTP-SO_3H) acid states (upper panel). Figure adapted from (Karisch and Neel, 2013), John Wiley and Sons license: 3281320820731.

The reversible oxidation of intracellular proteins can occur in response to a variety of different external or intracellular stimuli, such as growth factors, hormones, cytokines and cellular stress. The mechanisms triggering cellular redox signaling have been elucidated for many receptor classes, like integrins, cytokine receptors, G-protein-coupled receptors, RTKs and T- and B-cell receptors (Karisch and Neel, 2013). Here the RTK-mediated mechanism of reversible oxidation of PTPs will be described (figure 3A). Upon growth factor stimulation, receptor tyrosine kinases (RTK) get activated, leading to a transient ROS (H_2O_2) production. H_2O_2 is locally generated by NADPH oxidases (NOX) resulting in receptor phosphorylation and downstream signaling e.g regulating the Src family of kinases (Sorescu *et al*., 2002; Dewald *et al*., 1979; Yan and Berton, 1996).

PTPs are a viable target of intracellular H_2O_2 accumulation (Denu and Tanner, 1998). Because of the low pKa (4.5-5.5), the cysteine nucleophile of the PTPs exists as thiolate (S^-)

at physiological pH (Zhang *et al.*, 1994b). This enables nucleophilic attack of the substrate and makes the PTP accessible to oxidation (Salmeen and Barford, 2005). Due to intracellular ROS production, PTPs were found to be oxidized and inactivated. Reactions with ROS oxidize the PTP active site thiolate initially to the labile sulfenic acid (-SOH). Elevated levels of ROS lead to sulfinic ($-SO_2H$) or sulfonic ($-SO_3H$) acid derivatives (figure 3B). These kinds of modifications are irreversible. To prevent irreversible oxidation, a disulfide between the catalytic cysteine and a nearby "backdoor" cysteine is built in to stabilize the reversible oxidation state. This mechanism has been demonstrated for the PTPs SHP-1 and SHP-1 (Chen *et al.*, 2009), for Cdc25c and PTEN (Buhrman *et al.*, 2005; Leslie *et al.*, 2003). In addition, different family members are found to form a cyclic sulfenylamide with a neighbouring peptide backbone to protect the active site (Salmeen *et al.*, 2003). The disulfide and sulfenylamide states limit hyper-oxidation and can be reversed by reduction. How the recovery of PTP activity might occur is shown by the crystal structure of the oxidized PTP-1B (PDB: 1OEU). The structure reveals conformational changes in the PTP active site upon formation of the protective sulfenylamide intermediate, representing the inactive state (van Montfort *et al.*, 2003). The structural alterations are resulting in an exposure of the Sγ atom of the oxidized cysteine, making it more accessible for reduction. Little is known about the recovery of the oxidized PTPs *in vivo*. In general, the cellular redox status is controlled by e.g. H_2O_2-reducing enzymes such as catalase, peroxiredoxins (Prx), glutathione peroxidases and molecules like thioredoxin.

In conclusion, the regulation of the PTPs by reversible oxidation displays a fine tuning mechanism of pTyr phosphorylation levels. The oxidation of specific PTPs is required for optimal responses to various stimuli and implicated in diseases presenting increased ROS production like cancer, diabetes (Loh *et al.*, 2009) or ischemic stroke (Sandin *et al.*, 2011). Cancer cells develop high ROS levels driving PTPs into reversibly yet also irreversibly oxidized states (Lou, 2008). Decreased PTP activity has been shown in Bcr/Abl and Src transformed cells. Activity was recovered by antioxidants or protein tyrosine kinase inhibitors. The (reversible) oxidation of PTPs presents an important mechanism regulating normal and pathological/oncogenic signaling pathways (Gianni *et al.*, 2008; Sattler *et al.*, 2000).

1.4 The family of haloacid dehalogenase-type phosphatases

Members of the haloacid dehalogenases (HADs) form not only an extremely large, but also a very old superfamily. As an estimation, five genes encoding HADs were already present in the last universal common ancestor. The protein phosphatase family contains the active site sequence DxDx(T/V), and belongs to the of phosphoaspartate transferases (Koonin and Tatusov, 1994). The haloacid dehalogenase superfamily represents a large and ubiquitous class of enzymes with ~ 130,000 members in organisms across all domains of life (Pandya *et*

al., 2014). At least 40 genes encoding for HAD phosphatase catalytic subunits can be identified in humans, and some of them have important functions in physiology and disease (Seifried *et al*., 2013). While originally named after the haloacid dehalogenases that are found in prokaryotes (Motosugi *et al*., 1982; Liu *et al*., 1995; Copley, 1998; Kurihara *et al*., 2000; Kurihara and Esaki, 2008), HAD superfamily members in all organisms are quantitatively dominated by enzymes that catalyze the hydrolysis of a phosphate ester (phosphatase, ~79%) or anhydride (ATPase, ~20%) bond (Burroughs *et al*., 2006). HAD phosphatases carry out catalysis differently from other well-characterized phosphatase superfamilies like the family of PSPs (1.2) or PTPs (1.3). In contrast to these enzymes, HAD phosphatases use an aspartate residue in the active site for nucleophilic attack. This feature of HAD phosphatases also explains their lack of sensitivity against commonly employed phosphatase inhibitors and may have contributed to the slow understanding of their versatile roles in the mammalian system (Barford *et al*., 1998; Alonso *et al.,* 2004).

1.4.1 Structural and mechanistic features

1.4.1.1 Signature motifs

Although the overall sequence identity between HAD phosphatases is typically very low (<15%), the catalytic core residues are highly conserved and cluster into four signature motifs, corresponding to four active site loops (Aravind *et al*., 1998). The four conserved motifs compose the active core (figure 4A). Motif I with the consensus sequence hhhDxDx[T/V][L/V]h (h = hydrophobic residue, x = any residue) is located close to the N-terminus (Allen and Dunaway-Mariano, 2009). The first aspartic acid in motif I is essential for enzymatic activity (Collet *et al*., 1998). It catalyzes reactions initiated by nucleophilic attack (figure 4B). The carboxylate group of the Asp nucleophile and the carbonyl backbone of the second Asp (Asp+2) in motif I coordinate the essential Mg^{2+} in the active site (figure 4C). Motif II with the consensus sequence hhhhhh(S/T) contains a conserved Ser or Thr residue implicated in hydrogen binding to its transferring phosphoryl group and the orientation of the substrate for nucleophilic attack. Motif III is poorly conserved and comprises a conserved Lys residue. The function of the Lys is the stabilization of the negative charge of the reaction intermediate together with Ser/Thr of motif II. It is spaced 18-30 residues apart from motif IV (Lahiri *et al*., 2002a). Motif IV exhibits the consensus sequence (G/S)(D/S)x_{3-4}(D/E)hhhh, as an exception a DD signature is observed. Together with the Asp residues of motif I, the conserved motif IV acidic Asp or Glu residues coordinate Mg^{2+}. Motifs I–IV are arranged around a single binding cavity at the C-terminal end of the strands of the central sheet that forms the active site of HAD phosphatases (Allen and Dunaway-Mariano, 2004).

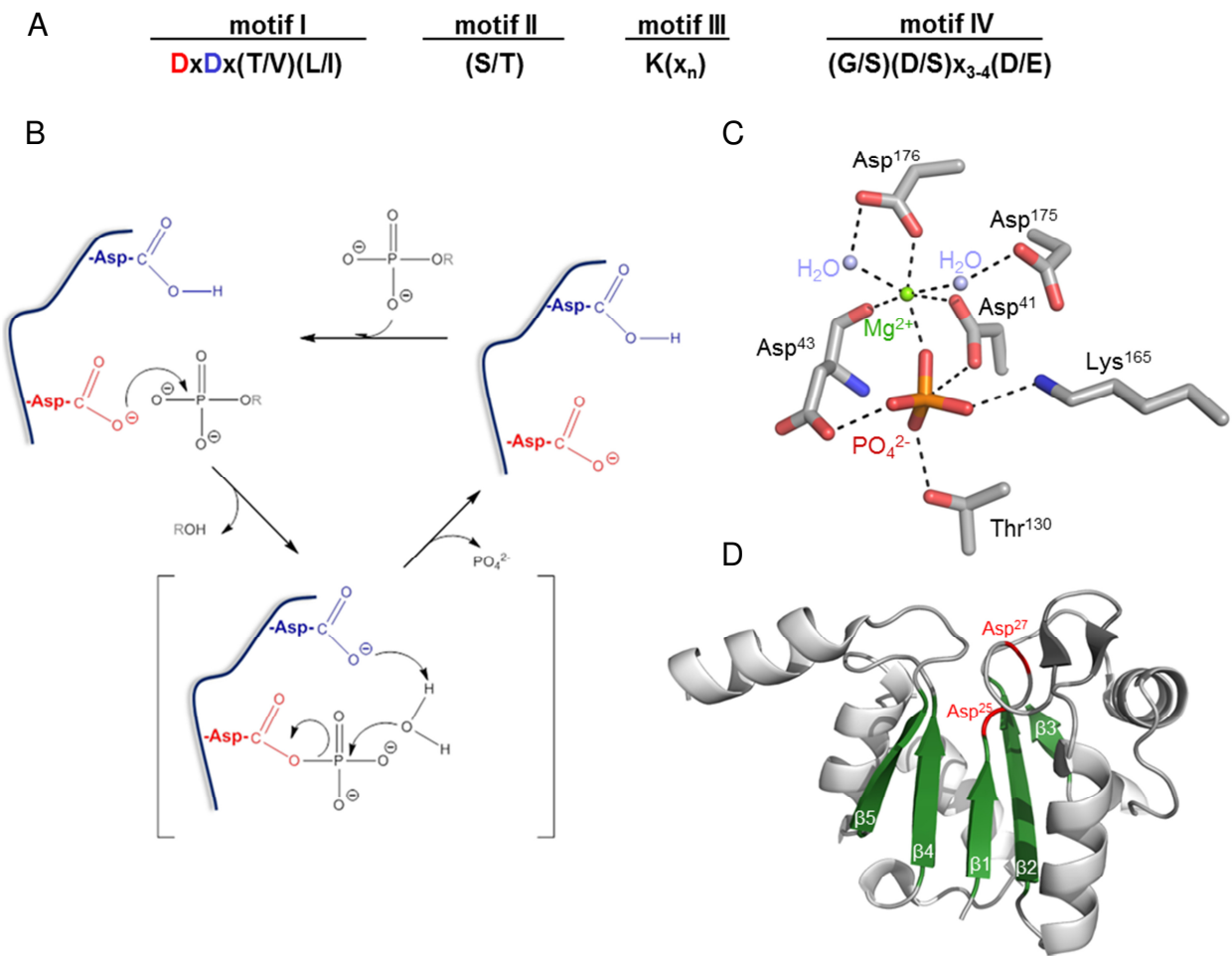

Figure 4: The HAD signature motifs. (A) Consensus sequence of the four catalytic motifs of the family of haloacid hehalogenase (HAD)-type phosphatases. First aspartate residue in motif I depicted in red, representing the nucleophile. X represents any amino acid, D: aspartic acid, V: valine, T: threonine, K: lysine, G: glycine, E: glutamic acid, L: leucine, S: serine, I: isoleucine. **(B)** The general catalytic mechanism of HAD phosphatases. Catalysis proceeds through an aspartylphosphate intermediate. The aspartate nucleophile is shown in red, aspartate+2 is depicted in blue. **(C)** Illustration of the steric orientation of the catalytic core residues in the four active site loops of the human mitochondrial deoxyribonucleotidase (adapted, PDB: 1MH9). Nitrogen atoms are blue, oxygen atoms are red, phosphate atoms are orange, and carbon atoms are gray. **(D)** The Rossmann-like fold of the catalytic core of chronophin (adapted, PDB: 2P69). The structure is reduced to the residues of the catalytic core. The Rossman fold of HAD phosphatases is formed by repeating β-α units. The central sheet consists of five β-strands sequentially arranged in a "54123" order (green). The two aspartates of HAD motif I are depicted in red, followed by the squiggle and flap domains in the first loop (shown in dark gray). For further details, see text.

1.4.1.2 Catalysis

Catalysis occurs in a two-step phosphoaspartyl transferase mechanism (figure 4B). First, the Asp nucleophile initiates a nucleophilic attack on the phosphoryl group of the substrate, which results in the formation of a phosphoaspartyl enzyme intermediate and the displacement of the substrate leaving group. Next, a phosphoryl transfer from the aspartyl-phosphate intermediate to a water molecule takes place, thus releasing free phosphate and regenerating the catalytic Asp. The second aspartate in motif I is positioned two residues C-terminal of the Asp nucleophile (designated Asp+2). It functions as a hydrogen bond

acceptor from the water nucleophile and as a hydrogen bond donor to the leaving group oxygen atom. This leads to the detachment of the dephosphorylated substrate.

The chemistry of this split reaction is shared by all aspartate-based phosphatases (Lahiri *et al.*, 2003). All HAD phosphoaspartyl transferases use Mg^{2+} as cofactor (figure 4C). Magnesium aids in the correct positioning of the substrate phosphoryl group relative to the Asp nucleophile, and electrostatically stabilizes the required close approximation of the anionic nucleophile to the dianionic substrate phosphomonoester (Peeraer *et al.*, 2004). Furthermore, it provides charge neutralization of the transition state. Together, the catalytic residues and the Mg^{2+} cofactor stabilize the trigonal bipyramidal transition state of both partial reactions (Tremblay *et al.*, 2006; Tremblay *et al.*, 2005).

1.4.1.3 The HAD superfold

Aside from the consensus sequence of the four motifs, all members of the HAD phosphatase superfamily share the same structural arrangement of the active core. The residues are ordered in a Rossmann fold built up out of a three stacked α/β sandwich comprised of repeating β-α units (figure 4D). The central sheet is parallel and generally composed of at least five strands in a 54123 sequential arrangement (Burroughs *et al.*, 2006). The structurally conserved core domain of the haloacid dehalogenase superfamily (HADSF) harbors the catalytic scaffold, therefore here referred to as “business part” (figure 6).

The Rossmann fold houses three more structural signatures that allow the enzyme to adopt distinct conformational states and that contribute to substrate specificity: the squiggle, flap, and cap domains. Two smaller signature elements, termed “squiggle” and “flap” are located immediately downstream of the β1-strand of the core rossmannoid fold. The structural motif “squiggle” assumes a nearly complete single helical turn while the downstream motif “flap” forms a β-hairpin turn. The helical turn can adopt loosely or tightly wound helical conformations, thereby inducing a movement in the β-hairpin immediately adjacent to the active site. This automatically generates various conformational states (Godinho and de Sa-Nogueira, 2011).

The phosphoaspartyl transferase mechanism is dependent on an initial reaction that facilitates solvent exclusion (Peisach *et al.*, 2004). For hydrolysis of the phosphoaspartyl intermediate, a subsequent reaction that involves extensive solvent contact is needed. Therefore, alternation between closed and open states of the active site cavity is predicted. The conformational changes exerted by the squiggle and flap domains appear to constitute the minimal machinery required for solvent exclusion and solvent access at the active site (Almo *et al.*, 2007).

1.4.1.4 The cap domain

The members of the HADSF family achieve structural and functional diversity due to cap domain insertions (~5-200 residues)(Pandya *et al.*, 2013). These additional, mobile inserts provide more extensive shielding for the catalytic cavity and supply binding determinants for substrate selectivity and are involved in oligomerization (Lu *et al.*, 2011). Despite their structural diversity, caps can be divided into three classes, C0, C1 and C2. They are similarly distributed across different phyla and all classes exist in the last universal common ancestor (Pandya *et al.*, 2014). Based on this domain organization, HAD phosphatases fall into three structural subfamilies (figure 5).

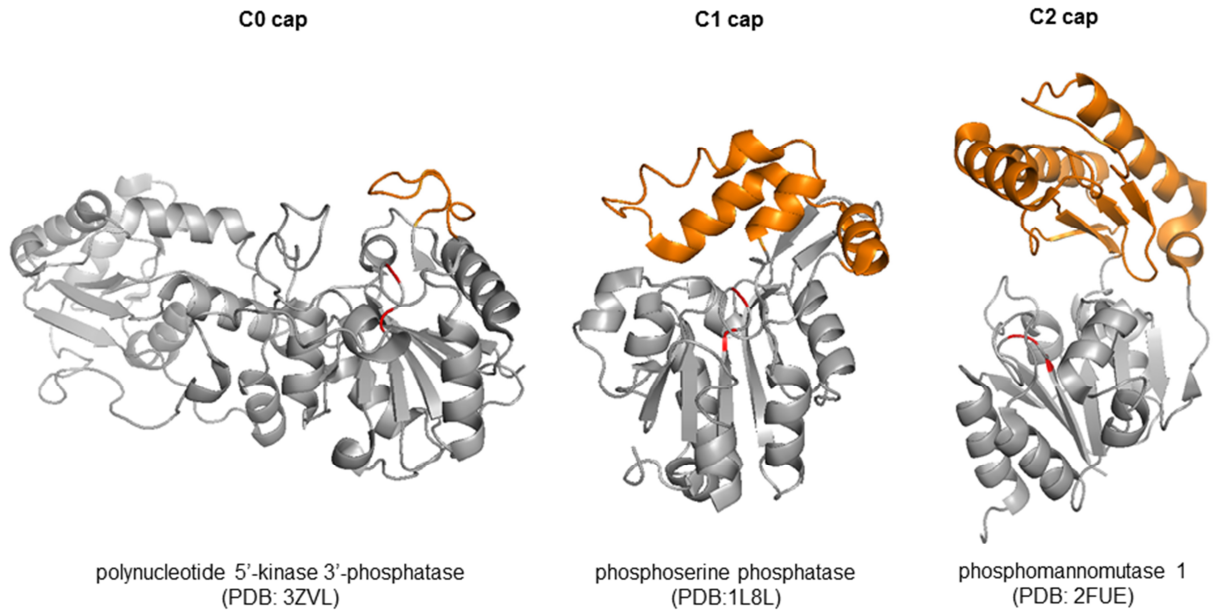

Figure 5: Structural diversity of HAD phosphatase cap domains.
X-ray crystal structures of PNKP (with an unstructured loop as C0 cap), PSPH (with a C1 cap consisting of a four-helical bundle), and PMM1 (with an α/β fold as a C2 cap) are presented. The catalytic domain is depicted in gray, and cap domains are colored in orange in cartoon representation. The catalytic aspartate and aspartate+2 are highlighted in red.

Type C0 and C1 structures are inserted in between the two β-strands of the flap, C2 caps are incorporated in the linker immediately after the β3 strand of the core domain. Whereas C0 elements are very small (Kamenski *et al.*, 2004), C1 and C2 caps fold into domains of considerable size.

The C0 caps represent the structurally simplest modules and can consist of loops or β-strands (Zhang *et al.*, 2006). As a member of the C0 subfamily the polynucleotide kinase/phosphatase (PNKP, PDB: 3ZVL) is depicted in figure 5 (Bernstein *et al.*, 2005).

The C1-type structures include HADs in which the small α-helical cap domain is inserted between motif I and motif II. The most common C1 caps are large enough to completely seal the enzyme's active site. The cN-I nucleotidase families harbor the most

basic α-helical cap. A more complex C1 cap, the tetra-helical bundle, is present in the phosphoserine phosphatase family (PSPH, PDB: 1L8L figure 5)(Kim *et al.*, 2002), whereas the C1 cap of Eyes absent 2 (Eya2) (PDB: 3GEB, 3HB0, 3HB1) folds into a large bundle of seven helices (Jung *et al.*, 2010).

The C2 caps are located between the second and third conserved motif and are highly diverse in structure and size. In general, they are composed of α+β domains with a core β-sheet of at least three strands. Other simple secondary structure elements can be added. The C2 cap class is additionally subdivided into C2a and C2b cap domains, based on the location and topology of the insert. Examples of C2a-capped HAD phosphatases include pyridoxal 5'-phosphatase [Pdxp/chronophin (PDB: 2OYC, 2P69)], phosphomannomutase 1 (PMM1, PDB: 2FUE) (Silvaggi *et al.*, 2006) and NagD (PDB: 2C4N)(Tremblay *et al.*, 2006). The cap residues form four α-helices and five β-strands in contrast to the α-helical bundle cap domain found in C1 subfamily members. This topology is distinct from the mixed α/β cap domain of the C2b members as seen in BT1666 from *B. thetaiotaomicron.* The mixed α/β fold cap has a αββ(αβαβ)αββ topology (PDB 3R4C) (Lu *et al.*, 2011). The phosphoserine phosphatase family simultaneously contains C1 and C2 caps (Peeraer *et al.*, 2003).

Structural analysis of C1- and C2-type phosphatases has revealed the existence of "substrate specificity domains" (Allen and Dunaway-Mariano, 2009; Rinaldo-Matthis *et al.*, 2002). These specificity modules are inserted in the cap domains and generally consist of residues that interact with the substrate leaving group. They define the electrostatic environment of the active site and activate the substrate for nucleophilic attack (Lahiri *et al.*, 2006). In addition, substrate binding may also stabilize the closed conformation of the cap domain, thereby providing specificity. In conclusion, compared to the core domain, the cap domains highly differ between the representatives of the HADSF and are thus here referred to as "private part" (figure 6).

1.4.1.5 Substrate selectivity

The described conserved features of the HADSF enable the members to employ similar catalytic mechanisms. Mammalian HAD phosphatases cover an exceptionally broad substrate space, and can specifically dephosphorylate lipids, various metabolites, DNA, and serine/threonine- or tyrosine-phosphorylated proteins. It is thought that the less conserved regions of the HADs, the cap domains, dictate substrate selectivity. Structural and biochemical approaches show that cap domains can additionally play a decisive role in the selectivity for low- or high molecular weight substrates. Therefore, the cap domain is considered to be the main regulator of substrate selectivity/specificity. C0 members such as PNKP or the RNA polymerase II C-terminal domain (CTD) phosphatases tend to process macromolecular substrates, and the bound substrate itself functions as a cap by excluding bulk solvent. In these cases, substrate selectivity may be provided by a number of invariant

residues that line the entrance to the active site. However, structures of bacterial HAD phosphatases indicate that uncapped phosphatases may also utilize small substrates due to "pseudocapping" by oligomerization via the flap segment (Lu *et al.*, 2009). The presence of distinct C1/C2-type cap modules (or the pseudocapping by oligomerization) sterically restricts access to the catalytic cavity, and allows phosphatases to act on small molecules, which can be sequestered within the active site by cap closure. Despite this, two capped phosphatases have been shown to act on macromolecular substrates: Eya, which can dephosphorylate the C-terminal tyrosyl residue of histone H2AX (Cook *et al.*, 2009), and Pdxp/chronophin, which dephosphorylates not only pyridoxal 5'-phosphate, but also pSer3 of the actin-binding factor cofilin (Gohla *et al.*, 2005). Therefore, capped proteins can be accessible to the termini of phosphoproteins. In contrast to these findings, new bioinformatic analyses have shown that different cap types can carry out similar chemistries (Pandya *et al.*, 2014). It is therefore currently thought that whereas the cap domain does not necessarily restrict the phosphatase to a particular substrate class (protein or small molecular weight substrate), single cap domain residues may be sufficient to determine substrate specificity.

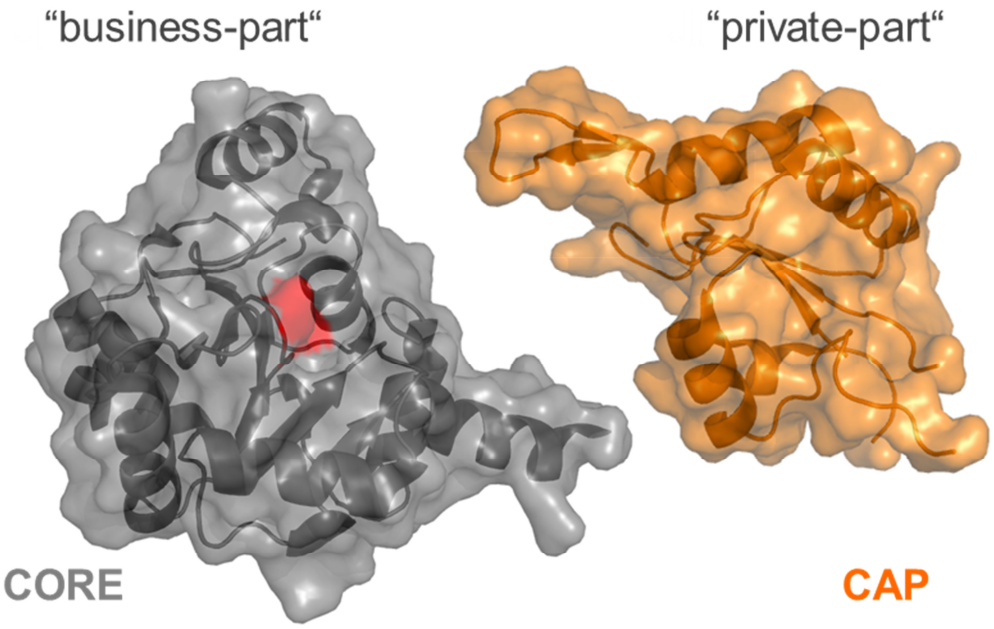

Figure 6: Domain structure of the human chronophin (adapted, PDB 2P69). The core (gray) and cap (orange) domain of chronophin are depicted as ribbon diagram, with transparent surface. The active site aspartate is highlighted in red. The core domain harbors the conserved Rossmann fold motif, responsible for catalysis, therefore defined as "business part". The structural elements of the cap domain vary among the cap classes. In addition, the amino acid sequence of the cap domain is less conserved. The cap domain is therefore defined as "private part".

Furthermore, HAD phosphatases can be fused to additional domains to specialize protein functions. Whereas many prokaryotic HAD phosphatases are small proteins that appear to consist of a single hydrolase domain, some human HAD phosphatases contain

additional domains that give some indications as to their subcellular localization and functions (figure 7).

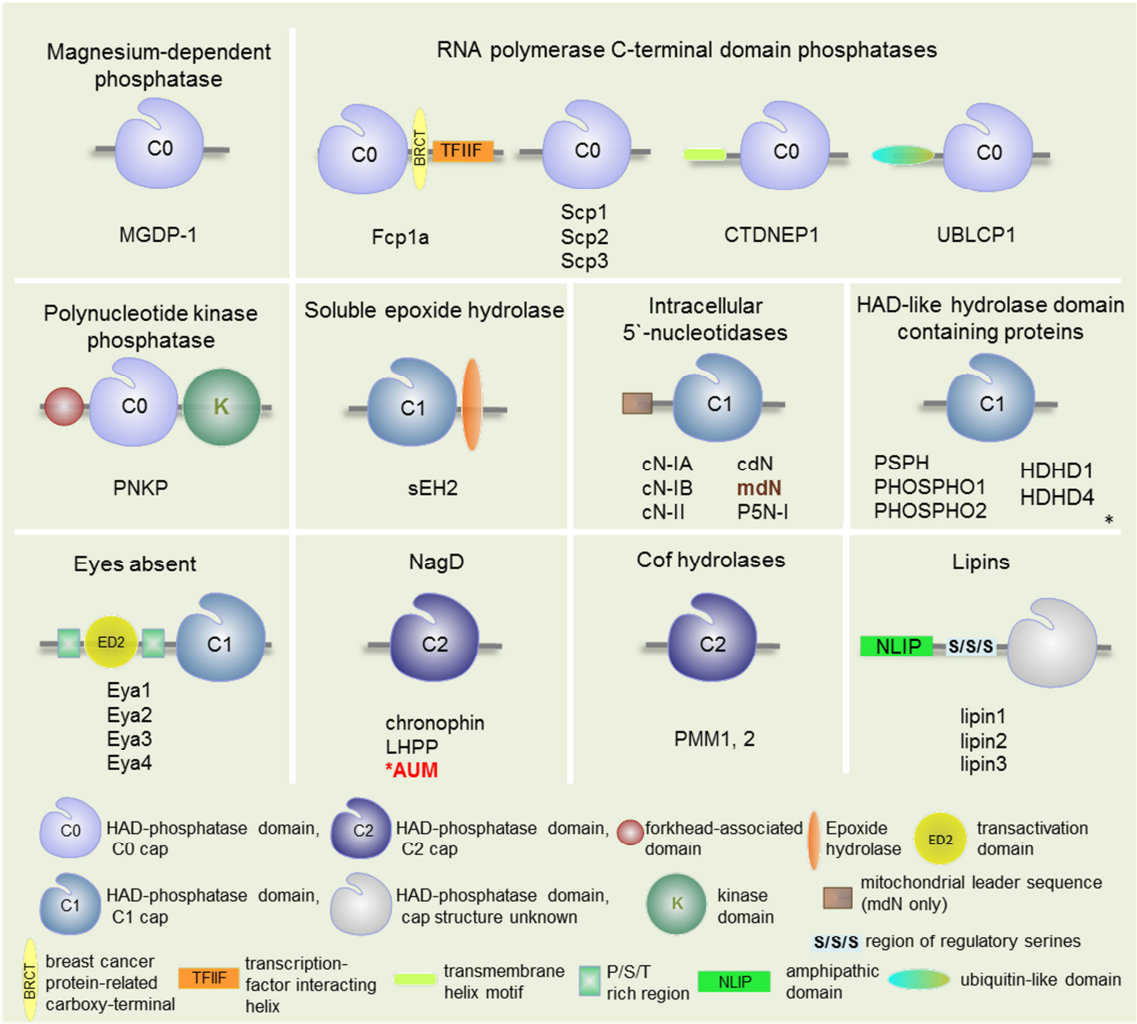

Figure 7: Schematic view of the domain structures of characterized human HAD phosphatases. *These proteins belong to different HAD families (PSPH, PHOSPHO1/2: phosphoserine phosphatases/pyrimidine 5'-nucleotidase) and HDHD1/4 (HAD-like hydrolase domain-containing proteins), but are grouped here due to their common C1 cap and the absence of other recognizable functional domains. For further details, see text.

While there are no known examples of HAD phosphatases with extracellular domains (as can be found in receptor PTPs), the C-terminal domain nuclear envelope phosphatase/dullard homolog (Kim *et al.*, 2007) has a transmembrane helix motif required for nuclear membrane targeting, and the mitochondrial deoxyribonucleotidase (mdNT) (Rinaldo-Matthis *et al.*, 2002) contains a mitochondrial leader sequence. The specialized functions of polynucleotide kinase 3`-phosphatase (PNKP) and soluble epoxide hydrolase 2 (sEH2) for DNA repair or lipid metabolism, respectively, have been accomplished by the fusion of HAD phosphatase domains with DNA kinase or epoxide hydrolase domains (Newman *et al.*, 2003; Bernstein *et al.*, 2005). PNKP additionally contains a DNA binding motif and a forkhead-associated domain that mediates binding to other DNA repair proteins. The Eya phosphatase

domain is embedded in a region that mediates protein-protein interactions with DNA binding proteins, and the catalytic domain is additionally fused to a transactivation domain flanked by P/S/T-rich regions (Rebay *et al.*, 2005). To fulfill their functions in lipid metabolism on intracellular membranes, lipin phosphatases contain an amphipathic α-helix responsible for membrane association. In addition, lipins contain a nuclear localization signal and coactivator motifs to regulate the transcription of genes involved in fatty acid metabolism(Donkor *et al.*, 2007; Csaki and Reue, 2010). The RNA polymerase II C-terminal domain (CTD) phosphatase Fcp1 contains a transcription factor TFIIF-interacting helix and a breast cancer protein-related carboxy-terminal (BRCT) domain that binds to the phosphorylated CTD (Ghosh *et al.*, 2008), whereas the Fcp1-related small CTD phosphatases (SCPs) lack the BRCT and TFIIF-binding domains (Zhang *et al.*, 2006), and the ubiquitin-like CTP phosphatase (UBLCP1) is additionally equipped with an ubiquitin-like domain. Thus, while some HAD phosphatases have an elaborate extra catalytic multidomain structure, others display no additional recognizable domains. These phosphatases may associate with regulatory or targeting subunits (although very few interacting proteins of HAD phosphatases have been described so far), or they may operate as single hydrolase domain entities whose catalysis and specificity is determined in an intrinsic fashion.

1.4.1.6 The identification of AUM

One of the members of the family of the mammalian HAD phosphatases is chronophin. Chronophin was first identified as the pyridoxal 5'-phosphate (PLP) phosphatase [Pdxp; (Fonda, 1992; Jang *et al.*, 2003)]. Pyridoxal-5'-phosphate, the metabolically active form of vitamin B_6, is involved in a wide range of enzymatic reactions including carbohydrate, amino acid, and fatty acid metabolism (Bowling, 2011). Besides its function as PLP phosphatase, chronophin is implicated in the dephosphorylation and activation of Ser3-phosphorylated cofilin (P-cofilin). It regulates actin remodeling during mitosis and cytokinesis (Gohla *et al.*, 2005). It has been implicated in cofilin activation in neutrophils (Sun *et al.*, 2007), and the formation of cofilin/actin-containing rods in neurons subjected to ATP-depletion (Huang *et al.*, 2008). Chronophin is involved in the β-arrestin-mediated cofilin regulation downstream of protease-activated receptor-2 (Zoudilova *et al.*, 2007) and was identified as phospho-serine/threonine phosphatase targeting the steroid receptor co-activator SRC-3 (Li *et al.*, 2008). The dual activity of chronophin as a protein phosphatase, involved in actin reorganization and as a PLP phosphatase has been linked to cytoskeletal changes observed during pyridoxine chloride-induced seizures in rats (Kim *et al.*, 2008). The human chronophin was crystallized with or without its substrate PLP and with its cofactor Mg^{2+} (PDB: 2OYC, 2P27, 2P69).

It was previously shown that HAD phosphatases are an active target of evolution in eukaryotes (Seifried *et al.*, 2013). Interestingly, chronophin represents a member of one of

the HAD subfamilies that was expanded independently in *D. melanogaster* and *C. elegans*, an event likely driven by the need for substrate diversification in metazoans. As the closest relative of chronophin, the phosphatase AUM (aspartate-based, ubiquitous, Mg^{2+}-dependent phosphatase; gene annotation: phosphoglycolate phosphatase, *PGP*) was identified by our group (PhD thesis, P. Duraphe). Human AUM (*PGP*) maps to chromosome 16p13 (Mulley *et al.*, 1990), whereas human chronophin/Pdxp (*PDXP*) is located on chromosome 22q12.3.

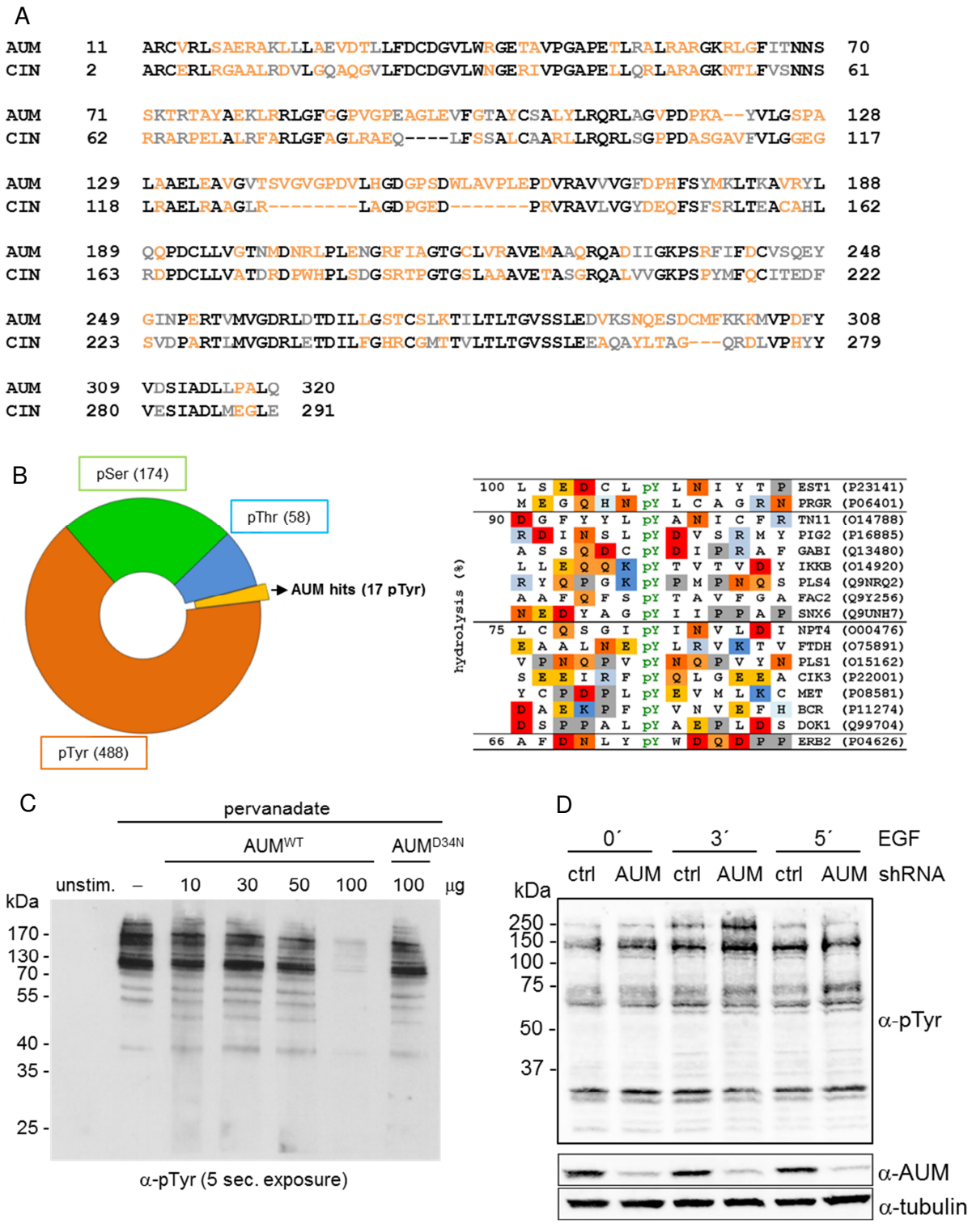

Figure 8: AUM (aspartate-based, ubiquitous, Mg^{2+}-dependent phosphatase) shows high sequence homology with chronophin and acts as a phospho-tyrosine directed phosphatase. **(A)** The sequence alignment of AUM and chronophin show high homology and identity on the amino acid level. Identical residues are shown in black, similar residues are shown in orange and different amino acids are shown in gray. **(B)** Activity of AUM in phosphopeptide array assays comprising phosphoserine (pSer), phosphothreonine (pThr) and phosphotyrosine (pTyr)-containing peptides. The left panel shows the distribution of the 720 tested phosphopeptides, which are all derived from human protein phosphorylation sites. AUM dephosphorylated 17 pTyr, but no pSer or pThr peptides, listed in the right panel. Acidic residues are highlighted in red, basic residues in blue and proline residues in gray. Swiss Prot accession numbers of the peptides are given on the right. **(C)** AUM dephosphorylates tyrosine-phosphorylated proteins in phosphatase overlay assays. After SDS gel electrophoresis, immunoblotting was performed. The membrane was cut and incubated in the absence or presence of 10-100 µg AUM^{WT} or 100 µg AUM^{D34N}. Protein tyrosine phosphorylation was analyzed with 4G10 α-phosphotyrosine antibodies. **(D)** Endogenous AUM regulates EGF-induced protein tyrosine phosphorylation. GC1 spg cells expressing AUM shRNA or control shRNA were stimulated with 100 ng/mL EGF for the indicated time points. Cellular tyrosine phosphorylation levels were assessed with 4G10 α-phosphotyrosine (pTyr) antibodies.

The previously uncharacterized enzyme AUM and chronophin share 45% identity on the amino acid level and 87% similarity of predicted secondary structure motifs (figure 8A). By Northern blot, real-time PCR and Western blot analysis, it was shown that AUM is broadly expressed in all major tissues (PhD thesis, P. Duraphe). Unexpectedly, in contrast to the PLP- (Fonda, 1992; Jang *et al.*, 2003; Galluzzi *et al.*, 2012) and Ser/Thr-directed phosphatase chronophin (Gohla *et al.*, 2005; Zoudilova *et al.*, 2007; Huang *et al.*, 2008; Sun *et al.*, 2007; Li *et al.*, 2008), AUM acts as a tyrosine-specific HAD-type phosphatase *in vitro* and in cells. In a pTyr-, pSer-, and pThr- peptide screen AUM was found to exclusively dephosphorylate a small fraction of pTyr peptides (figure 8B). In addition, active AUM directly hydrolyzes tyrosyl-phosphorylated proteins from HeLa cell extracts in a phosphatase overlay assay (figure 8C). Upon stimulation with the epidermal growth factor (EGF), an increase of tyrosine-phosphorylation of high molecular weight proteins was observed upon RNA interference-mediated depletion of endogenous AUM (figure 8D). In contrast to chronophin, which is inactive against standard pTyr-containing peptides and tyrosyl-phosphorylated proteins (Gohla *et al.*, 2005), AUM appears to act as a tyrosine phosphatase. Because of the biological importance of chronophin in the mammalian system (see above), the function of the newly discovered, chronophin-related phosphatase AUM is of interest.

1.5 Aim of the Study

Mammalian haloacid dehalogenase (HAD)-type phosphatases have been implicated in important physiological processes. Still, numerous members of the 40 identified human HADs remain structurally and functionally uncharacterized to date, and a general understanding of the mechanistic features of specificity and catalytic activity is lacking. AUM (aspartate-based, ubiquitous, Mg^{2+}-dependent phosphatase) is a previously unexplored member of the mammalian HAD phosphatase family. Its mechanistic properties and biological functions are currently unknown.

The aim of the present work is the biochemical and structural characterization of AUM
Three main questions were addressed:

(1) Characterization of the *in vitro* phosphatase properties of recombinant, purified AUM
(2) Analysis of the substrate preferences of AUM in comparison to its closest homolog chronophin, employing evolutionary analyses, biochemical and X-ray crystallographic approaches
(3) Investigation of possible regulatory mechanisms affecting the catalytic activity of AUM

This approach is expected to give first insights into the mechanistic features of AUM substrate specificity and regulation, and may provide a basis for a general molecular understanding of mammalian HAD phosphatases.

2 Materials and Methods

2.1 Materials

2.1.1 Chemicals and reagents

2-hydroxypropane-1,2,3-tricarboxylic acid	Merck Millipore
2-propanol	Carl Roth
4-(2-hydroxyethyl)-1-piperazine-1-ethanesulfonic acid (HEPES)	AppliChem
acetic acid	J.T. Baker
acrylamide/bisacrylamide (30%/0.8%)	Carl Roth
adenosine 5′-(β,γ-imido)triphosphate lithium salt hydrate (AMP-PNP)	Sigma Aldrich
adenosine 5′-(γ-thio)triphosphate tetralithium salt (ATP-γ-S)	Sigma Aldrich
adenosine 5′-diphosphate sodium salt (ADP)	Sigma Aldrich
adenosine 5′-triphosphate disodium salt hydrate (ATP)	Sigma Aldrich
agarose (gene technology quality, GTQ)	Carl Roth
ammonium persulfate (APS)	Sigma Aldrich
ammonium sulfate	Merck Millipore
ampicillin sodium salt	Sigma Aldrich
aprotinin	Sigma Aldrich
beryllium chloride ($BeCl_2$)	Sigma Aldrich
Biomol Green Reagent	Enzo Life Sciences
bovine serum albumin fraction V (BSA)	AppliChem
bromophenol blue	Merck Millipore
calcium chloride ($CaCl_2$)	Merck Millipore
calyculin A	Calbiochem
chloramphenicol	AppliChem
citric acid	Sigma Aldrich
Coomassie Brilliant Blue R-250	Thermo Scientific
deoxyribonucleotide triphosphates (dNTPs)	Invitrogen
dithiothreitol (DTT)	Sigma Aldrich
Dulbecco`s phosphate buffered saline [(w/o $MgCl_2$/$CaCl_2$), DPBS]	PAN Biotech GmbH
Dulbecco's modified Eagle's medium (DMEM)	PAN Biotech GmbH
ethanol	Carl Roth
ethidium bromide solution 1%	Carl Roth
ethylenediaminetetraacetic acid (EDTA)	Merck
fetal calf serum (FCS)	PAN Biotech GmbH
GeneRuler 1kb DNA Ladder	Fermentas

glacial acetic acid (CH_3CO_2H)	Sigma Aldrich
glucose	Merck Millipore
glycerol	AppliChem
glycine	Carl Roth
guanosine 5′-diphosphate sodium salt (GDP)	Sigma Aldrich
guanosine 5′-triphosphate sodium salt hydrate (GTP)	Sigma Aldrich
hydrochloric acid (HCl)	Carl Roth
imidazole	Fluka
isopropyl β-D-1-thiogalactopyranoside (IPTG)	Carl Roth
kanamycin sulfate	Carl Roth
LB-Agar-Powder according to Miller	AppliChem
LB-Medium (Luria/Miller)	Carl Roth
leupeptin	Carl Roth
L-glutamine	PAN Biotech GmbH
Lipofectamine 2000	Invitrogen
magnesium chloride ($MgCl_2$)	AppliChem
magnesium nitrate [$Mg(NO_3)_2$]	AppliChem
magnesium sulfate ($MgSO_4$)	Merck Millipore
methanol	Carl Roth
N, N, N', N'-tetramethylethylenediamine (TEMED)	Carl Roth
nonyl phenoxypolyethoxylethanol (NP-40)	Fluka
okadaic acid	Calbiochem
OPTIMEM	Invitrogen
Orange G	Carl Roth
*p*ara-nitrophenol (*p*NP)	Merck
para-nitrophenylphosphate (*p*NPP)	Calbiochem
Pefabloc SC	Sigma Aldrich
PEG 3350	Sigma Aldrich
penicillin G sodium salt	PAN Biotech GmbH
pepstatin A	Sigma Aldrich
phenylmethylsulfonylfluoride (PMSF)	Sigma Aldrich
phosphatase inhibitor cocktail I and II	Sigma Aldrich
*p*NPP substrate buffer	Calbiochem
Ponceau S	Invitrogen
potassium acetate (CH_3CO_2K)	Fluka
potassium chloride (KCl)	Merck
powdered non-fat milk	Carl Roth
Precision Plus Protein Standard Dual Color	Bio-Rad

prostacyclin sodium salt	Cayman
Protease Inhibitor Cocktail Tablets (complete, EDTA-free)	Roche
puromycin	Calbiochem
pyridoxal 5'-phosphate (PLP)	Sigma Aldrich
sodium azide (NaN_3)	Merck
sodium chloride (NaCl)	Carl Roth
sodium deoxycholate	Sigma Aldrich
sodium dihydrogen phosphate (NaH_2PO_4)	Merck
sodium dodecyl sulfate (SDS) ultra pure	Carl Roth
sodium fluoride (NaF)	Sigma Aldrich
sodium hydroxide (NaOH)	Carl Roth
sodium orthovanadate (Na_3VO_4)	Sigma Aldrich
sodium pyrophosphate	Sigma Aldrich
streptomycin sulfate	PAN Biotech GmbH
tetracycline	Roth
triethanolamine (TEA)	AppliChem
tris(2-carboxyethyl)phosphine hydrochloride (TCEP)	Sigma Aldrich
tris(hydroxymethyl)aminomethan (Tris) base/Tris-HCl	Carl Roth
trisodium 2-hydroxypropane-1,2,3-tricarboxylate	Sigma Aldrich
trisodium citrate	Sigma Aldrich
Triton X-100	Sigma Aldrich
Tween 20	AppliChem
yeast extract	AppliChem
β-glycerophosphate	Sigma Aldrich
β-mercaptoethanol	Sigma Aldrich

2.1.2 Technical equipment

5424 R Centrifuge	Eppendorf
ÄKTApurifier	GE Healthcare
An-50 Ti rotor	Beckman Coulter
Avanti J25	Beckman Coulter
BBD 6229 incubator	Heraeus
BDK Laminarflow	Thermo Scientific
C1000TM thermal cycler	Bio-Rad
Cell disruptor TS-Series	Constant Systems
E.A.S.Y Win32 gel documentation system	Herolab
EBA 12R centrifuge	Hettich
EnVision 2104 multilabel reader	Perkin Elmer

HiLoad 16/60 Superdex 200 pg	GE Healthcare
HisTrap HP	GE Healthcare
HoneyBee 963	Zinsser Analytic
Howorka-Ball 20 ml	VWR
ImageQuant LAS 4010 Digital Imaging System	GE Healthcare
ISF-1-W bacterial shaker	Kühner
ISF-1-X bacterial shaker	Kühner
J-810-150S spectropolarimeter	Jasco
JA-17 rotor	Beckman Coulter
JLA 8.1000 rotor	Beckman Coulter
Lab 850 pH meter	Schott Instruments
Lizzy 2002	Zinsser Analytic
Micromax HF-007	Rigaku
Mini-PROTEAN Tetra Cell electrophoresis system	Bio-Rad
MR Hei-MixL magnetic stirrer	Heidolph
NanoDrop 2000c spectrophotometer	Peqlab
Neubauer counting chamber	Marienfeld
Optima XL I analytical ultracentrifuge	Beckman Coulter
R-axis HTC image plate detector	Rigaku
RoboSeal	HJ-Bioanalytik
Stemi 2000-C Microscope	Zeiss
Superdex 200 10/300 GL	GE Healthcare
Systec V-150 autoclave	Systec
Thermomixer comfort 1.5 mL	Eppendorf
Trans-Blot SD semi-dry transfer cell	Bio-Rad
Unimax 1010 plate mixer	Heidolph
Universal 16R centrifuge	Hettich
VORTEX-GENIE 2 mixer	Scientific Industries

2.1.3 Consumable supplies

96-well Crystallization plate	Crystalgen
96-well plate Nunclon Delta Surface	Thermo Scientific
Amicon Ultra centrifugal Filter Units, 10,000 MWCO	Millipore
Bio-Spin Disposable Chromatography Columns, 10 mL	Bio-Rad
CNBr-activated Sepharose 4B	GE Healtcare
Culture dishes Nunclon Delta Surface	Nunc
Hybond C nitrocellulose membrane	Amersham
Omnifix F syringe (25G×5/8)	Braun

PIP Strips	Echelon Biosciences
Protein A-Sepharose CL-4B	GE Healthcare
rubber policeman	A. Hartenstein
Sartolon polyamide 0.2 µm filter,	Sartorius Biotech
Slide-A-Lyzer Dialysis Cassette G2, 10,000 MWCO	Thermo Scientific
Whatman paper	A. Hartenstein

2.1.4 Commercial kits

Gel Filtration LMW Calibration Kit	GE Healthcare
Micro BCA kit	Thermo Scientific
Plasmid Plus Midi kit	Qiagen
Platinum Pfx DNA polymerase kit	Invitrogen
QIAfilter plasmid purification Midi plus kit	Qiagen
Qiaquick Gel Extraction kit	Qiagen
Super Signal West Pico	Thermo Scientific

2.1.5 Commercial screens

Crystal Screen 1	Hampton Research
Crystal Screen 2	Hampton Research
Index	Hampton Research
JBScreen Phosphatase	Jena Bioscience
Nextal PEGs suite	Qiagen
The Nucleix Suite	Qiagen
Topaz OptiMix-3	Fluidigm
Topaz OptiMix-PEG	Fluidigm
Wizard Screen I	Emerald BioSystems
Wizard Screen II	Emerald BioSystems

2.1.6 Cell lines and animals

Escherichia coli (*E. coli*) BL21(DE3)	Merck Millipore
Escherichia coli (*E. coli*) DH5α	Invitrogen
CHO-K1 (CCL-61)	ATCC/LGC
COS-7 (CRL-1651)	ATCC/LGC
GC1 spg (CRL-2053)	ATCC/LGC
GC1 spg/AUM shRNA (m77)	P. Duraphe, PhD thesis
GC1 spg/ctrl. shRNA	P. Duraphe, PhD thesis

HEK AD-293	Stratagene
HeLa (CCL-2)	ATCC/LGC
C57BL/6 AUM$^{D34N/D34N}$ mice	generated by Ozgene
C57BL/6 AUM$^{D34N/D34N; Pf4 Cre}$ mice	generated by K. Hadamek
C57BL/6 mice	Charles River Laboratories

2.1.7 RNA interference tools

TARGET plus siCONTROL (catalog # D-001810-0X)	Thermo Scientific
ON-TARGETplus Human PGP siRNA (catalog # J-022877-05)	Thermo Scientific
MISSION non-targeting shRNA control (catalog # SHC002)	Sigma Aldrich
MISSION shRNA Program (catalog # SHCLND-NM_025954)	Sigma Aldrich

shRNA TRCN0000081477:
5`CCGGCTGTAGCCTGAAGACTATCCTCTCGAGAGGATAGTCTTCAGGCTACAGTTTTTG 3`

2.1.8 Antibodies

α-Actin (clone C4) mouse monoclonal	Merck Millipore
α-AUM full-length rabbit polyclonal antibodies, magnesium eluate	Charles River, present work
α-AUM full-length rabbit polyclonal antibodies, glycine eluate	Charles River, present work
α-AUM rabbit polyclonal anti-peptide antibodies,	Charles River, P. Duraphe, PhD thesis
α-chronophin rabbit monoclonal	Cell Signaling Technology
α-GAPDH (clone 14C10) mouse monoclonal	Cell Signaling Technology
α-GST	Sigma Aldrich
α-rabbit and α-mouse secondary antibodies, HRP-conjugated	Thermo Scientific

2.1.9 Phospholipids

PtdIns(4)P, (P-4008)	Echelon Biosciences
PtdIns(3,4,5)P_3, (P-3908)	Echelon Biosciences
PtdIns(3,4)P_2, (P-3408)	Echelon Biosciences
PtdIns(3,5)P_2, (P-3508)	Echelon Biosciences

2.1.10 Enzymes, proteins and commercial buffers

10x EcoRI buffer	New England BioLabs
apyrase	New England BioLabs
DNaseI	AppliChem
DpnI	AppliChem
EcoRI	New England BioLabs
HindIII	New England BioLabs
lysozyme	Carl Roth
MultiPIP Grip (LL5α-PH)	Echelon Biosciences
NcoI	New England BioLabs
PTEN, recombinant, purified	Echelon Biosciences
RNase A	Qiagen
trypsin/EDTA	PAN Biotech GmbH

2.1.11 Oligonucleotides

All nucleotides were synthesized by Eurofins MWG GmbH.

Table 1: List of primers

Insert	Oligonucleotides	Sequence (5'-3' direction)
AUM	AUM_NcoI_fwd	GGGCATGGCAGAGGCGGAAGCC
	AUM_EcoRI_rev	GGGGAATTCTTAACCTTGAAGGG CAGG
AUM(human)	hAUM_NcoI_fwd	GGGCCATGGCGGCGGCGGAGGC CGG
	HomAUM_HINDIII_F	GGGAAGCTTGCCACCATGGCGGC GGCGGAG
$AUM^{R41N; T44R; A45I}$	AUM/CIN1_fwd	GATGGCGTGCTGTGGAACGGTGAG AGGATCGTGCCGGGCGCGCCG
	AUM/CIN1_rev	CGGCGCGCCCGGCACGATCCTCTC ACCGTTCCACAGCACGCCATC
$AUM^{T67S; S71R; K72R; T73A}$	AUM/CIN2_fwd	CTGGGCTTCATCAGCAACAACAGCC GCAGGGCTCGCACGGCCTAC
	AUM/CIN2_rev	GTAGGCCGTGCGAGCCCTGCGGCT GTTGTTGCTGATGAAGCCCAG
AUM/CIN hybrid	AUM_fwd_hyb	GCAACAACAGCCGGCGCGCGCGCA CGGCCTACGCGGAG
	CIN_rev_hyb	CTCCGCGTAGGCCGTGCGCGCGCG CCGGCTGTTGTTGC
	CIN_NcoI_fwd	GGGCCATGGCAGAGGCGGAAGC
	AUM_EcoRI_rev	GGGGAATTCTTAACCTTGAAGGGCA GG
$AUM^{T67S; S71R; K72R; T73A}$	AUM/CIN2_T-rescue_fwd	GCGACTGGGCTTCATCACCAACAAC AGCCGCAGGGC
	AUM/CIN2_T-rescue_rev	GCCCTGCGGCTGTTGTTGGTGATG AGCCCAGTCGC

AUM$^{T67; K72R; T73A}$	AUM/CIN2_S-rescue_fwd	GCAACAACAGCAGCAGGGCTCGCACGG
	AUM/CIN2_S-rescue_rev	CCGTGCGAGCCCTGCTGCTGTTGTGC
AUM$^{T67S; S71R; T73A}$	AUM/CIN2_K-rescue_fwd	GCAACAACAGCAGCAGGGCTCGCAGGC
	AUM/CIN2_K-rescue_rev	GCCGTGCGAGCCTTGCGGCTGTTGTGC
AUM^{T73A}	AUM/CIN2_TSK-rescue_fwd	CTGGGCTTCATCACCAACAACAGCGCAAGGCTCGCACGGCCTAC
	AUM/CIN2_TSK-rescue_rev	GTAGGCCGTGCGAGCCTTGCTGCTGTTGTTGGTGATGAAGCCCAG
AUM^{L204H}	L204H_fwd	GGCACCAACATGGACAACCGGCACCCGCTAGAGAACGGCCG
	L204H_rev	CGGCCGTTCTCTAGCGGGTGCCGGTTGTCCATGTTGGTGCC
AUM^{D34N}	AUM_D34N_fwd	GTGGACACGCTGCTGTTCAACTGCGATGGCGTGCTGTGG
	AUM_D34N_rev	CCACAGCaCGCCAtCGCAGTTGAACAGCAGCGTGTCCAC
CAC	CIN(1-100)_fwd	CATGCCATGGGAATGGCGCGCTGCGAGC
	CIN(1-100)_rev	GCCGGCCAGCCGCTGGCGCAGGAGGCG
	AUM(109-211)_fwd	CGCCTCCTGCGCCAGCGGCTGGCCGGC
	AUM(109-211)_rev	TGTGATGCACTGGAACATGTAAGGGCTAGGCTTCCCGATGATGTCCGCCTGG
	CIN(208-292)_fwd	CCAGGCGGACATCATCGGGAAGCCTAGCCCTTACATGTTCCAGTGCATCACA
	CIN(208-292)_rev	TAAGAATGCGGCCGCTCAGTCCTCCAGCCCCTCCAT
AUM^{C13S}	C13Sfor	GGTGGCGACGAAGCCCGCTCCGTGCGGCTGAGCGCCGAGC
	C13Srev	GCTCGGCGCTCAGCCGCACGGAGCGGGCTTGGTCGCCACC
AUM^{C35S}	AUMC35S_for	GGACACGCTGCTGTTCGACTCCGATGGCGTGCTGTGGCGC
	AUMC35S_rev	GCGCCACAGCACGCCATCGGAGTCGAACAGCAGCGTGTCC
AUM^{C243S}	C243Sfor	CCTAGCCGCTTCATCTTCGACTCCGTGTCCCAGGAGTATGG
	C243Srev	CCATACTCCTGGGACACGGAGTCGAAGATGAAGCGGCTAGG

Additional information on AUM mutants is given in the Methods section 2.2.2.

2.1.12 Plasmids

Unless otherwise specified, the inserted regions coding for AUM, chronophin or hybrids are of murine origin.

pcDNA3	Invitrogen
pcDNA3_humAUM (human)	present work

pcDNA3_humAUM^{D34N} (human)	present work
pCMV-SPORT6_bovAUM (bovine)	ImaGenes
pdEYFP-C1-hAUM (human)	A. Saxena, PhD thesis
pdEYFP-C1-hAUM^{D34N}(human)	A. Saxena, PhD thesis
pETM11	EMBL
pETM11_ACA (AUM$^{1-113}$-chronophin$^{101-207}$-AUM$^{234-321}$)	Geneart
pETM11_AUM$^{R41N; T44R; A45I}$	present work
pETM11_AUM$^{S71R; K72R; T73A}$	present work
pETM11_AUM$^{T67S; S71R; K72R; T73A}$	present work
pETM11_AUM $^{\Delta 10}$	present work
pETM11_AUM	present work
pETM11_AUM/CIN hybrid (chronophin$^{1-65}$-AUM$^{75-312}$)	present work
pETM11_AUM^{C104S}	present work
pETM11_AUM$^{C104S; C243S}$	present work
pETM11_AUM^{C13S}	present work
pETM11_AUM^{C193S}	present work
pETM11_AUM^{C217S}	present work
pETM11_AUM^{C243S}	present work
pETM11_AUM^{C272S}	present work
pETM11_AUM^{C293S}	present work
pETM11_AUM^{C35S}	present work
pETM11_AUM$^{C35S; C104S}$	present work
pETM11_AUM^{D34N}	present work
pETM11_AUM$^{D34N; L204H}$	present work
pETM11_AUM^{L204H}	present work
pETM11_AUM$^{T67; K72R; T73A}$	present work
pETM11_AUM$^{T67S; S71R; T73A}$	present work
pETM11_AUM^{T73A}	present work
pETM11_bovAUM (bovine)	present work
pETM11_CAC (chronophin$^{1-100}$-AUM$^{114-233}$-chronophin$^{208-291}$)	G. Knobloch
pETM11_CAC^{L191H}	present work
pETM11_chronophin	G. Knobloch
pETM11_humAUM (human)	present work
pG-Tf2 (chaperone plasmid set)	Takara Bio Inc.
pMK_RQ_AUM^{C104S}	Geneart
pMK_RQ_AUM^{C193S}	Geneart
pMK_RQ_AUM^{C217S}	Geneart
pMK_RQ_AUM^{C272S}	Geneart

pMK_RQ_AUM^{C293S}	Geneart
ptd Tomato-N1	Clontech
pTrcHis A-mAUM^{D34N}	P. Duraphe, PhD thesis
pTrcHis A-mAUM^{WT}	P. Duraphe, PhD thesis

Plasmid generation is described in 2.2.2.1

2.1.13 Solutions and buffers

Unless otherwise noted, chemicals given in percent (%) designate volume per volume (v/v).

Acid citrate dextrose (ACD):	15 mM	trisodium citrate
	25 mM	glucose
	12 mM	citric acid
		pH 4.5
antibody diluent:	10 mM	HEPES
	0.5 M	NaCl
	1% (w/v)	BSA
	0.2%	Tween-20
	0.2% (w/v)	NaN_3
		pH 7.4
blocking buffer:	50 mM	Tris-HCl
	2 mM	$CaCl_2$
	80 mM	NaCl
	5% (w/v)	powdered milk
	0.2%	NP-40
		pH 8.0
SDS-PAGE sample buffer:	62.5 mM	Tris-HCl
	10%	glycerol
	5%	β-mercaptoethanol
	2% (w/v)	SDS
	0.02% (w/v)	Bromophenol Blue
		pH 6.8

lysis buffer (for tissues and IP):	20 mM	Tris-HCl
	150 mM	NaCl
	1%	Triton X-100
	1 mM	β-glycerophosphate
	2.5 mM	sodium pyrophosphate
	10 µg/mL	aprotinin
	10 µg/mL	leupeptin
	1 mM	PMSF
	1 mM	pepstatin
		pH 7.5
RIPA buffer:	50 mM	Tris-HCl
	150 mM	NaCl
	1%	NP-40
	0.1% (w/v)	SDS
	0.5% (w/v)	sodium deoxycholate
	10 µg/mL	aprotinin
	10 µg/mL	leupeptin
	1 mM	pepstatin
	1 mM	PMSF
		pH 8.0
running buffer (SDS-PAGE) :	25 mM	Tris base
	200 mM	glycine
	1% (w/v)	SDS
		pH 8.7
stripping buffer:	62.5 mM	Tris-HCl
	2% (w/v)	SDS
	100 mM	β-mercaptoethanol
		pH 6.7
anode buffer I:	0.5 M	Tris base
	40%	methanol
anode buffer II:	25 mM	Tris base
	40%	methanol

cathode buffer:	25 mM	Tris base
	40 mM	glycine
	10%	methanol

For high molecular weight proteins, 20% methanol was used in anode buffers I and II and 0.005% SDS was added to the cathode buffer.

Coomassie destaining solution:	20%	ethanol
	10%	CH_3CO_2H

Coomassie staining solution:	2.5 g/l	Coomassie Brilliant Blue R-250
	10%	acetic acid
	45%	methanol

phosphate buffer (PB):	100 mM	NaH_2PO_4
	1 mM	$MgSO_4$
	pH 7.5	

TMN:	50 mM	TEA
	5 mM	$MgCl_2$
	250 mM	NaCl
		pH 7.5

TMN “LOW”:	50 mM	TEA
	5 mM	$MgCl_2$
	250 mM	NaCl
	10 mM	imidazole
		pH 7.5

TMN “HIGH”:	50 mM	TEA
	5 mM	$MgCl_2$
	250 mM	NaCl
	400 mM	imidazole
		pH 7.5

TMN “FRACTIO“:	30 mM	TEA
	1 mM	$MgCl_2$
	150 mM	NaCl
	10 µg/mL	aprotinin
	10 µg/mL	leupeptin
	1 mM	pepstatin
	1 mM	Pefabloc
		pH 7.5
TMN “LOW-chronophin”:	100 mM	TEA
	500 mM	NaCl
	20 mM	imidazole
	5 mM	$MgCl_2$
		pH 7.4
TMN “HIGH-chronophin”:	50 mM	TEA
	250 mM	NaCl
	500 mM	imidazole
	5 mM	$MgCl_2$
		pH 7.4
TMN “chronophin”:	50 mM	TEA
	250 mM	NaCl
	5 mM	$MgCl_2$
		pH 7.4
TBS:	25 mM	Tris-HCl
	140 mM	NaCl,
	2.7 mM	KCl
		pH 7.4
PIP-Strip dilution buffer:	10 mM	HEPES
	500 mM	NaCl
	1% (w/v)	BSA
	0.2%	Tween 20
	0.02% (w/v)	NaN_3
		pH 7.4

Ponceau S solution:	0.1% (w/v)	Ponceau S
	5%	CH_3CO_2H
P1 buffer:	50 mM	Tris-HCl
	10 mM	EDTA
	100 µg/mL	RNase A
		pH 8.0
P2 buffer:	200 mM	NaOH
	1% (w/v)	SDS
P3 buffer:	3 M	CH_3CO_2K
		pH 5.5
SDS-PAGE running gel (12%):	12% (w/v)	acrylamide
	0.05%	APS
	0.003%	TEMED
	0.1%	SDS
	375 mM	Tris-HCl
		pH 8.8
SDS-PAGE stacking gel:	4% (w/v)	acrylamide
	0.02%	APS
	0.002%	TEMED
	0.1%	SDS
	125 mM	Tris-HCl
		pH 6.8
SOC-medium:	2%	tryptone
	0.5%	yeast extract
	8.5 mM	NaCl
	2.5 mM	KCl
	10 mM	$MgCl_2$
	10 mM	$MgSO_4$
	20 mM	glucose
		pH 7.0

TAE:	40 mM	Tris base
	20 mM	CH_3CO_2H
	1 mM	EDTA
		pH 8.5
binding buffer:	100 mM	$NaHCO_3$
	500 mM	NaCl
		pH 8.3
tris buffer:	100 mM	Tris-HCl
	500 mM	NaCl
		pH 8.5
acetate buffer:	100 mM	$C_2H_3O_2Na$
	500 mM	NaCl
		pH 4.0
washing buffer:	50 mM	Tris-HCl
	50 mM	NaCl
		pH 7.5
collection buffer I:	50 mM	Tris-HCl
	50 mM	NaCl
		pH 7.5
elution buffer magnesium:	50 mM	Tris base
	3.5 M	$MgCl_2$
collection buffer II:	1 M	Tris-HCl
	50 mM	NaCl
		pH 8.8
elution buffer glycine:	200 mM	glycine
		pH 2.5

Tyrode`s buffer	137 mM	NaCl
	2.7 mM	KCl
	12 mM	$NaHCO_3$
	5 mM	HEPES
	1 mM	$MgCl_2$
	0.5 mM	$CaCl_2$
	0.1%	glucose
LOW SALT buffer:	10 mM	HEPES
	150 mM	NaCl
	10 mM	$MgCl_2$
	5%	glycerol
		pH 7.5
HIGH SALT buffer:	10 mM	HEPES
	500 mM	NaCl
	10 mM	$MgCl_2$
	5%	glycerol
		pH 7.5

2.1.14 Software and databases

BLAST	NCBI
ClustalW	EMBL
DSSP	(Kabsch and Sander, 1983)
ExPASy Server	Swiss Institute of Bioinformatics
GBlocks	(Talavera and Castresana, 2007)
GraphPad Prism version 4.01	GraphPad software
HMMDiverge	(Huang and Golding, 2012)
ImageJ	(Schneider *et al.*, 2012)
iMosflm	(Battye *et al.*, 2011)
MrBayes	(Ronquist *et al.*, 2012)
Muscle	(Edgar, 2004)
PAML	(Yang, 2007)
PFAM	(Punta *et al.*, 2012)
Phaser	(McCoy *et al.*, 2007)
Phenix	(Adams *et al.*, 2010)
PhyML	(Dereeper *et al.*, 2008)
pro origami system	(Stivala *et al.*, 2011)
PyMOL	Schrödinger, LLC
Scala	(Evans, 2006)
SDPfox	(Mazin *et al.*, 2010)
SEDFIT, NIH software	(Schuck, 2000)
The PISA online tool	(http://www.ebi.ac.uk/pdbe/prot_int/pistart.html)

2.2 Methods

2.2.1 Phylogenetic analysis of AUM and chronophin

Metazoan chronophin and AUM phosphatases were identified using PFAM 25.0, clan CL0137, and human sequences were used as queries for BLAST searches of the indicated genomes. The sequences were aligned with Muscle and curated with GBlocks. The phylogenetic tree was calculated using PhyML with default parameters. Conserved sites were identified as 90% consensus in chronophin and AUM, respectively (http://www.hiv.lanl.gov/content/sequence/CONSENSUS/AdvCon.html). Site specific evolutionary rates were identified using MrBayes with a gamma model for the rate distribution and ten categories considering the AUM and chronophin subfamilies. Differently conserved sites were identified with SDPfox. To test for sites under different selective pressure, HMMDiverge was used. All sites with a probability of ≥0.8 that the evolutionary rate is higher in one family were selected. Branch-specific rate analyses were performed with PAML. The following models were tested: (1) one rate for the whole tree; (2) one additional rate for the branches of chronophin and AUM, respectively, following the duplication; (3) one additional rate for the chronophin and the AUM subbranch, respectively. To test for significance, the doubled difference of the log likelihood was compared with the $\chi 2$ value taking into account the different degrees of freedom. Neither model 2 nor model 3 fitted the data significantly ($p<0.05$) better than the simple model 1. Phylogenetic analysis of AUM and chronophin was carried out by Prof. Jörg Schultz (Department of Bioinformatics, University of Würzburg).

2.2.2 Molecular cloning

2.2.2.1 Polymerase Chain Reaction

The polymerase chain reaction was used to amplify DNA regions (standard PCR), or to insert point mutations in generated constructs (site-directed mutagenesis), by employing defined oligonucleotides (2.1.11). All described amplification protocols were performed in a C1000 thermal cycler using the Platinum Pfx DNA polymerase kit.

For protein expression in *E. coli,* the AUM sequence and AUM sequence variants were inserted into pETM11 via NcoI and EcoRI restriction sites. For eukaryotic expression, AUM and AUM mutants were inserted into pcDNA3 via HindIII and EcoRI restriction sites. To amplify murine AUM^{D34N}, pTrcHis A-$mAUM^{D34N}$ was used as a template. All murine AUM point mutants were generated via site-directed mutagenesis using pETM11_AUM as a template. Human AUM wildtype and AUM^{D34N} were subcloned using pdEYFP-C1-hAUM or pdEYFP-C1-$hAUM^{D34N}$. The bovine wildtype AUM was subcloned using pCMV-

SPORT6_bovAUM. The murine chronophin$^{1-100}$-AUM$^{114-233}$-chronophin$^{208-292}$ (pETM11_CAC) hybrid was provided by Gunnar Knobloch. The murine AUM$^{1-113}$-chronophin$^{101-207}$-AUM$^{234-321}$ (pETM11_ACA) hybrid was obtained by gene synthesis after optimizing the nucleotide sequence for maximal protein production without changing the murine AUM or chronophin amino acid sequences (Geneart). The murine AUM^{C104S}, AUM^{C193S}, AUM^{C217S}, AUM^{C272S}, AUM^{C293S} in pMK_RQ were obtained by gene synthesis (Geneart) and then subcloned into pETM11 via the AUM_NcoI_fwd and AUM_EcoRI_rev primers. To generate the constructs pETM11_AUM^{C35_104S} and pETM11_AUM^{C104_243S}, pETM11_AUM^{C104S} was used as a template. To insert the additional mutation, the primer pairs AUMC35S_for and AUMC35S_rev or C243Sfor and C243Srev were applied in site-directed mutagenesis experiments. All constructs were verified by sequencing (Eurofins MWG GmbH).

Standard PCR

To amplify AUM and variants for insertion into the pETM-11 or pcDNA3 plasmid, standard PCR was performed. The PCR reaction mix (50 µL final volume) contained: 5 µL Pfx 10x enhancer solution, 5 µL Pfx 10x amplification buffer, 0.5 mM $MgSO_4$, 10 ng DNA template, 0.3 mM dNTPs, 0.8 pM of each forward and reverse primer, 0.5 mL Pfx polymerase. Sterile $H_2O_{dest.}$ was added to reach the final volume.

PCR protocol (30 reaction cycles):

(1) initialization step: 95°C → 1 min
(2) denaturation step: 95°C → 1 min
(3) annealing step: 50°C → 1 min
(4) elongation step: 68°C → 1.5 min
→ (2) to (4): 30 repeats
(5) final elongation step: 68°C → 5 min
(6) final hold: 12°C → ∞

Site-directed mutagenesis

To insert point mutations, site-directed mutagenesis was performed. Primers encoding for one to four point mutations, flanked by 15-20 bases on each side were generated. The PCR reaction mix (50 µL final volume) contained: 100 ng DNA template, 0.3 mM dNTPs, 0.8 pM of each forward and reverse primer, 0.5 mM $MgSO_4$, 5 µL 10x Pfx amplification buffer, 5 µL 10x PCR enhancer solution, 1 µL Pfx polymerase and sterile $H_2O_{dest.}$ to reach the final volume.

PCR protocol (12 reaction cycles):

(1) initialization step:	95°C → 3 min
(2) denaturation step:	95°C → 0.5 min
(3) annealing step:	42-65°C → 1 min
(temperature depending on primer length and GC content)	
→ (2) to (4): 12 repeats	
(4) elongation step:	68°C → 9 min
(5) final elongation step:	68°C → 5 min
(6) final hold:	12°C → ∞

After amplification, the PCR mixture was incubated for 3-12 h with 10 U of DpnI at 37°C to remove the methylated templates by digestion. The PCR product (2, 5, and 10 µL) was transformed into chemically competent *E. coli* DH5α, and plated on LB plates containing 50 µg/mL kanamycin for pETM11 constructs. Antibiotic-resistant colonies were screened for the desired mutation by sequencing.

2.2.2.2 Agarose gel electrophoresis

To separate DNA fragments after PCR or restriction digestion, agarose gel electrophoresis was performed. Gels were prepared by melting 1% agarose (w/v) in TAE buffer. DNA samples were mixed with orange G DNA loading dye (3:1). TAE was used as running buffer and a 1 kb DNA ladder was used as a standard. DNA was separated electrophoretically according to molecular size at a constant voltage of 90 V. For UV-light detection, the agarose gel was stained in 0.3‰ ethidium bromide solution for 10 min and analyzed using a gel documentation system.

2.2.2.3 DNA purification

PCR products were purified via the Qiagen gel extraction kit. After amplification, the DNA was mixed with 300 µL of QG buffer, pipetted into the provided spin column and centrifuged for 1 min at 15,700 x *g* to bind the DNA to the column. Afterwards, the flow-through was discarded and 750 µL of PE buffer were added on the filter for DNA purification. After centrifugation (1 min, 15,700 × *g*), the flow-through was again discarded and after an additional centrifugation step the DNA was eluted with 30 µL of sterile $H_2O_{dest.}$ (1 min, 15,700 × *g*). DNA was stored at -20°C until use.

2.2.2.4 Restriction digestion

For insertion into pETM11, NcoI and EcoRI restriction site sequences were added on the 3` (NcoI) and 5` (EcoRI) end of the AUM sequence via amplification primers (specified in 2.1.11 and 2.2.2.1). To insert the AUM^{WT} or AUM^{D34N} sequence into pcDNA3, HindIII (3` position) and EcoRI (5` position) restriction sites were used (specified in 2.1.11 and 2.2.2.1). For enzymatic digestion of the plasmid and the PCR product, DNA was incubated with both restriction enzymes for 2 h at 37°C. The digestion reaction mixture consisted of 5 µL 10x EcoRI buffer, 20 U of each restriction enzyme, the purified PCR product or 1 µg plasmid, and was adjusted to a final volume of 50 µL by adding $H_2O_{dest.}$. A single digest was performed as a positive control: 0.5 µg of plasmid were incubated with 10 U EcoRI or NcoI, 2.5 µL 10x EcoRI buffer, $H_2O_{dest.}$ to a total volume of 25 µL. The efficiency of digestion was checked by agarose gel electrophoresis.

2.2.2.5 DNA gel extraction

After agarose gel electrophoresis, DNA extraction was performed by using the Qiagen gel extraction kit. The piece of interest was cut out of the agarose gel and melted with 750 µL of QG buffer at 50°C. For improving the isolation of large DNA fragments, 100 µL of isopropanol was added after melting. Samples were applied on a spin column and centrifuged for 1 min at 15,700 × *g*. The flow-through was discarded and 750 µL of PE buffer was added followed by centrifugation under the same conditions. The flow-through was discarded and DNA was eluted with 30 µL of sterile $H_2O_{dest.}$ (1 min, 15,700 × *g*).

2.2.2.6 Ligation

The purified restriction products were ligated using the T4 ligase and the appropriate T4 ligation buffer. The DNA concentration of the linearized plasmid and the digested insert were measured using a Nanodrop spectrophotometer (A_{260nm}). The following formula was used to calculate the required amount of insert to obtain a molar ratio of plasmid DNA to insert DNA of 1:5: [5 × (100 ng plasmid × 1 kb insert / 6 kb plasmid)]. Ten µL 2× T4 DNA ligation buffer and 1 µLT4 DNA ligase were added, and the ligation reaction mixture was adjusted to a total volume of 20 µL by adding $H_2O_{dest.}$. The ligation was carried out overnight at 16°C.

2.2.2.7 Transformation of competent *E. coli*

For transformation, 5-10 ng plasmid DNA was added to 50 µL of chemically competent *E. coli* DH5α or BL21 (pGTF-2) cells, followed by incubation on ice for 20 min. After heat shock (1 min, 42°C) and subsequent incubation on ice for 20 min, 1 mL SOC-medium was added. Cells were then incubated for 45 min at 37°C in a shaker at 650 rpm. Afterwards,

cells were centrifuged (2 min, 2,700 × *g*), resuspended in approximately 100 µL of supernatant, and plated on LB agar plates containing appropriate antibiotics. After overnight incubation at 37°C, antibiotic-resistant colonies were either inoculated for a small-scale plasmid preparation, or used for a preculture prior to protein expression.

2.2.2.8 Small-scale plasmid preparation

To screen *E. coli* DH5α colonies for successful mutagenesis, plasmid preparations were performed. Five mL of LB medium containing 50 µg/mL kanamycin for pETM11 constructs or 50 µg/mL ampicillin for pcDNA3 constructs were inoculated with a single bacterial colony and incubated overnight at 37°C under constant agitation. Two mL of culture were pelleted (2 min, 2,700 × *g*) and resuspended in 200 µL P1 buffer. After adding 200 µL of P2 buffer and 200 µL of P3 buffer, each sample was mixed by repeatedly inverting the tubes, followed by centrifugation (15 min, 25,200 × *g*, 4°C). The supernatant was transferred to a new tube, and 1 mL of 100% ethanol was added to precipitate the DNA. After centrifugation (30 min, 25,200 × *g*, 4°C), the supernatant was removed, and the pellet was resuspended in 400 µL of 70% ethanol and centrifuged again (30 min, 25,200 × *g*, 4°C). The supernatant was discarded, the DNA was air-dried at room temperature, and subsequently resuspended in 30 µL sterile $H_2O_{dest.}$ Plasmid DNA was further analyzed by agarose gel electrophoresis and sequencing. Plasmid DNA was stored at -20°C.

2.2.2.9 Large-scale plasmid preparation

For isolating high amounts of plasmid DNA out of *E. coli* DH5α, the Qiagen Plasmid Plus Midi Kit was used according to the manufacturer's instructions. Buffers and materials are named as described in the manufacturer`s manual. One hundred mL of LB medium containing 50 µg/mL kanamycin or 50 µg/mL ampicillin (regarding the used vector) were inoculated with a single bacterial colony and incubated overnight at 37°C under constant agitation. Fifty mL of the bacterial culture were pelleted by centrifugation (15 min, 2,500 × *g*, 4°C) and resuspended in 4 mL of P1 buffer. Four mL of P2 buffer were added, gently mixed by inverting the tube, and incubated at room temperature for 3 min. Four mL of S3 buffer were added, and the lysate was mixed immediately by inverting the tube 4-6 times. The lysate was transferred to the Qiafilter cartridge, incubated at room temperature for 10 min, and filtered into a 50 mL tube. To clear the lysate, 2 mL buffer BB were added and mixed by inversion 4-6 times. Cleared lysate was transferred to a Qiagen Plasmid Plus Midi spin column with a tube extender and attached to a vacuum source to draw the solution through the column. To wash column-bound DNA, 700 µL buffer ETR was added and drawn through the column. As a second washing step, 700 µL PE buffer was added, and the liquid was completely removed. To elute the purified DNA from the column, 200 µL sterile $H_2O_{dest.}$ was added and

the spin column was placed into a 1.5 mL microcentrifuge tube. After 1 min of incubation, samples were centrifuged for 1 min at 10,000 × *g*. Plasmid DNA was stored at -20°C.

2.2.3 Protein expression and purification

2.2.3.1 Expression and purification of AUM and AUM variants

For recombinant protein expression, pETM11 constructs encoding for His_6-tagged AUM^{WT} and AUM variants were transformed into *E. coli* BL21 (DE3) (pG-Tf2). LB medium was supplemented with 20 µg/mL chloramphenicol and 50 µg/mL kanamycin. To increase protein solubility, 1 ng/mL tetracycline was added to express the chaperones groES, groEL and trigger factor, encoded by pG-Tf2. After induction with 0.5 mM isopropyl β-D-1-thiogalactopyranoside (IPTG), expression was performed for 20 h at 28°C. Cells were harvested by centrifugation (8,000 × *g*, 10 min) and resuspended in TMN LOW buffer supplemented with complete EDTA-free protease inhibitor cocktail tablets (1 tablet/50 mL buffer). Cells were lysed in the presence of 150 U/mL DNase I using a cell disruptor, and cell debris was removed by centrifugation (10,000 × *g*, 30 min, 4°C). For the purification of recombinant AUM, cleared bacterial lysates were loaded onto a Ni-NTA agarose column (His Trap HP, 5 mL bed volume) coupled to an ÄKTApurifier FPLC system, operated with a flow rate of 5 mL/min. After the washout/removal of unbound proteins, the sample was eluted using a linear 10-400 mM imidazole gradient (up to 100% TMN HIGH). Peak fractions were tested for phosphatase activity using *p*NPP as a substrate (2.2.6). Active fractions were pooled and concentrated to a volume of 10 mL. The sample was then subjected to tobacco etch virus (TEV) protease cleavage (0.5%) in a dialysis cassette (10 kDa excision size) towards TMN (4°C, 4 days) to avoid the inhibition of the protease by imidazole. Subsequently, cleaved AUM was separated from uncleaved AUM and from the His-tagged TEV protease on a HisTrap HP column. The untagged AUM was recovered in the column flow through. Active fractions containing untagged AUM were pooled, concentrated (10 kDa molcular weight cut-off) and applied to a Superdex size exclusion chromatography column (Superdex 200 Hiload 16/60 or Superdex 75 10/300 GL, depending on the sample volume), and eluted with TMN buffer. All purification steps were carried out at 4°C. All buffers that were applied to the ÄKTA system were filtered and degassed before use. Purified proteins were subjected to SDS-PAGE and stained with Coomassie Blue to monitor enzyme purity.

2.2.3.2 Expression and purification of chronophin and CAC

Chronophin and the CAC hybrid were expressed and purified by G. Knobloch as described above for AUM with the following modifications: His_6-tagged enzymes were expressed for 18 h at 20°C after induction with IPTG. After centrifugation, cells were resuspended in TMN "LOW-chronophin" buffer and lysed using a cell disruptor in the presence of protease

inhibitors and DNase I. Cleared supernatants were loaded on a HisTrap HP column equilibrated with TMN “LOW-chronophin” buffer, and His_6-tagged proteins were eluted using a linear gradient of up to 50% TMN “HIGH-chronophin” buffer. The fractions containing His_6-chronophin were pooled, the His_6-tag was cleaved with TEV protease, and untagged chronophin was isolated using a HisTrap HP column and further purified on a HiLoad 16/60 Superdex 200 pg size exclusion chromatography column in TMN “chronophin”.

2.2.4 Protein analytics

2.2.4.1 Sodium dodecyl sulfate polyacrylamide gel electrophoresis

Sodium dodecyl sulfate polyacrylamide gel electrophoresis (SDS-PAGE) was performed to separate proteins according to their molecular mass. First, proteins were denatured by boiling in SDS-PAGE sample buffer for 10 min. AUM, chronophin and their respective variants were run on 12% SDS-PAGE gels (Laemmli, 1970). Electrophoresis was carried out in running buffer. Proteins were concentrated in the stacking gel at a constant voltage of 80 V. Proteins were separated at a constant voltage of 150 V in the running gel according to their molecular mass. To visualize and monitor the purity of recombinant, purified proteins, SDS-PAGE gels were stained with Coomassie Blue staining solution for 20 min. Afterwards, the gels were destained with Coomassie Blue destaining solution until the gel background was clear. Gels were scanned for documentation.

2.2.4.2 Western Blot analysis

Western blot analysis was performed for protein detection in whole cell- or tissue lysates. After separation of the proteins contained in the lysates by SDS-PAGE, proteins were transferred onto nitrocellulose membranes via semi-dry transfer. To this end, a nitrocellulose membrane was first soaked in $H_2O_{dest.}$. For the bottom part of the blotting sandwich, two sheets of Whatman paper were submerged in anode buffer I and one sheet was submerged in anode buffer II. The nitrocellulose membrane was immersed in anode buffer II and added to the Whatman paper sheets, followed by the SDS-PAGE gel rinsed in cathode buffer. Three sheets of Whatman paper equilibrated in cathode buffer were placed on top of this sandwich. Proteins were blotted at a constant electric current of 70 mA per sandwich for 40 min. After blotting, the nitrocellulose membranes were stained with Ponceau S to monitor protein transfer. Membranes were scanned for documentation. The membranes were subsequently blocked with blocking buffer (15 min, constant agitation) to avoid unspecific binding of the antibodies. After rinsing with $H_2O_{dest.}$, the blots were incubated with primary antibodies. Commercial antibodies were diluted according to the manufacturer’s instructions. In general, antibodies were diluted 1:1000 in antibody diluent and incubated with the membrane overnight at 4°C under constant agitation. Afterwards, the membrane was rinsed

with $H_2O_{dest.}$, followed by an incubation (1h, RT, constant agitation) with horseradish peroxidase (HRP)-labelled secondary antibodies (diluted 1:10,000 in blocking buffer). The blot was developed using Super Signal West Pico Stable Peroxide Solution and Luminol/Enhancer Solution mixed in a ratio of 1:1 for 3 to 5 min. The signals were detected using ImageQuant LAS 4010 Digital Imaging System. Bands were densitometrically analyzed with ImageJ.

2.2.4.3 Analytical size exclusion chromatography

To define the oligomeric state of AUM in solution, analytical size exclusion chromatography was performed using a HiLoad 16/60 Superdex 200 pg column. The column was equilibrated with TMN and then calibrated with the Gel Filtration LMW Calibration Kit containing ferritin (440 kDa), aldolase (158 kDa), conalbumin (75 kDa), ovalbumin (43 kDa), carboanhydrase (29 kDa), ribonuclease A (13.7 kDa) and aprotinin (6.5 kDa). Blue dextran (2000 kDa) was used to determine the void volume of the column. After calibration, purified AUM^{WT} (1 mg) was loaded onto the column. Proteins were eluted isocratically with TMN buffer. Protein elution volumes were determined by monitoring the absorption at 280 nm. The partition coefficient (K_{av}) was calculated with the equation $K_{av} = (V_e-V_o)/(V_t-V_o)$, where V_e is the elution volume, V_o the void volume and V_t the total column volume. The apparent molecular weight was then derived from the inverse logarithm of the partition coefficient.

2.2.4.4 Analytical ultracentrifugation

Sedimentation velocity analytical ultracentrifugation was carried out using a Beckman Optima XL I analytical ultracentrifuge (Beckman Coulter) with an eight hole An-50 Ti rotor at 40,000 rpm and 20°C. Four hundred µL of highly purified, recombinant murine AUM, murine chronophin or reference buffer solution were loaded in standard double-sector charcoal-filled Epon centerpieces equipped with sapphire windows. Protein concentrations corresponded to an OD_{280} of 0.25-0.8. Data were collected in continuous mode at a step-size of 0.003 cm, using absorption optical detection at a wavelength of 280 nm. Data were analyzed using the NIH software SEDFIT to determine continuous distributions for solutions c(s) to the Lamm equation. Analysis was performed with regularization at confidence levels of 0.68 and floating frictional ratio (f/fo ~1.22 ± 0.04 for AUM and f/fo ~1.32 ± 0.02 for chronophin, suggesting a globular conformation for both enzymes), time-independent noise, baseline, and meniscus position, to root mean square deviation (RMSD) values <0.0064 for AUM and <0.012 for chronophin. Consistent results were obtained in three independent experiments. Analytical size exclusion experiments were supervised by Ingrid Tessmer (Rudolf-Virchow-Center). Christian Kestler analyzed the sedimentation velocities of chronophin.

2.2.4.5 Circular dichroism spectroscopy

In order to monitor the effect of reducing and oxidizing agents on protein folding and to estimate structural similarities or differences between AUM and chronophin, circular dichroism (CD) spectroscopy was performed. CD measurements in the far UV range (190-260 nm) provide quantitative secondary structure assessments of peptides and proteins. With this method, an estimation of the α-helical and β-sheet content or the random coil conformation of a protein can be obtained. All buffer substances interfering with CD spectroscopy were removed by overnight dialysis at 4°C against phosphate buffer (PB) or TMN for CD spectroscopy using Slide-A-Lyzer 10K dialysis cassettes. After dialysis, the protein samples were diluted to a protein concentration of 0.2 mg/mL and transferred to Quartz SUPRASIL 110-QS9 precision cells for measurements. The determination of CD spectra was performed on a Jasco J-810-150S spectropolarimeter, purged with nitrogen and with the sample cell set to a temperature of ~20°C. For scans, the following parameters were used:

band width:	2 nm	scanning speed:	20 nm/min
response:	1 sec	accumulation:	5
sensitivity:	Standard	cell length:	0.1 cm
data pitch:	1 nm	emperature:	19.98 °C

measurement range: 260-194 nm (terminated as soon as the voltage needed for a sufficient signal exceeded 600V)

2.2.4.6 Phospholipid overlay assay

Hydrophobic membranes spotted with 15 different biologically active lipids (lysophosphatidic acid (LPA), lysophosphocholine (LPC), phosphatidylinositol (PtdIns), phosphatidylinositol (3) phosphate (PtdIns(3)P), phosphatidylinositol (4) phosphate (PtdIns(4)P), phosphatidylinositol (5) phosphate (PtdIns(5)P), phosphatidylethanolamine (PE), phosphatidylcholine (PC), sphingosine 1-phosphate (S1P), phosphatidylinositol (3,4) bisphosphate ($PtdIns(3,4)P_2$), phosphatidylinositol (3,5) bisphosphate ($PtdIns(3,5)P_2$), phosphatidylinositol (4,5) bisphosphate ($PtdIns(4,5)P_2$), phosphatidylinositol (3,4,5) trisphosphate ($PtdIns(3,4,5)P_3$), phosphatidic acid (PA), phosphatidylserine (PS); catalog #P-6001, listed as PIP Strips) were blocked in blocking buffer for 1 h at room temperature. Purified murine AUM^{WT} and AUM^{D34N} were diluted in PIP-Strip dilution buffer to a final concentration of 20 µg/mL. The blocked membranes were incubated with the AUM variants or MultiPIP GripTM (recombinant GST-tagged LL5α-PH, #G-9901) for 1 h at room temperature. After rinsing with $H_2O_{dest.}$, the membranes were probed for associated proteins with α-AUM or α-GST antibodies (Sigma).

2.2.5 Protein crystallization and data collection

Vapor diffusion is the most common method for protein crystallization, and was used in the various AUM or AUM variant crystallization screens. The protein solution was mixed at a 1:1 ratio in the crystallization drop with the precipitant from the reservoir solution. In a closed system, different concentrations of solutes in the crystallization drop and in the buffer reservoir start to equilibrate by vapor diffusion. H_2O and other volatile compounds diffuse out of the drop into the reservoir. The volume of the crystallization drop thus decreases, while the protein as well as the precipitant concentrations in the crystallization drop increase. The H_2O absorption of the reservoir finally leads to supersaturation of the crystallization drop enabling protein nucleation and potential crystal growth. Two different experimental setups for vapor diffusion are established: In the hanging drop experiment, the crystallization drop is hanging from a cover slide, which also closes the reservoir, whereas in the sitting drop experiment the crystallization drop is placed on a shelf above the reservoir. To crystallize AUM and variants, sitting drop experiments were performed in 96-well crystallization plates. After purification of the protein, the samples were dialyzed towards the desired crystallization buffer. The protein samples were highly concentrated to reach the supersaturated state, and initial screening was performed at protein concentrations of 10 mg/mL. Depending on the proportion of buffer conditions yielding protein precipitates as opposed to clear drops (indicating no protein precipitates) in the first screens, the protein concentration was either reduced or increased for subsequent screens. For AUM in TMN buffer, protein concentrations of ~ 10-15 mg/mL were suitable. Samples were centrifuged (30 min, 16,100 × *g*, 4°C) to remove aggregates. For co-crystallization experiments, the protein was pre-incubated for 1 h with the additives. The standard screen was pipetted with the HoneyBee crystallization robot using 40 µL of reservoir solution and crystallization drops consisting of 0.3 µL reservoir and 0.3 µL protein solution. Proteins were screened with different commercially available crystallization screens (2.1.1). The screens were closed with an adhesive sealing foil by the sealing robot RoboSeal. The screens were incubated at 20 °C and evaluated after several time points at the Stemi 2000-C (Zeiss) Microscope. The following table summarizes the various AUM proteins and crystallization conditions that have been tested.

Table 2: Tested crystallization conditions

Protein	Concentration (mg/mL)	Crystallization buffer	Additives/ modifications
AUM^{WT} (murine)	17, 15, 14, 12, 10	50 mM TEA, 200 mM NaCl, 1 mM $MgCl_2$, pH 7.5	
AUM^{WT} (murine)	17, 15, 14, 12, 10	50 mM NaH_2PO_4, 200 mM NaCl, 1 mM $MgCl_2$, pH 7.5	
	12	10 mM TEA, 30 mM NaCl, 1 mM $MgCl_2$, pH 7.5	
		10 mM TEA, 100 mM NaCl, 1 mM $MgCl_2$, pH 7.5	
		10 mM NaH_2PO_4, 30 mM NaCl, pH 7.5	
		10 mM TEA, 30 mM NaCl pH 7.5	
		10 mM TEA, 150 mM NaCl pH 7.5	
		10 mM NaH_2PO_4, 100 mM NaCl, 1 mM $MgCl_2$, pH 7.5	
		10 mM NaH_2PO_4, 100 mM NaCl, pH 7.5	
		10 mM TEA, 100 mM NaCl, 1 mM $MgCl_2$, pH 7.5	drop size 1 µL
		10 mM TEA, 100 mM NaCl, 1 mM $MgCl_2$, pH 7.5	4°C
His_6-AUM^{WT} (murine)		10 mM TEA, 100 mM NaCl, 1 mM $MgCl_2$, pH 7.5	
AUM^{WT} (bovine)	20	10 mM TEA, 100 mM NaCl, 1 mM $MgCl_2$, pH 7.5	
	12	10 mM TEA, 100 mM NaCl, 1 mM $MgCl_2$, pH 7.5	
	20	10 mM NaH_2PO_4, 100 mM NaCl, 1 mM $MgCl_2$, pH 7.5	
	12	10 mM NaH_2PO_4, 100 mM NaCl, 1mM $MgCl_2$,	

		pH 7.5	
AUM^{WT} (human)		10 mM TEA, 100 mM NaCl, 1 mM $MgCl_2$, pH 7.5	
		10 mM NaH_2PO_4, 100 mM NaCl, 1 mM $MgCl_2$, pH 7.5	
$AUM^{\Delta 10}$ (murine)		10 mM TEA, 100 mM NaCl, 1 mM $MgCl_2$, pH 7.5	
AUM^{WT} (murine)		10 mM TEA, 100 mM NaCl, 1 mM $MgCl_2$, pH 7.5	1 mM $BeCl_2$, 10 mM NaF
		10 mM TEA, 100 mM NaCl, 1 mM $MgCl_2$, pH 7.5	25 mM $BeCl_2$, 250 mM NaF
		10 mM TEA, 100 mM NaCl, 1 mM $MgCl_2$, pH 7.5	50 mM $BeCl_2$, 250 mM NaF
		10 mM TEA, 100 mM NaCl, 1 mM $MgCl_2$, pH 7.5	100 mM Na_3VO_4
		10 mM TEA, 100 mM NaCl, 1 mM $MgCl_2$, pH 7.5	10 mM Na_3VO_4
		10 mM TEA, 100 mM NaCl, 1 mM $MgCl_2$, pH 7.5	2.5 mM ATP-γ-S
		10 mM TEA, 100 mM NaCl, 1 mM $MgCl_2$, pH 7.5	2.5 mM AMP-PNP
AUM^{D34N} (murine)		10 mM TEA, 100 mM NaCl, 1 mM $MgCl_2$, pH 7.5	*p*-NPP (3.5; 7; 10 mM)
		10 mM TEA, 100 mM NaCl, 1 mM $MgCl_2$, pH 7.5	2.5 mM ADP
		10 mM TEA, 100 mM NaCl, 1 mM $MgCl_2$, pH 7.5	
		10 mM NaH_2PO_4, 100 mM NaCl, 1mM $MgCl_2$, pH 7.5	
$AUML^{204H}$ (murine)		10 mM TEA, 100 mM NaCl, 1 mM $MgCl_2$, pH 7.5	
		10 mM TEA,	6 mM PLP

		100 mM NaCl, 1 mM $MgCl_2$, pH 7.5	
		10 mM HEPES, 150 mM NaCl, 10 mM methionine, 10% glycerol, 5 mM DTT	6 mM PLP
		10 mM HEPES, 150 mM NaCl, 10 mM methionine, 10% glycerol, 5 mM DTT	
		10 mM NaH_2PO_4, 100 mM NaCl, 1mM $MgCl_2$, pH 7.5	
AUML$^{204H; D34N}$ (murine)		10 mM TEA, 100 mM NaCl, 1 mM $MgCl_2$, pH 7.5	6 mM PLP
		10 mM TEA, 100 mM NaCl, 1 mM $MgCl_2$, pH 7.5	
		10 mM HEPES, 150 mM NaCl, 10 mM methionine, 10% glycerol, 5 mM DTT	6 mM PLP
		10 mM HEPES, 150 mM NaCl, 10 mM methionine, 10% glycerol, 5 mM DTT	
		10 mM NaH_2PO_4, 100 mM NaCl, 1mM $MgCl_2$, pH 7.5	
		10 mM TEA, 100 mM NaCl, 1 mM $MgCl_2$, pH 7.5	trypsin (1 mg/mL; 0.5 mg/mL; 0.05 mg/mL)
ACA (murine)	9	10 mM TEA, 100 mM NaCl, 1 mM $MgCl_2$, pH 7.5	
CAC (murine)	10	10 mM TEA, 100 mM NaCl, 1 mM $MgCl_2$, pH 7.4	15% PEG 3350 + 0.2 M $Mg(NO_3^-)_2$

Crystals of the chronophin$^{1-100}$-AUM$^{114-233}$-chronophin$^{208-291}$ (CAC) hybrid were grown at 20°C in 15% PEG 3350 and 0.2 M $Mg(NO_3^-)_2$ using the sitting-drop vapor diffusion method, by mixing 0.6 µL protein solution with 0.4 µL reservoir solution. CAC crystals appeared as thin plates with dimensions of 0.25 × 0.5 × 0.05 mm after 2-3 days, and the majority of crystals displayed very high mosaicity. Crystals were cryoprotected for flash-cooling in liquid nitrogen by soaking in mother liquor containing 30% (v/v) glycerol. Diffraction data were collected on

an R-axis HTC imagine plate detector mounted on a Micromax HF-007 rotating anode X-ray generator. Data were processed using iMosflm and scaled with Scala from the CCP4 program suite. The structure was solved by molecular replacement with the program Phaser with human pyridoxal 5'-phosphatase (PDB entry 2OYC) as a search model. The structure was refined at 2.5 Å resolution with Phenix, incorporating torsion angle NCS restraints. Data collection and refinement statistics are summarized in Table 3. The X-ray crystal structure of the murine CAC protein has been deposited in the Protein Data Bank under accession code 4BKM. The figures of the chronophin and CAC structures were generated with PyMOL. Topology diagrams were generated with the pro origami system using PDB files 2P69 and 4BKM. Dimer interface calculations were performed with the PISA online tool. G. Knobloch crystallized the CAC hybrid, and Prof. Hermann Schindelin and G. Knobloch (Rudolf-Virchow-Center) performed data collection and -processing.

Table 3: Data collection and refinement statistics

Data collection	
Wavelength (Å)	1.5418
Space group	P 2_1
Unit cell parameters	
a, b, c (Å)	67.50, 91.96, 105.92
α, β, γ (°)	90, 90.2, 90
Resolution range (Å) [a]	41.74 - 2.65 (2.79 - 2.65)
R_{sym} [b]	0.125 (0.816)
$R_{p.i.m.}$ [c]	0.070 (0.456)
$\langle I / \sigma I \rangle$ [d]	6.6 (1.4)
Completeness (%)	96.2 (94.9)
Multiplicity	4.1 (4.1)
Total reflections	150275
Unique reflections	36203 (3531)
Refinement	
Wilson B-factor (Å²)	50.0
Average B-factor (Å²)	86.9
Macromolecules	87.4
solvent	64.0
R_{cryst} [e]	0.1976 (0.2878)
R_{free} [e]	0.2564 (0.3290)
Number of non H-atoms	9450
Macromolecules	9236
Ligands	12
Water	202
R.m.s. deviations in	
bond lengths (Å)	0.004
bonds angles (°)	0.83
planar groups (Å)	0.004
dihedral angles (°)	13.54
Coordinate error (Å) [f]	0.36
Ramachandran statistics [g]	
favored (%)	97.68
allowed (%)	2.07
outliers (%)	0.25
MolProbity clashscore [h]	12.17

[a] Numbers in parentheses refer to the respective highest resolution data shell in the data set.

[b] $R_{sym} = \Sigma_{hkl}\Sigma_i|I_i - \langle I \rangle| / \Sigma_{hkl}\Sigma_i I_i$, where I_i is the i^{th} measurement, and $\langle I \rangle$ is the weighted mean of all measurements of I.

[c] $R_{p.i.m.} = \Sigma_{hkl} (1/(n-1))^{1/2} \Sigma_i|I_i - \langle I \rangle| / \Sigma_{hkl}\Sigma_i I_i$, where n is the multiplicity of the observed reflection.

[d] $\langle I / \sigma I \rangle$: Indicates the average of the intensity divided by its S.D. value.

[e] $R_{cryst} = \Sigma|F_o - F_c| / \Sigma|F_o|$ where F_o and F_c are the observed and calculated structure factor amplitudes. R_{free}, same as R_{cryst} for 5% of the data randomly omitted from the refinement.

[f] Estimated coordinate error based on R_{free}.

[g] Ramachandran statistics indicate the fraction of residues in the favored, allowed and disallowed regions of the Ramachandran diagram, as defined by MolProbity (Chen *et al.*, 2010).

[h] number of serious clashes per 1000 atoms (Chen *et al.,* 2010).

2.2.6 Phosphatase activity assays

2.2.6.1 *In vitro p*NPP assay

For assays using *para*-nitrophenylphosphate (*p*NPP) as a substrate, 0.8 µg of the purified protein was pre-incubated for 30 min at 37°C in TMN, in the presence or absence of additives or their respective solvent controls. The reaction was started by the addition of *p*NPP (final concentration ranging from 0.5-9 mM in a total assay volume of 100 µL, and 3.5 mM for single point assays). The kinetics of *para*-nitrophenol (*p*NP) generation were followed spectrophotometrically by measuring the absorbance at 405 nm every 30 sec on a microplate reader. *p*NP generation was quantitated using *p*NP standard curves. To derive K_M and k_{cat} values, the data were fit by nonlinear regression to the Michaelis-Menten equation using GraphPad Prism, version 4.01.

Inhibitors

To test the effect of diverse phosphatase inhibitors on AUM activity, the enzyme was preincubated for 30 min at 37°C with the inhibitor or solvent control in TMN buffer. To study the effect of NaF or of BeF_3^- on phosphatase activity, AUM was preincubated with 1 mM NaF or with 1 mM NaF + 0.1 mM $BeCl_2$ (BeF_3^-). To assess the effect of okadaic acid and calyculin A, inhibitor concentrations of 0-1000 nM were tested with DMSO as a control. Na_3VO_4 (dissolved in TMN) was tested at concentrations ranging from 0-1000 µM. The tested inhibitors were also added to the buffer controls in the absence of enzyme to exclude possible effects on *p*NPP.

Reducing and oxidizing agents

To test the effect of DTT, TCEP, β-MEOH and H_2O_2 on AUM activity, the enzyme was preincubated for 30 min at 37°C with the reagent in closed tubes in order to avoid vapor diffusion. AUM activity was tested in the presence of 0-5 mM DTT, TCEP, β-MEOH or 0-25 mM H_2O_2. To calculate enzyme velocity the slope of the first 7.5 min of the reaction directly after the addition of *p*NPP was determined. To measure the re-activation of AUM activity after inhibition via H_2O_2, the enzyme was oxidized for 30 min at 37°C. After the addition of *p*NPP the pNP generation was quantified for 30 min. Then the measurement was stopped, the desired concentration of DTT (1-5 mM, according to the performed assay) was added using a multichannel pipet, and measurements were continued. Five minutes after adding DTT, the slope of *p*NP development over time was determined for 10 min to calculate enzyme velocity. DTT and H_2O_2 were also added to the buffer controls without enzyme to exclude an effect on *p*NPP.

2.2.6.2 *In vitro* malachite green assay

For a quantitative measurement of inorganic free phosphate after dephosphorylation of potential substrates, a malachite green assay was performed. AUM (0.16 µg of protein/well) was pre-incubated for 10 min at 22°C in TMN. The reactions were started by the addition of a substrate candidate, and stopped after 5.5 min by the addition of 100 µL malachite green solution. Released phosphate was determined by measuring A_{620} and extrapolating the values to a phosphate standard curve, and K_M and k_{cat} values were calculated using GraphPad Prism, version 4.01.

Pyridoxal 5'-phosphate (PLP)

PLP was used to verify the PLP-phosphatase activity of chronophin, and to test for a potential PLP activity of AUM and AUM variants. The enzyme was incubated with a final PLP concentration ranging from 0-1 mM in a total volume of 50 µL. The tested concentrations of PLP were also added to the buffer controls w/o enzyme to measure the amount of basal hydrolysis due to solvent, light and temperature.

Nucleotides

To test nucleotides (ADP, ATP, GDP, GTP) as potential substrates of recombinant AUM, nucleotides were tested at concentrations ranging from 0-3 mM. Nucleotides were also added to the buffer controls w/o enzyme to measure the amount of basal hydrolysis due to solvent, light and temperature.

Phospholipids

Recombinant, purified AUM (0.16 µg/well) was incubated at 37°C for 1h with 1.5 nM phospholipids [PtdIns(3,4)P_2 ; PtdIns(3,4,5)P_3; PtdIns(3,5)P_2; PtdIns(4)P] in an assay volume of 25 µL TBS supplemented with 10 mM DTT. Free inorganic phosphate was detected by incubation with 100 µL malachite green solution/well for 20 min at RT, and the absorbance of the resulting phosphomolybdate complex was measured at 620 nm. Recombinant, purified PTEN was used as a positive control. The tested concentrations of phospholipids and DTT were also added to the buffer controls without enzyme, to measure the amount of basal hydrolysis due external influences.

All phosphatase activity assays were conducted in 96-well microtiter plates. All *p*NPP and malachite green phosphatase assays were performed with three independently purified protein batches.

2.2.6.3 Fractionation based AUM phosphatase activity assay

Cell culture

To measure the phosphatase activity of endogenous AUM in cell lysates, GC1 spg and HEK AD-293 cells were used. The cell lines were cultured in Dulbecco's modified Eagle's medium (DMEM) containing 4.5 g/l glucose, supplemented with 10% FCS, 2 mM L-glutamine, 100 U/mL penicillin and 100 µg/mL streptomycin (and 1 µg/mL puromycin for GC1 spg AUM or control shRNA cells) at 7% CO_2 and 37°C in a standard cell culture incubator. Endogenous AUM was downregulated by RNA interference. To this end, AUM-directed or control shRNA was introduced by lentiviral transduction, and stable cell lines were generated by cell culture in the presence of puromycin to select for cells expressing control or AUM shRNA (yielding GC1 spg/ctrl. shRNA and GC1 spg/AUM shRNA lines; P. Duraphe, PhD thesis). For the re-expression of AUM^{WT} or AUM^{D34N}, RNA interference-insensitive human AUM^{WT} or human AUM^{D34N} were transfected in GC1 spg/AUM shRNA cells. As a control, ptdTomato-N1 was transfected in GC1 spg/ctrl. shRNA cells. GC1 spg cells were seeded at low density (approximately 200,000 cells) the day before transfection on a 10 cm dish. The next day, 1 µg plasmid DNA and 18 µL Lipofectamine 2000 were mixed separately with 1.5 mL OPTIMEM in polystyrene tubes. After a 5 min incubation, DNA and Lipofectamine 2000 solution were combined and incubated for another 20 min. Cells were washed (5 mL OPTIMEM) and 6 mL OPTIMEM and the Lipofectamine/OPTIMEM mix were added. Cells were incubated in a cell culture incubator for 4 hours. After that, the transfection medium was replaced with 10 mL of standard growth medium. Proper transfection efficiency was verified by visualizing the expression of the red fluorescent tomato protein in control cells by fluorescence microscopy 24 h after transfection. Cells were then trypsinized and counted in a Neubauer counting chamber. The desired number of cells was pelleted (3 min, 1,300 × *g*, RT) and resuspended in 750 µL ice cold TMN "FRACTIO". Afterwards, cells were lysed on ice by repeatedly drawing into a syringe (25G × 5/8 inch needle), and insoluble material was removed by centrifugation at 10,000 × *g* for 12 min at 4°C.

RNA interference

Cellular AUM expression was downregulated using a transient transfection of synthetic siRNA oligoribonucleotides into HEK AD-293 cells. The day before transfection, 5×10^4 cells/well were seeded (3 cm dish). Next day, 25 nM siRNA oligoribonucleotides (#5 or control siRNA) and 3 µL Lipofectamin 2000 reagent were mixed separately with 0.5 mL or 0.25 mL OPTIMEM in polystyrene tubes and were incubated for 5 min at room temperature. Afterwards siRNA and Lipofectamin 2000 solutions were mixed and incubated for 20 min at RT. In parallel, cells were washed once with 1 mL OPTIMEM and 500 µL OPTIMEM was added. As a next step, 500 µL of the siRNA mix was added, and the cells were incubated in a cell culture incubator for 4 h. After that, the transfection medium was replaced with 2 mL of

standard growth medium. Cells were trypsinized 72 h after transfection and counted in a Neubauer counting chamber. HEK AD-293/ctrl. siRNA and HEK AD-293/AUM siRNA (150.000 cells) were pelleted and resuspended in TMN "FRACTIO". Afterwards, cells were lysed on ice via shearing force by repeatedly drawing into a syringe (25G × 5/8 inch needle) and insoluble material was removed by centrifugation at 10,000 × *g* for 12 min at 4°C.

Platelet isolation

For platelet isolation, C57BL/6 AUM$^{D34N/D34N}$ and C57BL/6 AUM$^{D34N/D34N;\ Pf4\text{-}Cre}$ mice were bled from the retroorbital plexus under deep isoflurane anesthesia using 20 µL heparin capillary tubes (performed by the group of Prof. Nieswandt, RVZ). Approximately 600 µL of blood were collected into a tube containing 250 µL acid citrate dextrose (ACD). Blood was centrifuged at 1,800 rpm for 5 min at RT (no brake). The supernatant was transferred into a new tube and centrifuged at 800 rpm for 5 min at RT (no brake) to obtain platelet rich plasma. The supernatant was supplemented with 0.5 µM prostacyclin and again centrifuged at 2,800 rpm. To prepare washed platelets, the pellet was resuspended in 1 mL Tyrode's buffer containing 0.5 µM prostacyclin and 0.02 U/mL apyrase. After 5 min incubation at 37°C, the sample was centrifuged at 2,800 rpm for 5 min. After a second washing step, the platelet pellet was resuspended in 750 µL TMN „FRACTIO", and platelets were lysed by shear force by repeatedly drawing into a syringe (25G × 5/8 inch needle). All centrifugation steps were performed in the EBA 12 R Hettich centrifuge.

Fractionation of cell lysates

To perform the fractionation based activity assay, lysates were prepared as described above and separated by size exclusion chromatography. For this, an ÄKTApurifier FPLC system and a Superdex 200 10/300 GL column were used. The column was equilibrated with TMN "FRACTIO", and the cleared lysates (final volume, 0.75 mL), were injected with a 1 mL loop. Afterwards, proteins were eluted in TMN "FRACTIO" with a flow of 0.75 mL/min. The flow-through was collected in 1 mL fractions. Fractionation was carried out at 4°C. All buffers that were applied to the ÄKTA system were filtered and degased before use. This approach yielded 24 fractions that were analyzed for the presence of AUM by Western blot.

Activity assay

The fractionated lysates were tested for phosphatase activity towards *p*NPP. A volume of 100 µL of each of the obtained fractions was pipetted into a well of a 96-well microtiter platecontaining 3.5 mM *p*NPP and 2 µL of the *p*NPP-buffer. According to the performed assay, 0-5 mM of DTT was added and the plate was incubated for 30 min at 37°C. *p*NP generation was followed spectrophotometrically by measuring the absorbance at 405 nm every 30 sec on a microplate reader for 60 min. Appropriate buffer controls were included and used as a blank.

2.2.7 Antibody purification and characterization

2.2.7.1 Antibody purification

To generate a polyclonal antibody specific for full-length AUM, AUM^{D34N} was recombinantly expressed in *E. coli* and purified to homogeneity. Charles River Laboratories performed immunization of rabbits and serum extraction.

The antibody was purified from rabbit serum by affinity chromatography. To this end, recombinant AUM^{D34N} was immobilized on cyanogen bromide (CNBr)-activated sepharose to create an affinity matrix. The active groups cyanate esters and imidocarbonates of the CNBr-activated sepharose immobilize ligands containing primary amines. One gram of CNBr-activated sepharose was suspended in 100 mL 1 mM HCl. A first acidic washing step is recommended to remain the activated groups stable (Mannik and Stage, 1971). Afterwards the medium was washed with 25 mL H_2O and equilibrated with 15 mL binding buffer. Purified AUM^{D34N} (12 mg/1 g CNBr-activated sepharose) was suspended in 3 mL binding buffer and incubated with the sepharose at 4°C overnight under constant rotation. The loaded sepharose was washed with 15 mL binding buffer. To block remaining active groups of the matrix, an excess of small primary amines was added (1 M ethanolamine, pH 8.0) and incubated for 2 h at 4°C under constant rotation. After blocking, the sepharose was washed six times with 9 mL Tris buffer and with 9 mL acetate buffer in an alternating manner.

For a pre-purification of the antibodies, the rabbit serum was first centrifuged for 30 min, 3,000 × *g* at 4°C, and the resulting supernatant was subjected to a two-step ammonium sulfate precipitation. For this the ammonium sulfate was pulverized in a mortar and small amounts were added slowly over the course of hours to the serum. First, ammonium sulfate was added to 25% saturation (under stirring on ice for 10 hours) to deplete more insoluble, non-antibody proteins from the serum and to thus enrich for antibodies in the supernatant. After re-centrifugation, the obtained supernatant was subjected to an additional ammonium sulfate precipitation. Since immunoglobulines precipitate at 40-50% ammonium sulfate saturation, the serum was incubated with ammonium sulfate to yield 50% saturation (overnight at 4°C). The precipitate was pelleted for 30 min, 3,000 × *g*, at 4°C. The pellet (antibody fraction) was resuspended in 4 mL binding buffer and dialyzed towards 3 L of binding buffer overnight at 4°C. The sample was loaded for 72 h on the sepharose, for antibody binding (4°C, constant rotation). Afterwards the medium was washed with 500 mL washing buffer.

Sepharose-bound antibodies were then eluted in two consecutive elution steps. For an efficient elution of polyclonal antibodies, two different elution conditions were employed. Two types of elution were performed (1) high ionic strength (magnesium elution buffer), (2) low pH (glycine elution buffer). First, an elution under mild conditions was performed by

altering the ionic strength with 3 mL magnesium elution buffer. Second, the antibody was eluted with 4 mL glycine elution buffer. Each elution was performed twice and only the second elution pool was collected. Antibodies obtained with the second magnesium elution were directly collected in 7 mL collection buffer I. The eluate of the second glycine elution was collected in 500 µL collection buffer II. Both fractions were concentrated to a volume of 1 mL and dialyzed 3 times towards 1 L TBS.

2.2.7.2 Tissue and cell lysate preparation

The AUM-directed antibody was characterized by Western blot analysis of mouse tissues and of cell lysates. For this, an adult C57BL/6 male mouse was sacrificed by cervical dislocation, dissected, and the indicated tissues/organs were immediately snap-frozen and pulverized in liquid nitrogen. One hundred mg of the respective tissue powders were solubilized in 1 mL of tissue lysis buffer supplemented with phosphatase inhibitor cocktails I and II. Insoluble material was removed by centrifugation at 21,000 × *g* for 10 min at 4°C. All cell lines (2.1.6) were cultured in DMEM containing 4.5 g/L glucose supplemented with 10% FCS, 2 mM L-glutamine, 100 U/mL penicillin and 100 µg/mL streptomycin. Cell lysates were prepared in ice-cold RIPA buffer containing freshly added protease inhibitors (10 µg/mL aprotinin, 10 µg/mL leupeptin, 1 mM pepstatin, 1 mM Pefabloc), and insoluble material was removed by centrifugation at 21,000 × *g* for 10 min at 4°C. Protein concentrations were determined using the Micro BCA kit, according to the manufacturer`s instructions.

2.2.7.3 Immunoprecipitation

To validate the generated AUM antibody for immunoprecipitation of endogenously expressed protein, the GC1 spg cell line was used. Immunoprecipitation experiments were performed in RIPA buffer, lysis buffer for tissues and immunoprecipitation, or HIGH SALT/LOW SALT lysis buffer. For each condition, GC1 spg cells from three confluent 10 cm dishes were used. Cells were washed with Ca^{2+}/Mg^{2+}-free DPBS, and then lysed in 500 µL ice-cold lysis buffer, supplemented with freshly added protease inhibitors. The cells were scraped from the plate using a rubber policeman on ice and homogenized by repeatedly drawing into a syringe (25G × 5/8 inch needle). Cells were then lysed by incubating in the respective lysis buffers for 20 min at 4°C under constant agitation. Insoluble cell components were removed by centrifugation at 10,000 × *g* for 12 min at 4°C. The supernatant was supplemented with 5 µL of α-AUM magnesium eluate or α-AUM glycine eluate. For a beads control, antibody addition was omitted. The lysate/antibody mix was incubated for 2 h at 4°C under constant agitation. In parallel, protein A sepharose beads were equilibrated in the respective lysis buffer and blocked in 3% BSA for 1 h at 4°C. Afterwards, lysates with or without antibody were incubated in the presence of 20 µL beads for another 2 h at RT. After washing the beads

three times in the respective buffer, protein complexes were eluted from the beads by incubation in 30 µL boiling SDS-PAGE sample buffer for 5 min. The efficiency of immunoprecipitation was assessed by immunoblotting. The beads control eluate and lysates before and after immunoprecipitation were used as control.

3 Results

3.1 Biochemical characterization of AUM

To characterize the intrinsic phosphatase activity of AUM, several AUM wildtype and mutant proteins from various species were utilized for biochemical and structural characterization. In the first experiments the expression and purification of AUM and its variants was established. Further, the phosphatase activity of AUM was tested against diverse small molecular weight substrates and AUM phosphatase activity was profiled in the presence of phosphatase inhibitors.

3.1.1 Cloning and purification of AUM and AUM variants

For biochemical measurements and protein crystallography the purity and homogeneity of a protein is of great importance. The different AUM proteins were purified using the same protocol (2.2.3). As a first step, murine AUM was cloned into the pETM11 expression vector with an N-terminal hexahistidine tag in a T7-promotor-controlled region with a kanamycin resistance gene for selection. The protein production was induced via IPTG. Because of the insolubility of the protein, a co-transformation with pG-Tf2 was performed. The pG-Tf2 plasmid encodes for the *E. coli* chaperones groEL, groES and tig. The highest expression of AUM was achieved in an overnight expression at 28 °C, which was used for the following high scale expressions. Representative expression levels of AUM are shown in figure 9A after SDS-PAGE and Coomassie Brilliant Blue-staining of the gels. Overexpressed proteins are clearly visible as a thick band migrating slightly below the 37 kDa marker band. Murine AUM has a molecular mass of around 34.5 kDa, indicating that the appearing band most likely represents AUM fused to the hexahistidine tag. The expression of AUM after induction was also confirmed by immunoblot analysis (figure 9B). After the production of AUM in *E. coli* and cell lysis, the protein was purified to homogeneity. The expressed protein was isolated from the *E. coli* cell lysate by affinity chromatography utilizing its N-terminal hexahistidine tag and afterwards separated from contaminations and aggregated protein by size-exclusion chromatography (SEC). For the nickel affinity chromatography, a pre-packed HisTrap column connected to an ÄKTA chromatography system was used. Cleared cell lysate was loaded onto the equilibrated column and AUM was eluted from the column with a gradient of 10 to 400 mM imidazole (figure 9C). Protein samples from every step and the peak fractions were analyzed via SDS-PAGE (figure 9D). Elution fractions of high purity were used for the second step of purification. The hexahistidine tag was cleaved via TEV-protease, and removed by a second nickel affinity chromatography. The success of the cleavage was monitored by SDS-

PAGE (figure 9E). The flow-through, containing the cleaved sample, was subsequently applied to the size-exclusion column (HiLoad 16/60 Superdex 200 pg). The sample was eluted and the elution profile was composed of 2 characteristic peaks (figure 9F). Samples from each peak were analyzed on SDS-PAGE (figure 9G). The fractions of the peaks displayed high purity. They were pooled and concentrated (figure 9H). The described expression and purification protocol was also successful for the other AUM variants investigated in this thesis.

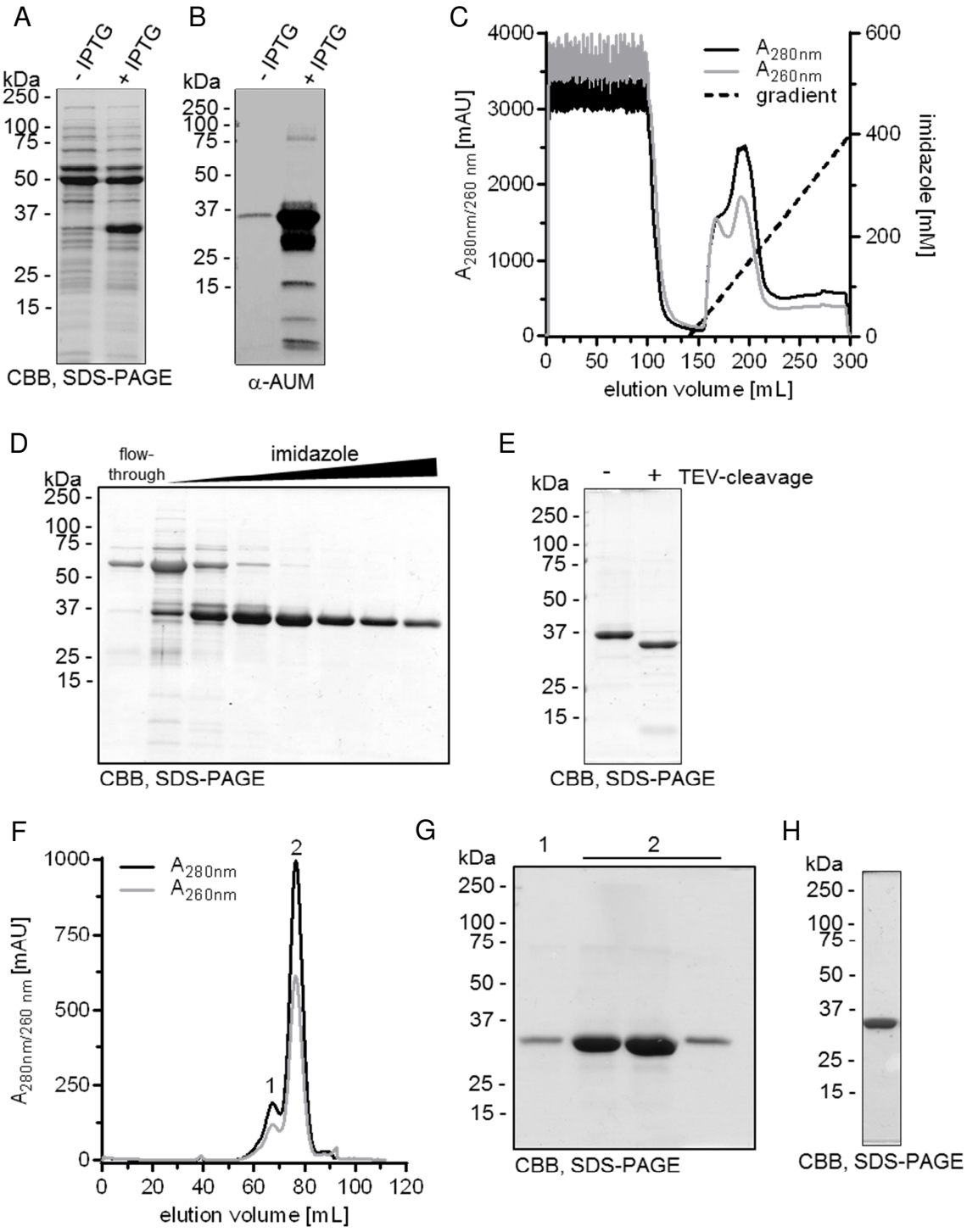

Figure 9: AUM expression and purification. (A) Coomassie Brilliant Blue (CBB) stained SDS-PAGE of *E. coli* BL21 (DE3) lysates transformed with pETM11_AUM and pg-Tf2 before and after the induction of protein expression with 500 µM of IPTG. **(B)** Immunoblot analysis of the recombinant expression of AUM before and after the induction with IPTG. **(C)** Chromatogram of a Ni-NTA affinity purification (HisTrap HP) with a linear imidazole gradient (dashed line), absorption at 280 nm (black) and 260 nm (gray) are shown **(D)** CBB-stained SDS-PAGE of HisTrap purification. Protein content of the flow-through fraction and elution fractions are shown. **(E)** CBB-stained SDS-PAGE of AUM before and after TEV-cleavage **(F)** Chromatogram of a size exclusion chromatography (HiLoad 16/60 Superdex 200 pg); the absorption at 280 nm is shown in black and at 260 nm in gray. **(G)** CBB-stained SDS-PAGE showing the elution fractions after size exclusion chromatography (peak 1 and 2 corresponding to the peaks labeled in (F)) **(H)** CBB-stained SDS-PAGE of AUM after completion of all purification steps.

To analyze the two appearing peaks in the size exclusion chromatogram, analytical size exclusion chromatography (SEC) was performed using a Superdex column (HiLoad 16/60 Superdex 200 pg), calibrated with globular proteins of known molecular weight (see 2.2.4.3). The oligomeric states of highly purified, untagged recombinant murine AUM were analyzed. Figure 10A shows that AUM (theoretical molecular mass, 34.5 kDa) has a peak elution volume that corresponds to a calculated molecular mass of 79.6 kDa (see peak 2, figure 9F), indicating that the protein forms a stable dimer in solution. AUM predominantly elutes as a dimer (80.6%); interestingly, 19.3% of AUM elute at a volume corresponding to a tetramer (see peak 1, figure 9F). The calculated molecular mass for the tetrameric form of AUM is 163.6 kDa (figure 10A). In addition, analytical ultracentrifugation (AUC) sedimentation velocity experiments were performed (2.2.4.4). The AUC analysis confirmed the existence of a dimeric (88.26%) and a tetrameric (11.74%) form of AUM. Chronophin, the closest AUM relative, has also been reported to elute as a dimer from size exclusion columns (Fonda, 1992; Jang *et al.*, 2003). Figure 10B shows an overlay of AUC analyses of AUM with chronophin. Only 2.25% of chronophin particles sediment in a tetrameric state, while the majority of chronophin particles (97.75%) form dimers. These data show that AUM exists in equilibrium between dimers and tetramers in solution, and has a greater propensity for tetramer formation than chronophin.

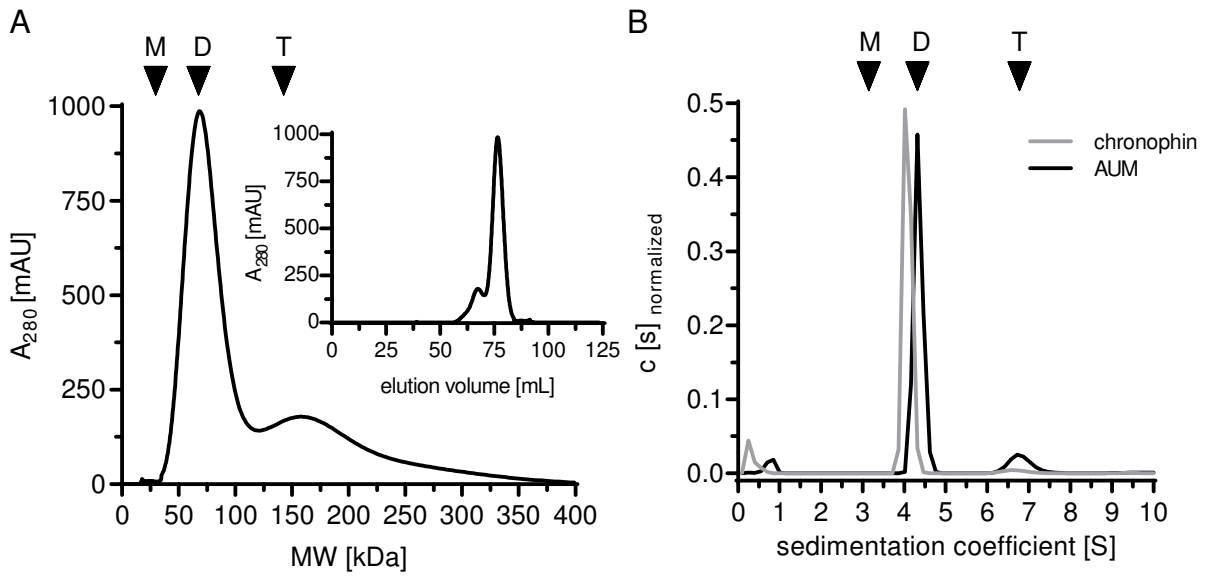

Figure 10: AUM exists as a stable dimer in solution, which can transiently form tetramers.
(A) Molecular weight profile of purified, untagged murine AUM on a size exclusion chromatography column (HiLoad 16/60 Superdex 200 pg). The inset shows the corresponding elution profile. AUM predominantly elutes as a homodimer, and a fraction of AUM exists in the tetrameric state. **(B)** Analytical ultracentrifugation sedimentation velocity experiments of purified AUM (black) and chronophin (gray). AUM exists in equilibrium between dimers and tetramers. (A, B), n = 3. Arrowheads indicate the expected/observed position of AUM monomers (M), dimers (D) and tetramers (T).

3.1.2 The phosphatase activity of AUM

To verify the intrinsic phosphatase activity of AUM, the enzyme kinetics of recombinant AUM against *para*-nitrophenyl phosphate (*p*NPP), a generic phosphatase substrate, were examined. To test whether AUM indeed functions as a phosphatase, the enzyme kinetics of bacterially expressed murine AUM against *p*NPP were determined. The pure enzyme (figure 9H) was used to determine the enzymatic properties of AUM in *in vitro* phosphatase assays (2.2.6.1). A pH/rate profile (figure 11D), as measured by *p*NPP hydrolysis, revealed that AUM has a pH optimum at pH 7.5 (with 7.56% or 47.74% of the maximal activity at pH 5 or pH 10, respectively); all subsequent phosphatase assays were therefore performed at this pH. Figure 11A shows, that AUM dephosphorylates *p*NPP with a K_M of 3.13 mM and a k_{cat} of 0.47 s^{-1} for the murine enzyme.

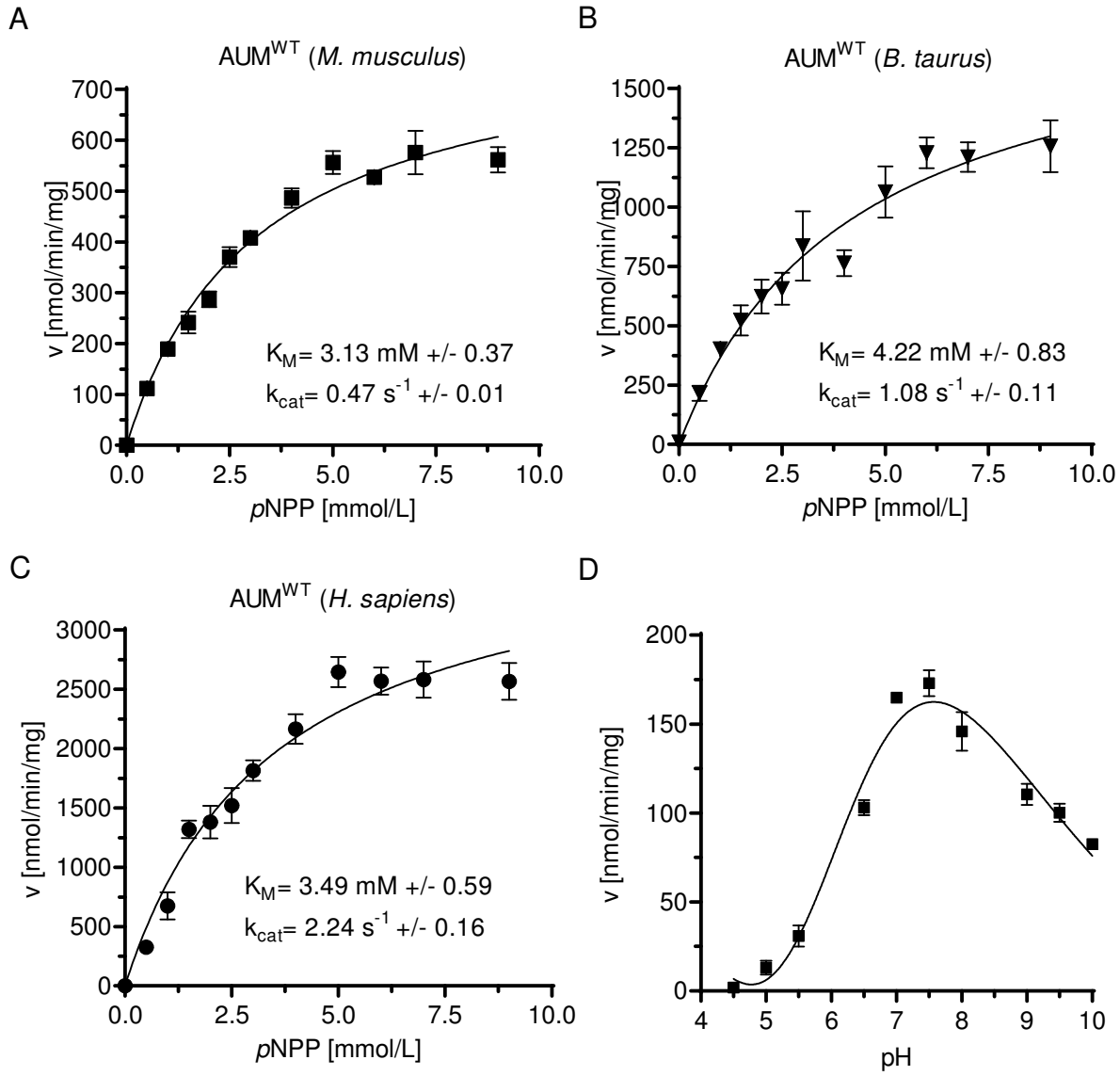

Figure 11: AUM orthologs from different mammalian species dephosphorylate *p*NPP at neutral pH. Steady-state kinetic measurements of the phosphatase activity of the murine **(A)**, the bovine **(B)** and the human AUM **(C)** towards *p*NPP. **(D)** pH/rate profile of *p*NPP dephosphorylation by murine AUM. Results are mean values ± SEM of three independent experiments performed in triplicates with three independently purified protein batches.

To verify that other mammalian AUM orthologs also have intrinsic phosphatase activity, two additional AUM species were tested. The AUM encoding sequences of *Homo sapiens* (*H. s.*; NCBI reference: NP_001035830.1) and of *Bos taurus* (*B. t.*; NCBI reference: NP_001033261.1) were cloned in pETM11, expressed and purified as described for the AUM protein of *Mus musculus* (2.2.3). The murine and human AUM share 91% identity, while the murine and bovine AUM share 90% identity on amino acid level. The human and bovine AUM share 91% identity on amino acid level. Steady-state enzyme kinetics of human and the bovine AUM were tested towards the substrate *p*NPP. Both enzymes show a K_M towards *p*NPP that is comparable to murine AUM than murine AUM, (figure 11B, C).

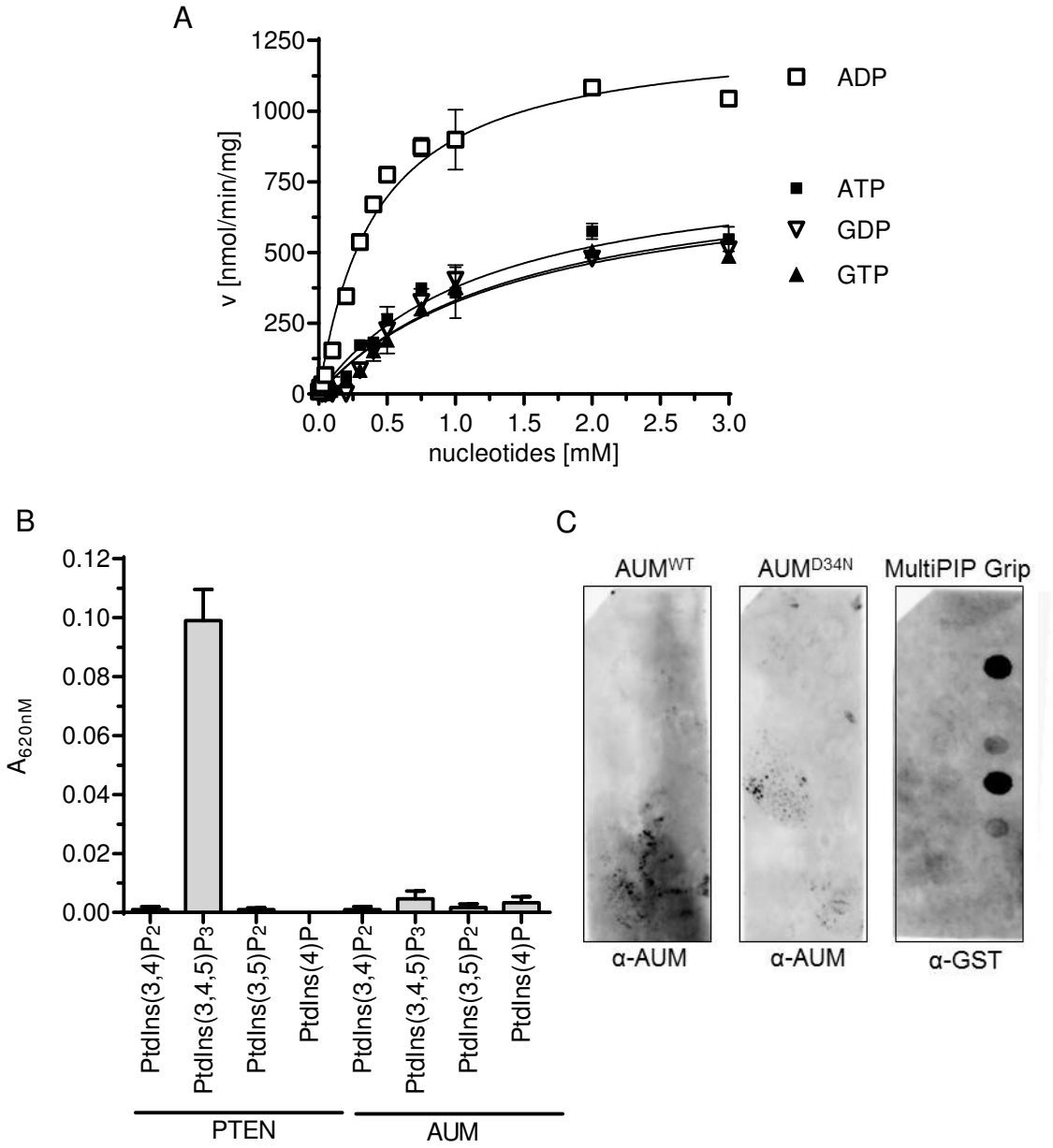

Figure 12: AUM shows activity towards nucleotides but no activity/affinity towards phospholipids. (A) AUM dephosphorylates adenine and guanine nucleotide di- and triphosphates. Nucleotides were tested at concentrations ranging from 0-3 mM in an *in vitro* malachite green assay with 0.16 µg/well of a 96-well microtitter plate of protein. Results are mean values ± SEM of three independent experiments performed in triplicates with three independently purified protein batches. **(B)** AUM shows no phosphatase activity towards phosphataidyl-inositol phosphates. Purified AUM (0.16 µg) was incubated with 1.5 nM phosphatidyl-inositol phosphates in the presence of 10 mM DTT. Recombinant, purified PTEN was used as a positive control. Results are mean values ± SEM of three independent experiments performed in triplicates with three independently purified protein batches. **(C)** AUM^{WT} and AUM^{D34N} does not bind to the tested phospholipids in a protein-lipid overlay assay. Purified AUM (20 µg/ml) was incubated with hydrophobic membranes, spotted with 100 pmol of 15 lipids. MultiPIP Grip-GST was used as positive binding control and detected with α-GST. All assays were performed with recombinant, purified murine AUM.

The generic phosphatase substrate *p*NPP is well suited for kinetic measurements of phosphatase activity, and it is widely accepted as a tool for phosphatase characterization, in case the physiological phosphatase substrate is unknown. Nevertheless, other,

physiological, potential candidates of small molecular substrates were tested in *in vitro* malachite green assays (2.2.6.2). Since the Rossman fold is a classic nucleotide-binding motif (Rossmann *et al.*, 1974), the activity of AUM towards adenine and guanine nucleotides was tested.

AUM dephosphorylates adenine and guanine nucleotide di- and triphosphates (ADP>ATP≈GDP≈GTP; figure 12A; table 4). Given the role of some HAD phosphatases for lipid metabolism (Newman *et al.*, 2003; Han *et al.*, 2006; Peterfy *et al.*, 2001), phospholipids as potential substrates or binding partners of AUM were tested. AUM shows no detectable phosphatase activity towards the phospholipids (PtdIns(3,4)P_2 ; PtdIns(3,4,5)P_3; PtdIns(3,5)P_2; PtdIns(4)P; figure 12B). Besides this, neither AUM^{WT} nor AUM^{D34N} bind phospholipids in a phospholipid overlay assay, excluding PIPs as potential substrates or binding partners.

Table 4: Catalytic constants of AUM towards nucleotides

	K_M (mM)	v_{max} (nmol/mg/min)	k_{cat} (s^{-1})
ADP	0.42 ± 0.04	1279 ± 40	0.73 ± 0.02
ATP	1.23 ± 0.19	840 ± 62	0.48 ± 0.03
GDP	1.48 ± 0.31	821 ± 88	0.47 ± 0.05
GTP	1.47 ± 0.21	802 ± 59	0.46 ± 0.03

Nucleotide dephosphorylation was measured with malachite green.
Results are means ± SEM; *n* = 3.

3.1.3 AUM belongs to the family of haloacid dehalogease-type phosphatases

Next it was tested, whether AUM displays characteristics typical of HAD-type phosphatases. The alignment in figure 13A shows the presence of the four conserved HAD motifs in the AUM sequences and also highlights the similarity of these regions to other members of the HADSF (chronophin, PMM1 and PMM2).

A

	motif I DxDx(T/V)(L/I)	motif II (S/T)	motif III K(X$_n$)	motif IV (G/S)(D/S)X$_{3-4}$(D/E)	
AUM					
M. musculus	^{31}LLFDCDGVLW^{40}	^{65}FITNNS^{70}	^{232}IIGKPS^{237}	^{259}GDRLDTDILLG^{269}	(NP_080230.2)
R. norvegicus	^{31}LLFDCDGVLW^{40}	^{65}FITNNS^{70}	^{232}IIGKPS^{237}	^{259}GDRLDTDILLG^{269}	(NP_001162623.1)
H. sapiens	^{31}LLFDCDGVLW^{40}	^{65}FITNNS^{70}	^{232}IIGKPS^{237}	^{259}GDRLDTDILLG^{269}	(NP_001035830.1)
M. mulatta	^{32}LLFDCDGVLW^{41}	^{66}FITNNS^{71}	^{233}IIGKPS^{238}	^{260}GDRLDTDILLG^{270}	(XP_001084229.2)
B. taurus	^{31}LLFDCDGVLW^{40}	^{65}FITNNS^{70}	^{232}IIGKPS^{237}	^{259}GDRLDTDILLG^{269}	(NP_001033261.1)
M. domestica	^{31}LLFDCDGVLW^{40}	^{65}FVTNNS^{70}	^{233}IIGKPS^{238}	^{260}GDRLDTDILLG^{270}	(XP_001363637.1)
A. carolinensis	^{29}VLFDCDGVLW^{38}	^{69}YVTNNS^{74}	^{239}IVGKPS^{244}	^{266}GDRLDTDILMG^{276}	(XP_003229206.1)
D. rerio	^{24}VLFDCDGVIW^{33}	^{58}FVTNNS^{63}	^{217}VVGKPS^{222}	^{244}GDRLDTDIMLG^{254}	(AAH45860.1)
X. tropicalis	^{24}VLFDCDGVLW^{33}	^{58}FLTNNS^{63}	^{217}VIGKPS^{222}	^{244}GDRLDTDIQMG^{254}	(XP_002932481.1)
	:*******:*	::****	::****	********.:*	
chronophin (*M.m.*)	^{22}VLFDCDGVLW^{32}	^{56}FVSNNS^{61}	^{210}VVGKPS^{215}	^{233}GDRLETDILFG^{243}	(NP_064667.2)
AUM (*M.m.*)	^{31}LLFDCDGVLW^{40}	^{65}FITNNS^{70}	^{232}IIGKPS^{237}	^{259}GDRLDTDILLG^{269}	(NP_080230.2)
PMM1 (*M.m.*)	^{16}CLFDVDGTLT^{25}	^{52}GGSDYS^{57}	^{195}GWDKRY^{201}	^{220}TSPGGNDFEIY^{230}	(NP_038900.1)
PMM2 (*M.m.*)	^{5}CLFDMDGTLT^{14}	^{41}GGSDFE^{46}	^{182}GWDKRY^{187}	^{207}TMPGGNDHEIF^{217}	(NP_058577)

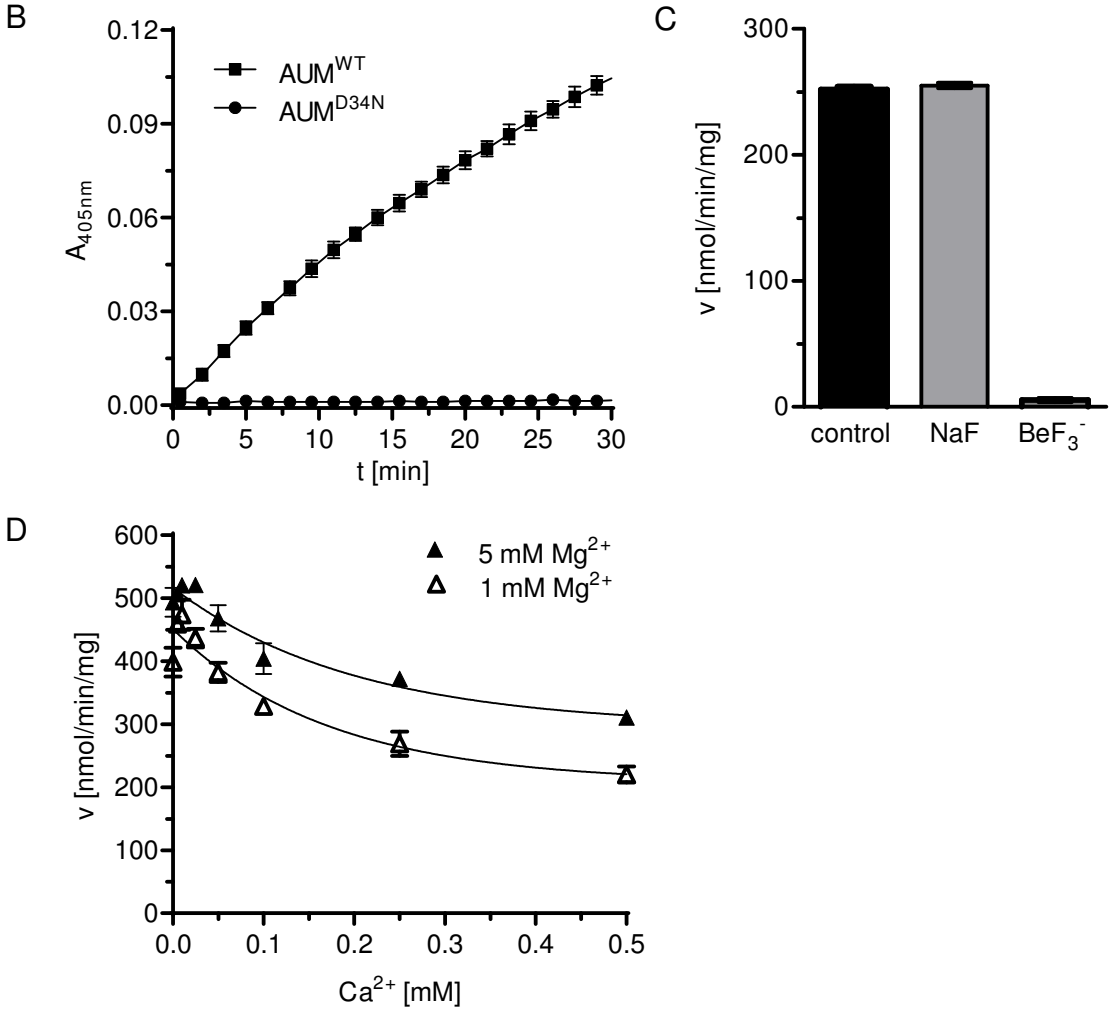

Figure 13: AUM is an aspartate-dependent phosphatase. (A) Alignment of the four conserved HAD motifs of vertebrates AUM orthologes in comparison to murine chronophin and murine phosphomannomutase (PMM) 1 and 2. **(B)** *In vitro* phosphatase assays with AUM^{WT} and AUM^{D34N} using *p*NPP as a substrate. The generation of the dephosphorylated product *p*NP is measured colorimetrically over time at $A_{405\ nm}$. (**C**) *p*NPP phosphatase activity of AUM in dependence of NaF (1 mM) and BeF_3^- (1 mM NaF + 0.1 mM $BeCl_2$) is shown. (D) The effect of Ca^{2+} (0-0.5 mM) on AUM activity in presence of 1 and 5 mM of Mg^{2+} was measured in *in vitro* *p*NPP assays. (**A - C**): For all shown activity assays 0.8 µg AUM and 3.5 mM *p*NPP in a total assay volume of 100 µL were used. Results are means ± SEM of three independent experiments performed in triplicates with three independently purified protein batches.

It has been previously demonstrated that the first Asp in HAD motif I is essential for mammalian HAD phosphatase activity (Gohla *et al.*, 2005). To further validate AUM as a member of the HADSF, the effect of the replacement of the putative nucleophilic Asp in AUM for Asn (AUM^{D34N}) on phosphatase activity was tested. The *p*NPP phosphatase activity of the recombinant purified murine AUM^{D34N} is completely abolished, demonstrating that AUM is indeed an aspartate-dependent phosphatase (figure 13B). Next, AUM activity was measured in the presence of berylliumfluoride (BeF_3^-). HAD phosphatases form a stable complex with BeF_3^- that structurally mimics their phosphoaspartate transition state by binding to the active site aspartate and to the other catalytic core residues, and by coordinating the catalytically essential Mg^{2+} (Cho *et al.*, 2001; Rinaldo-Matthis *et al.*, 2002). AUM is insensitive to NaF, whereas its hydrolytic activity is completely blocked by BeF_3^- (figure 13C). These results indicate that similar to other HAD superfamily members, the AUM-catalyzed dephosphorylation reaction proceeds via a pentacovalent phosphoaspartate intermediate. The critical role of Mg^{2+} for HAD-type phosphatases has been characterized for many members of the HADSF. Ca^{2+} can displace Mg^{2+} from the active site and interfere with the nucleophilic attack of the catalytic aspartate side chain oxygen atoms on the substrate's phosphate moiety (Peeraer *et al.*, 2004). Figure 13D shows that increasing concentrations of added Ca^{2+} reduced AUM phosphatase activity, while elevated Mg^{2+} concentrations protected the enzyme partly against Ca^{2+}-mediated inhibition. Taken together, these results support the classification of AUM as a Mg^{2+}-dependent HAD phosphatase.

3.1.4 Inhibitor studies

To further characterize the HAD-type phosphatase activity of AUM, established inhibitors of classical phosphatases were tested. In line with an aspartate-based catalytic mechanism, AUM was insensitive to inhibitors of serine/threonine protein phosphatases, such as okadaic acid and calyculin A (figure 14A, B). Okadaic acid is an inhibitor of PP1(IC_{50} = 15 nM) and PP2A (IC_{50} = 0.1 nM) (Cohen *et al.*, 1989), it does not inhibit acid and alkaline phosphatases, nor protein tyrosine phosphatases (Bialojan *et al.*, 1988). The protein phosphatase inhibitor calyculin A potently inhibits PP1 and PP2A (Ishihara *et al.*, 1989). Sodium orthovanadate (Na_3VO_4) is a commonly used general inhibitor for protein tyrosine phosphatases (PTPs) as well as for ATPases, alkaline phosphatases (Huyer *et al.*, 1997). The phosphatase AUM, indicated to be phospho-tyrosine directed (figure 8), was incubated with up to 1 mM of orthovanadate. AUM concentration-dependent inactivation occurred with an IC_{50} of 41.4 µM (figure 14C).

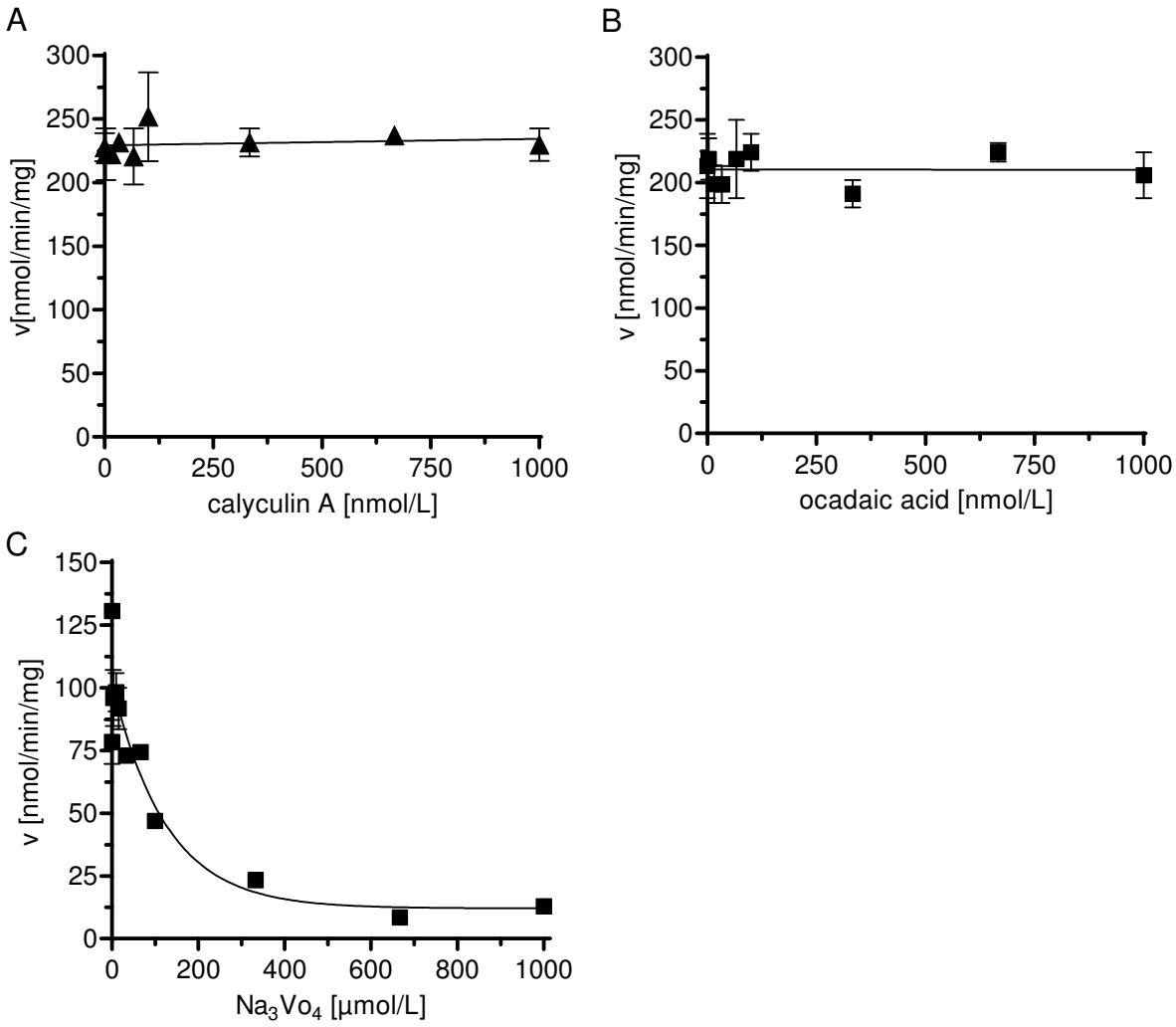

Figure 14: AUM activity in the presence of phosphatase inhibitors.
Phosphatase activity of AUM in dependence of calyculin A (0-1 µM; **A**), ocadaic acid (0-1 µM; **B**) and sodium orthovanadate (0-1 mM; **C**) was measured in *in vitro p*NPP assays. For all shown activity assays 0.8 µg AUM and 3.5 mM *p*NPP were used. Results are means ± SEM of three independent experiments performed in triplicates with independently purified protein batches.

3.1.5 Antibody purification and validation

To generate AUM specific antibodies, rabbits were immunized with purified murine AUM^{D34N}. The antibody was purified by using $(NH_4)_2SO_4$-precipitation and affinity chromatography on immobilized AUM^{D34N} protein from the serum (2.2.7). The specificity and sensitivity of the antibody was analyzed by immunoblotting, using purified, recombinant AUM and AUM endogenously expressed in cells. Because of the extensive sequence identity between AUM and chronophin, a potential cross-reactivity of the AUM antibody with chronophin was analyzed. For this purpose, different protein amounts of recombinant, purified, murine AUM and chronophin (0.1-2.5 µg) were separated on the same SDS-PAGE gel and immunoblotting was performed (figure 15A). The membranes were cut and incubated with purified α-AUM antibodies (glycine eluate) or with α-chronophin antibodies. The α-AUM

antibody was able to reliably detect as little as 100 ng of recombinant, purified AUM, and no cross-reactivity was observed between AUM- or chronophin-directed antibodies.

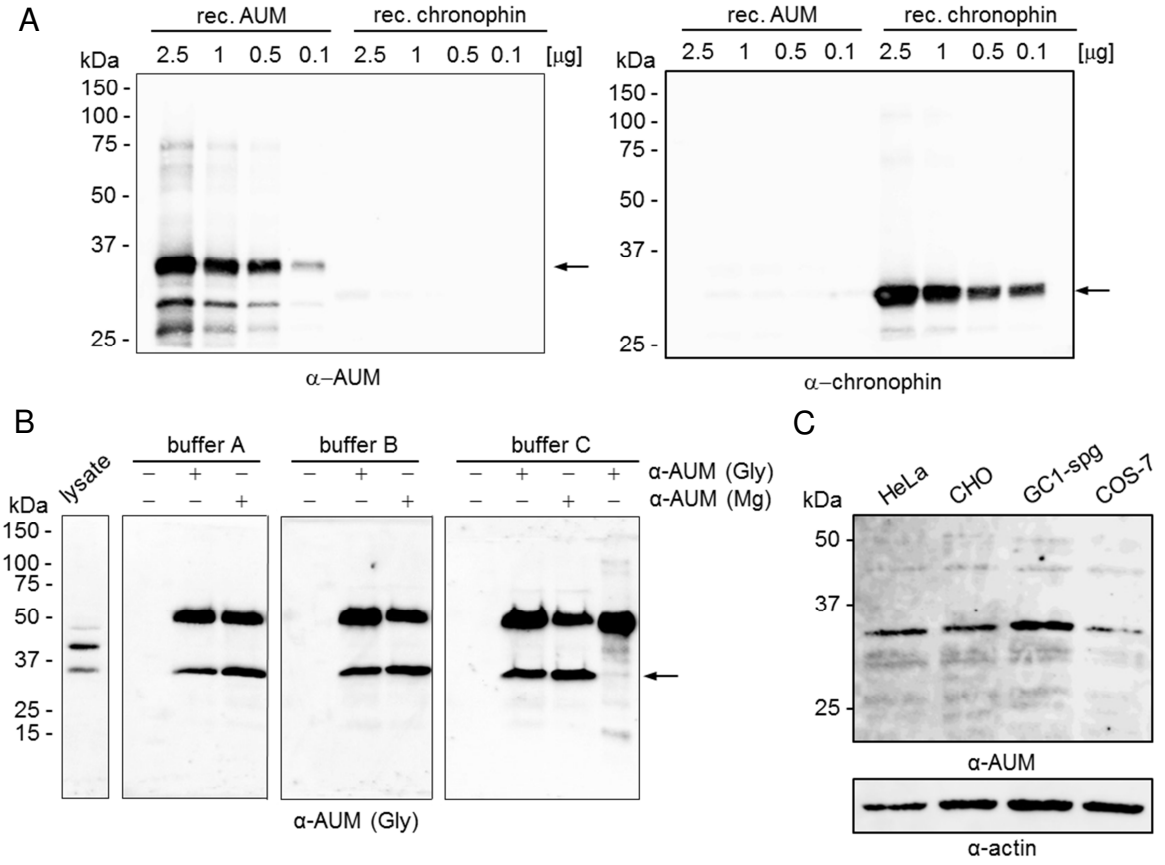

Figure 15: The α-AUM antibody generated against full-length AUM recognizes AUM specifically and can be used for immunoprecipitation. (A) The indicated amounts of purified, recombinant (rec.) AUM and chronophin were separated by SDS-PAGE and probed with α-AUM (upper panel) or α-chronophin antibodies (lower panel). No antibody cross-reactivity is observed. The faster migrating bands on the upper blot are AUM degradation products. Arrows show the expected size for AUM or chronophin. **(B)** Glycine (Gly) and magnesium (Mg) eluate α-AUM antibodies were used for immunoprecipitation of endogenous AUM from GC1 spg cell lysates using three different buffer conditions (buffer A: RIPA buffer; buffer B: lysis buffer; buffer C: HIGH SALT/LOW SALT). Immunoprecipitates were resolved by SDS-PAGE, blotted onto nitrocellulose, and probed with α-AUM antibodies. A beads control (no antibody), the cell lysate and the antibody itself (last row) are shown as controls. The arrow indicates the expected size of AUM. **(C)** The α-AUM antibody detects endogenous AUM in human cervical carcinoma (HeLa), chinese hamster ovary (CHO), mouse spermatogonial (GC1 spg), and monkey kidney (COS7) cells.

To test whether the newly generated antibody is suitable for immunoprecipitation (IP, 2.2.7.3) GC1 spg cells were used (figure 15B). The cells were lysed in three different buffers [RIPA buffer (buffer A), lysis buffer (buffer B) or HIGH SALT/LOW SALT lysis buffer (buffer C)], and immunoprecipitation experiments were performed. Both magnesium and glycine eluates were able to precipitate endogenous AUM under the three tested conditions. A strong band of around 35 kDa was detected with α-AUM antibodies. The molecular mass of this band corresponds to endogenous AUM as detected in GC1 spg cell lysates run in parallel on the

gel. Under the tested conditions, AUM did not bind non-specifically to the beads (beads control, no antibody used). When the glycine eluate itselve was separated by SDS-PAGE and probed with α-AUM antibodies, no band at ~35 kDa was detected, indicating that the antibody eluates were not contaminated with AUM protein derived from the column (figure 15B, last row). As a next step, the protein expression patterns of commercially available cell lines were investigated by immunoblotting to validate the newly generated α-AUM antibody for endogenous AUM levels. The full-length antibody was able to detect AUM in all tested cell lines, including the mouse spermatogonial cell line GC1 spg (figure 15C).

3.2 Regulation of AUM specificity

On the basis of the criteria that define the HAD family of phosphatases [presence of a rossmannoid structure, active site signature DxDx(V/T)], 40 different human genes and their corresponding protein products were identified by database mining (Seifried *et al.*, 2013). They specifically dephosphorylate carbohydrates, lipids, metabolites, DNA and serine-, threonine- or tyrosine-phosphorylated proteins. Dephosphorylation takes place via the first aspartate of the conserved motif DxDx(T/V) located in the core domain. HAD phosphatases share additional inserts termed cap domains. The caps provide more extensive shielding for the catalytic cavity, supply binding determinants for substrate selectivity, and can be involved in phosphatase oligomerization. The structural diversity of these domains is of high interest when it comes to the question of specificity of HAD phosphatases. The question arises if it is possible to identify conserved residues that are responsible for binding of particular substrate classes, like strategically placed amino acid residues framing the active site motif DxDx(T/V) or amino acids positioned in the cap domain. To address this question, specificity determinants of chronophin and AUM should be identified.

3.2.1 Comapartive studies of AUM and chronophin

By database mining, AUM was identified as the closest homolog of chronophin in mammalian cells. A polyclonal antibody (2.2.7.1, figure 15) against murine AUM was raised to compare the expression levels of AUM and chronophin. AUM was found to be ubiquitously expressed with highest expression levels in testis (figure 16). The highest expression of chronophin was detected in brain. In all investigated tissues, the AUM antibody detected a predominant band corresponding to the expected AUM size of ~35 kDa. In addition, faint lower molecular weight bands were detected, suggesting degradation products of AUM.

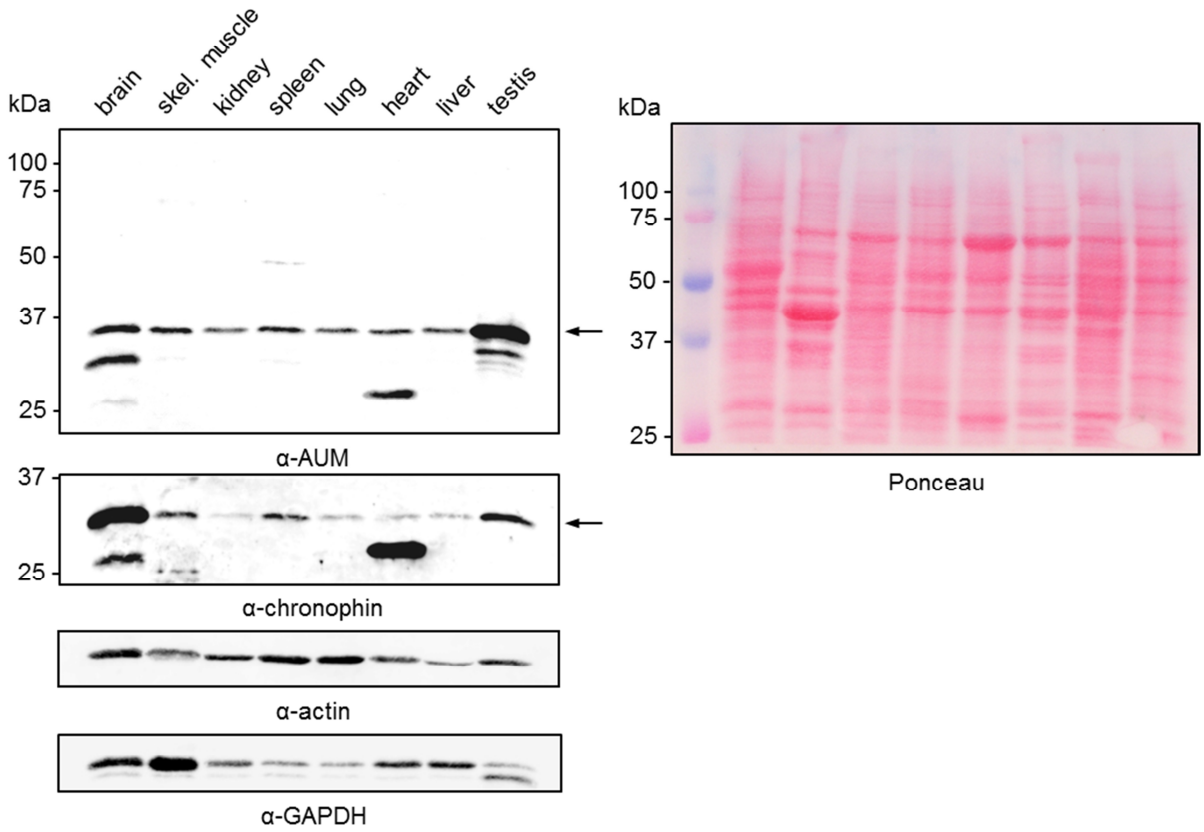

Figure 16: Comparison of AUM and chronophin expression levels in murine tissues
Mouse tissue lysates (50 µg of protein) were separated by SDS-PAGE and analyzed by immunoblotting with α-AUM antibodies. The blot was stripped and reprobed with α-chronophin antibodies. Blots were reprobed with α-actin and α-GAPDH antibodies to test for comparable protein loading, which is also documented on the Ponceau-stained membrane. Like chronophin, AUM is expressed in all investigated mouse tissues, with high AUM levels found in testis. The bands corresponding to the expected AUM or chronophin molecular weights are indicated by arrows.

After the comparison of AUM and chronophin expression levels, it was focused on the structural characteristics of the two phosphatases. Both share 45% identity on amino acid level and 87% similarity of predicted secondary structure motifs. To confirm this, CD spectroscopy was performed (2.4.4.5). With this technique the overall secondary structure content of a protein can be qualitatively analyzed, defining a characteristic fingerprint of the native protein structure. In an overlay, the CD spectra of AUM and chronophin show almost identical minima at 209 nm and 222 nm, characteristic of a high alpha helical content (figure 17A).

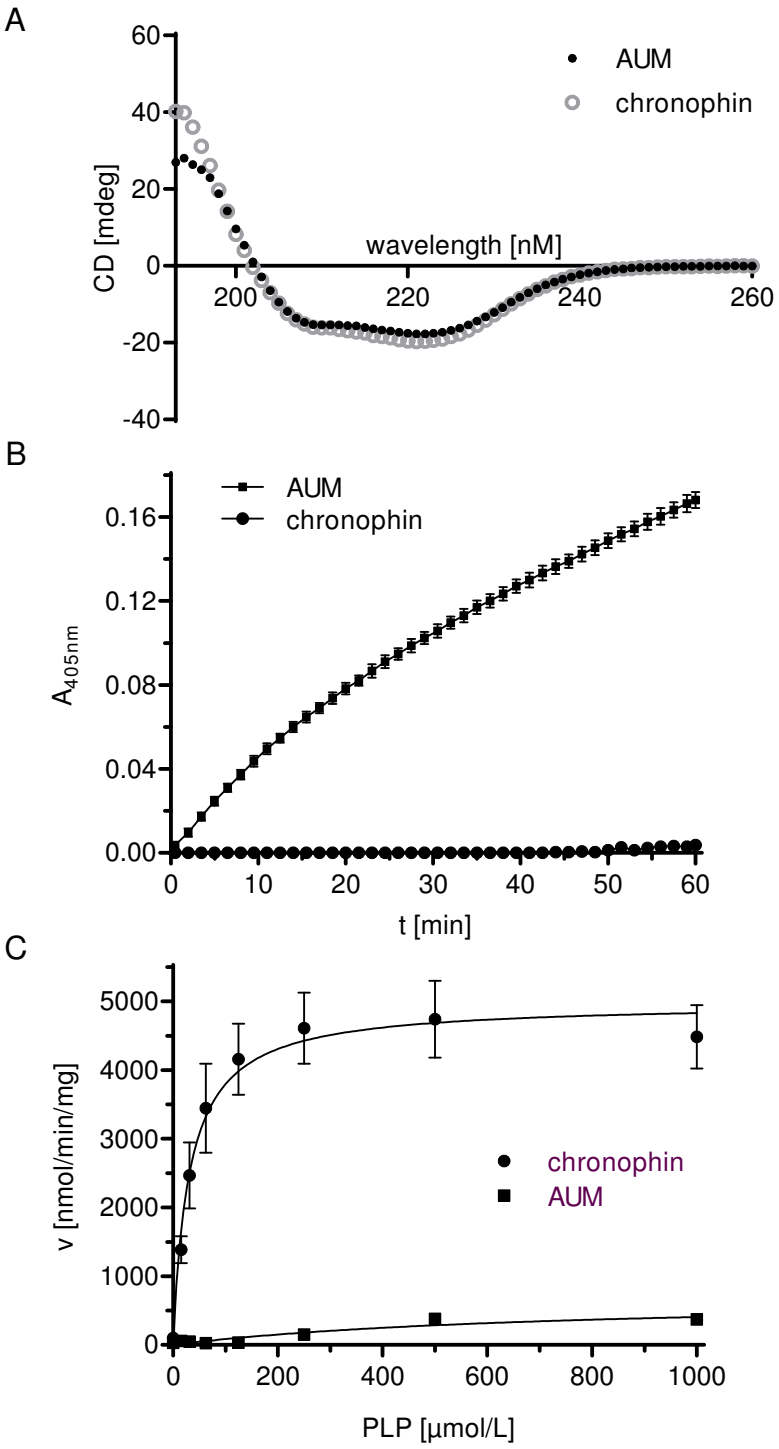

Figure 17: Comparison of AUM and chronophin secondary structure arrangement and phosphatase activities. (A) Shown is the CD spectroscopy analysis of recombinant, purified AUM (black) and chronophin (gray). The mean values of five measurements are shown for each protein. **(B)** *In vitro* phosphatase assays with AUM and chronophin using *p*NPP as a substrate. The generation of the dephosphorylated product *p*NP is measured colorimetrically over time at A_{405nm}. **(C)** AUM displays no activity against the low molecular weight chronophin substrate pyridoxal 5'-phosphate (PLP). The production of inorganic phosphate was detected with malachite green and measured at 620 nm. The results in A and B are means ± SEM of three independent experiments performed in triplicates with independently purified protein batches.

Despite the exceptional homology of AUM and chronophin on the primary and secondary structure level, there is a striking difference in function between these two enzymes. Both phosphatases differ in substrate choice: AUM is phospho-tyrosine directed (figure 8), and dephosphorylates *p*NPP and adenine and guanine nucleotides (figure 11). Chronophin was identified as a serine3-phosphocofilin phosphatase and as a pyridoxal-5'-phosphate (PLP) phosphatase (Pdxp) (Gohla *et al.*, 2005; Fonda, 1992). In contrast, AUM dephosphorylates the low molecular weight chronophin substrate PLP only poorly (figure 17C), whereas chronophin exhibits no measurable activity against *p*NPP as a substrate (figure 17B). To elucidate the basis of this striking difference in substrate preference in the closely related AUM and chronophin phosphatases, the evolutionary relationship of these two proteins was investigated.

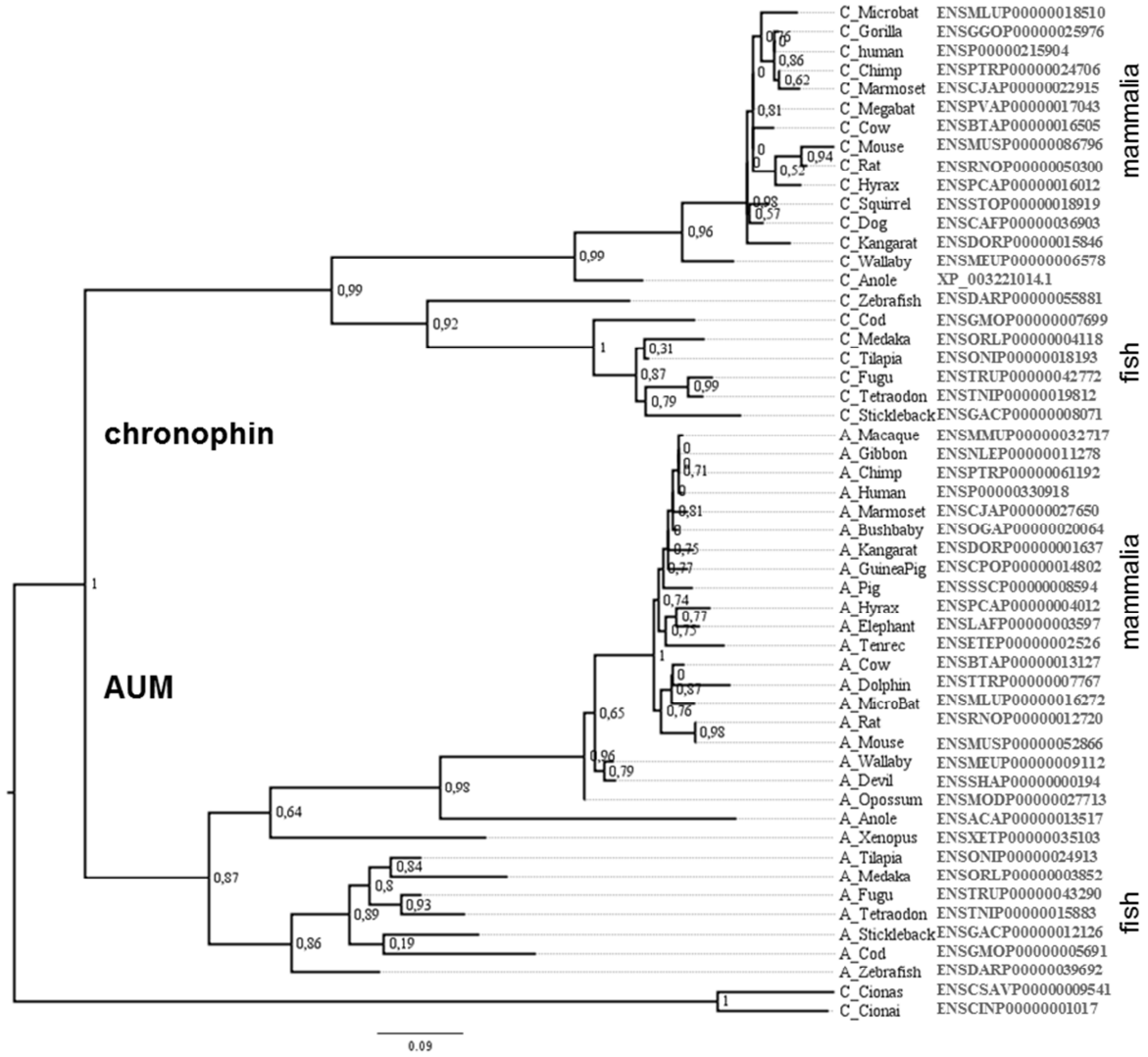

Figure 18: AUM is a chronophin paralog. Shown is a phylogenetic tree of vertebrate AUM and chronophin proteins together with urochordate sequences predating the duplication of a common ancestor.

The AUM/chronophin family evolved via a duplication of an ancestral gene at the origin of vertebrates (figure 18). Retained duplicated genes usually undergo either neofunctionalization (i.e., one of the genes evolves a new function), or subfunctionalization (i.e., each gene retains a subset of the original function) (Lynch and Conery, 2000). A typical indication of neofunctionalization is an increased evolutionary rate in one of the two duplicated genes. To test for such a rate difference, models allowing for different evolutionary rates at the base of each subgroup as well as in the whole subgroups were compared with models allowing only a single rate over the whole phylogenetic tree. However, none of the complex models improved the fit to the data significantly ($p<0.05$). Thus, the evolutionary rate of both genes cannot be distinguished, disagreeing with a classical model of neofunctionalization. Nevertheless, the experimental data (figure 8) show that the substrate specificities, and therefore most likely also the functions of AUM and chronophin differ substantially. To elucidate the basis of substrate specificity in this HAD phosphatase subfamily, comparative evolutionary, biochemical and mutational analyses of AUM and chronophin were performed.

3.2.2 Generation of AUM mutants

To investigate the structural basis of the substrate specificity differences between AUM and chronophin, amino acid residues in AUM for the corresponding chronophin residues in regions of AUM/chronophin sequence divergence were exchanged. Based on available chronophin structures (2OYC, 2P27, 2P69) and on amino acid alignments, regions of interest were chosen. For a first analysis, regions that are unstructured in chronophin and located in close proximity to the nucleophile were exchanged. In addition, the cap domains were exchanged (figure 19). In this project the following mutants were generated:

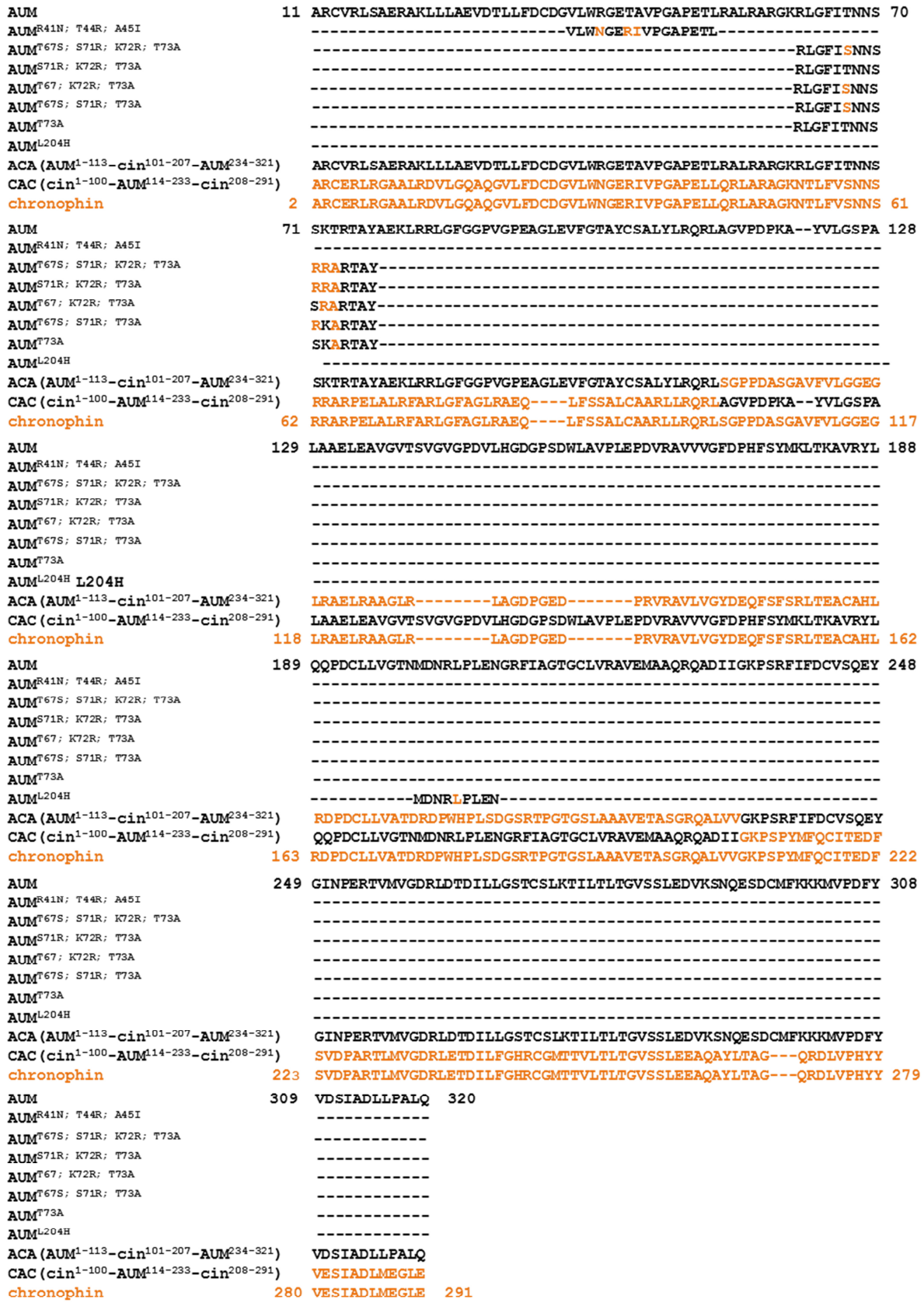

Figure 19: Alignment of the analyzed swapping mutants:
cin stands for chronophin. Multiple sequence alignments were performed with ClustalW.

Table 5: Mutants generated for swapping experiments

mutagenesis close to DxDx(T/V) motif
$AUM^{R41N; T44R; A45I}$
N-terminal hybrid ($chronophin^{1-65}$-AUM^{75-312})
mutagenesis close to putative substrate entry site
$AUM^{T67S; S71R; K72R; T73A}$
$AUM^{S71R; K72R; T73A}$
$AUM^{T67S; K72R; T73A}$
$AUM^{T67S; S71R; T73A}$
AUM^{T73A}
mutagenesis of the cap domain
AUM^{L204H}
CAC^{L191H}
ACA (AUM^{1-113}-$chronophin^{101-207}$-$AUM^{234-321}$)
CAC ($chronophin^{1-100}$-$AUM^{114-233}$-$chronophin^{208-291}$)

The recombinant proteins were overproduced in *E. coli* and purified via affinity- and size exclusion chromatography (2.2.3). The $AUM^{R41N; T44R; A45I}$, $AUM^{S71R; K72R; T73A}$, AUM^{T73A}, AUM^{L204H}, ACA, and the CAC mutant were as soluble as the wild-type enzymes, whereas the mutants $AUM^{T67S; S71R; K72R; T73A}$, $AUM^{T67; K72R; T73A}$ and $AUM^{T67S; S71R; T73A}$ showed decreased solubility and impurities (figure 20).

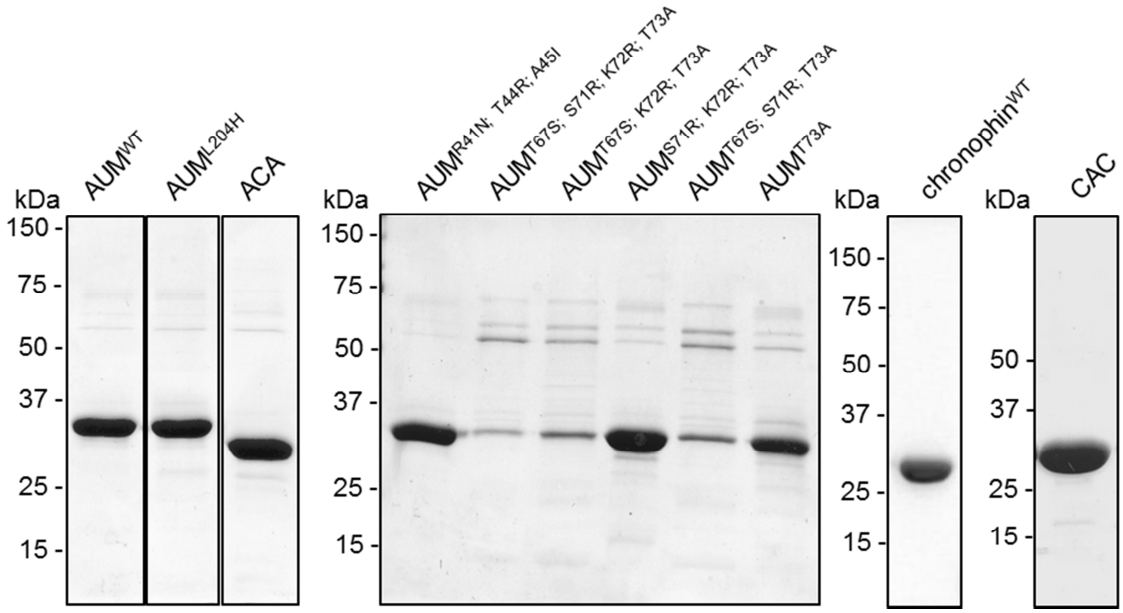

Figure 20: Purity of the employed recombinant proteins.
Shown are Coomassie Brilliant Blue stained gels.

To compare the amounts of the various AUM mutants, proteins were run on SDS-PAGE gels and stained with Coomassie Blue. Protein concentrations were estimated by A_{280nm} measurements and additional densitometric analysis were performed with ImageJ after scanning the gels. The mutant CAC^{L191H} and the N-terminal hybrid were insoluble and therefore could not be further analyzed.

3.2.3 Enzymatic activity measurements

To elucidate the substrate preference of the mutants, phosphatase activity assays with *p*NPP or PLP as substrate were performed.

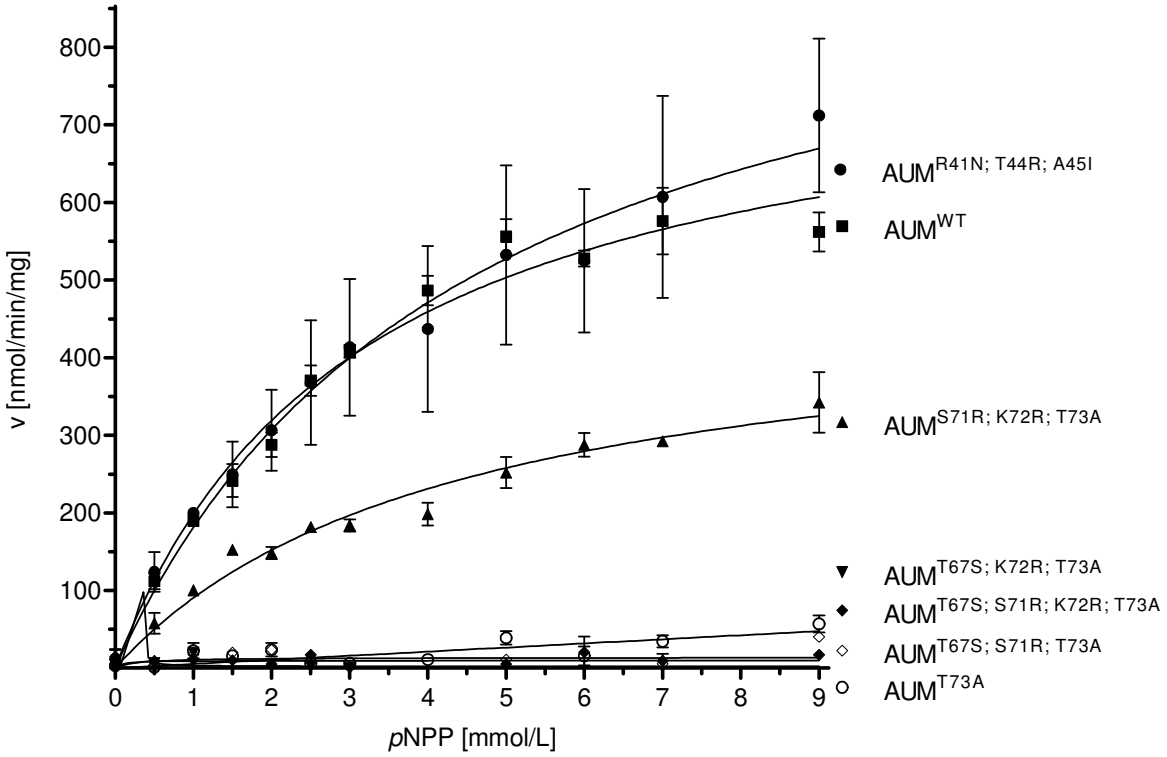

Figure 21: Swapping mutations in the core domain affect AUM activity.
*In vitro p*NPP phosphatase activity of purified core domain swapping mutants. Results are mean values ± SEM of three independent experiments performed in triplicates with three independently purified protein batches.

Figure 21 shows that the exchange of three divergent amino acids adjacent to HAD motif I to the corresponding chronophin residues ($AUM^{R41N;\ T44R;\ A45I}$) slightly elevated the activity towards *p*NPP (~123.5% of AUM^{WT}). Next the function of residues in the region surrounding the AUM/chronophin HAD motif II was investigated. This motif contains a conserved Ser or Thr that contributes to the orientation of the substrate for nucleophilic attack by forming a hydrogen bond with the substrate's phosphoryl group. The swap of four AUM residues for the corresponding chronophin residues in the seven amino acid stretch of AUM that starts with

the conserved HAD motif II Ser/Thr (AUM$^{T67S;\ S71R;\ K72R;\ T73A}$) abolished AUM phosphatase activity towards *p*NPP. To determine which of these residues are required for AUM activity, all divergent residues of this domain were swapped in a stepwise fashion. Only the reverse mutation of Ser67 back to the original Thr67 AUM residue (AUM$^{S71R;\ K72R;\ T73A}$) partially recovered the *p*NPP phosphatase activity (~58.7% of AUM^{WT}). These results point to an important function of the conserved Thr67 in HAD motif II for the phosphatase activity of AUM. In contrast, AUM variants that contain the other three reverse mutations remained catalytically strongly impaired (AUM$^{T67S;\ K72R;\ T73A}$, AUM$^{T67S;\ S71R;\ T73A}$, or AUM^{T73A}). None of the investigated AUM variants had detectable phosphatase activity towards the chronophin substrate PLP, the catalytic constants towards *p*NPP are summarized in table 6. These results show that the residues exchanged in the swapping mutants of the core domains did not contribute to substrate specificity. Next, mutants with amino acid exchanges in the cap domains were analyzed in *in vitro* phosphatase assays. The exchange of the AUM and chronophin cap modules resulted in a clear change of substrate specificity (figure 22A, B). While the phosphatase hybrid consisting of the chronophin cap and the AUM core domain (AUM$^{1-113}$-chronophin$^{101-207}$-AUM$^{234-\ 321}$, ACA) is inactive against *p*NPP (0.46% activity compared to AUM^{WT} activity), the presence of the chronophin cap on the AUM core is sufficient for PLP dephosphorylation (k_{cat}: 3.73 ± 0.36 s^{-1}). In contrast, the presence of the AUM cap connected to the chronophin core (chronophin$^{1-100}$-AUM$^{114-233}$-chronophin$^{208-291}$, CAC) abolished phosphatase activity against PLP. Consistent with the role of the AUM core domain residues for efficient substrate dephosphorylation (figure 21), the *p*NPP phosphatase activity of the CAC hybrid is reduced compared to AUM^{WT}, but comparable with the basal *p*NPP activity of chronophin^{WT}. The results show that determinants of both the core and the cap domain of AUM contribute to phosphatase activity and specificity towards *p*NPP.

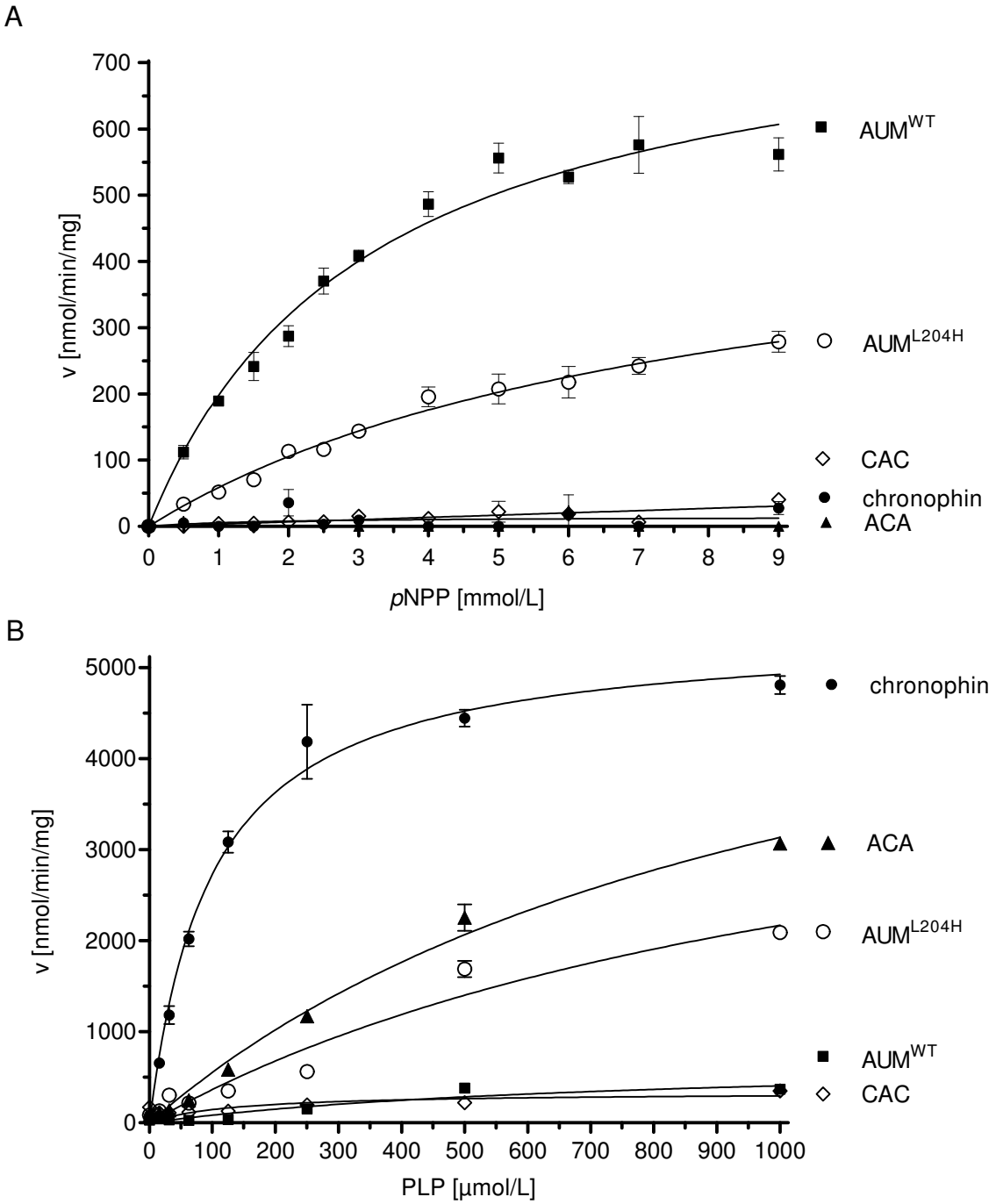

Figure 22: The cap domain of AUM and chronophin dictates substrate specificity.
The indicated proteins were tested for their *in vitro* phosphatase activity towards *p*NPP **(A)** and PLP **(B)**. His182 in the chronophin cap is essential for PLP dephosphorylation, and the substitution of the corresponding Leu204 in AUM for a His residue transfers chronophin-like activity onto AUM. Results are means ± SEM of $n = 3$ independent experiments

Because of the experimental finding, that the chronophin cap is essential for PLP dephosphorylation, residues that are in contact with PLP, based on the available PLP-bound chronophin X-ray crystal structures (PDB: 2P69) were analyzed. His182 in the chronophin cap is oriented towards the catalytic cleft by a β-hairpin structure, and the His imidazole ring

directly coordinates the PLP pyridine ring (figure 25A). To explore the contribution of this residue to substrate specificity, the His residue in the corresponding AUM position was exchanged. AUM^{L204H} dephosphorylates PLP almost as well as $chronophin^{WT}$ with a turnover rate of k_{cat} 2.76 ± 0.58 s^{-1} (figure 22B). In contrast, AUM^{L204H} only has markedly impaired (64.3%) activity against *p*NPP compared to AUM^{WT} (figure 22A). This result confirms that the introduction of a His residue at position 204 in the AUM cap module can transfer chronophin-like activity onto AUM, while simultaneously attenuating *p*NPP dephosphorylation. This position is therefore critical for the substrate specificity of chronophin and AUM.

Table 6: Catalytic constants of AUM, AUM mutants and chronophin towards *p*NPP

	K_M (mM)	k_{cat} (s^{-1})
AUM^{WT}	3.13 ± 0.36	0.47 ± 0.023
$AUM^{R41N; T44R; A45I}$	4.58 ± 1.55	0.57 ± 0.096
$AUM^{T67S; S71R; K72R; T73A}$	0.09 ± 0.60	0.006 ± 0.002
$AUM^{T67S; K72R; T73A}$	n.d.	n.d.
$AUM^{T67S; S71R; T73A}$	0.28 ± 0.84	0.008 ± 0.003
AUM^{T73A}	n.d.	n.d.
$AUM^{S71R; K72R; T73A}$	4.31 ± 0.74	0.28 ± 0.023
AUM^{L204H}	7.97 ± 1.58	0.30 ± 0.04
ACA	3.75 ± 0.36	0.001 ± 0.001
CAC	n.d.	n.d.
chronophin	n.d.	n.d.

The catalytic constants of $AUM^{T67S; K72R; T73A}$, AUM^{T73A}, the CAC hybrid and chronophin could not be determined (n.d.) because the *p*NPP activity of these proteins was too low. Results are means ± SEM; $n = 3$.

3.2.4 Structural insights into AUM/chronophin specificity

Further insights into the structural basis of the different substrate specificities of chronophin and AUM were obtained from X-ray crystallographic studies. While experiments to crystallize full-length AUM were not successful, the CAC hybrid containing the AUM cap domain inserted into the chronophin catalytic core was crystallized and analyzed. The atomic model of the CAC hybrid was refined to 2.65 Å with an R-factor of 19.8% and an R_{free} of 25.6%. The protein crystallized in the space group P1 21 1 with four molecules (two homodimers) per asymmetric unit (table 3; PDB entry 4BKM).

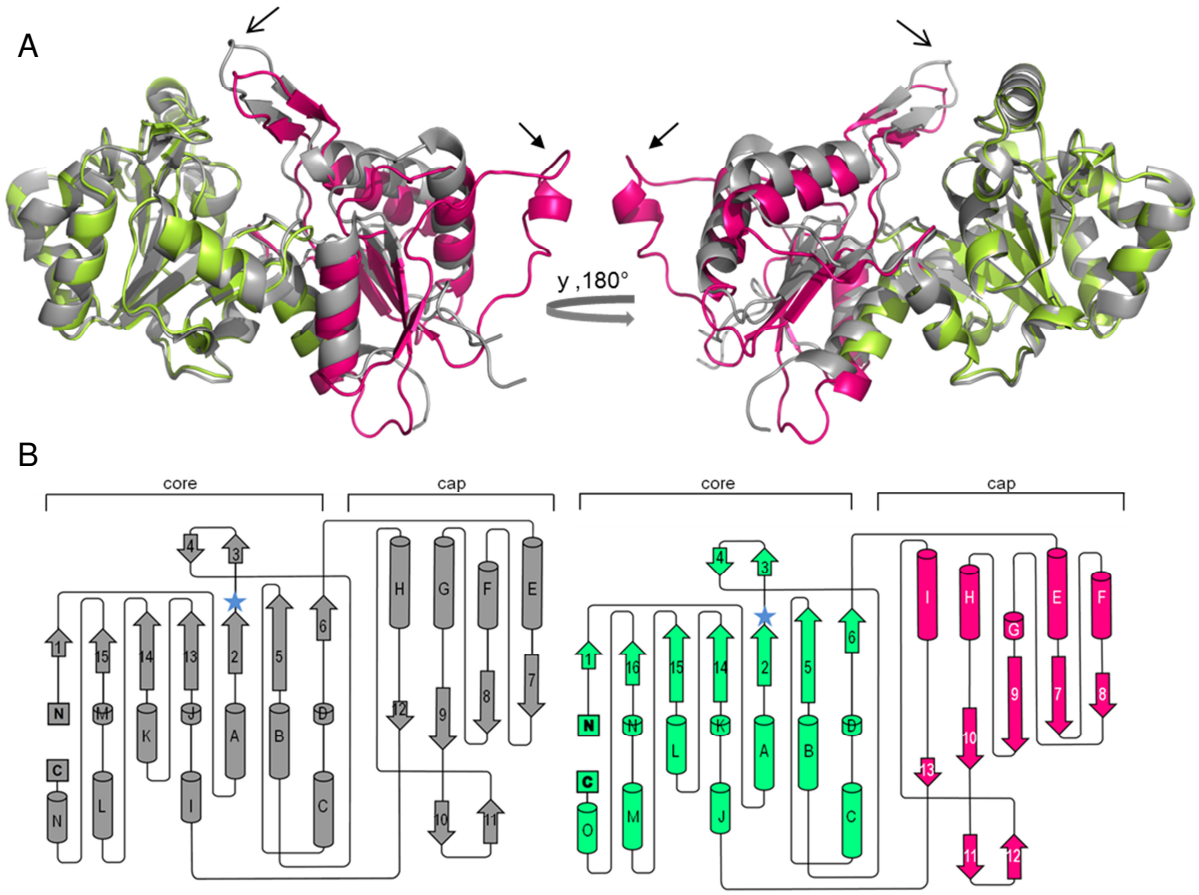

Figure 23: Crystal structure of the murine chronophin core/AUM cap hybrid (CAC).
(A) Overall structure of the murine CAC (PDB: 4BKM) compared to human chronophin (PDB: 2P69). Structures are rendered as ribbon diagrams. Human chronophin is represented in the PLP-bound state and shown in gray. The core domain of murine chronophin in the CAC hybrid is in lime color, and the AUM capping domain is in pink. The two core domains were aligned and the structures were superimposed. Shown is a side view that is horizontally turned by 180° in the right panel. **(B)** Topology diagrams of chronophin and CAC. The organization of chronophin is shown in gray (left panel). The CAC core domain is depicted in lime and the CAC cap domain is shown in pink (right panel). The β-sheets are numbered consecutively and α-helices are labeled in alphabetical order from the N- to the C-terminus. The position of the nucleophilic Asp25 is marked with a blue star.

Figure 23A shows that, as expected from the high degree of sequence identity (~93%) between human and murine chronophin, the overall structure of the murine CAC hybrid is highly similar to human chronophin. When the Cα-atoms of the full length proteins are aligned, they show a root mean square deviation (RMSD) of 1.1 Å, indicating a high structural homology of the two proteins. The superimposition of only the catalytic cores of the chronophin and CAC structures reveals that the orientation of the capping domain in the CAC hybrid is slightly tilted relative to the catalytic core, resulting in a more open conformation of the cap relative to the core domain. The catalytic domains of the two orthologs are organized in a superimposable manner, consisting of a typical rossmannoid fold composed of seven central parallel β-sheets in a 1-15-14-13-2-5-6 orientation for chronophin and a 1-16-15-14-2-5-6 organization for CAC, which are surrounded by α-helices. When only the amino acids corresponding to the catalytic core of human chronophin (PDB: 2P69) and the catalytic core of murine chronophin in the CAC hybrid (PDB: 4BKM) are

structurally aligned (residues 1-100 and 207-291 in chronophin, or 1-100 and 200-306 in CAC, respectively), a RMSD of 0.582 Å indicates that the introduction of the AUM capping domain has no major impact on the folding of the catalytic core of chronophin.

The overall structures of the AUM and chronophin capping domains are closely related in terms of structural elements and folding with a RMSD of 1.281 Å, although remarkable differences exist (figure 23A). Both caps consist of a central parallel β-sheet in 7-8-9-12 (chronophin) or 8-7-9-10-13 (CAC) orientation, with α-helices (chronophin: E, F, G, H; CAC: F, E, G, H, I) connecting the strands of the sheet (figure 23B). Preceding strand 9 (chronophin) or 10 (CAC), an α-hairpin (residues 181-191 in chronophin, 201-211 in AUM, 190-200 in CAC; Leu204 in AUM corresponds to Leu191 in the CAC hybrid) followed by a helix (H in chronophin, I in CAC) is inserted into the capping domain. In chronophin, this β-hairpin covers the entrance of the active site and harbors the His182 residue (specificity loop). Compared to the orientation of this β-hairpin in the chronophin cap, the corresponding β-hairpin is notably skewed in AUM (figure 23A, open arrow). The AUM cap also features an additional extensive loop (transverse loop) not present in chronophin (residues 140-164 in AUM, 127-151 in CAC; closed arrow in figure 23A).

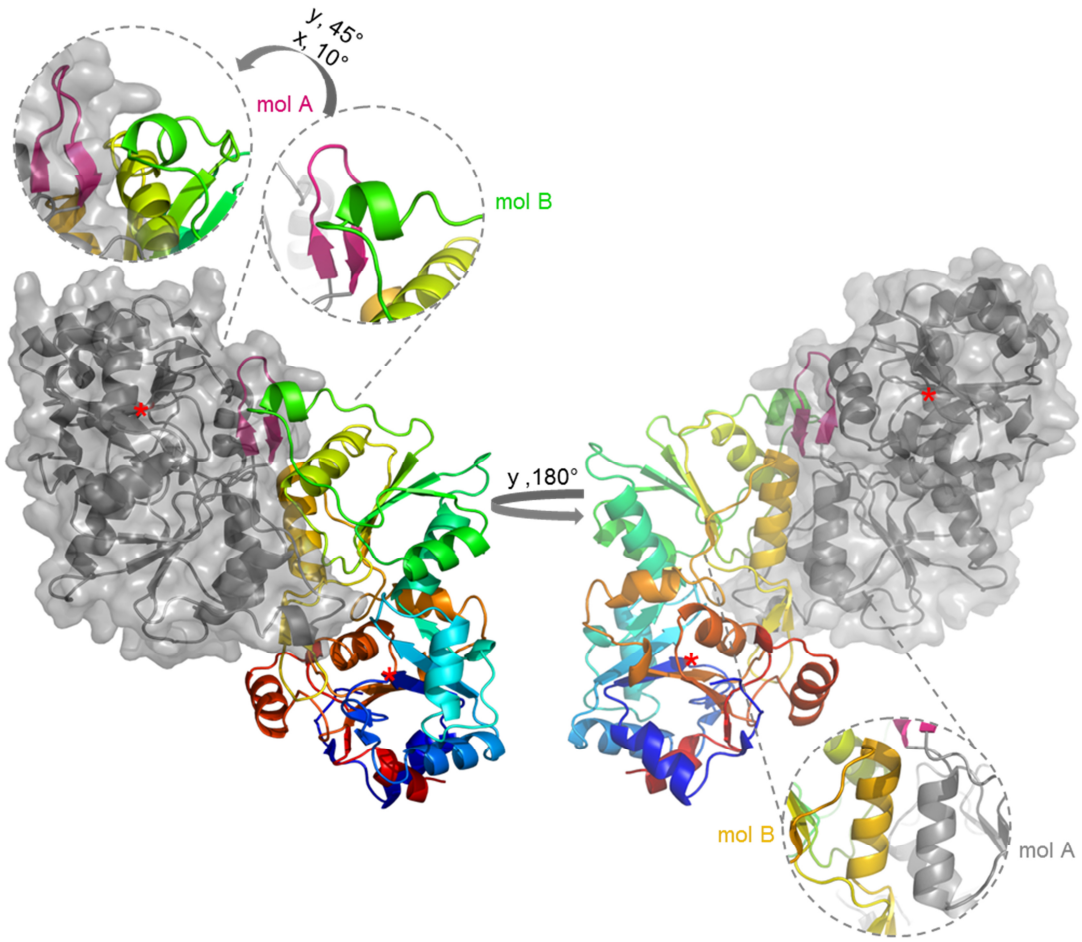

Figure 24: Overall structure of the CAC homodimer.
One protomer (mol A) is represented as a ribbon and surface diagram (gray) with the substrate specificity loop marked in pink. Mol B is depicted in rainbow colors, starting with blue at the N-terminus. Two orientations are given. One insert shows the magnified spatial arrangement of the small helix in the additional, transverse loop of the AUM cap (mol B, green, residues 140 - 143) and the specificity loop of the AUM cap (mol A, pink, residues 190 - 120). The second insert shows helix I (residues 202-214) of mol A (gray) and of mol B (orange) forming the dimer interface. The position of the nucleophilic Asp25 is marked with a red star.

Figure 24 shows the overall orientation of the two CAC protomers in the homodimeric structure. The average AUM homodimer interface buries an accessible surface area of ~1525 Å² [A/B: 1484.8 Å² (ΔiG p-value=0.004), C/D: 1565.3 Å² (ΔiG p-value=0.006)], compared to a chronophin dimer interface of 989.1 Å² (PDB: 2P69). In contrast, the CAC interfaces that form the tetramers have a contact area of <400 Å². A predominantly dimeric state of AUM is also in agreement with size exclusion chromatography and AUC analyses (figure 10). The dimerization of the CAC hybrid is mediated via the AUM capping domain, mainly by helices H and I between strand 9/10 of the β-sheet and following the α-hairpin substrate specificity loop. Interestingly, the additional loop in the AUM cap of molecule A in the dimer is positioned in close proximity to the substrate specificity loop in the molecule B

cap. Arg197 in the β-hairpin and Leu144 in the additional loop (corresponding to Arg201 and Leu157 in AUM) may be important residues for this interaction between two CAC protomers. This characteristic loop in the AUM cap also partially occludes the active site entrance of the adjacent protomer. Thus, both the substrate specificity loop and the large and presumably flexible additional loop are likely to determine AUM phosphatase substrate accessibility and selectivity.

The amino acid residues that form the active site in chronophin vs. the CAC hybrid are shown in figure 25A, with a detailed view of the chronophin/PLP binding interface given in panel I, and the corresponding view of the CAC active site depicted in panel II. The core domain of chronophin contains the conserved motif I (Asp25, Asp27), motif II (Ser58, Ser61), motif III (Lys213) and motif IV (Asp243, Asp238) residues that build up the binding site for the substrate's phosphate moiety and constitute the catalytic machinery in chronophin and most HAD superfamily enzymes. In AUM, motif I consists of Asp34 and Asp36, motif II of Thr67 and Ser70, motif III of Lys235, and motif IV of Asp260 and Asp265. Thus, with the exception of the motif II Thr67 in AUM, all residues that are directly involved in the reaction mechanism are conserved among AUM and chronophin, indicating that these two phosphatases function by the same catalytic mechanism. Asp25/34 most likely makes a nucleophilic attack on the phosphate moiety of the substrate by forming a pentavalent intermediate, and Asp27/36 donates a proton to the leaving group. Ser58 in chronophin, which is replaced by Thr67 in AUM, helps to orient the substrate for nucleophilic attack by forming a hydrogen bond with its transferring phosphoryl group. Interestingly, the presence of an additional methyl group in the AUM Thr residue at this position appears to be critical for AUM *p*NPP activity (see Table 6 and figure 21).

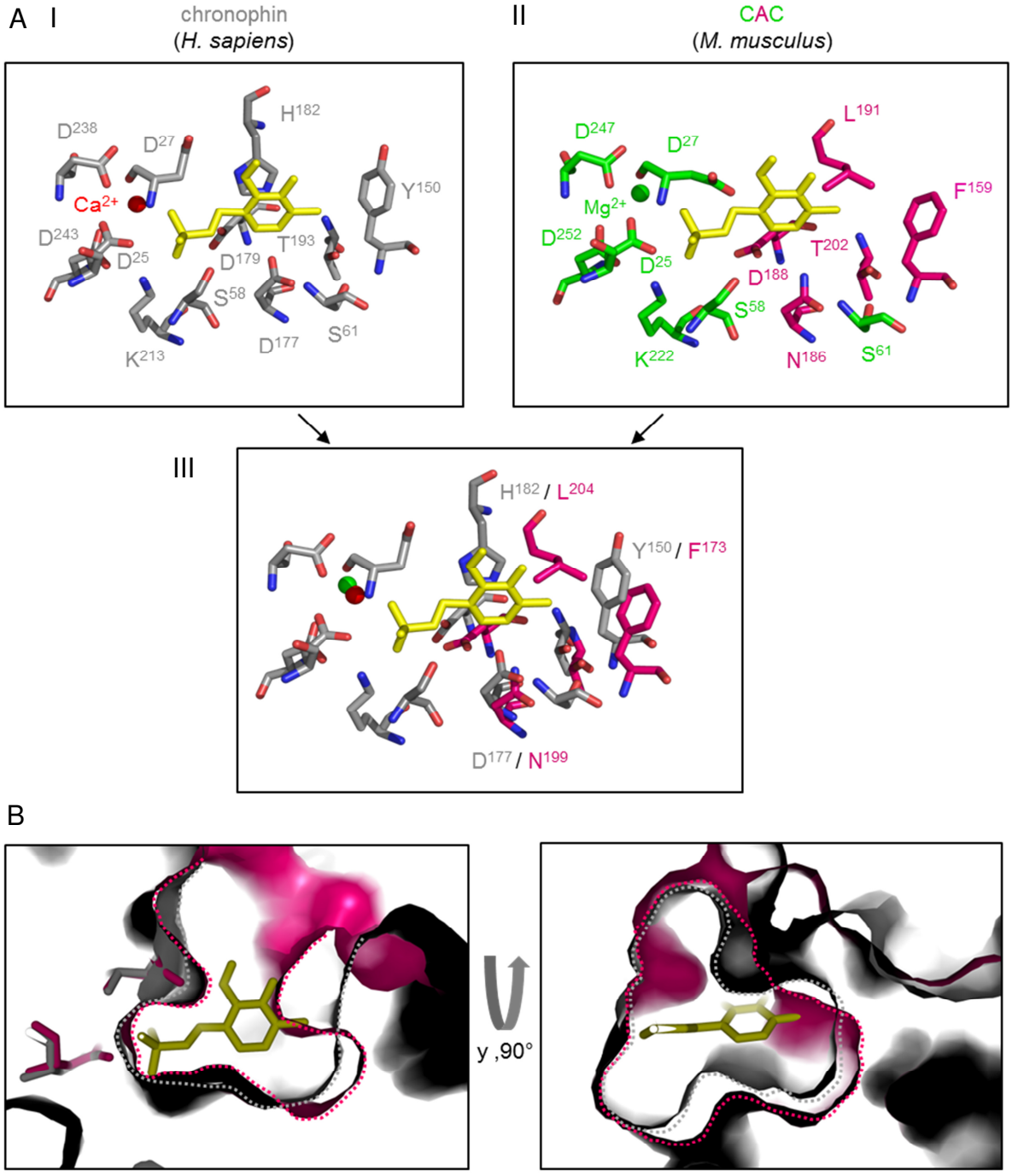

Figure 25: The active site of the human chronophin in comparison to the murine CAC hybrid
(A) I, View of the chronophin/PLP binding interface (PDB: 2P69). PLP is shown in yellow; residues involved in substrate binding are in gray. II, View into the active center of the CAC hybrid (PDB: 4BKM). The catalytic residues of the murine chronophin core domain are shown in green, the residues of the AUM cap domain are shown in magenta. The amino acid residues are labeled according to their position in the CAC hybrid. The PLP molecule (yellow) is modeled according to the human chronophin structure. III, Superposition of the active site residues of human chronophin in the PLP-bound state (gray) and the corresponding residues of the AUM cap domain in the CAC hybrid (magenta). The amino acid residues are labeled according to their position in murine chronophin and in murine AUM, not after their numbering in the CAC hybrid. (**B**) Superposition of the CAC (pink, PDB: 4BKM) and chronophin (gray, PDB: 2P69) active sites as surface representation. Shown is a zoom in the active site underneath the nucleophilic Asp25 (left panel). A lateral view is presented in the right panel. The different spatial arrangements of the substrate binding pocket residues of CAC and chronophin towards PLP are shown.

Residues His182, Asp177, Asp179, Thr193 and Tyr150 in the chronophin cap interact with the chronophin substrate PLP. The imidazole ring of His182 in chronophin directly coordinates and orients the PLP pyridine ring, thus explaining its critical function for substrate recognition (figure 22). His182 is replaced by Leu191 in CAC. Panel II in figure 25A illustrates that the aliphatic Leu is unable to coordinate the PLP pyridine ring. The superposition of the active site residues of chronophin in the PLP-bound state and the corresponding residues of the AUM cap domain of the CAC hybrid (figure 25A, panel III) shows that Leu204 in AUM is also shifted relative to the position of His182 in chronophin. Two other notable amino acid exchanges are the replacement of the acidic Asp177 in chronophin for the charge-neutral Asn186 in CAC (Asn199 in AUM), and the substitution of Tyr150 in chronophin for Phe159 in CAC (Phe173 in AUM).

The topological comparison of the catalytic clefts in chronophin and the CAC hybrid. illustrates that in the CAC hybrid cap, the portion of the active site pocket that is dedicated to substrate recognition is deeper than in the chronophin pocket (figure 25). This result is consistent with the observed AUM phosphatase activity towards the pTyr-mimetic *p*NPP substrate (figure 11) and towards Tyr-phosphorylated peptides and proteins (figure 8), and indicates that in contrast to the shallower binding groove of chronophin, the conformation of the substrate binding pocket of AUM may allow for the accommodation of bulkier pTyr residues.

3.2.5 Phylogenetic analysis of substrate specificity of AUM and chronophin

The substrate selectivities of AUM and chronophin differ substantially. The biochemical and structural analysis reveal that a single amino acid residue in the AUM or chronophin cap domain dictates the specificity of either phosphatase towards low molecular weight substrates. To generalize this approach and to predict residues of specificity, a comparative evolutionary approach was adopted (2.2.1). Regarding the common phylogenetic background of AUM and chronophin, branch-specific rate analysis was performed. If, upon gene duplication, the function of two paralogs changes, sites that determine the substrate preference of an enzyme are typically conserved only in one of the subfamilies (class I residues), or are conserved in both subfamilies, but harbor a different amino acid (class II residues).

Table 7: Sites differently conserved between AUM and chronophin (class II residues).

position in AUM	position in chronophin	amino acid in AUM	amino acid in chronophin	amino acid in *Ciona*	Z-score
204	182	L	H	M	6.88
203	181	R	W	R	6.58
199	177	N	D	N	6.56
128	117	A	G	A	6.55
244	222	V	I	I	5.87
263	241	D	E	N	5.58
178	156	Y	F	Y	5.56
217	195	C	S	C	5.47
101	88	T	S	T	5.35
72	63	K	R	K	5.34
268	246	L	F	F	5.31
136	125	V	A	L	5.00
197	175	G	A	A	4.96
169	147	V	L	L	4.94
226	204	A	S	A	4.80
100	87	G	S	S	4.78

Indeed, 16 positions are notably differently conserved between AUM and chronophin (table 7). Of these, the exchange of histidine in position 182 of chronophin and leucine in position 204 of AUM was identified as the most significant candidate residue with a Z-score of 6.88. Meaning, they are strictly retained in the respective orthologs. In terms of phylogentic analysis this site is a prime candidate for the functional differences between AUM and chronophin. Taken together, the biochemical (3.2.2), structural (3.2.3) and phylogenetic approach clearly demonstrate that this position is critical for the substrate specificity of chronophin and AUM.

Additionally, 15 class II sites have been identified that may be involved in functional differentiation. Mapping these sites on the AUM cap structure (figure 26A) reveals that residues Asp177, Asp179, Thr193 and Tyr150 in the chronophin cap interact with the chronophin substrate PLP. Of the corresponding residues in the CAC cap (Leu191, Asn186, Asp188, Thr202 and Phe159), only Asp188 and Thr202 are conserved between chronophin and AUM. Some differentially conserved residues stand out as candidates involved in the determination of substrate specificity. Asn199 in AUM (Asp177 in chronophin) is located in the substrate recognition part inside the active cleft (see also figure 25A). The replacement of the acidic Asp177 in chronophin for the charge-neutral Asn186 in CAC (Asn199 in AUM), represents a notable amino acid exchange. The residue Arg203 in AUM (Trp181 in chronophin) maps to the substrate specificity loop, but is oriented towards the outer protein surface and may thus function in substrate recognition at the entrance to the active cleft. Similarly, Lys72 in AUM (Arg63 in chronophin, figure 26C, cyan) is located at the entrance to the active pocket (see also figure 21 for biochemical indications on the relevance of this residue). Other differentially conserved residues, including Ala128, Tyr178, Cys217 and

Ala226 in AUM are exposed on the cap surface and may play a role in regulatory protein-protein interactions.

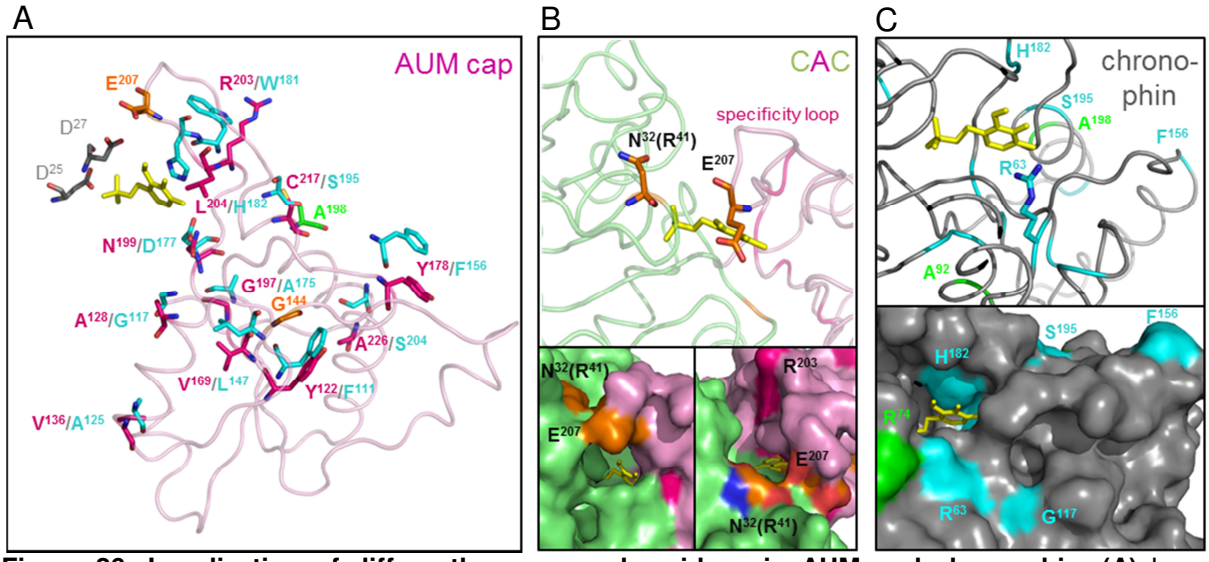

Figure 26: Localization of differently conserved residues in AUM and chronophin. (A) Loop diagram representing the overall structure of the AUM cap domain (in pink; Asp$^{25/27}$ of the chronophin core in gray, PLP in yellow). Differently conserved AUM or chronophin residues are labeled in pink or cyan, respectively (residue numbering according to murine AUM or chronophin). Chronophin residues are shown according to their spatial orientation in the chronophin cap (the chronophin cap is not shown for clarity) after structural alignment with and superimposition onto the CAC structure. Sites conserved in one subfamily, but not in the other are labeled in orange (AUM) or green (chronophin). **(B)** Loop diagram (upper panel) and surface representation (lower panel, two different orientations are shown) of a zoom into the active site of the CAC hybrid (chronophin core domain in lime, AUM cap domain in pink, PLP in yellow). The position of Glu207 in the AUM cap and the putative position of AUM^{Arg41} (corresponding to chronophin^{Asn32}) in the chronophin core is shown in orange. **(C)** Loop diagram (upper panel) and surface representation (lower panel) of a magnification of the active center of human chronophin (PDB code 2P69). Residues differently conserved in chronophin and AUM are marked in cyan.

Sites involved in functional differentiation can also be highly conserved in one paralog, but under poor selection constraint in the other (class I sites; see table 8). Of interest, Glu207 in AUM is positioned on top of the specificity loop and may be involved in initial substrate contact of AUM, but not of chronophin (figure 26B), and Arg41 in AUM is located at the entrance to the active cleft (figure 26B and 21 for biochemical indications on the relevance of this residue). Both residues are conserved in AUM, but not in chronophin.

Table 8: Sites conserved in one family, but not in the other (class I residues)

position in AUM	position in chronophin	amino acid	same rate	high rate in AUM	high rate in chronophin
		in chronophin			
105	92	A	0.04	0.96	0.00
83	74	R	0.04	0.96	0.00
96	83	E	0.05	0.95	0.00
22	13	R	0.14	0.86	0.00
220	198	A	0.20	0.80	0.00
		in AUM			
207	185	E	0.03	0.00	0.97
317	292	P	0.06	0.00	0.94
41	32	R	0.16	0.00	0.84
144	132	G	0.20	0.00	0.80

3.3 Regulation of AUM catalysis

After having elucidated AUM specificity determinants, the next task was to investigate possible regulatory mechanisms that may affect AUM catalysis. In contrast to the regulatory mechanisms conserved in Ser/Thr phosphatases and protein tyrosine phosphatases, it is currently unclear whether -and if so, how- the catalytic activity of HAD phosphatases is regulated. In eukaryotes, the HAD-hydrolase domain can be fused to targeting domains or to other functional domains, thereby regulating e.g. the subcellular localization of the phosphatase or additional (enzymatic) activities (Seifried *et al.*, 2013). In contrast, regulatory domains, subunits or modifications that influence the catalysis of HAD phosphatases have so far not been identified. Arguably the simplest way of modulating intrinsic phosphatase activity is through the posttranslational modification of single amino acid residues, and the potential relevance of such a mechanism was therefore investigated for AUM.

The starting point was the finding that the purified AUM^{WT} enzyme can be activated by reducing agents. *In vitro* AUM phosphatase assays using *p*NPP as a substrate showed an activation upon dithiothreitol (DTT) treatment (figure 27A). The pre-incubation of recombinant, purified AUM with increasing amounts of DTT led to a robust stimulation of AUM-mediated *p*NPP dephosphorylation, with a 10-fold increase of activity. Already 1 µM DTT doubled AUM activity while a maximal activation is observed with 50 µM DTT (figure 27A, B). Similar effects were observed with TCEP and β-MEOH (figure 45).

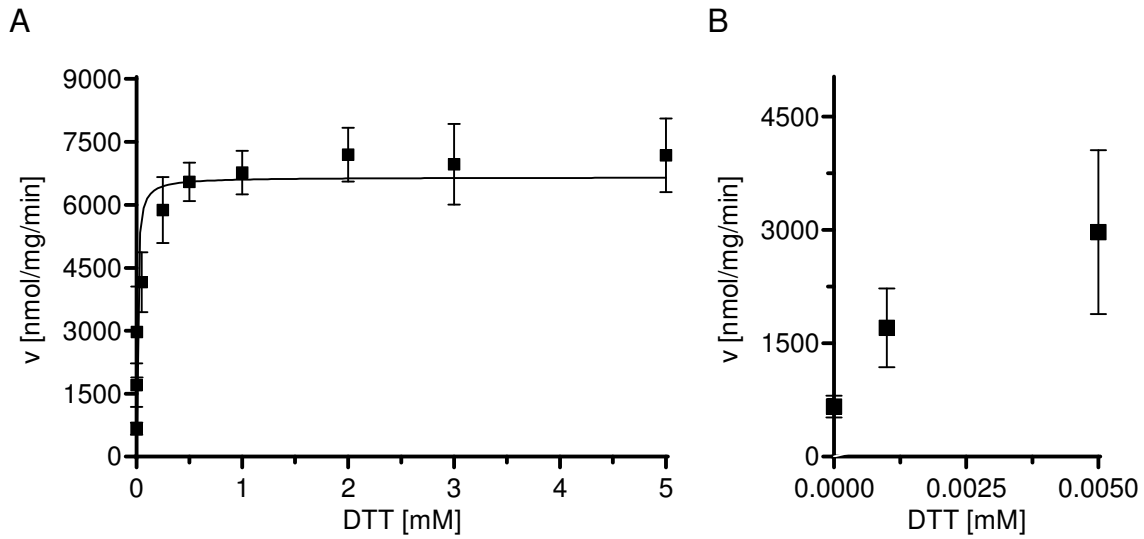

Figure 27: AUM activity increases upon treatment with the reducing agent DTT: (A) Kinetic measurements of the phosphatase activity of the murine AUM with increasing amounts of DTT. Purified AUM^{WT} (0.8 µg) was pre-incubated with 0.001-5 mM of DTT for 30 minutes and the phosphatase activity towards *p*NPP was measured. (**B)** Detail view of A. Results are mean values ± SEM of three independent experiments performed in triplicates with three independently purified protein batches.

In return, the enzyme can be inhibited by the oxidizing agent hydrogen peroxide H_2O_2 (figure 28A). After a pre-incubation of the purified AUM^{WT} with increasing amounts of H_2O_2 the phosphatase activity towards *p*NPP was monitored. Already 41 µM H_2O_2 reduced AUM activity by half, and AUM activity was completely abolished at a concentration of 1 mM H_2O_2.

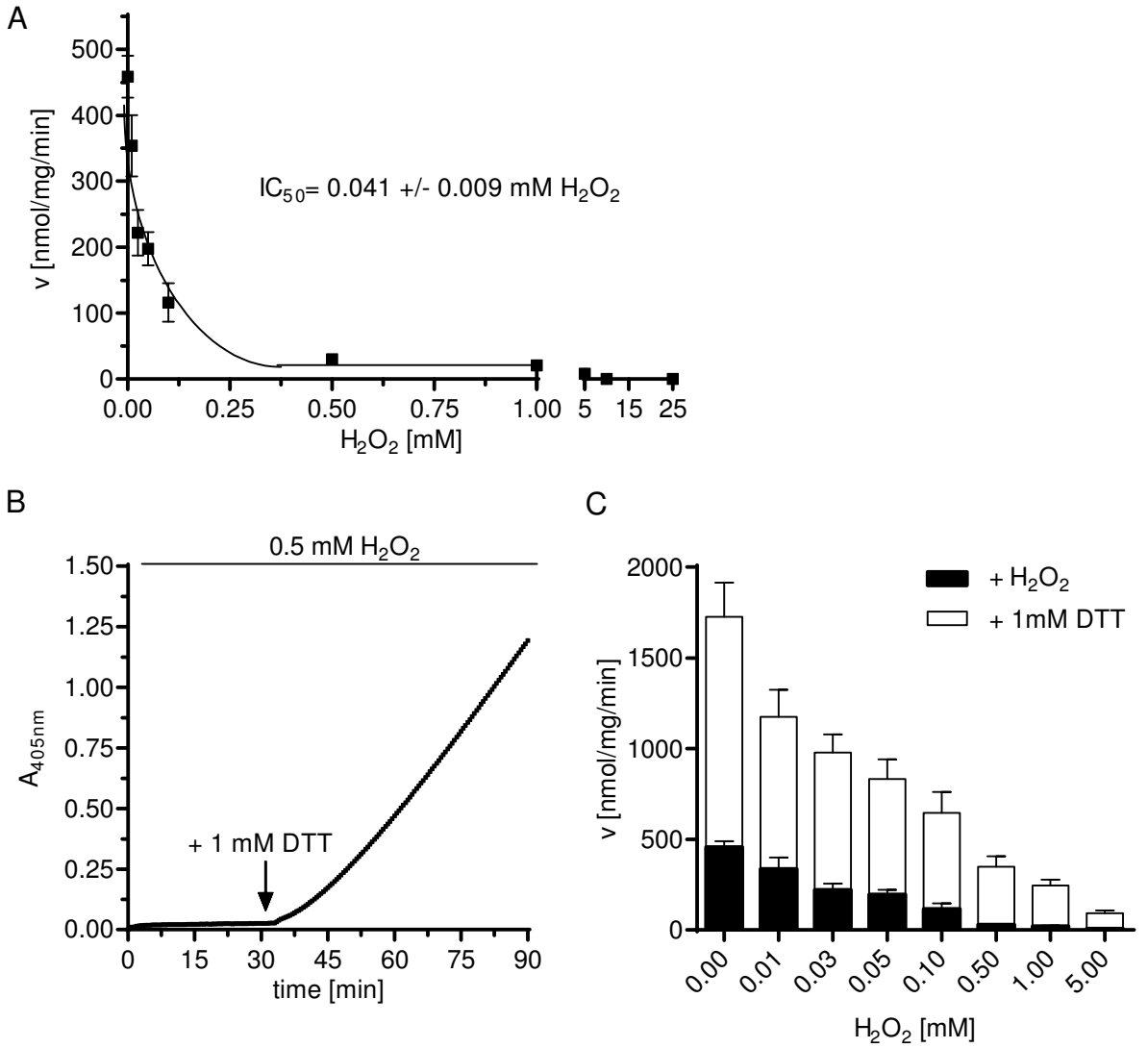

Figure 28: Hydrogen peroxide inhibits AUM, and AUM activity can be recovered with DTT. (A) *In vitro p*NPP assay with increasing amounts of H_2O_2. Purified AUM^{WT} (0.8 µg) was pre-incubated with 0.01-25 mM of H_2O_2 for 30 minutes. **(B)** Shown is an *in vitro* phosphatase assay with AUM^{WT} using *p*NPP as a substrate. The enzyme was pre-incubated with 0.5 mM H_2O_2 for 30 minutes. Afterwards, the generation of the dephosphorylated product *p*NP is measured colorimetrically over time at $A_{405\ nm}$. After 30 minutes 1 mM DTT was added (arrowhead) and phosphatase activity was continuously monitored for 1 hour. **(C)** Inhibition of AUM activity by H_2O_2 can be relieved by the addition of DTT. AUM^{WT} was pre-incubated with increasing amounts of H_2O_2 for 30 minutes, and phosphatase activity was detected over 30 minutes (black columns). Afterwards, 1 mM of DTT was added, and phosphatase activity was monitored over 30 minutes (clear columns). The black bar at 0 mM H_2O_2 represents basal AUM activity in the absence of DTT. Results of A and C are mean values ± SEM of three independent experiments performed in triplicates with three independently purified protein batches.

As a next step it was tested whether the inhibition of AUM activity in the presence of oxidizing agents can be counteracted upon treatment with reducing agents. For this, AUM was pre-incubated with increasing amounts of H_2O_2 and phosphatase activity was monitored using *p*NPP as a substrate. After a measurement period of 30 minutes, 1 mM of DTT was added. AUM^{WT} activity immediately increased upon DTT addition, as shown in the $A_{405\ nm}$ measurement of a single experiment in figure 28B. AUM^{WT} activity was partly recovered by

DTT addition after inhibition with up to 5 mM H_2O_2 (figure 28C). The reversibility of the H_2O_2-mediated AUM inhibition leads to the hypothesis that AUM can be regulated by reversible oxidation. The difference in AUM activation in figure 27A and 28C can be explained with the differences in the experimental setup (2.2.6.1).

3.3.1 Generation of AUM mutants

Redox modifications of proteins mostly occur at thiol groups. The amino acids cysteine and methionine contain reactive thiol groups that can confer redox sensitivity to proteins (Lizama-Manibusan and McLaughlin, 2013). Similarly, the amino acid histidine is a good target, although only few examples of this kind of modification are known (Takayama *et al.*, 2008). In addition, less reactive amino acids including tyrosine, phenylalanine, valine, proline, arginine and tryptophane can be oxidized (Dean *et al.*, 1997; Davies, 2005). The majority of oxidative protein modifications are observed at cysteine, methionine, tyrosine, and tryptophane residues (Rinalducci *et al.*, 2008). However, only the oxidation of cysteines (to cysteine sulfenic acid) and methionines (to methionine sulfoxide) are reversible. Cysteine oxidation can be induced by hydrogen peroxide, superoxide, nitric oxide and derivatives and highly reactive species such as hydroxyl radicals (Jacob *et al.*, 2004). The reversible oxidation of the active site cysteine in the PTPs is a well-known, key regulatory mechanism in this family of tyrosine phosphatases (Ostman *et al.*, 2011). For chronophin, the closest homolog of AUM, a reactive cysteine has been described in the active center (Gao and Fonda, 1994) but the potential involvement of this residue in redox regulation has not been addressed. To elucidate the possible mechanism underlying reversible oxidation and to identify the reactive amino acid(s), the cysteine residues of AUM were analyzed.

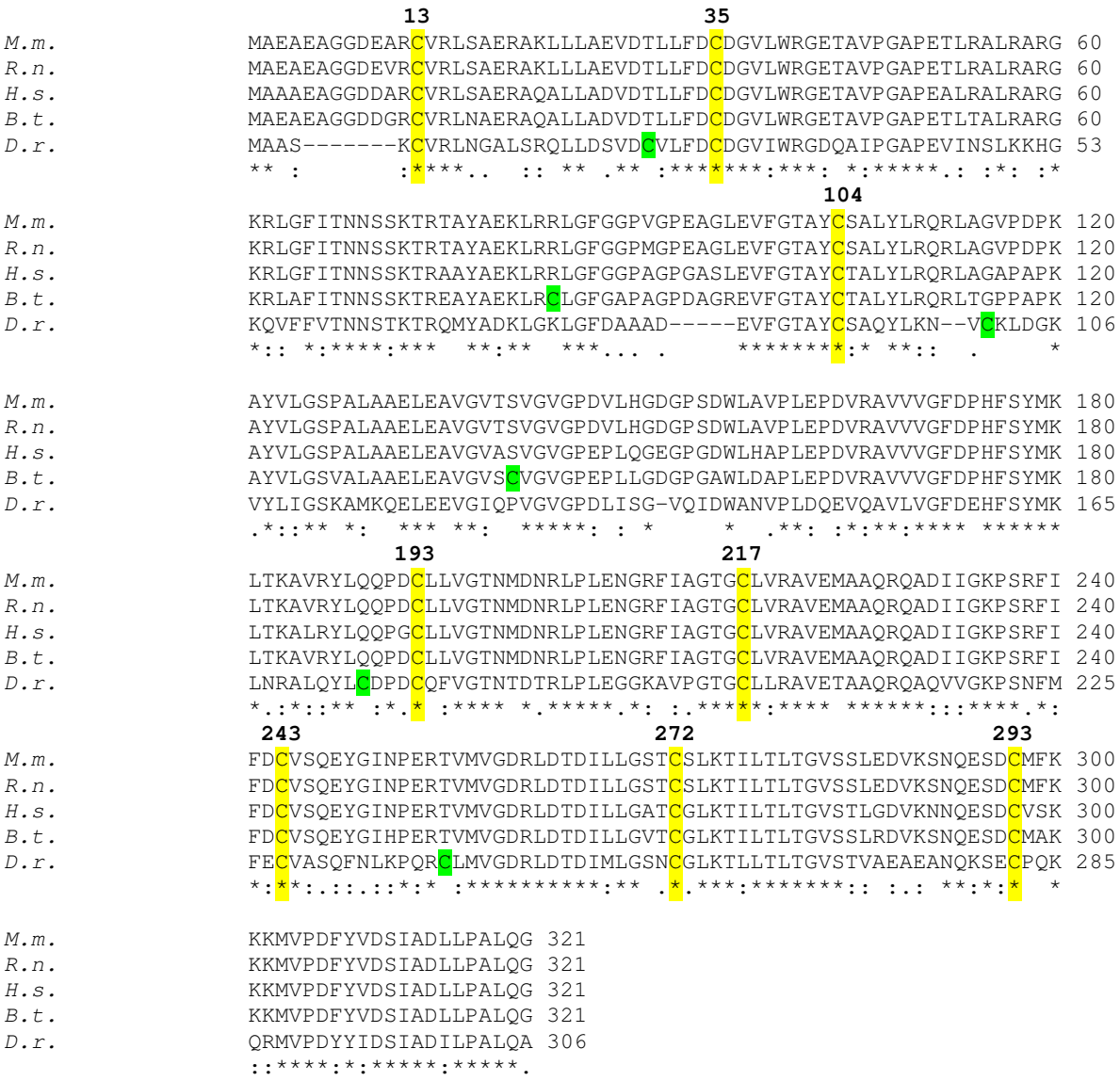

Figure 30: Conserved cysteine residues in different AUM species.
Conserved cysteine residues are marked in yellow, non-conserved cysteine residues are marked in green. The alignment was performed with ClustalW. (*M.m.: Mus musculus, R.n: Rattus norvergicus, H.s.: Homo sapiens, B. t.: Bos taurus, D.r.: Danio rerio*)

AUM harbors eight cysteine residues which are conserved in vertebrates (figure 30). The cysteine residues at position 13, 35, 104, 243, 272, 293 (numbering according to murine AUM) are located in the core domain, while residues 193, 217 are located in the cap domain of the phosphatase. Cys217 was identified as residue contributing to the dimer interface (figure 24), and it was also identified as a site differently conserved between AUM and chronophin (table 7). For a first analysis, all cysteine residues in AUM were successively exchanged to a serine (CS mutants). In this project the following mutants were generated:

Table 9: Cysteine to serine substitutions in murine AUM
core domain
AUM^{C13s}
AUM^{C35S}
AUM^{C104S}
AUM^{C243S}
AUM^{C272S}
AUM^{C293S}
$AUM^{C35S; C104S}$
$AUM^{C104S; C243S}$
cap domain
AUM^{C193S}
AUM^{C217S}

All cysteine residues in AUM were exchanged to a serine via site-directed mutagenesis, using pETM11_AUM as a template (2.2.2.1). The resulting single or double point mutants were produced in *E. coli* and purified via affinity- and size exclusion chromatography (2.2.3, figure 31).

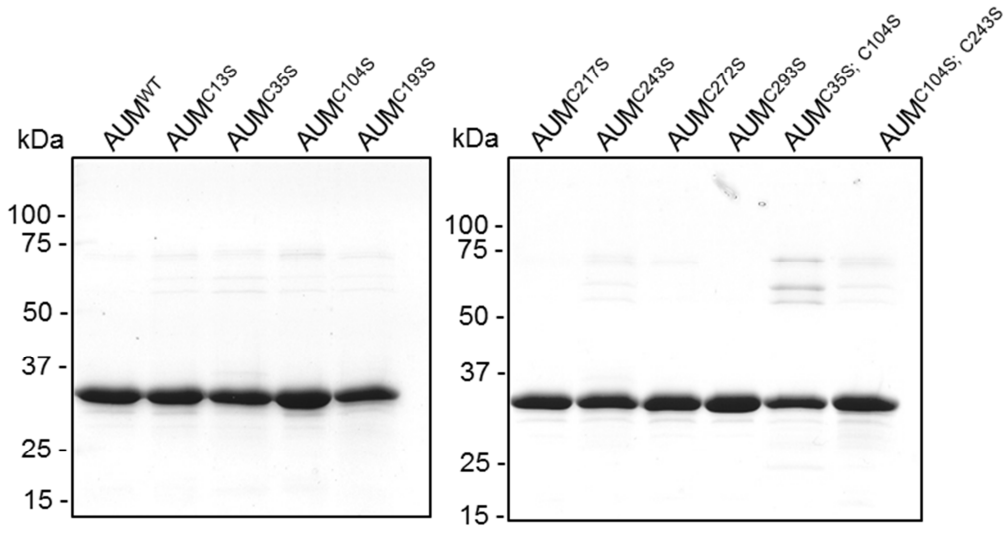

Figure 31: Purity of the employed, recombinant AUM cysteine to serine mutants.
Shown are Coomassie Brilliant Blue stained gels.

3.3.2 Enzymatic activity measurements

To elucidate the impact of the cysteine residue replacements on the phosphatase activity of AUM, *in vitro p*NPP assays were performed in the absence and presence of DTT (2.2.6.1).

The substitution of each cysteine led to a change in phosphatase activity compared to the AUM^{WT} enzyme. The basal activity of AUM^{C13S}, AUM^{C193S}, AUM^{C217S}, AUM^{C243S}, $AUM^{C104; 243S}$ was attenuated compared to the wildtype enzyme, and the phosphatase activity of the AUM^{C35S} and $AUM^{C35S; C104S}$ was almost abolished. In contrast, the AUM^{C104S}, AUM^{C272S} and AUM^{C293S} mutants showed enhanced *p*NPP phosphatase activity compared to AUM^{WT} (figure 32A).

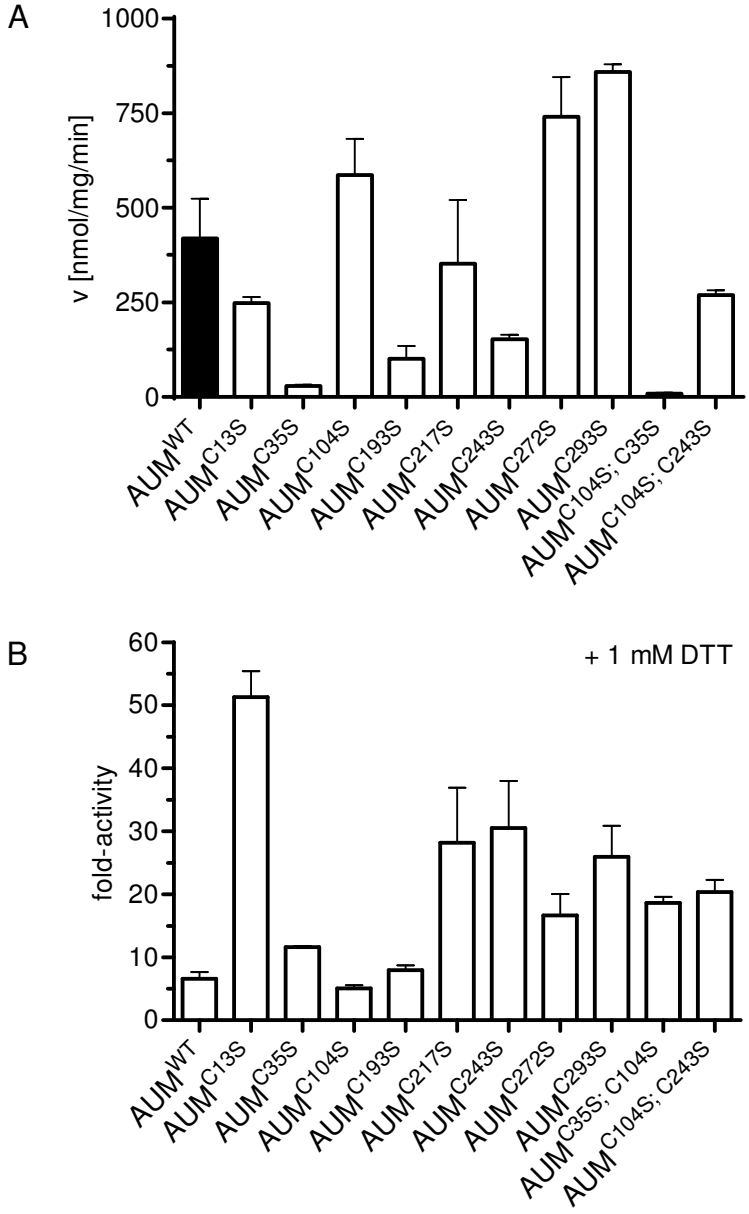

Figure 32: The tested cysteine to serine mutations influence *p*NPP phosphatase activity of AUM, while none of the mutations led to a loss of DTT-induced AUM activation. (A) Velocity of *p*NPP dephosphorylation of AUM and the CS mutants (0.8 µg) in the presence of 3.5 mM *p*NPP. **(B**) Fold-activation of the phosphatase activity of AUM and the CS mutants in the presence of 1 mM DTT. Results are mean values ± SEM of three independent experiments performed in triplicates with two independently purified protein batches.

To test if a cysteine substitution results in a loss of sensitivity towards reducing agents, phosphatase activity was measured after DTT addition (figure 32B). Although the basal activity of the AUM-CS mutants compared to the wildtype enzyme was changed, each mutant showed an increase of phosphatase activity under reduced conditions compared to non DTT-treated conditions. AUM^{C35S}, AUM^{C104S}, AUM^{C193S} and AUM^{WT} showed a <10-fold activation upon treatment with reducing agents. All other AUM-CS mutants showed an increased activation compared to AUM^{WT}: AUM^{C35S}, AUM^{C272S}, $AUM^{C104S;\ C243S}$ showed >10<21-fold activation, AUM^{C217S}, AUM^{C293S} and AUM^{C35}S; C104S showed >21<30 fold activation, AUM^{C13S} and AUM^{C243S} showed >30 fold activation. The maximal activation of the AUM-CS mutants upon DTT treatment is summarized in table 10 and dose response curves are given in the supplement (figure 46).

Table 10: Maximal activation of AUM-wildtype and AUM-mutant phosphatase activity upon DTT treatment.

	max. fold of activation
AUM^{WT}	7.35 +/- 0.54
AUM^{C13S}	48.73 +/- 2.20
AUM^{C35S}	16.44 +/- 1.80
AUM^{C104S}	5.00 +/- 0.28
AUM^{C193S}	7.75 +/- 0.59
AUM^{C217S}	24.45 +/- 3.38
AUM^{C243S}	44.54 +/- 3.66
AUM^{C272S}	16.11 +/- 0.09
AUM^{C293S}	27.25 +/- 2.35
$AUM^{C35S;\ C104S}$	25.96 +/- 4.60
$AUM^{C104S;\ C243S}$	20.70 +/- 1.11

Since all CS mutants showed increased activity upon DTT treatment, the reactive residue(s) could not be unequivocally identified with this type of experiments. As a next step it was analyzed, if oxidizing conditions lead to an inhibition of the CS mutants. The enzymes were pre-incubated with increasing amounts of H_2O_2 (0.01-5 mM) for 30 minutes and *p*NPP phosphatase activity was monitored (figure 33). The mutants AUM^{C13S}, AUM^{C193S}, AUM^{C217S}, AUM^{C272S} and AUM^{C293S} were as sensitive to H_2O_2 as AUM^{WT}, and enzyme activity was abolished upon treatment with 1 mM H_2O_2 (figure 33A). In contrast, the mutants AUM^{C35S}, AUM^{C104S} and AUM^{C243S} were less sensitive to oxidation-induced inhibition. A minor phosphatase activity could be detected even at a concentration of 5 mM H_2O_2 (figure 33B). These results indicate that the cysteines C35, C104 and C243 are likely the target residues of interest, because the loss of their thiol groups protects the enzyme from complete oxidation-induced inhibition.

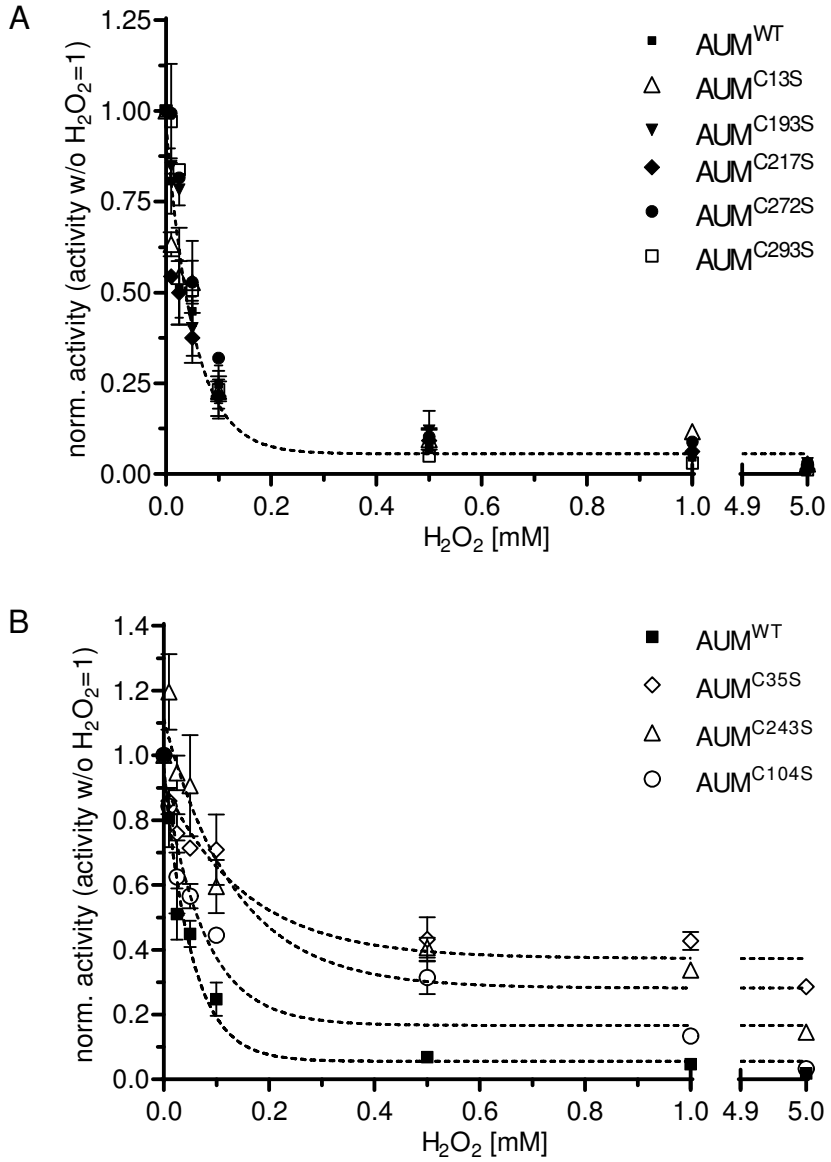

Figure 33: Oxidation inhibits AUM CS mutants in a differential manner. *In vitro p*NPP phosphatase assays of the purified AUM^{WT}, AUM^{C13S}, AUM^{C193S}, AUM^{C217S}, AUM^{C272S}, AUM^{C293S} mutants **(A)** and of AUM^{C35S}, AUM^{C243S}, AUM^{C104S} mutants **(B)** in the presence of increasing amounts of H_2O_2 (0.01-5 mM). Shown are normalized values, with the activity without inhibitor set to 1. Results are mean values ± SEM of three independent experiments performed in triplicates with three independently purified protein batches.

Nevertheless, this single cysteine to serine mutants are still sensitive to oxidation-induced inhibition, leading to the idea that more than one cysteine is responsible for the effect. Therefore, these mutations were combined. The double mutants AUM$^{C35S;\ C104S}$ and AUM$^{C104S;\ C243S}$ were generated, and the proteins were recombinantly expressed as described, and *in vitro p*NPP assays were performed (figures 31, 32).

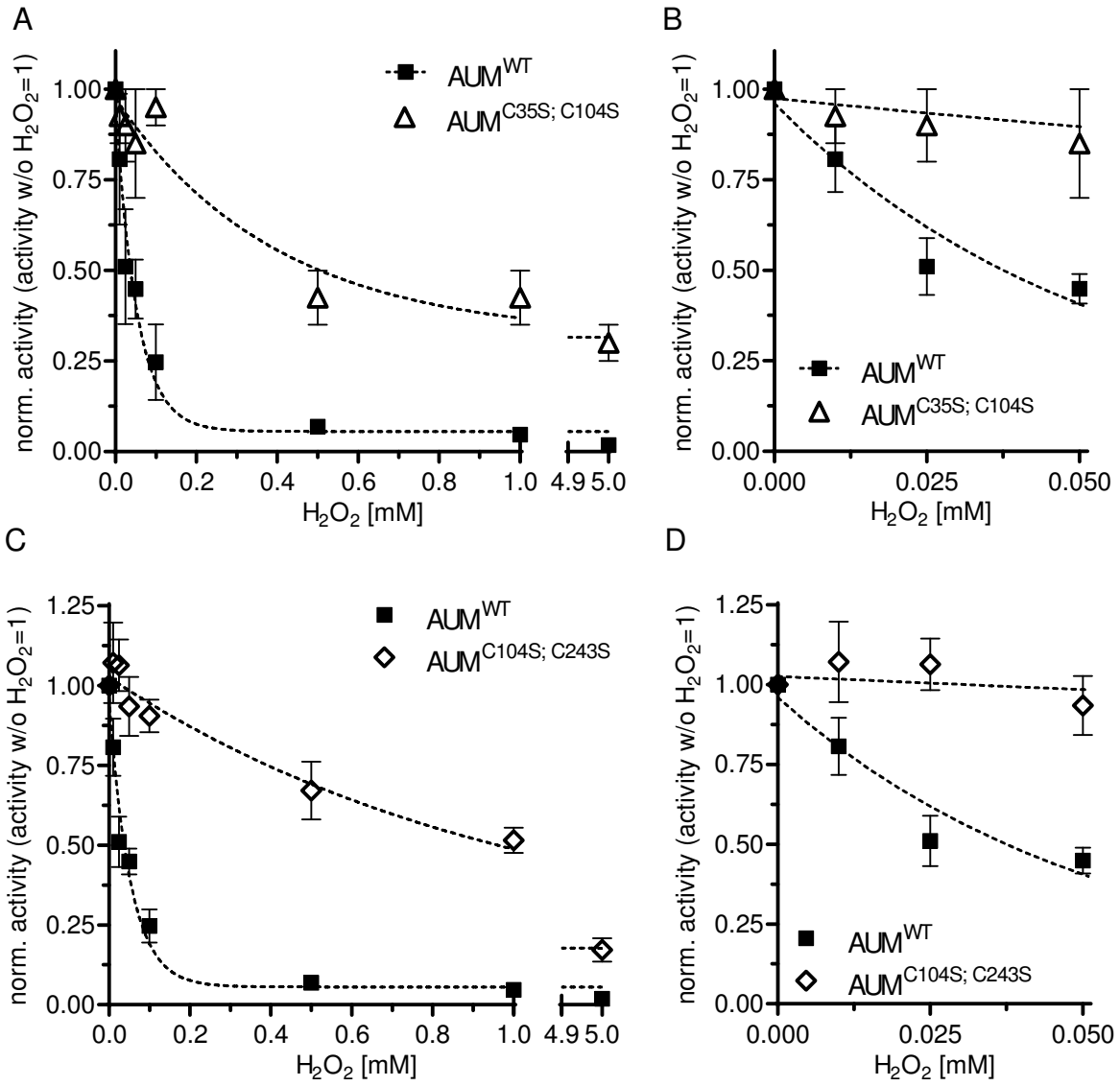

Figure 34: Sensitivity of the double mutants AUM$^{C35S; C104S}$ and AUM$^{C104S; C243S}$ to oxidation. **(A)** AUM$^{C34S; C104S}$ and AUM^{WT} phosphatase activity in the presence of H_2O_2 (0.01–5 mM) was measured in *in vitro* *p*NPP assays. **(B)** Detail view of A. **(C)** *p*NPP activity assay of AUM$^{C104S; C243S}$ and AUM^{WT} in the presence of increasing concentrations of H_2O_2. **(D)** Detail view of C. Shown are normalized values, and the phosphatase activity in the absence of H_2O_2 was set to 1. Results are mean values ± SEM of three independent experiments performed in triplicates with three independently purified protein batches.

Strikingly, the double mutants showed little sensitivity towards H_2O_2 treatment in comparison to the AUM^{WT} and the single point mutants AUM^{C35S}, AUM^{C104S} and AUM^{C243S} (figure 34A). Remarkably, the enzymes could not be inhibited with low concentrations of H_2O_2 (figure 34B, D). The IC_{50} for AUM^{WT} was determined as 41 µM H_2O_2 (figure 28A). In contrast, at a concentration of 50 µM H_2O_2, AUM$^{C35S; C104S}$ and AUM$^{C104S; C243S}$ were not inhibited at all.

These results lead to the conclusion, that all three cysteine residues (Cys35, Cys104, Cys243) are responsible for the inhibitory effect of H_2O_2 on AUM phosphatase activity.
To test the reversibility of the H_2O_2-induced effects, the different AUM-CS mutants were first treated with H_2O_2, and then subjected to an incubation with 1 mM of DTT, followed by the measurement of phosphatase activity.

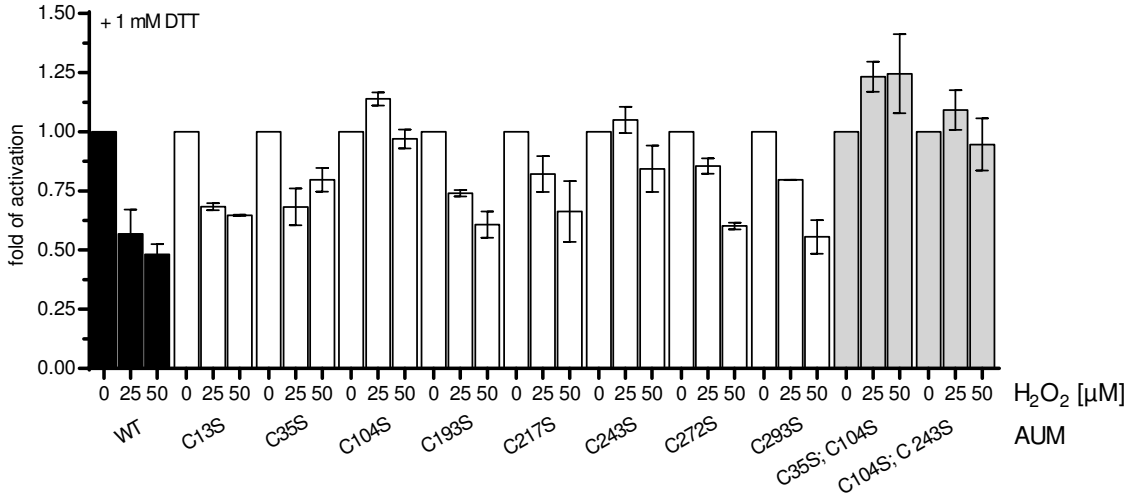

Figure 35: Reversible oxidation of the CS mutants. AUM^{WT} and the CS mutants were pre-incubated with 25 and 50 µM of H_2O_2 for 30 minutes. Phosphatase activity was detected over 30 minutes, followed by an addition of 1 mM DTT. The activation upon DTT treatment after inhibition is shown for AUM^{WT} (black), the single point mutants (white) and the double mutants (gray). Shown are normalized values, activity without inhibitor was set to 1. Results are mean values ± SEM of three independent experiments performed in triplicates with two independently purified protein batches

The H_2O_2-inhibited phosphatase activities of AUM^{WT} and AUM^{C13S}, AUM^{C35S}, AUM^{C193S}, AUM^{C217S}, AUM^{C272} andAUM^{C293S} were only partially recovered by DTT compared to the non-H_2O_2-pretreated enzymes (figure 35). The phosphatase activities of AUM^{C104S} and AUM^{C243S} (the mutants that showed reduced sensitivity towards oxidation, see figure 33B), were similar in the absence and presence of 25 and 50 µM H_2O_2. The DTT-stimulated activation of the double mutants $AUM^{C35S; C104S}$ and $AUM^{C104S; C243S}$, which were also not inhibited by 25 or 50 µM H_2O_2, was comparable to the non-H_2O_2-treated enzyme (figure 47 shows the complete range of tested H_2O_2 concentrations for each mutant).
To summarize, the residues Cys35, Cys104 and Cys243 are clearly responsible for AUM sensitivity towards oxidation. However, these data do not allow to pinpoint which one(s) of these residues are required for DTT-dependent re-activation of AUM phosphatase activity. The analysis of the X-ray crystal structures of chronophin and the CAC mutant, as well as the amino acid sequence alignments of chronophin and AUM shows that Cys35 has a prominent position located in between the nucleophile Asp34 and Asp36 (figure 30). The oxidation of Cys35 might influence the nucleophilic nature of Asp34 as well as the function of Asp36 during dephosphorylation. In contrast, the residues Cys104 and Cys243 are not located in

the active site of the enzyme, but rather expected to be exposed on the surface of the enzyme. The corresponding Cys residues of chronophin build a disulfide bridge, thereby connecting the cap with the core domain (figure 34). Upon a redox switch, this connection might be broken and so a change of enzyme flexibility might occur. To test this possible open/close mechanism for AUM, the impact of reduction and oxidation on structure and folding was investigated.

3.3.3 Impact of redox changes on structure and folding

As described earlier in this thesis, AUM exists as a stable dimer in solution, which can transiently form tetramers (figure 10). In addition, the CAC hybrid of chronophin and AUM crystallized as a dimer (figure 24). An assembly of higher oligomers can be mandatory for enzyme activation (Marianayagam *et al.*, 2004; Neet and Timm, 1994), and it is well-known that oligomerization can be mediated by disulfide-bridges between the protomers. To elucidate the potential role of the cysteine residues of AUM for oligomerization, SEC with the AUM^{WT} enzyme in the presence of 5 mM DTT was performed (figure 36). No monomeric species were observed, and only a small increase of the dimeric species was detected under reducing conditions. A redox status-dependent dimerization of AUM can therefore be excluded. Interestingly, a reduction of the tetramer species was observed in the presence of DTT, indicating a role of (a) cysteine(s) for tetramerization. To confirm this, SEC profiles of all CS mutants were generated. Only the elution profile of the AUM^{C293S} mutant was consistent with a lack of tetrameric species (figure 36 inset). These results thus clearly show that Cys293 is responsible for the tetramerization of AUM.

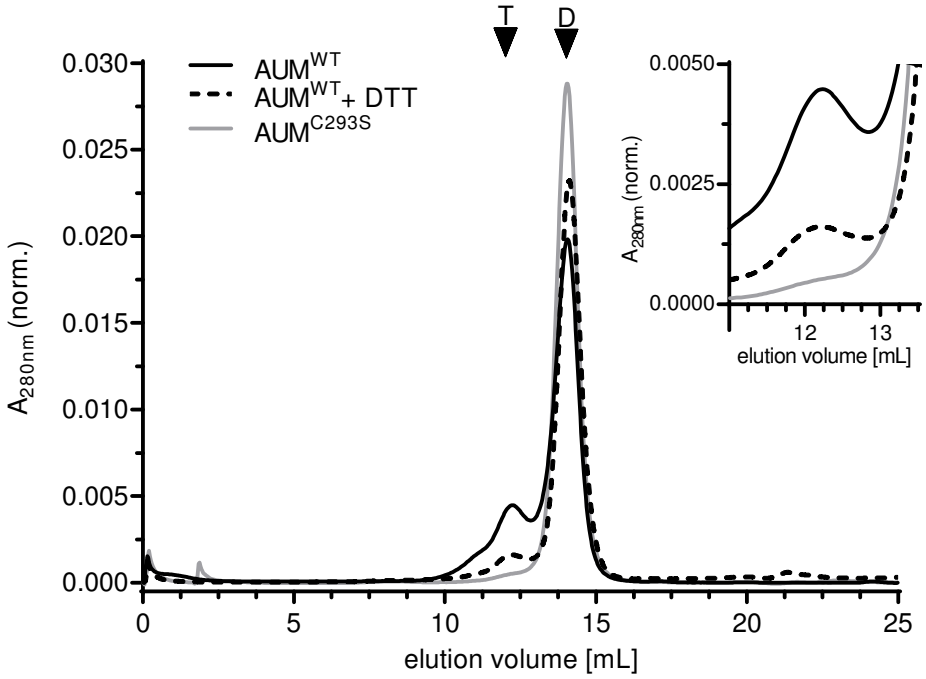

Figure 36: Cysteine 293 is responsible for the tetramerization of AUM. Elution profile of purified, untagged murine AUM (black line), AUM pre-treated with 5 mM DTT (dashed line) and AUM^{C293S} (gray line) after size exclusion chromatography (Superdex 200 10/300 GL). The inset shows a detail view of the elution profiles at volumes corresponding to the tetramer peak of AUM^{WT}.

As shown, Cys293 has an effect on the oligomerization of AUM, but the cysteine in this position has no impact on the redox mediated activity switch (figure 32, 33, 35). The findings of Cys104 and Cys243 are targets for oxidation point to the possibility that an intramolecular disulfide bond is responsible for AUM activation and inhibition. To test potential structural changes upon a redox switch, CD spectroscopy was performed. This technique monitors structural changes in proteins (Zhukova *et al.*, 2004; Link *et al.*, 1996). For this, AUM^{WT} was measured under reducing and oxidizing conditions in two buffer systems: the assay buffer in which the whole mechanism was analyzed (TMN), and a phosphate buffer (PB), an ideal buffer to perform CD spectroscopy. It has to be noted, that DTT itself has UV absorbance properties and so disturbs the measurement at high concentrations. Because of this, the appropriate buffer controls are shown to exclude artefacts due to the use of DTT. The WT enzyme shows the same spectrum (compare also to figure 17 A) in both buffer conditions (blue and yellow symbols, figure 37). Next, the WT enzyme was pre-incubated with 5 mM of H_2O_2, the molar concentration of H_2O_2 that led to complete inhibition of phosphatase activity (figure 32). Upon oxidation a small positive shift at 222 nm is observed in TMN buffer as well as in phosphhate buffer (green symbols). To reach maximal AUM activation, 5 mM DTT were used. Strikingly, the reduction of AUM led to a large negative shift at a wavelength of

222 nm, suggesting an intramolecular rearrangement (orange symbols). In conclusion, a redox switch induces a structural change in AUM supporting the hypothesis of the open/close mechanism mediated via an intramolecular disulfide.

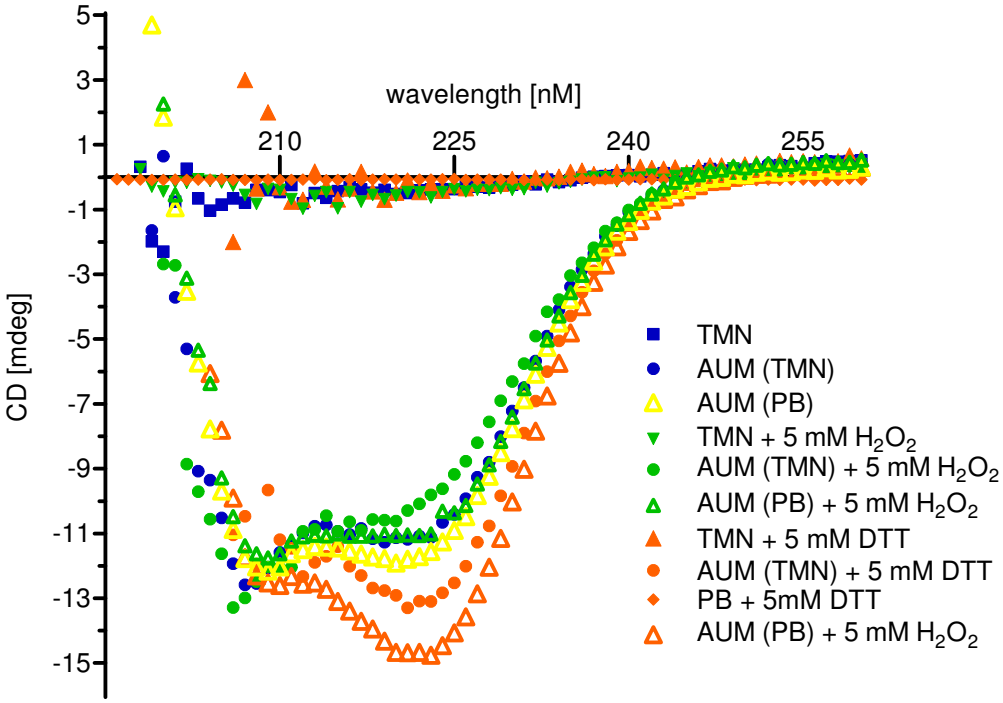

Figure 37: CD-spectroscopy analysis of AUM in different redox states. Shown is the CD-spectroscopy analysis of recombinant, purified murine AUM in TMN or phosphate buffer (blue and yellow symbols), subjected to 5 mM of H_2O_2 (green symbols) or DTT treated (5 mM, orange symbols).

3.3.4 Fractionation based AUM phosphatase activity assay

To determine the potential role of AUM modifications in a cellular system, an *in vivo* assay as an AUM activity readout was developed. The biological substrate of AUM is unknown, therefore its dephosphorylation cannot be measured. *p*NPP was described as a suitable substrate to monitor AUM phosphatase activity with recombinant purified protein (figure 11). However, since *p*NPP acts as a general substrate for phosphatases, it cannot be used for whole cell lysates to specifically measure AUM activity. Another option would be the activation of AUM via DTT to create a more intense signal. However, phosphatase activation via reducing agents is an established mechanism for the family of PTPs (1.3). That is why DTT treatment would not only enhance AUM activity but also the activity of several members of the PTPs. Still, *p*NPP and DTT are currently the only available tools to monitor AUM activity. To create a specific AUM readout, cellular AUM has to be partly separated or enriched to exclude other *p*NPP-phosphatases that are sensitive to DTT. As a strategy, a fractionation based activity assay was designed.

3.3.4.1 Experimental setup

To separate endogenous AUM of whole cell lysates, size exclusion chromatography was used. This method represents a mild separation of proteins via size with no influence on the native folding of the enzymes. Furthermore it was shown, that AUM activity is not influenced upon SEC. In activity assays with purified enzyme the TMN buffer system was found to be ideal to measure AUM activity towards *p*NPP. For the fractionation based activity assay the TMN "FRACTIO" buffer was composed of 30 mM TEA, 1 mM $MgCl_2$, 50 mM NaCl, 10 µg/mL aprotinin, 10 µg/mL leupeptin, 1 mM pepstatin, 1 mM Pefabloc at pH 7.5. To test endogenous AUM activity, cells with or without AUM were cultured in full medium without additional stimulus (2.2.6.3). When confluence was reached the cells were trypsinized and counted. Afterwards, equal numbers of cells were pelleted and resuspended in 75 µL ice cold TMN FRACTIO. Cell lysis was performed in the absence of detergents by repeatedly drawing the cell suspensions into a syringe. Afterwards, cell debris were removed via centrifugation and the cleared lysates were inserted into a 1 ml loop connected to the ÄKTApurifier FPLC system. For SEC a column with a small bed volume was used (24 mL, Superdex 200 10/300 GL) to keep dilution as small as possible. Before injection of the lysate the column was equilibrated with one column volume of TMN FRACTIO. Afterwards the proteins were eluted with a constant flow of 0.7 mL/min. The eluting proteins were collected in a volume of 1 mL resulting in 24 fractions. As a next step *p*NPP-phosphatase activity was measured in each fraction. For this 100 µL of each fraction was pipetted into a well of a 96 well plate. Next, 2 µL of *p*NPP and 2 µL of *p*NPP substrate buffer were added. The 96 well plate was incubated for 30 minutes at 37 °C and phosphatase activity was monitored at A_{405nm}. To detect in which fraction AUM elutes from the column, immunoblotting was performed. 20 µL of each fraction were separated on a SDS-PAGE, proteins were transferred to a nitrocellulose membrane and AUM was detected with the generated full length α-AUM antibody (3.1.3).

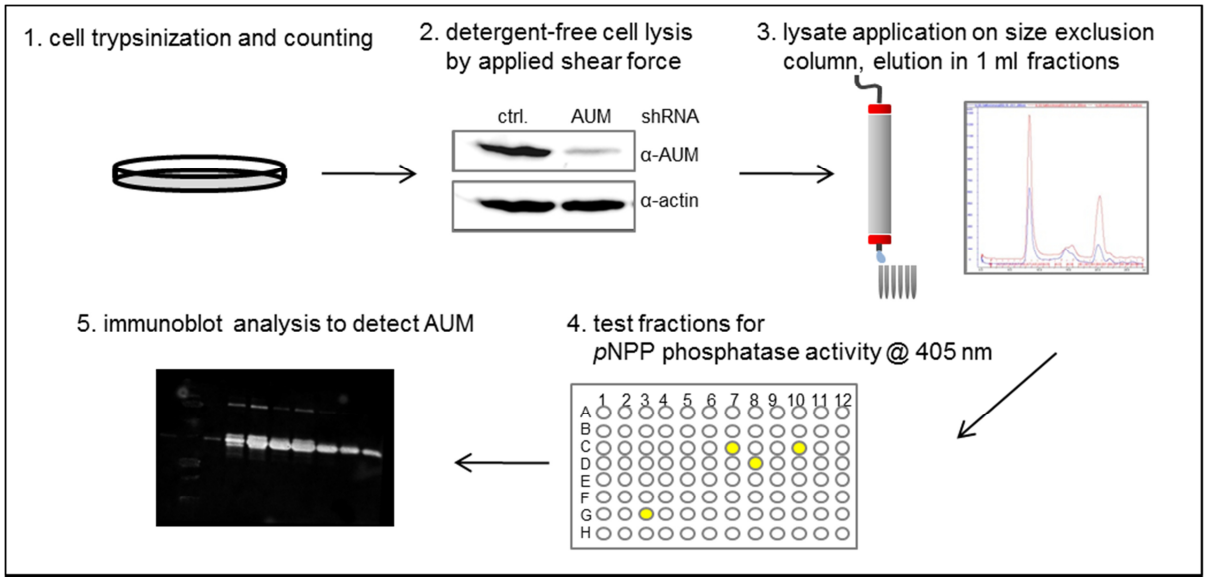

Figure 38: Experimental setup of the fractionation based AUM phosphatase activity assay.

3.3.4.2 Activity assay in cell lines and primary cells

As shown in 3.1.3 the mouse spermatogonial cell line GC1 spg expresses high levels of AUM. To validate the assay setup, a GC1 spg/ctrl. shRNA and GC1 spg/AUM shRNA cell line were used (PhD thesis, P. Duraphe). AUM expression was down-regulated via RNA interference (figure 39A). Cells were trypsinized and 5 million cells per cell line were subjected to cell lysis. As described, lysates were fractionated via size exclusion chromatography. GC1 spg/ctrl. shRNA and GC1 spg/AUM shRNA lysates showed an identical elution profile at $A_{280\ nm}$, indicating equal protein amounts (figure 39B). Afterwards, AUM was detected exclusively in fractions F13-F15 of the GC1 spg/ctrl. shRNA cell line via immunoblot analysis (figure 39C).

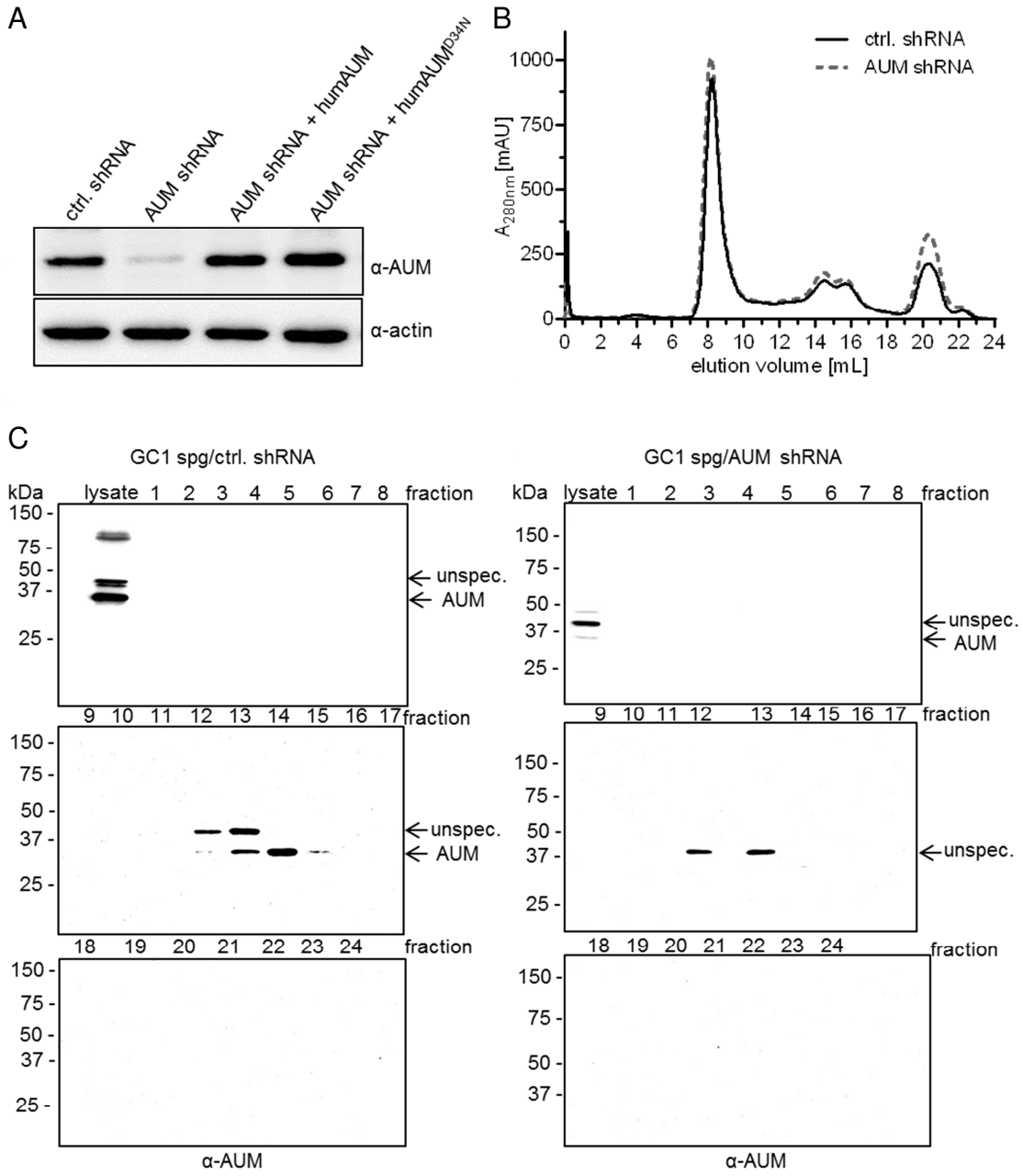

Figure 39: Fractionation of GC1 spg/ctrl. shRNA and GC1 spg/AUM shRNA cell lysates. (A) Downregulation of AUM via shRNA in GC1 spg cells and rescue experiments with human AUM and human AUM^{D34N} are shown in immunoblot analysis. **(B)** Elution profile at A_{280nm} of GC1 spg/ctrl. shRNA cell lysate (black line) and GC1 spg/AUM shRNA cell lysate (dashed line, Superdex 200 10/300 GL). **(C)** Immunoblot analysis of the elution fractions of GC1 spg/ctrl. shRNA and GC1 spg/AUM shRNA cell lysates. Arrows point to an unspecific band or indicate the expected size of AUM. Lysates are shown as a control.

All fractions were tested for *p*NPP-phosphatase activity. In agreement with the immunoblot analysis, only the fractions F13-F15 of the GC1 spg/ctrl shRNA cells showed phosphatase activity, while the fractions of lysates of the AUM depleted cell line (GC1 spg/AUM shRNA) showed no activity (figure 40A, B).

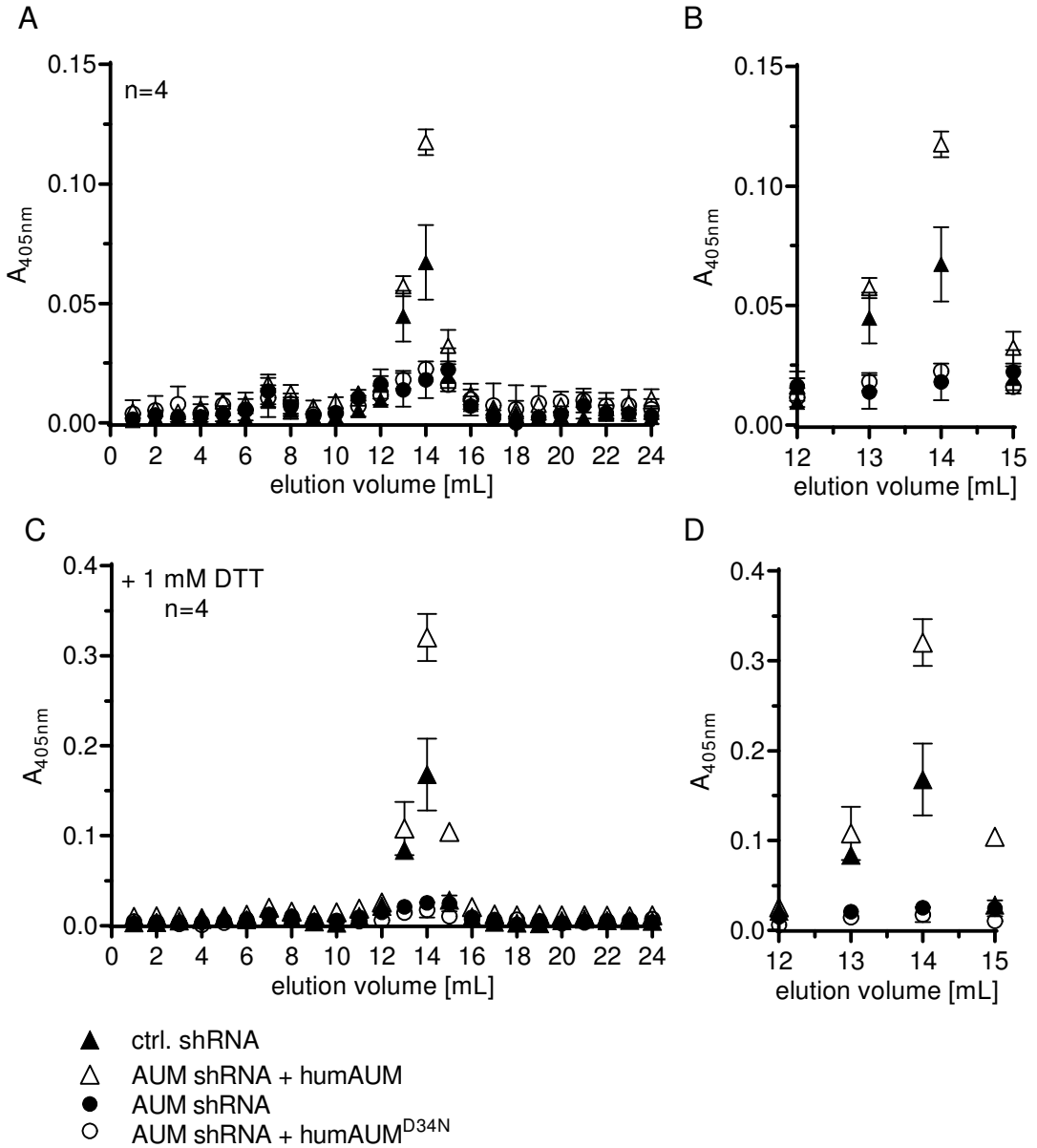

Figure 40: *p*NPP phosphatase activity in fractions of GC1 spg cell lysates with or without DTT stimulus. (A) GC1 spg/ctrl., GC1 spg/AUM shRNA, GC1 spg/AUM shRNA_humAUM and GC1 spg/AUM shRNA_humAUM^{D34N} cell lysates were fractionated and 100 µl of each fraction was tested for *p*NPP-phosphatase activity, measured at A_{405nm}. **(B)** Magnification of elution volume 12 to 15 ml of A. **(C)** *p*NPP phosphatase activity assay of GC1 spg/ctrl., GC1 spg/AUM shRNA, GC1 spg/AUM shRNA_humAUM and GC1 spg/AUM shRNA_humAUM^{D34N} cell lysates after fractionation and a pre-incubation with 1 mM DTT for 30 minutes. **(D)** Magnification of C. Results are mean values ± SEM four independent experiments.

To perform rescue experiments, a construct encoding for untagged human AUM or a construct encoding for untagged human AUM^{D34N} was transfected in AUM depleted cells (figure 39A). After fractionation, the lysates of the GC1 spg/AUM shRNA_humAUM showed phosphatase activity in F13-F15, while no activity was observed in the fractions of the GC1 spg/AUM shRNA_humAUM^{D34N} cells expressing the inactive mutant of AUM (figure 40A, B). Thus, *p*NPP-phosphatase activity could be measured exclusively in fractions comprising active AUM. To increase the readout signal, the different fractions were supplemented with 1

mM of DTT. Strikingly, phosphatase activity was increased three-fold in the presence of DTT, allowing a clear differentiation between cell lysates with or without active AUM (figure 40B, C).

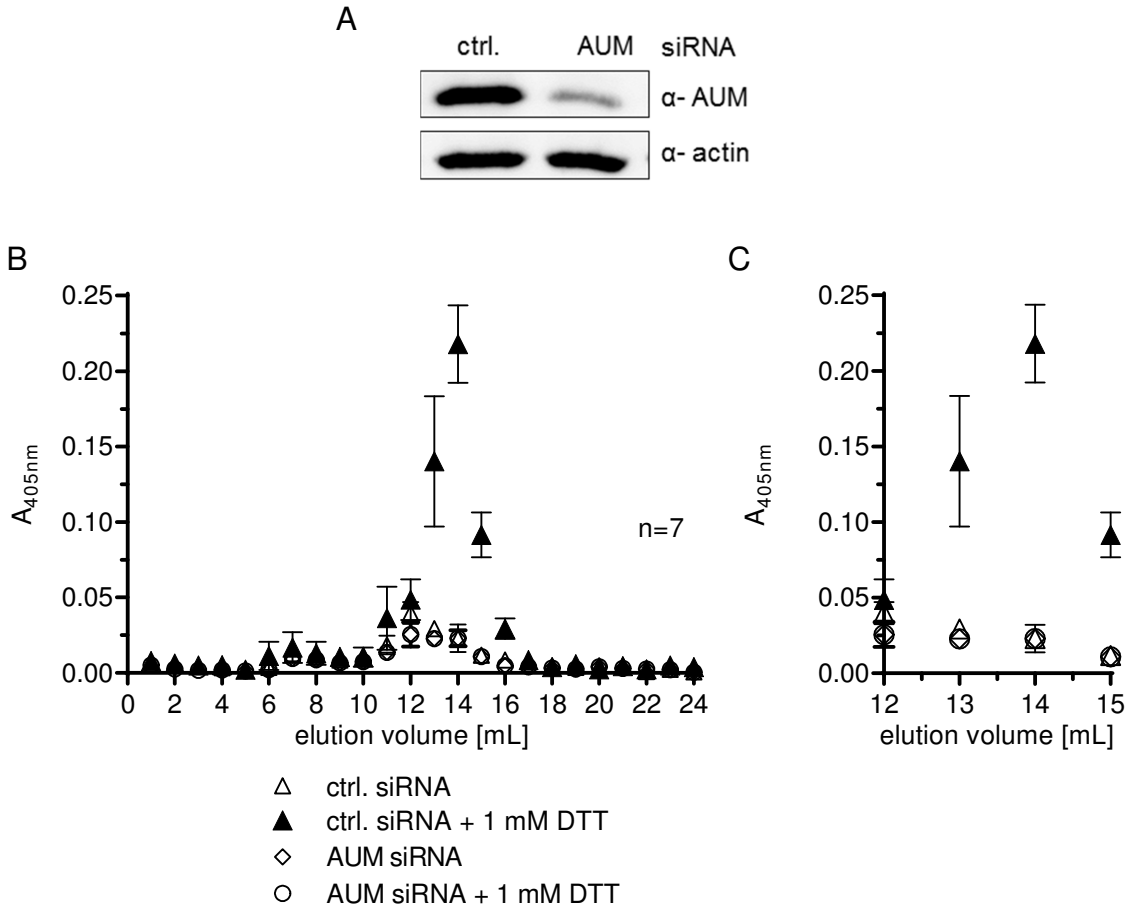

Figure 41: *p*NPP phosphatase activity in fractions of HEK AD-293 cell lysates with or without DTT stimulus. (A) HEK AD 293/ctrl. siRNA and HEK AD 293/AUM siRNA cell lysates were separated by SDS-PAGE and analyzed by immunoblotting with α-AUM and α-actin antibodies. **(B)** HEK AD 293/ctrl. siRNA and HEK AD 293/AUM siRNA cell lysates were fractionated and each fraction was tested for *p*NPP activity at A_{405nm} with or without pre-incubation with 1 mM DTT. Results are mean values ± SEM of seven independent experiments.

To confirm that the AUM activity readout in the fractionation based activity assay was specific for AUM, an additional cell line was tested. While the spermatogonial cell line GC1 spg is less frequently used, HEK AD-293 cells represent a commonly used cell line in molecular and cellular biology. Immunoblot analysis showed a AUM expression in HEK cells (figure 15 C). Cellular AUM expression was downregulated using a transient transfection of synthetic siRNA oligoribonucleotides into HEK AD-293 cells creating HEK AD-293/ctrl. siRNA cells and HEK AD-293/AUM siRNA cells (figure 41A). Cells were lysed and fractionated as described above and *p*NPP-phosphatase activity was tested. Phosphatase activity was detected after DTT treatment (1 mM) in F13-F15 in the HEK-AD 293/ctrl. siRNA lysates, whereas no *p*NPP

dephosphorylation was observed in the AUM-knockdown lysates, again verifying the specific readout of the activity assay.

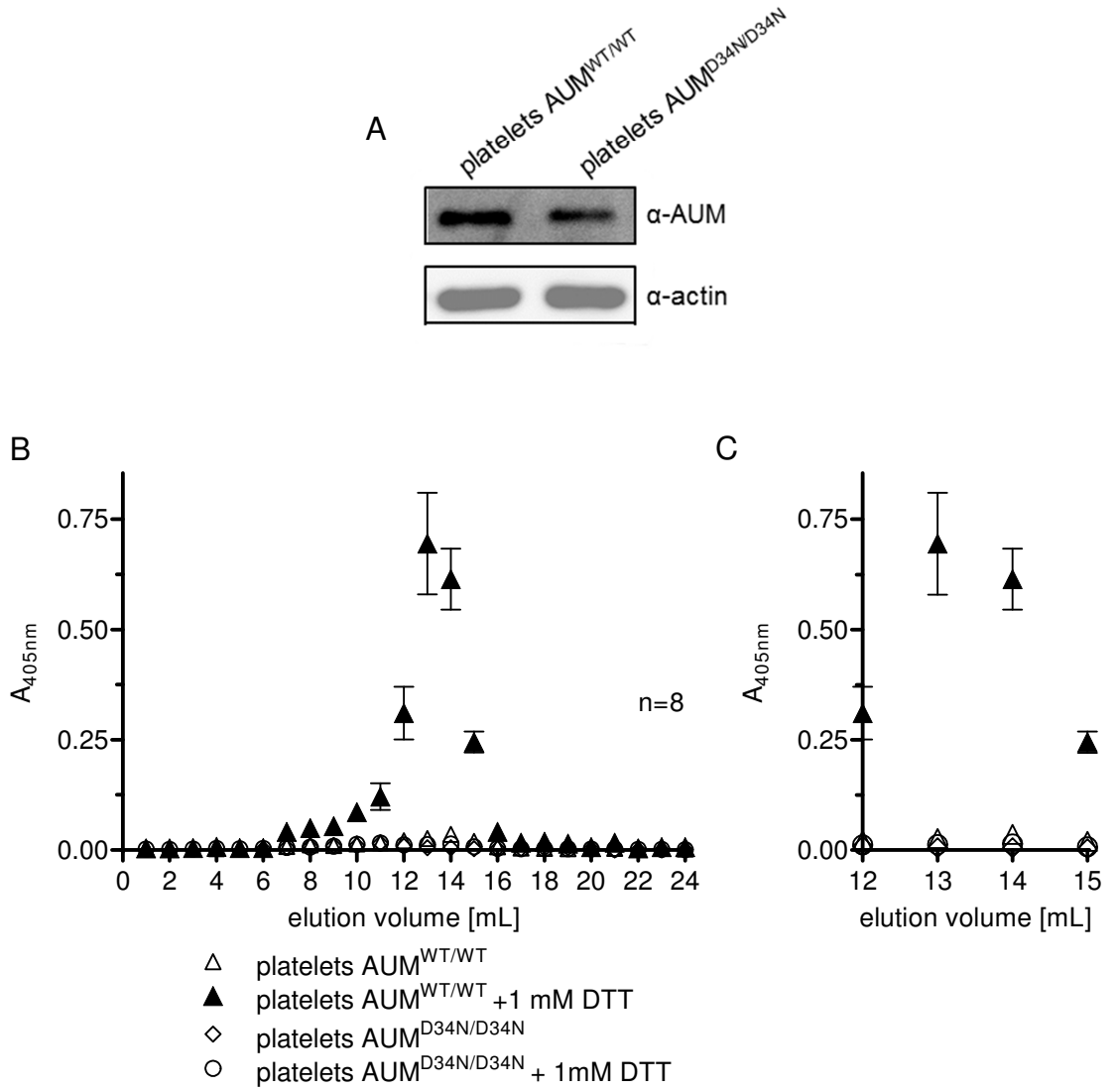

Figure 42: *p*NPP phosphatase activity in fractions of WT and AUM-inactivated mouse platelets with or without DTT stimulus. (A) WT and AUM-inactivated mouse platelets lysates were separated by SDS-PAGE and analyzed by immunoblotting with α-AUM and α-actin antibodies. **(B)** WT and AUM-inactivated mouse platelets lysates were fractionated and each fraction was tested for *p*NPP activity at A_{405nm} with or without pre-incubation with 1 mM DTT. **(C)** Magnification of B. Results are mean values ± SEM of eight independent experiments.

The fractionation assay was also performed with primary cells isolated from genetically AUM-inactivated mice. For this, WT and AUM-inactivated mouse platelets (platelets $AUM^{D34N/D34N}$) were isolated from AUM-fl/fl and AUM fl/fl x PF4-Cre mice, lysed and fractionated as described above. Again, AUM was detected exclusively in fractions F13-F15 via immunoblot analysis. Phosphatase activity was detected after DTT treatment in F13-F15 in the AUM-WT

platelet lysates, whereas no *p*NPP dephosphorylation was observed in the AUM-inactivated platelet lysates.

Taken together the first cellular readout system for AUM-specific phosphatase activity has been successfully established. For this, a promiscuous substrate was combined with a general stimulus to create a specific AUM activity readout. This fractionation-based assay is the first tool to differentiate between cell lines or tissues with different AUM concentrations or activities.

4 Discussion

This study characterizes the structural and biochemical properties of the previously unexplored chronophin paralog AUM. The first crystal structure of the AUM capping domain is presented, which reveals the structural basis of the divergent substrate specificities of AUM and chronophin. These results provide novel insights into the mammalian HAD phosphatase substrate specificity code. In addition, the catalytic properties of AUM are investigated, identifying a mechanism of reversible oxidation and thus potentially of AUM regulation in cells. In this context, the first cell-based AUM activity assay was developed.

4.1 AUM acts on proteins and on low molecular weight substrates

The gene encoding for human AUM was previously mapped to cytogenetic band 16p13.3 and annotated as phosphoglycolate phosphatase (PGP) based on genetic linkage analyses (Eiberg *et al.*, 1993), indicating that AUM can act as a small molecular weight substrate phosphatase. PGP is proposed to have a salvage function in the metabolism of the 2-phosphoglycolate formed during DNA repair (Teresa Pellicer *et al.*, 2003). However, except for genetic linkage analyses suggesting PGP activity of AUM, the biochemical and structural properties of the isolated mammalian protein encoded by the *PGP* gene have remained untested until now. It was not possible to directly analyze the potential PGP activity of AUM in this thesis because 2-phosphoglycolate is not commercially available any more. However, there are several facts that may argue against a PGP function of AUM. (I) Besides being members of the HADSF and containing the four conserved HAD motifs, previously characterized phosphoglycolate phosphatases from different species show only very low sequence similarity with AUM. (II) X-ray crystal structures have been solved of phosphoglycolate phosphatases from bacteria and archaea: *Aquifex aeolicus* (PDB: 2NYV; 2YY6), *Thermoplasma acidophilum* (PDB: 1KYT; 1L6R), *Pyrococcus horikoshii* (PDB: 1WR8), *Haemophilus somnus* (PDB: 2HSZ), *Lactobacillus plantarum* (PDB: 2HDO) *Lactobacillus delbrueckii* (PDB: 2HI0). Structural alignments show no relationship between these enzymes and the chronophin/AUM hybrid protein CAC (PDB: 4BKM; described in this study) or chronophin, the closest homolog of AUM (PDB: 2P69; 2OYC), except for the conserved rossmanoid fold of the active core residues. In addition, the cap types of these PGPs also vary (NYV/2YY6, 2HSZ, 2HDO, 2HI0: C1; 1KYT/1LR6, 1WR8: C2). (III) Moreover, the substrate binding pocket of the high specificity *T. acidophilum* PGP (PDB 1L6R) is surrounded by a network of acidic residues that interact with the glycolate leaving group (Kim *et al.*, 2004), which contrasts with the properties of the substrate binding pocket of AUM (see figure 25). Taken together, the structural divergence between designated PGP orthologs and murine AUM supports the idea that PGP and AUM represent distinct enzymes.

Interestingly, AUM can act as a protein tyrosine phosphatase (figure 8). AUM activity was assayed in peptide arrays, and shown to exclusively dephosphorylate pTyr peptides. In phosphatase overlay assays, it was shown that AUM was able to directly and concentration-dependently hydrolyze tyrosyl-phosphorylated proteins in HeLa cell extracts. In addition, endogenous AUM is involved in the EGF-dependent phosphoregulation of tyrosyl-phosphorylated proteins (Seifried *et al.*, 2014). Because of the fact that chronophin, the closest relative of AUM, acts as both a protein phosphatase and as a small molecule (pyridoxal 5'-phosphate/PLP) phosphatase, AUM activity towards small molecular weight substrates was tested (3.1.2). AUM dephosphorylates the low molecular weight chronophin substrate PLP only poorly (figure 17C) and shows no phosphatase activity against phosphatidyl-inositol phosphates (figure 12B). In contrast, AUM effectively dephosphorylates adenine and guanine nucleotide di- and triphosphates (ADP>ATP≈GDP≈GTP; table 4). While ATP is needed to activate phosphatases such as PP2A (Guo *et al.*, 2014), there is little evidence for the existence or requirement of an intracellular phosphonucleotide phosphatase in the mammalian system (Wass and Butterworth, 1971). The potential physiological relevance of these findings is therefore currently unclear.

In general, ATP-hydrolysis is required to drive active transport across membranes and this can be performed by the catalytic subunits of P-type ATPases, a subclass of the HADSF (Ridder and Dijkstra, 1999). Sequence alignments showed that P-type ATPases harbor the four conserved motifs as well as the rossmanoid fold. As in HAD-type phosphatases, an aspartate residue was identified as the nucleophile in P-type ATPases. A comparison of the reaction mechanism of P-type ATPases with that of HAD phosphatases indicates that the underlying chemistry is very similar (Aravind *et al.*, 1998). The observed ATP dephosphorylation by AUM is thus consistent with these structural and mechanistic similarities between P-type ATPases and HAD phosphatases. HAD phosphatases hydrolyze a phosphate ester and the ATPases a phosphate anhydride. Both reactions could occur to dephosphorylate phosphonucleotides since they contain a phosphate ester and anhydride bond.

Nevertheless, there are currently no experimental data to support the *in vitro* findings that AUM can function as an ADP/ATP/GTP/GDP phosphatase. To validate the role of AUM as a potential ATP phosphatase, a luciferase assay could be performed. The luciferase assay requires ATP as a co-factor for the enzymatic reaction. The levels of ATP can be compared to the production of luminescent light. With this, ATP levels in AUM^{WT} and AUM^{D34N} primary cells or GC1 spg/ctrl shRNA and GC1 spg/AUM shRNA cells could be compared. In addition the level of total adenine nucleotides could be assayed by high pressure liquid chromatography (Eguchi *et al.*, 1997). To directly visualize ATP levels in AUM-WT and AUM depleted cells, Förster resonance energy transfer (FRET) can be used. The indicator, named ATeam is a FRET-based sensor for ATP. It is composed of the ε subunit of the bacterial

F_oF_1-ATP synthase sandwiched by the cyan- and yellow-fluorescent proteins (Imamura *et al.*, 2009).
The structural analysis of adenine and guanine nucleotide substrates bound to CAC might also be helpful to draw conclusions about the steric nature and charge of physiological low molecular weight AUM substrates.

In this work, the *in vitro* phosphatase activity of AUM and its variants was characterized using *p*NPP as a surrogate substrate. *p*NPP is a non-proteinaceous, non-specific substrate that was initially used to characterize the enzymatic properties of alkaline phosphatase (Hiwada and Wachsmuth, 1974). In the course of time it was established as general tool to characterize phosphatases with unknown substrates. Especially the family of PTPs shows activity towards this substrate (Pot *et al.*, 1991; Niu *et al.*, 1999). The enzyme kinetics of bacterially expressed murine (K_M= 3.13 mM; k_{cat}= 0.47 s^{-1}), bovine (K_M= 4.22 mM k_{cat}= 1.08 s^{-1}) and human AUM (K_M= 3.49 mM ; k_{cat}= 2.24 s^{-1}) towards *p*NPP were analyzed (figure 11A, B, C). The catalytic efficiency of AUM is comparable to the *p*NPP phosphatase activity of the murine protein tyrosine phosphatase Eya3 (Tootle *et al.*, 2003; Rayapureddi *et al.*, 2003) and the human small C-terminal domain phosphatase SCP1 (Zhang *et al.*, 2010), both members of the HADSF. In contrast, the detected AUM activity is much lower than the *p*NPP phosphatase activity of classical tyrosine phosphatases such as PTP1B, TC-PTP or SHP-1 (Ren *et al.*, 2011; Rayapureddi *et al.*, 2003). Despite being an artificial substrate, *p*NPP turned out to be a practical tool to characterize AUM activity. In contrast to the malachite green-based endpoint assays that detect free inorganic phosphate liberated from pTyr peptides or phosphonucleotides, AUM activity towards *p*NPP can be measured continuously over time.

In conclusion, the present work demonstrates that AUM can dephosphorylate tyrosyl-phosphorylated proteins and that it can additionally act on some small molecular weight substrates, at least *in vitro*. These findings lead to the speculation that -similar to its closest relative chronophin- AUM might also operate as a small molecular weight substrate-directed phosphatase with metabolic functions *in vivo*. To assign the function of AUM as small molecular weight substrate phosphatase, an activity-based metabolomic profiling (AMP) approach could be applied. Here an extract of polar metabolites from tissue extracts (e.g. liver, brain, testis) is used as a library of potential *in vitro* substrates. This small-molecule extract could be incubated with purified AUM^{WT} and AUM^{D34N}. Liquid-chromatography mass spectrometry (LC-MS) can then be used to analyze the impact of the recombinant enzyme on the cellular extract and the potential substrates and products (de Carvalho *et al.*, 2010; Larrouy-Maumus *et al.*, 2013).

4.2 Inhibitor studies

Enzyme inhibitors are important research tools. To further characterize the phosphatase activity of AUM, established inhibitors of classical phosphatases were tested. There are several natural toxin inhibitors of the PSP family of enzymes. These include microcystins, calyculins, tautomycin and okadaic acid. Okadaic acid is a tumor-promoting polyether fatty acid produced by marine dinoflagellates. The compounds of the okadaic acid class are selective inhibitors of several protein serine/threonine but not tyrosine phosphatases. Okadaic acid is an inhibitor of PP1 (IC_{50} = 15 nM) and PP2A (IC_{50} = 0.1 nM) (Cohen *et al.*, 1989), it does not inhibit acid and alkaline phosphatases, nor protein tyrosine phosphatases (Bialojan *et al.*, 1988). The crystal structure of PP1:okadaic acid (PDB: 1JK7) reveals the binding mode of the toxin to the catalytic subunits of PSPs (Maynes *et al.*, 2001). Calyculin A, isolated as a cytotoxin from the marine sponge *Discodermia calyx*, consists of a polyketide and a dipeptide with a phosphate group in the polyketide portion. The protein phosphatase inhibitor potently inhibits PP1 (IC_{50}: 2 nM) and PP2A (IC_{50}: 0.5-1 nM) (Ishihara et al., 1989). A structure of the complex between calyculin A and the γ isoform of PP1 (PDB: 1IT6) was solved, representing the key interactions with the enzyme (Kita *et al.*, 2002). AUM was insensitive to inhibitors of serine/theorine protein phosphatases, okadaic acid and calyculin A up to a concentration of 1 µM inhibitor (figure 14). This is consistent with the aspartate-based catalytic mechanism typical of HAD-phosphatases such as AUM. Sodium orthovanadate (Na_3VO_4) is a commonly used inhibitor for protein tyrosine phosphatases (PTPs) as well as for ATPases, alkaline and tyrosine phosphatases. The VO_4^{3-} ion binds to the active site nucleophile, mimicking a transition state of the phosphoryl transfer. Vanadate occupies the active site by a covalent binding of the thiol of the catalytic cysteine. It acts as a competitive inhibitor of PTP1B with a K_i of 0.38 µM (Huyer *et al.*, 1997). Consistent with its phospho-tyrosine directed activity, AUM was inactivated by VO_4^{3-} with an IC_{50} of 41.4 µM. The mechanism of VO_4^{3-} mediated AUM inhibition is currently unclear, because an AUM:VO_4^{3-} crystal structure is not yet available. It may be speculated that VO_4^{3-} binds to Cys35, adjacent to the Asp34 nucleophile of AUM.

4.3 AUM is a member of the HADSF

The present work, as well as former studies from the group (PhD thesis, P. Duraphe), classify AUM as a member of the family of mammalian haloacid dehalogenase-type phosphatases. The enzyme harbors all for conserved HAD motifs (figure 13A) and the exchange of the nucleophile Asp34 to an asparagine leads to a complete inactivation of the phosphatase (figure 13B). The catalytic mechanism of the HADSF is known to be magnesium-dependent, and Ca^{2+} has been shown to inhibit HAD phosphatases (Almo *et al.*, 2007). Co-crystallization studies of the HAD phosphatase phosphoserine phosphatase with

Mg^{2+} or Ca^{2+} have provided insights into the inhibitory effect of Ca^{2+} on this enzyme family. In the presence of Ca^{2+}, the sixfold coordinated Mg^{2+} ion is replaced with a sevenfold coordinated Ca^{2+} ion in the active site. A Mg^{2+} ion coordinates one oxygen atom of the catalytic Asp residue, while the Ca^{2+} ion ligates both side chain oxygen atoms. With this Ca^{2+} prevents the nucleophilic attack of one of the aspartate side chain oxygen atoms on the phosphorus atom of the substrate (Peeraer *et al.*, 2004). Ca^{2+} has already been described as a competitive inhibitor of chronophin (Fonda and Zhang, 1995). The phosphatase activity of AUM was therefore tested in the presence of Mg^{2+} and Ca^{2+}. AUM phosphatase activity was reduced by increasing concentrations of added Ca^{2+}, while elevated Mg^{2+} concentrations protected the enzyme partly against Ca^{2+}-mediated inhibition (figure 13B). This observation confirms the magnesium-dependent catalytic mechanism of AUM that has been described for all members of the HADSF.

To further investigate the catalytic mechanism of a HAD phosphatase, the effect of the inhibitor beryllium fluoride (BeF_3^-) can be tested. The compound is a common crystallographic and biochemical tool in the field of HADSF to investigate function and mechanism of this type of phosphatases. HAD phosphatases form a stable complex with BeF_3^- that structurally mimics their tetragonal phosphoaspartate intermediate. BeF_3^- binds the active-site aspartate in a tetrahedral geometry similar to the phosphoryl group. The compound has the capability to accept pairs of electrons to complete an octet with available covalent bond donors. Potential donors are oxygen atoms of a phosphate group or an aspartate carboxylate group. The use of BeF_3^- as an analog of a phosphate ion for biological studies was first reported for transducin, the G protein of the retinal rods (Bigay *et al.*, 1987). BeF_3^- has been used to generate an analog of aspartyl phosphate in the response regulator CheY (Yan *et al.*, 1999; Lee *et al.*, 2001). Since then, BeF_3^- has been employed as an inhibitor for aspartate based phosphatases. A specific inhibition of the catalytic activity with BeF_3^- has been shown e.g. for Scp1 and Fcp1 (PDB: 3EF1), the mammalian protein phosphatase Dullard (Kim *et al.*, 2007), murine chronophin (PDB: 4BX2), the human deoxyribonucleotidase dNT-2 (PDB: 1MH9) and PSP of *Methanococcus jannaschii* (PDB: 1J97). The solved structures provide new insights into the mechanism of substrate binding and the phosphotransfer reaction mechanism. In the crystal structure of the BeF_3^-:PSP complex from *M. jannaschii*, BeF_3^- is coordinated to Mg^{2+}, and is bound to the catalytic Asp and the surrounding conserved residues of the active site. When comparing the structure of bound BeF_3^- and bound phosphate, no significant changes of the residues can be observed (Cho *et al.*, 2001; Kamenski *et al.*, 2004; Rinaldo-Matthis *et al.*, 2002; Ghosh *et al.*, 2008). Figure 13C shows that the hydrolytic activity of AUM is completely blocked by BeF_3^-, indicating a similar catalytic mechanism as seen for the described HAD phosphatases above. The use of this compound overcomes the difficulty of visualizing the labile phosphoaspartate.

and BeF_3^- therefore represents a potent and valuable reagent for future structural studies on AUM or the CAC hybrid. Taken together, the performed experiments (figure 13) consolidate the HAD identity of AUM.

4.4 Intrinsic specificity determinants of AUM

Phosphatases play critical roles in a wide variety of cellular processes, and they can act on highly diverse substrate classes. Given the diversity of phosphorylated substrates in mammalian cells, the question of phosphatase substrate specificity is a core issue. Mammalian HAD-type phosphatases represent an emerging family of structurally unique enzymes implicated in the regulation of metabolism (Possemato et al., 2011; Csaki and Reue, 2010), proteasome activity (Guo *et al.*, 2011), nuclear membrane biogenesis (Kim *et al.*, 2007), cytoskeletal dynamics (Gohla *et al.*, 2005), DNA repair (Weinfeld *et al.*, 2011), apoptosis or survival decisions (Cook *et al.*, 2009) and transcription (Yeo *et al.*, 2005). In contrast to classical Ser/Thr-directed phosphatases that instrumentalize a vast array of regulatory subunits to precisely target their substrates (Virshup and Shenolikar, 2009), but similar to classical Tyr-phosphatases that have acquired their specificity by domain fusion events (Alonso *et al.*, 2004), HAD phosphatases have specialized their functions by the fusion of a “generic” catalytic core with structurally diversified cap domains (Burroughs *et al.*, 2006; Moorhead *et al.*, 2009; Meng and Babbitt, 2011). Crystallographic studies on prokaryotic HAD phosphatases and on mammalian HAD-type nucleotidases have led to the realization that HAD caps can provide specificity domains, yet no experimental evidence has been available so far to support this presumed role (Lu *et al.*, 2005; Lahiri *et al.*, 2004; Rinaldo-Matthis *et al.*, 2002; Wallden *et al.*, 2007).

While being a key task in the elucidation of HAD functions, the basis of HAD phosphatase substrate specificity has thus remained elusive. To address this, a comparative evolutionary, biochemical and structural analysis of the closely related murine AUM and chronophin enzymes was conducted. The AUM/chronophin family evolved via a duplication of an ancestral gene at the origin of the vertebrates (figure 18). Belonging to the C2a class of the HADSF (figure 23) both share 45% identity on amino acid level and 87% similarity of predicted secondary structure motifs (figure 8A, 17A). AUM, with a molecular mass of 34.5 kDa (monomer) exists as a stable dimer in solution, which can transiently form tetramers (figure 10). Although the physiological substrate of AUM is currently still unknown, the results presented here show that the enzyme is phospho-tyrosine directed (figure 8 B-D) and dephosphorylates nucleotide di- and triphosphates (table 4) as well as *p*NPP (figure 11) *in vitro.* Taken together, the common origin and the different substrate preferences of AUM and

chronophin make the two phosphatases an ideal model to address the question of substrate specificity in two closely related members of the mammalian HADSF.

For PTPs it has been described that residues lining the substrate entry site and those that determine the electrostatic potential of the enzyme surface contribute to intrinsic substrate specificity (Barr *et al.*, 2009). In line with this idea and based on the published chronophin structures, residues corresponding to those in close proximity to motif I and motif II, located in unstructured flexible elements and lining the substrate entry site of chronophin were substituted in AUM ($AUM^{R41N; T44R; A45I}$, $AUM^{T67S; S71R; K72R; T73A}$, $AUM^{S71R; K72R; T73A}$, $AUM^{T67S; K72R; T73A}$, $AUM^{T67S; S71R; T73A}$, AUM^{T73A}). All these exchanges affected the activity of the respective AUM variants towards *p*NPP in comparison to AUM^{WT} (figure 21). Interestingly, the swapping mutants in the seven amino acid stretch of AUM that starts with the conserved HAD motif II Ser/Thr ($AUM^{T67S; S71R; K72R; T73A}$) abolished AUM phosphatase activity towards *p*NPP. Recombinant $AUM^{T67S; S71R; K72R; T73A}$ protein was characterized by limited solubility, indicating an important role of the exchanged residues for the structure and folding of AUM. The reverse mutation of Ser58 back to the original Thr67 AUM residue ($AUM^{S71R; K72R; T73A}$) partially recovered *p*NPP phosphatase activity and enzyme solubility. This finding points to an important function of the conserved Thr67 in HAD motif II for the phosphatase activity of AUM. The CAC structure confirms this finding. Ser58 in chronophin, which is replaced by Thr67 in AUM, helps to orient the substrate for nucleophilic attack by forming a hydrogen bond with its transferring phosphoryl group (figure 25A). The presence of an additional methyl group in the AUM Thr residue at this position appears to be critical for AUM *p*NPP activity. The selected residues did not interfere with substrate specificity even though they are in close contact to the substrate. These findings contribute to the idea that the core domain (“business part”) codes for residues important for catalysis, while specificity is encoded by the cap domain (“private part”).

After excluding a contribution of core domain residues for AUM/chronophin specificity, swapping mutants of the AUM/chronophin cap domains were generated. The generation of functional HAD phosphatase cap hybrids between two HAD paralogs has not been reported in the literature before (figure 22). *In vitro* phosphatase assays show that these domain swaps can toggle between chronophin- and AUM-like phosphatase activities. The transfer of the chronophin cap to the catalytic core of AUM (ACA hybrid) transforms a *p*NPP phosphatase into a PLP phosphatase. Thus, the chronophin cap domain comprises all residues necessary for specificity towards the chronophin substrate PLP. Supporting this idea, the transfer of the AUM cap to the chronophin core domain (CAC hybrid) abolishes PLP activity. As may be expected for an artificial substrate, this cap transfer does nevertheless not result in enhanced *p*NPP dephosphorylation. Thus, the AUM cap may only provide specificity towards (currently unknown) physiological AUM substrates. In agreement with the

role of HAD motif II residues for AUM activity (figure 21), these data may indicate that in addition to residues placed in the AUM cap, the AUM core domain harbors residues that are required for efficient (*p*NPP) dephosphorylation.

The cap domains of AUM and chronophin are highly similar on the amino acid level and in terms of predicted secondary structures. Therefore, the question arises if strategically placed, different residues that are responsible for the specificity of the cap domain can be identified. To address this question, the chronophin structure in complex with PLP (PDB: 2P69) was analyzed and cap residues in close proximity of the substrate were further investigated. The swapping mutant AUM^{L204H} was generated. *In vitro* phosphatase assays demonstrate the functional importance of this single residue for substrate specificity (figure 22). The exchange of this single leucine residue confers chronophin-like PLP activity onto AUM.

This finding can be explained with the CAC structure. Structural analysis of the CAC (chronophin/AUM cap hybrid) present the first partial structure of AUM. An overlay of human chronophin in its PLP bound state and the CAC hybrid (figure 23) reveals first insights in the difference of substrate recognition between AUM and chronophin. The cap residue (H182 in chronophin, L204 in AUM) is positioned by a characteristic β-hairpin structure, covering the active site (figure 26A). This structural element is described as substrate specificity loop (Lu *et al.*, 2005; Lahiri *et al.*, 2006). The structure of human chronophin shows the coordination of the PLP pyridine ring via the imidazole ring of His182 in the active site. Due to the exchange L204H in AUM, the coordination of PLP is abolished. The identification of L204/H182 as residues that contribute to substrate specificity in AUM or chronophin is also supported by the evolutionary analysis of sites differently conserved between AUM and chronophin (table 7, class II residues).

Interestingly, evolutionary analysis of two mammalian C2 members of the HADSF, phosphomannomutase 1 (PMM1) and PMM2, support the presented findings. PMM1 corresponds to the brain inosine monophosphate sensitive glucose-1,6-bisphosphatase, while PMM2 is insensitive to inosine monophosphate and exhibits only very low glucose-1,6-bisphosphatase activity (Pirard *et al.*, 1999; Veiga-da-Cunha *et al.*, 2008). As shown for AUM and chronophin (this study), PMM1 and -2 also share a common vertebrate ancestor (Matthijs *et al.*, 1997). Comparative evolutionary analysis identified class II residues in PMM1/PMM2, similar to the His182 or L204 residues identified for chronophin or AUM, respectively (table 7) (Quental *et al.*, 2010). In the future it could be tested, if the identified class II residues are responsible for the different substrate preference of PMM1 and PMM2. This approach could support the idea of the comparative studies of AUM and chronophin, that in general, predictable single residues at conserved position of the cap domain are

important for substrate specificity of human HADSF. A global approach identifying class II residues in related HAD phosphatases could be conducted. In comparison with known phosphatase:substrate structures a general conclusion of residues responsible for substrate specificity in the HADs could be drawn.

Residues coding for substrate specificity are located in the substrate specificity loop of the AUM (and chronophin) cap domain. In the future, these regions will likely be of importance to determine the physiological substrate of AUM. The cap-located specificity elements of the HADSF might be comparable with the WPD-loop of the family of PTPs. The WPD loop closes the entrance of the PTP active site, sequestering the nucleophile-substrate intermediate from water molecules, thus promoting substrate hydrolysis (Yang *et al.*, 1998; Barr *et al.*, 2009). Residues located in the WPD-loop of PTPs are targeted to generate substrate trapping mutants. For substrate trapping, a phosphatase point mutant is generated in which the affinity for the substrate remains similar, but the catalytic activity is reduced in order to enable the isolation of enzyme:substrate complexes. A mutation of the invariant catalytic acid (Asp181 in PTP1B) of the WPD-loop converts an active enzyme into a "substrate trap". Several substrate trapping mutants of PTPs have been characterized so far and potential protein substrates were isolated and identified with this technique (Flint *et al.*, 1997; Agazie and Hayman, 2003; Blanchetot *et al.*, 2005). Since the residues that determine AUM substrate specificity are also important for substrate affinity because they bind to the substrate's leaving group, they might not be the right targets to generate "substrate traps". According to the findings on PTP1B, Asp36 of AUM might be a good candidate for the generation of a substrate trapping mutant. It acts as an acid/base residue during catalysis, similar to Asp181 in PTP1B. In the future the identified class I and class II residues can contribute to the design of a HAD-Type "substrate-trap". These findings lay the groundwork for the generation of tools that may facilitate the identification of physiological AUM substrates and potentially also of AUM inhibitors.

Besides a possible prediction of the substrate nature or potent inhibitors of phosphatases the identified residues might be linked to health and disease. Single nucleotide polymorphisms (SNPs) are the most common type of genetic variation representing a difference in a single nucleotide. The mutations can result in an amino acid substitution with importance for protein function. The phospholysine phosphohistidine inorganic pyrophosphate phosphatase (LHPP) is a member of the human C2a HADSF, belonging to the NagD family, like AUM and chronophin. LHPP SNPs are interacting genetic risk factors in major depression (Neff *et al.*, 2009). While the SNPs of LHPP are not characterized on enzyme level, there are known examples, where SNPs change enzyme specificity. The endoplasmic-reticulum aminopeptidase-2 (ERAP-1) regulates the adaptive immune response. Coding SNPs have

been described with preposition to human diseases like autoimmunity and cancer. Biochemical and X-ray analysis revealed alterations in activity and specificity of the enzyme due to amino acid substitution caused by SNP (Evnouchidou *et al*., 2012). Studies like this confirm the important role of the residues coding for specificity. There is no SNP, implicated in disease, identified in the AUM sequence. However, the presented study highlights how in the future residues coding for specificity in other members of the human HADs can be identified.

Protein Ser/Thr phosphatases determine substrate specificity due to association with regulatory subunits. They regulate activity by restricting substrate specificity via occupying substrate sites. For the family of HADSF no associated regulatory subunits providing substrate specificity are known, while HAD hydrolase dimerization can contribute to substrate specificity. In the family of C2a-capped HAD phosphatases homodimerization is a conserved and common feature contributing to substrate specificity by correct substrate coordination. The homodimerization of chronophin is needed for the proper positioning of the substrate specificity loop and efficient PLP dephosphorylation (Kestler *et al*., 2014). SEC and AUC analysis revealed dimeric and tetrameric species of AUM (figure 10). Cys293 is responsible for the tetramerization of AUM (figure 36). The disruption of the tetramer interface has no impact on substrate specificity towards *p*NPP (figure 32A). The AUM dimer interface is shown in the CAC structure (figure 24). Similar to chronophin, it appears likely that AUM dimerization is also required for the positioning of the substrate specificity loop. Thus, AUM homodimerization represents an additional mechanism to provide substrate specificity.

In future the relevance of the identified conserved residues (class I and class II) should be further investigated. Their detailed role for substrate specificity can be systematically explored once a physiological AUM substrate has been identified. Some of the residues, located at the AUM cap domain, are exposed (figure 26 A). They can provide necessary information about possible docking sites for regulatory protein-protein interactions. In addition the impact of the additional feature of the AUM cap, the identified transverse loop (figure 23 A), is still unknown. It may serve to orient the substrate specificity loop of the adjacent monomer in the homodimer. Its role for specificity and catalysis or as a potential interaction interface has to be investigated.

4.5 The reversible oxidation of AUM

The presented biochemical characterization, the inhibitor studies and the elucidation of the CAC structure confirm AUM as member of the HAD phosphatases with catalysis based on Asp34 as the nucleophile. Next, the question arises if the catalytic activity itself may be subject to regulation. Currently, there is no evidence reported in the literature that the catalytic activity of HAD phosphatases is regulated. As presented in the introduction, there are known targeting domains or other functional domains fused to other human HADs, however these fusion domains do not affect catalysis (1.4.1.5). Regulatory subunits like those described for the Ser/Thr phosphatases (1.2), or modifications regulating catalysis such as those described for the PTP family (1.3) have so far not been identified for HAD-type phosphatases. The characterization of the swapping mutants of the catalytic core of AUM (figure 21) identified residues necessary for proper catalysis, indicating a possible intrinsic regulation of AUM activity. Intrinsic modulation of enzyme catalytic activity can be provoked by modifications. With this background, the second part of the present thesis focuses on an intrinsic type of regulation, the reversible oxidation of AUM. Reversible oxidation has been described as a modification that regulates the catalytic activity of PTPs, yet so far this type of regulation has not been described for HAD phosphatases.

Initially it was found that AUM activity can be increased by a treatment with DTT (figure 27), suggesting that reducing conditions can activate AUM. This finding was confirmed using the reducing agents β-MEOH and TCEP. In contrast, the incubation of AUM with the oxidant H_2O_2 dose-dependently inhibited AUM phosphatase activity (figure 28A) in a reversible manner (figure 28 B, C). This mechanism can be classified as a reversible oxidation: Upon treatment with oxidative agents, catalysis is shut down. The reduction of the oxidized enzyme recovers catalytic activity. Members of the family of PTPs have likewise been shown to be subject to reversible oxidation *in vitro* and in cells. For example, activation of receptor tyrosine kinases can stimulate the intracellular production of reactive oxygen species (ROS) by mitochondria or NADH oxidases (NOX). NOX activation leads to an increase of endogenous H_2O_2 levels, resulting in a transient inactivation of PTPs. Besides H_2O_2, ROS comprise different chemical oxidants such as superoxide anion, singlet oxygen and hydroxyl radicals. This ROS production is not only a harmful byproduct of aerobic metabolism, but ROS can also serve as important signaling molecules for e.g. regulating the inflammatory response or protein modification as here discussed for phosphatase regulation. The inhibition by oxidation gets reversed by antioxidant molecules in the presented data mimicked by DTT. The mechanism, rate and identity of the thiol regenerating the active site cysteine of PTPs are poorly understood. A complex web of antioxidant molecules regulates the maintenance of the intracellular redox homeostasis. Antioxidants are e.g superoxide dismutase and

peroxiredoxins, the thioredoxin and glutaredoxin family. GSH, thioredoxin, glutharedoxin and sulfiredoxin are described to recover PTPs upon oxidation (Parsons and Gates, 2013; Dagnell *et al.*, 2013).
As a next step it has to be investigated whether AUM activity is also redox-regulated in cells. So far, only H_2O_2 has been identified as possible ROS species inhibiting AUM *in vitro*. In addition an antioxidant system has to be identified, recovering AUM activity. The effect of small protein antioxidants such as GSH and thioredoxin should be addressed in AUM activity assays to confirm the findings with DTT.

After the identification of AUM as potential redox regulated phosphatase, the responsible residues were investigated. The regulation of the PTP family occurs by oxidizing the active site cysteine. Due to its unique properties (e.g. low pKa), the cysteine side chain is responsible for the thiol-based redox switches in redox regulated proteins (for further details see introduction). As mentioned above, AUM catalysis is based on Asp34 as the nucleophile. In contrast to the cysteine-based PTPs the redox-sensitivity observed for AUM is therefore not likely to be mediated by the nucleophile itself. It has to be noted, that aspartate oxidases exist in the mammalian system. However, this type of enzymes can be excluded for the investigated mechanism, because they only act on free D- or L- aspartate (Katane and Homma, 2010). To investigate the molecular mechanism of the reversible oxidation of AUM it was focused on the cysteines of the phosphatase. To identify the regulatory cysteine, single point mutants were generated. To study the effect of a cysteine on the protein of interest it is usually exchanged to a serine residue or an alanine residue. The exchange to an alanine would remove the side chain for interactions while it may introduce a small cavity in the interior of the protein. The exchange to a serine residue is critical if interactions based on a disulfide are investigated. The hydroxyl side chains of serine residues can also form (non-covalent hydrogen or salt) bridges, and may therefore maintain intra/intermolecular interaction in a manner similar to cysteine side chains. Most of the cysteines of AUM are predicted to be internal, which is why for this approach a cysteine to serine exchange was performed to avoid affecting the structural arrangement of AUM. AUM contains eight cysteines: C13, C35, C104, C193, C217, C243, C272, C293. The CAC structure reveals the structural arrangement of the AUM cap. Here the location and orientation of Cys193 and Cys217 can be observed, while no direct structural information is available for the other cysteines contained in the AUM core domain.

As a first step, an effect of the Cys to Ser substitutions on the oligomerization of AUM was investigated. Oligomerization can be regulated by redox switches, if a disulfide is involved. Depending on cellular H_2O_2 formation, protein kinase A was observed forming an interprotein disulfide bond between its two regulatory RI subunits (Brennan *et al.*, 2006). Peroxiredoxins

(Prxs) are known to build dimers or decamers regulated by a redox-sensitive dimer to decamer transition (Wood *et al*., 2002). AUM forms dimers and tetramers (figure 10) and the CAC structure confirms the dimeric state of AUM while tetramerization is unlikely (figure 24). The interaction of the two protomers is mediated by a cap to cap interaction with one protomer rotated by 180° with respect to the other protomer. The CAC structure reveals that AUMCys217 is located in the dimer interface, yet it cannot form a disulfide bridge with Cys217 of the opposing protomer due to 180° rotation (figure 43 II). With this and the SEC experiments performed in the presence of DTT (figure 36), a disulfide mediating the dimerization of AUM can be excluded. The dimerization of AUM is not redox dependent. Strikingly, the tetramer species decreases upon DTT treatment (figure 36), indicating a redox-sensitive tetramer binding site. The purified CS mutants were analyzed via SEC, and the results clearly show that Cys293 is responsible for AUM tetramerization. The SEC profile of AUM^{C293S} shows no tetramer species (figure 36). In contrast to the dimer interface, tetramerization is mediated by the core domain. For chronophin, no tetramerization is observed. This difference can be now traced back to the fact that a Cys residue corresponding to Cys293 in AUM is not present in chronophin (figure 43 I). Whether AUM can also exist as tetramers in cells and whether oligomerization is potentially regulated by a redox switch currently remains an open question.

In *p*NPP activity assays it was shown that all CS mutants show altered activity compared to AUM^{WT} as a result of the amino acid substitution(s) (figure 32A). All single CS mutants could be re-activated by reducing agents (figure 32B). In contrast, the single point mutants AUM^{C35S}, AUM^{C104S} and AUM^{C243S} were less sensitive to H_2O_2 (figure 33B). For the double mutants $AUM^{C35S;\ C104S}$ and $AUM^{C104S;\ C243S}$ no inhibition by oxidation up to a concentration of 100 µM H_2O_2 was detected (AUM^{WT}: IC_{50}: 41 µM H_2O_2; figures 28A, 34). These findings indicate that more than one Cys is involved in the inactivation of AUM and that Cys35, Cys104 and Cys243 are the responsible residues for this kind of regulation. Notably, no Cys of the cap domain is involved, the regulation is mediated by Cys located in the core domain.

Based on the chronophin structure and the CAC structure a possible mechanism is proposed. Cys35 is located in between the nucleophile Asp34 and Asp36 in motif I (figure 43 III). Already the exchange to a serine residue resulted in a strong reduction of AUM activity towards *p*NPP. This reveals the importance of the thiol group of Cys35 for catalysis. Even though it is not understand how, the Cys residue has direct impact on the ability of Asp34 to act as the nucleophile. Oxidation could lead to a local change of the pH needed for proper catalysis. Chronophin also harbors a Cys in between the nucleophile Asp25 and Asp+2 which is sensitive to thiol-specific reagents (Gao and Fonda, 1994). The mechanism of reversible oxidation has not been addressed. Anyways it is important to note, that Cys26 of

chronophin is not oriented towards PLP or to the two aspartates (PDB 2P69; see also figure 43 III). Thus, no conclusions about the impact of Cys35 on AUM activity can currently be drawn from the CAC structure.

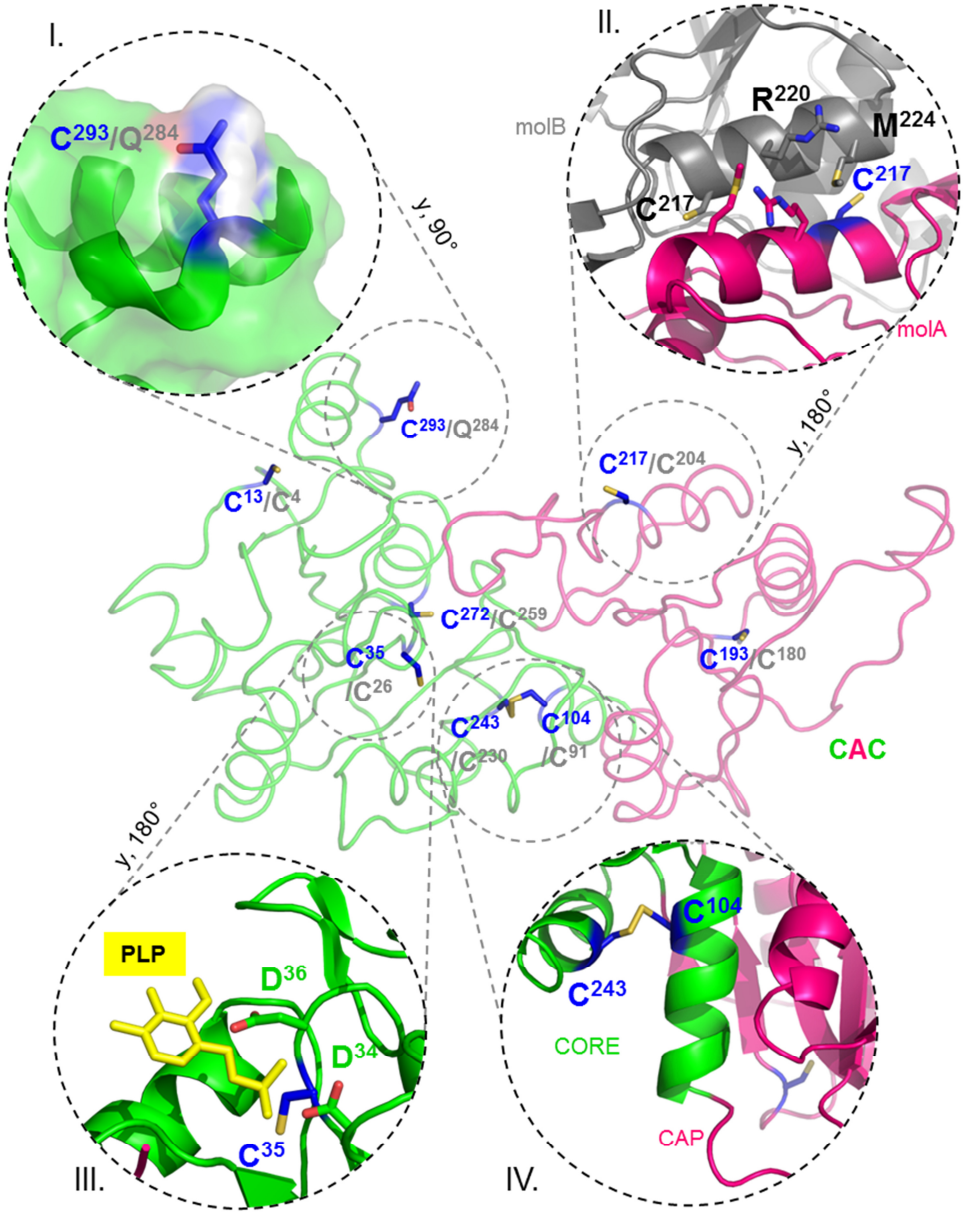

Figure 43: Model of the proposed roles of the AUM cysteines. The CAC structure is depicted as loop diagram (PDB: 4BKM). The chronophin core domain is colored in green, the AUM cap domain is colored in pink. The amino acid residues are labeled according to their position in the murine AUM (blue) and according to their position in the CAC hybrid (gray). The PLP molecule (yellow) is modeled according to the human chronophin structure (PDB: 2P69). I: Cys293 is located at the C-terminus of AUM, mediating tetramerization. II: The dimer interface of AUM. III: Cys35 is located in between the nucleophile Asp34 and Asp36. IV: A disulfide between Cys243 and Cys104 connects the core and cap domain of AUM/chronophin.

Next to Cys35, Cys104 and Cys243 of AUM are targeted by oxidation. The replacement of Cys104 by a Ser increases AUM activity, while the replacement of Cys243 by a Ser decreases the basal activity of these mutants compared to AUM^{WT}. Notably, the exchange to a serine makes both mutants less sensitive to H_2O_2. In contrast to Cys35, Cys104 and

Cys243 are not located in close proximity to one of the conserved motifs responsible for catalysis. Cys104 is part of an α-helix, located N-terminal of the cap domain, followed by a loop region containing 9 residues. Cys243 is part of an α-helix, located C-terminal of the cap domain with a loop region of 13 residues ahead. The two α-helices determine the interface of the core/cap interaction. The position of the two cysteines is also conserved in chronophin (Cys91, Cys230). Except for 2OYC, all known human and murine structures of chronophin and the CAC structure present a disulfide formed by Cys91 and Cys230 (murine chronophin), connecting core and cap domain (figure 43 IV). Whereas there is no structural information available for Cys104 and Cys243 of AUM, the observed disulfide in chronophin could be also present in AUM. Disulfide formation during oxidation may lead to the observed inactivation of AUM due to H_2O_2 treatment, while reduction of the disulfide may lead to the re-activation of AUM. Because of the prominent position of the proposed disulfide, directly linking the core and the cap domain, a structural rearrangement of the two domains to each other may occur. This could result in an open/close mechanism, making the active site more accessible for the substrate, explaining the activation of AUM by reduction.

Such an open/close mechanism, regulating HAD phosphatase activity has already been proposed. The split phosphoaspartyl transferase mechanism is dependent on an initial reaction that requires solvent exclusion (to favor the Asp-based nucleophilic attack), and a subsequent reaction that involves extensive solvent contact (leading to the hydrolysis of the aspartylphosphate intermediate). Therefore, an essential aspect of catalysis is the alternation between closed and open states of the active site cavity. It is assumed, that the more flexible elements, such as the “squiggle” and “flap” signature elements and C1 class cap domains can perform this task (Burroughs *et al.*, 2006; Lahiri *et al.*, 2002b). The cooperation of core and cap acting on the substrate is described as highly dynamic. No general structural consensus of the interplay between cap and core domain has been defined so far. Solved structures of the phosphoserine phosphatase of *M. jannaschii* present the open (PDB: 1F5S) and closed (PDB: 1RKU) conformation (Wang *et al.*, 2001), mediated by the C1 cap. For members of the C2 subclass of the HADSF, such as AUM and chronophin, no extensive cap movements have been described till date. To address the question, whether the observed activation and inhibition of AUM due to a redox switch are a result of structural changes, CD spectroscopy was performed. Upon oxidation, no changes were observed. This result supports the hypothesis of a closed conformation based on a disulfide that is stabilizing the unstructured regions lining the cap domain. The CD spectrum of reduced AUM showed clear changes compared to the untreated enzyme suggesting an open conformation due to disulfide reduction. Of course the open/close mechanism in AUM depending on a redox switch is still speculative and structural evidence has to support these findings in the future.

switch is still speculative and structural evidence has to support these findings in the future.

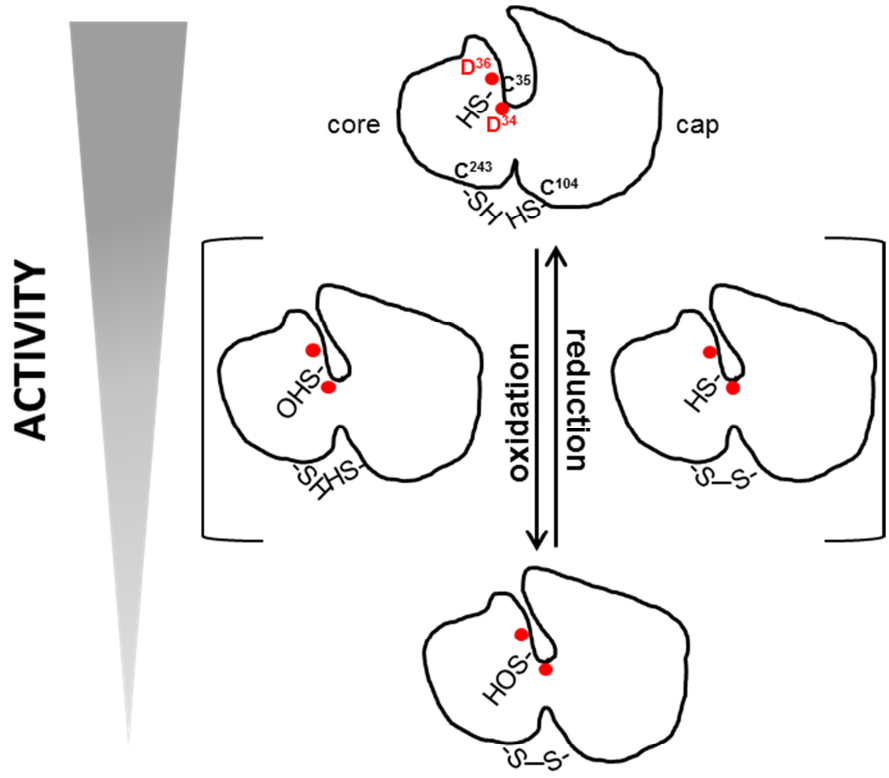

Figure 44: Model of the predicted mechanism of reversible oxidation of AUM (for details see the text below).

For the described mechanism, Cys35 and a Cys of the proposed disulfide is needed. The interplay of the identified residues is unclear. For SHP-1 and SHP-2, “backdoor” cysteines have been described. After oxidation, a disulfide between the catalytic cysteine and a nearby “backdoor” cysteine is built to stabilize the reversible oxidation state (Chen *et al.*, 2009). Since there is no structure of the AUM core available, the connection remains unclear.

Still, a hypothesis on how reversible regulation of AUM may take place can be proposed from the biochemical data (figure 44). Under the reducing conditions present in the cytoplasm, all cysteine residues of AUM are likely to be reduced, the enzyme is fully active and in its open conformation (experimentally mimicked by DTT). By e.g. ROS-mediated oxidative stress, the thiol groups of Cys35, Cys104 and Cys243 get oxidized. Oxidation of these Cys residues could either happen simultaneously or in a stepwise fashion based on differences in accessibility of the single residues. Inhibition of AUM takes place by a conformational change allowing the building of the disulfide resulting in the closure of the active site. Additionally, tetramerization by Cys293 could take place. The mechanism is reversible. By the reduction of the disulfide the enzyme opens up, Cys35 gets accessible to reduction and AUM activity is recovered. In conclusion, the data present the first evidence for the regulation of AUM catalysis by reversible oxidation. This finding is unique in the field of HAD phosphatases.

As a next step the proposed mechanism has to be investigated in a cellular system. As described, ROS production and the reduction of proteins by antioxidant complexes is a very local and temporary event due to a stimulus, here described for growth factor signaling (figure 3). Meaning phosphatase inhibition contributes to fine tuning events in cell signaling. If AUM is a target of RTK mediated oxidation, a predominant localization close to the plasma membrane should be observed. However, preliminary data from our group show that endogenous AUM is mostly diffusely distributed in the cytoplasm. In addition to plasma membrane-proximal ROS generation, cellular compartments such as mitochondria and peroxisomes are described as “redox hotspots” (Ivashchenko *et al.*, 2011). In the future, AUM activity has to be linked to local redox events or to redox-active compartments presenting redox switches. This could be done by colocalization experiments with members of the RTK or NOX family or with mitochondria/peroxisome markers. For this type of experiments the generated and characterized AUM antibody (figure 15, 16) will be a helpful tool.

Next to this, the developed fractionation based AUM activity assay can be used to investigate the role of reversible oxidation of AUM in cells and tissues. When used in combination with the activation of AUM via reducing agents, this fractionation based activity assay is the first tool to differentiate between cell lines or tissues with different AUM concentrations or activities. While the physiological substrate of AUM is still unknown, there is evidence for a tyrosine phosphorylated protein substrate, and this thesis additionally presents the ability of AUM to act on small molecular weight substrates. *In vitro* protein phosphatase assays are quite challenging. One of the difficulties that have to be overcome for these assays is to properly recapitulate the physiological conditions that may be essential for dephosphorylation of the respective protein substrate (for example, factors present in a particular subcellular compartment). In addition, the isolation of the phosphorylated substrate or the appropriate phosphorylation of the substrate *in vitr*o can be challenging. Alternatively, phospho-peptides can be used as substrates, but in this case the transfer of peptide-based results to intact proteins data can be problematic (Zhang *et al.*, 1994a). Because of these issues, artificial substrates are commonly used to detect phosphatase activity in cell lysates. The most practical substrate to monitor AUM activity is *p*NPP. As described in chapter 4.1, *p*NPP serves as a substrate for a variety of phosphatases like PTP-1B and SHP-2 (Parsons and Gates, 2013). To overcome this issue, the AUM activity assay presented in this thesis is based on a fractionation of the cell lysate protein content by size. With this, AUM should be dissociated from other *p*NPP phosphatases and molecules that may disturb the assay. In addition, the TMN buffer system was shown to provide suitable conditions for measuring AUM activity and restricting the activity of other phosphatases. The fractionation of cell lysates (GC1 spg, HEK AD 293) and platelets made a specific readout of AUM activity

possible (figures 40-42). This is proven by using cell lines lacking (active) AUM (GC1 spg/shRNA AUM, HEK AD 293/siRNA AUM) and platelets expressing AUM^{D34N} instead of AUM^{WT}. These cell lysates contained no detectable *p*NPP phosphatase activity. To increase the assay readout, the reducing agent DTT was added. The readout signal increased and only fractions including active AUM showed phosphatase activity. With this, an unspecific stimulus was combined with a general phosphatase substrate to generate a specific AUM activity readout. In the future, this assay will be employed to investigate the mechanism of reversible oxidation of AUM and to distinguish between AUM^{WT} and AUM^{D34N} expressing tissues.

Taken together, novel modes of AUM regulation and determinants of specificity have been identified and investigated in structural and mechanistic detail. As a key message, residues of the core domain are responsible for the regulation of catalysis and residues of the cap domain define the substrate specificity of AUM and chronophin. This fully supports the idea of the conserved core acting as “business part” and the variable cap domain acting as “private part” for phosphatases of the HADSF. In addition, the interplay between both domains is functionally important. The substrate leaving group and the phosphoryl group are bound by the cap and core domains, and specificity and catalysis can therefore not be independent of each other. Substrate binding and catalysis are based on the functional co-dependence between the core and the cap domain. It is important to note, that even though the overall structure and mechanism of mammalian HAD phosphatases is conserved, small differences on the amino acid level make each member functionally unique. A thorough biochemical characterization of each member of the HAD phosphatase family is therefore essential to understand their roles in the complex system of phospho-regulation in the mammalian system.

5 Summary

Mammalian haloacid dehalogenase (HAD)-type phosphatases are an emerging family of enzymes with important functions in physiology and disease. HAD phosphatases can target diverse metabolites, lipids, DNA, and serine/threonine or tyrosine phosphorylated proteins with often high specificity (Seifried *et al.*, 2013). These enzymes thus markedly enlarge the repertoire and substrate spectrum of mammalian phosphatases. However, the basis of HAD phosphatase substrate specificity is still elusive and a number of mammalian HAD phosphatases remain uncharacterized to date. This study characterizes the biochemical and structural properties of AUM (aspartate-based, ubiquitous, Mg^{2+}-dependent phosphatase), a previously unexplored mammalian HAD phosphatase.

In vitro phosphatase assays of purified, recombinant AUM showed phosphatase activity towards *para*-nitrophenyl phosphate and adenine and guanine nucleotide di- and triphosphates. Inhibitor studies indicated that similar to other HAD superfamily members, the AUM-catalyzed dephosphorylation reaction proceeds via a pentacovalent phosphoaspartate intermediate. In line with an aspartate-based catalytic mechanism, AUM was insensitive to inhibitors of serine/threonine phosphatases. The characterization of the purified recombinant murine enzyme also revealed that AUM exists in equilibrium between dimers and tetramers.

AUM was identified as the closest, yet functionally distinct relative of chronophin, a pyridoxal 5'-phosphate and serine/threonine-directed phosphatase. Phylogenetic analyses showed that AUM and chronophin evolved via duplication of an ancestral gene at the origin of the vertebrates. In contrast to chronophin, AUM acts as a tyrosine-specific HAD-type phosphatase *in vitro* and in cells. To elucidate how AUM and chronophin achieve these distinct substrate preferences, comparative evolutionary analyses, biochemical approaches and structural analyses were combined. Swapping experiments of less homologous regions between AUM and chronophin were performed. The mutational analysis revealed residues important for AUM catalysis and specificity. A single differently conserved residue in the cap domain of AUM or chronophin is crucial for phosphatase specificity (AUM^{L204}, $chronophin^{H182}$). The X-ray crystal structure of the AUM cap fused to the catalytic core of chronophin (CAC, PDB: 4BKM) was solved to 2.65 Å resolution. It presents the first crystal structure of the murine AUM capping domain. The detailed view of the catalytic clefts of AUM and chronophin reveals the structural basis of the divergent substrate specificities. These presented findings provide insights into the design principles of capped HAD phosphatases and show that their substrate specificity can be encoded by a small number of predictable residues.

In addition, the catalytic properties of AUM were investigated, identifying a mechanism of reversible oxidation regulating the activity of AUM *in vitro*. AUM phosphatase activity is inhibited by oxidation and can be recovered by reduction. The underlying molecular mechanism was revealed by mutational analyses. The cysteines C35, C104 and C243, located in the AUM core domain, are responsible for the inhibition of AUM by oxidation. C293 mediates the redox-dependent tetramerization of AUM *in vitro*. Based on the chronophin and CAC structure, a direct impact of the oxidation of C35 on the nucleophile D34 is proposed. In addition, a redox-dependent disulfide bridge (C104, C243), connecting the core and cap domain of AUM may be important for an open/close-mechanism. This hypothesis is supported by CD spectroscopy experiments that demonstrate a structural change in AUM upon reduction. These data present the first evidence for the regulation of AUM catalysis by reversible oxidation. This finding is so far unique in the field of HAD phosphatases.

In this context, the first cell-based AUM activity assay was developed. For this, the artificial substrate *p*NPP was combined with the reducing agent DTT to create a specific AUM activity readout. This fractionation-based assay is the first tool to differentiate between cell lines or tissues with different AUM concentrations or activities.

Taken together, the presented biochemical characterization reveals the specificity determinants and catalytic properties of AUM. General insights into structural determinants of mammalian HAD phosphatase substrate recognition are provided and reversible oxidation as possible regulatory mechanism for AUM is proposed. These findings constitute a framework for further functional analyses to elucidate the biomedical importance of AUM.

Zusammenfassung

Enzyme der Klasse der Haloazid Dehalogenase (HAD)-Typ Phosphatasen in Säugern sind an einer Vielzahl biologischer Prozesse mit unmittelbarer Relevanz für Erkrankungen beteiligt. Ihre Funktionen sind jedoch nach wie vor nur rudimentär verstanden. Es ist bekannt, das HAD Phosphatasen, unterschiedliche Metabolite, Lipide und DNA, sowie an Serin/Threonin- oder Tyrosinresten phosphorylierte Proteine spezifisch dephosphorylieren (Seifried *et al.*, 2013). Der Mechanismus dieser Substratspezifität ist bislang weitgehend unerforscht und einige HAD Phosphatasen in Säugern sind nach wie vor nicht charakterisiert. Diese Arbeit beschreibt die biochemischen und strukturellen Eigenschaften von AUM (Aspartat-basierte, ubiquitäre, Mg^{2+}-abhängige Phosphatase), eine der bisher uncharakterisierten HAD Phosphatasen.

In vitro Phosphatase-Assays mit gereinigtem, rekombinantem AUM zeigten, dass AUM kleinmolekulare Substrate wie z. B das artifizielle Substrat *para*-Nitrophenylphosphat und Adenin- und Guaninnukleotid Di- und Triphosphate dephosphorylieren kann. Inhibitorstudien bestätigten den Asparat-basierten Mechanismus der Katalyse für AUM. Des Weiteren zeigte die Charakterisierung des gereinigten rekombinanten murinen Enzyms, dass AUM in Lösung in einem dynamischen Verhältnis von Dimeren und Tetrameren vorliegt.

AUM wurde als nächster Verwandter der Pyridoxal 5`-Phosphat und Serin/Threonin-gerichteten Phosphatase Chronophin identifiziert. Phylogenetische Analysen zeigten, dass AUM und Chronophin durch Duplikation eines gemeinsamen Vorläufergens zu Beginn der Vertebraten-Evolution entstanden sind. Beide Enzyme sind jedoch funktionell unterschiedlich; im Unterschied zu Chronophin zeigt AUM in Zellen und *in vitro* eine Tyrosin-gerichtete Phosphatase-Aktivität.

Um die Basis der unterschiedlichen Substratpräferenz von AUM und Chronophin aufzuklären, wurden in der vorliegenden Arbeit evolutionsbiologische Analysen, biochemische Versuche und Strukturanalysen kombiniert. Durch den Austausch von Regionen geringer Homologie in AUM und Chronophin und die Bestimmung der Substratpräferenz der so generierten Mutanten wurden Reste identifiziert die für die Katalyse und Spezifität von AUM ausschlaggebend sind. So ist ein unterschiedlich konservierter Rest in der Cap-Domäne von AUM oder Chronophin (AUM^{L204}, $Chronophin^{H182}$) entscheidend für die Spezifität der Phosphatasen. Die Struktur des CAC-Fusionsproteins (Cap-Domäne von AUM fusioniert mit der Core-Domäne von Chronophin) wurde röntgenstrukturanalytisch charakterisiert. Die gelöste CAC Struktur (2.65 Å, PDB: 4BKM) stellt die erste Struktur einer murinen AUM Cap-Domäne dar. Die Detailansicht der katalytischen Zentren von AUM und Chronophin zeigt den molekularen Aufbau der Substratspezifität der beiden Phosphatasen. Diese Daten geben Einblicke in den prinzipiellen Aufbau von HAD Phosphatasen mit Cap-

Domäne und belegen, dass die Substratspezifität durch eine kleine Anzahl an vorhersagbaren Resten definiert werden kann.

Zusätzlich wurden die katalytischen Eigenschaften von AUM untersucht. Es konnte gezeigt werden, dass die AUM-Aktivität *in vitro* durch reversible Oxidation reguliert wird. Die Phosphataseaktivität wird durch Oxidation inhibiert und kann durch Reduktion wiederhergestellt bzw. gesteigert werden. Der zugrunde liegende molekulare Mechanismus wurde mittels Mutationsanalysen aufgeklärt. Die Cysteine C35, C104 und C243 sind für die durch Oxidation ausgelöste Inhibition von AUM verantwortlich. Die identifizierten Reste sind an, für die Katalyse wichtigen Positionen, der AUM Core-Domäne lokalisiert. Abgeleitet aus der Chronophin und CAC Struktur hat die Oxidation von C35 möglicherweise Einfluss auf die Eigenschaften des Nukleophils D34 und trägt so zur Inhibition der Phosphatasefunktion von AUM bei. Zusätzlich könnte eine Disulfidbrücke (C104, C243), welche die AUM Cap- und Core-Domäne verknüpft; für einen Redox-abhängingen *open/close*-Mechanismus des Enzyms verantwortlich sein. Diese Hypothese wird durch CD-spektroskopische Analysen gestützt mit welchen eine strukturelle Veränderung von AUM unter reduzierenden Bedingungen nachgewiesen wurde. Eine Redox-vermittelte Modulation der AUM Struktur könnte so zur Inhibition beitragen. Diese Daten sind ein erster Hinweis auf eine mögliche Regulation von AUM durch reversible Oxidation. Bis jetzt ist diese Beobachtung für HAD Phosphatasen einzigartig.

In diesem Zusammenhang wurde auch der erste zellbasierte AUM-Aktivitäts-Assay entwickelt. Durch die Kombination des artifiziellen Substrats *p*NPP und des Reduktionsmittels DTT konnte spezifisch AUM Phosphatase-Aktivität in diversen Zelllysaten gemessen werden. Dieser Assay, basierend auf der säulenchromatografischen Fraktionierung von Zell- oder Gewebelysaten, macht es nun möglich, Zelllinien oder Gewebe mit unterschiedlichen AUM Konzentrationen oder mit unterschiedlichen AUM-Aktivitäten zu differenzieren.

Die Substratspezifität von Enzymen sowie die Modulation von zellulären Prozessen durch Oxidation sind wichtige Bestandteile der Signaltransduktion. Durch die vorliegende biochemische Charakterisierung konnten die Determinanten der Spezifität und der katalytischen Eigenschaften der HAD-Typ Phosphatase AUM aufgeklärt werden. Des Weiteren wurde die reversible Oxidation von AUM als möglicher Mechanismus zur Regulation der Enzymaktivität identifiziert. Die präsentierten Daten können als Grundlage für zukünftige Arbeiten zur Aufklärung einer biomedizinischen Relevanz der Phosphatase AUM dienen.

6 References

ADAMS, P. D., AFONINE, P. V., BUNKOCZI, G., CHEN, V. B., DAVIS, I. W., ECHOLS, N., HEADD, J. J., HUNG, L. W., KAPRAL, G. J., GROSSE-KUNSTLEVE, R. W., MCCOY, A. J., MORIARTY, N. W., OEFFNER, R., READ, R. J., RICHARDSON, D. C., RICHARDSON, J. S., TERWILLIGER, T. C. & ZWART, P. H. 2010. PHENIX: a comprehensive Python-based system for macromolecular structure solution. *Acta Crystallogr D Biol Crystallogr,* 66**,** 213-21.

AGAZIE, Y. M. & HAYMAN, M. J. 2003. Development of an efficient "substrate-trapping" mutant of Src homology phosphotyrosine phosphatase 2 and identification of the epidermal growth factor receptor, Gab1, and three other proteins as target substrates. *J Biol Chem,* 278**,** 13952-8.

ALLEN, K. N. & DUNAWAY-MARIANO, D. 2004. Phosphoryl group transfer: evolution of a catalytic scaffold. *Trends Biochem Sci,* 29**,** 495-503.

ALLEN, K. N. & DUNAWAY-MARIANO, D. 2009. Markers of fitness in a successful enzyme superfamily. *Curr Opin Struct Biol,* 19**,** 658-65.

ALMO, S. C., BONANNO, J. B., SAUDER, J. M., EMTAGE, S., DILORENZO, T. P., MALASHKEVICH, V., WASSERMAN, S. R., SWAMINATHAN, S., ESWARAMOORTHY, S., AGARWAL, R., KUMARAN, D., MADEGOWDA, M., RAGUMANI, S., PATSKOVSKY, Y., ALVARADO, J., RAMAGOPAL, U. A., FABER-BARATA, J., CHANCE, M. R., SALI, A., FISER, A., ZHANG, Z. Y., LAWRENCE, D. S. & BURLEY, S. K. 2007. Structural genomics of protein phosphatases. *J Struct Funct Genomics,* 8**,** 121-40.

ALONSO, A., SASIN, J., BOTTINI, N., FRIEDBERG, I., OSTERMAN, A., GODZIK, A., HUNTER, T., DIXON, J. & MUSTELIN, T. 2004. Protein tyrosine phosphatases in the human genome. *Cell,* 117**,** 699-711.

ANDERSEN, J. N., JANSEN, P. G., ECHWALD, S. M., MORTENSEN, O. H., FUKADA, T., DEL VECCHIO, R., TONKS, N. K. & MOLLER, N. P. 2004. A genomic perspective on protein tyrosine phosphatases: gene structure, pseudogenes, and genetic disease linkage. *FASEB J,* 18**,** 8-30.

ARAVIND, L., GALPERIN, M. Y. & KOONIN, E. V. 1998. The catalytic domain of the P-type ATPase has the haloacid dehalogenase fold. *Trends Biochem Sci,* 23**,** 127-9.

BARFORD, D., DAS, A. K. & EGLOFF, M. P. 1998. The structure and mechanism of protein phosphatases: insights into catalysis and regulation. *Annu Rev Biophys Biomol Struct,* 27**,** 133-64.

BARFORD, D., FLINT, A. J. & TONKS, N. K. 1994. Crystal structure of human protein tyrosine phosphatase 1B. *Science,* 263**,** 1397-404.

BARFORD, D., JIA, Z. & TONKS, N. K. 1995. Protein tyrosine phosphatases take off. *Nat Struct Biol,* 2**,** 1043-53.

BARR, A. J., UGOCHUKWU, E., LEE, W. H., KING, O. N., FILIPPAKOPOULOS, P., ALFANO, I., SAVITSKY, P., BURGESS-BROWN, N. A., MULLER, S. & KNAPP, S. 2009. Large-scale structural analysis of the classical human protein tyrosine phosphatome. *Cell,* 136**,** 352-63.

BATTYE, T. G., KONTOGIANNIS, L., JOHNSON, O., POWELL, H. R. & LESLIE, A. G. 2011. iMOSFLM: a new graphical interface for diffraction-image processing with MOSFLM. *Acta Crystallogr D Biol Crystallogr,* 67**,** 271-81.

BENNETT, A. M., TANG, T. L., SUGIMOTO, S., WALSH, C. T. & NEEL, B. G. 1994. Protein-tyrosine-phosphatase SHPTP2 couples platelet-derived growth factor receptor beta to Ras. *Proc Natl Acad Sci U S A,* 91**,** 7335-9.

BERNSTEIN, N. K., WILLIAMS, R. S., RAKOVSZKY, M. L., CUI, D., GREEN, R., KARIMI-BUSHERI, F., MANI, R. S., GALICIA, S., KOCH, C. A., CASS, C. E., DUROCHER, D., WEINFELD, M. & GLOVER, J. N. 2005. The molecular architecture of the mammalian DNA repair enzyme, polynucleotide kinase. *Mol Cell,* 17**,** 657-70.

BIALOJAN, C., RUEGG, J. C. & TAKAI, A. 1988. Effects of okadaic acid on isometric tension and myosin phosphorylation of chemically skinned guinea-pig taenia coli. *J Physiol,* 398**,** 81-95.

BIGAY, J., DETERRE, P., PFISTER, C. & CHABRE, M. 1987. Fluoride complexes of aluminium or beryllium act on G-proteins as reversibly bound analogues of the gamma phosphate of GTP. *EMBO J,* 6**,** 2907-13.

BILWES, A. M., DEN HERTOG, J., HUNTER, T. & NOEL, J. P. 1996. Structural basis for inhibition of receptor protein-tyrosine phosphatase-alpha by dimerization. *Nature,* 382**,** 555-9.

BLANCHETOT, C., CHAGNON, M., DUBE, N., HALLE, M. & TREMBLAY, M. L. 2005. Substrate-trapping techniques in the identification of cellular PTP targets. *Methods,* 35**,** 44-53.

BOWLING, F. G. 2011. Pyridoxine supply in human development. *Semin Cell Dev Biol,* 22**,** 611-8.

BRENNAN, J. P., BARDSWELL, S. C., BURGOYNE, J. R., FULLER, W., SCHRODER, E., WAIT, R., BEGUM, S., KENTISH, J. C. & EATON, P. 2006. Oxidant-induced activation of type I protein kinase A is mediated by RI subunit interprotein disulfide bond formation. *J Biol Chem,* 281**,** 21827-36.

BUHRMAN, G., PARKER, B., SOHN, J., RUDOLPH, J. & MATTOS, C. 2005. Structural mechanism of oxidative regulation of the phosphatase Cdc25B via an intramolecular disulfide bond. *Biochemistry,* 44**,** 5307-16.

BURROUGHS, A. M., ALLEN, K. N., DUNAWAY-MARIANO, D. & ARAVIND, L. 2006. Evolutionary genomics of the HAD superfamily: understanding the structural adaptations and catalytic diversity in a superfamily of phosphoesterases and allied enzymes. *J Mol Biol,* 361**,** 1003-34.

CASELLI, A., MARZOCCHINI, R., CAMICI, G., MANAO, G., MONETI, G., PIERACCINI, G. & RAMPONI, G. 1998. The inactivation mechanism of low molecular weight phosphotyrosine-protein phosphatase by H2O2. *J Biol Chem,* 273**,** 32554-60.

CHEN, C. Y., WILLARD, D. & RUDOLPH, J. 2009. Redox regulation of SH2-domain-containing protein tyrosine phosphatases by two backdoor cysteines. *Biochemistry,* 48**,** 1399-409.

CHEN, V. B., ARENDALL, W. B., 3RD, HEADD, J. J., KEEDY, D. A., IMMORMINO, R. M., KAPRAL, G. J., MURRAY, L. W., RICHARDSON, J. S. & RICHARDSON, D. C. 2010. MolProbity: all-atom structure validation for macromolecular crystallography. *Acta Crystallogr D Biol Crystallogr,* 66**,** 12-21.

CHO, H., WANG, W., KIM, R., YOKOTA, H., DAMO, S., KIM, S. H., WEMMER, D., KUSTU, S. & YAN, D. 2001. BeF(3)(-) acts as a phosphate analog in proteins phosphorylated on aspartate: structure of a BeF(3)(-) complex with phosphoserine phosphatase. *Proc Natl Acad Sci U S A,* 98**,** 8525-30.

CHU, Y., LEE, E. Y. & SCHLENDER, K. K. 1996. Activation of protein phosphatase 1. Formation of a metalloenzyme. *J Biol Chem,* 271**,** 2574-7.

COHEN, P. 1992. Signal integration at the level of protein kinases, protein phosphatases and their substrates. *Trends in Biochemical Sciences,* 17**,** 408-413.

COHEN, P. 2000. The regulation of protein function by multisite phosphorylation--a 25 year update. *Trends Biochem Sci,* 25**,** 596-601.

COHEN, P. 2002. The origins of protein phosphorylation. *Nat Cell Biol,* 4**,** E127-30.

COHEN, P., KLUMPP, S. & SCHELLING, D. L. 1989. An improved procedure for identifying and quantitating protein phosphatases in mammalian tissues. *FEBS Lett,* 250**,** 596-600.

COLLET, J. F., STROOBANT, V., PIRARD, M., DELPIERRE, G. & VAN SCHAFTINGEN, E. 1998. A new class of phosphotransferases phosphorylated on an aspartate residue in an amino-terminal DXDX(T/V) motif. *J Biol Chem,* 273**,** 14107-12.

COOK, P. J., JU, B. G., TELESE, F., WANG, X., GLASS, C. K. & ROSENFELD, M. G. 2009. Tyrosine dephosphorylation of H2AX modulates apoptosis and survival decisions. *Nature,* 458**,** 591-6.

COPLEY, S. D. 1998. Microbial dehalogenases: enzymes recruited to convert xenobiotic substrates. *Curr Opin Chem Biol,* 2**,** 613-7.

CSAKI, L. S. & REUE, K. 2010. Lipins: multifunctional lipid metabolism proteins. *Annu Rev Nutr,* 30**,** 257-72.

DADKE, S., COTTERET, S., YIP, S. C., JAFFER, Z. M., HAJ, F., IVANOV, A., RAUSCHER, F., 3RD, SHUAI, K., NG, T., NEEL, B. G. & CHERNOFF, J. 2007. Regulation of protein tyrosine phosphatase 1B by sumoylation. *Nat Cell Biol,* 9**,** 80-5.

DADKE, S., KUSARI, A. & KUSARI, J. 2001. Phosphorylation and activation of protein tyrosine phosphatase (PTP) 1B by insulin receptor. *Mol Cell Biochem,* 221**,** 147-54.

DAGNELL, M., FRIJHOFF, J., PADER, I., AUGSTEN, M., BOIVIN, B., XU, J., MANDAL, P. K., TONKS, N. K., HELLBERG, C., CONRAD, M., ARNER, E. S. & OSTMAN, A. 2013. Selective activation of oxidized PTP1B by the thioredoxin system modulates PDGF-beta receptor tyrosine kinase signaling. *Proc Natl Acad Sci U S A,* 110**,** 13398-403.

DAVIES, M. J. 2005. The oxidative environment and protein damage. *Biochim Biophys Acta,* 1703**,** 93-109.

DE CARVALHO, L. P., ZHAO, H., DICKINSON, C. E., ARANGO, N. M., LIMA, C. D., FISCHER, S. M., OUERFELLI, O., NATHAN, C. & RHEE, K. Y. 2010. Activity-based metabolomic profiling of enzymatic function: identification of Rv1248c as a mycobacterial 2-hydroxy-3-oxoadipate synthase. *Chem Biol,* 17**,** 323-32.

DEAN, R. T., FU, S., STOCKER, R. & DAVIES, M. J. 1997. Biochemistry and pathology of radical-mediated protein oxidation. *Biochem J,* 324 (Pt 1)**,** 1-18.

DENU, J. M. & TANNER, K. G. 1998. Specific and reversible inactivation of protein tyrosine phosphatases by hydrogen peroxide: evidence for a sulfenic acid intermediate and implications for redox regulation. *Biochemistry,* 37**,** 5633-42.

DEREEPER, A., GUIGNON, V., BLANC, G., AUDIC, S., BUFFET, S., CHEVENET, F., DUFAYARD, J. F., GUINDON, S., LEFORT, V., LESCOT, M., CLAVERIE, J. M. & GASCUEL, O. 2008. Phylogeny.fr: robust phylogenetic analysis for the non-specialist. *Nucleic Acids Res,* 36**,** W465-9.

DEWALD, B., BAGGIOLINI, M., CURNUTTE, J. T. & BABIOR, B. M. 1979. Subcellular localization of the superoxide-forming enzyme in human neutrophils. *J Clin Invest,* 63**,** 21-9.

DONKOR, J., SARIAHMETOGLU, M., DEWALD, J., BRINDLEY, D. N. & REUE, K. 2007. Three mammalian lipins act as phosphatidate phosphatases with distinct tissue expression patterns. *J Biol Chem,* 282**,** 3450-7.

EDGAR, R. C. 2004. MUSCLE: multiple sequence alignment with high accuracy and high throughput. *Nucleic Acids Res,* 32**,** 1792-7.

EGUCHI, Y., SHIMIZU, S. & TSUJIMOTO, Y. 1997. Intracellular ATP levels determine cell death fate by apoptosis or necrosis. *Cancer Res,* 57**,** 1835-40.

EIBERG, H., EWALD, H. & MORS, O. 1993. Suggestion of linkage between manic-depressive illness and the enzyme phosphoglycolate phosphatase (PGP) on chromosome 16p. *Clin Genet,* 44**,** 254-7.

EVANS, P. 2006. Scaling and assessment of data quality. *Acta Crystallogr D Biol Crystallogr,* 62**,** 72-82.

EVNOUCHIDOU, I., BIRTLEY, J., SEREGIN, S., PAPAKYRIAKOU, A., ZERVOUDI, E., SAMIOTAKI, M., PANAYOTOU, G., GIASTAS, P., PETRAKIS, O., GEORGIADIS, D., AMALFITANO, A., SARIDAKIS, E., MAVRIDIS, I. M. & STRATIKOS, E. 2012. A common single nucleotide polymorphism in endoplasmic reticulum aminopeptidase 2 induces a specificity switch that leads to altered antigen processing. *J Immunol,* 189**,** 2383-92.

FALET, H., PAIN, S. & RENDU, F. 1998. Tyrosine unphosphorylated platelet SHP-1 is a substrate for calpain. *Biochem Biophys Res Commun,* 252**,** 51-5.

FISCHER, E. H. & KREBS, E. G. 1955. Conversion of phosphorylase b to phosphorylase a in muscle extracts. *J Biol Chem,* 216**,** 121-32.

FLINT, A. J., TIGANIS, T., BARFORD, D. & TONKS, N. K. 1997. Development of "substrate-trapping" mutants to identify physiological substrates of protein tyrosine phosphatases. *Proc Natl Acad Sci U S A,* 94**,** 1680-5.

FONDA, M. L. 1992. Purification and characterization of vitamin B6-phosphate phosphatase from human erythrocytes. *J Biol Chem,* 267**,** 15978-83.

FONDA, M. L. & ZHANG, Y. N. 1995. Kinetic mechanism and divalent metal activation of human erythrocyte pyridoxal phosphatase. *Arch Biochem Biophys,* 320**,** 345-52.

FRANGIONI, J. V., ODA, A., SMITH, M., SALZMAN, E. W. & NEEL, B. G. 1993. Calpain-catalyzed cleavage and subcellular relocation of protein phosphotyrosine phosphatase 1B (PTP-1B) in human platelets. *EMBO J,* 12**,** 4843-56.

GALLUZZI, L., VITALE, I., SENOVILLA, L., OLAUSSEN, K. A., PINNA, G., EISENBERG, T., GOUBAR, A., MARTINS, I., MICHELS, J., KRATASSIOUK, G., CARMONA-GUTIERREZ, D., SCOAZEC, M., VACCHELLI, E., SCHLEMMER, F., KEPP, O., SHEN, S., TAILLER, M., NISO-SANTANO, M., MORSELLI, E., CRIOLLO, A., ADJEMIAN, S., JEMAA, M., CHABA, K., PAILLERET, C., MICHAUD, M., PIETROCOLA, F., TAJEDDINE, N., DE LA MOTTE ROUGE, T., ARAUJO, N., MOROZOVA, N., ROBERT, T., RIPOCHE, H., COMMO, F., BESSE, B., VALIDIRE, P., FOURET, P., ROBIN, A., DORVAULT, N., GIRARD, P., GOUY, S., PAUTIER, P., JAGEMANN, N., NICKEL, A. C., MARSILI, S., PACCARD, C., SERVANT, N., HUPE, P., BEHRENS, C., BEHNAM-MOTLAGH, P., KOHNO, K., CREMER, I., DAMOTTE, D., ALIFANO, M., MIDTTUN, O., UELAND, P. M., LAZAR, V., DESSEN, P., ZISCHKA, H., CHATELUT, E., CASTEDO, M., MADEO, F., BARILLOT, E., THOMALE, J., WISTUBA, II, SAUTES-FRIDMAN, C., ZITVOGEL, L., SORIA, J. C., HAREL-BELLAN, A. & KROEMER, G. 2012. Prognostic impact of vitamin B6 metabolism in lung cancer. *Cell Rep,* 2**,** 257-69.

GAO, G. & FONDA, M. L. 1994. Identification of an essential cysteine residue in pyridoxal phosphatase from human erythrocytes. *J Biol Chem,* 269**,** 8234-9.

GARTON, A. J. & TONKS, N. K. 1994. PTP-PEST: a protein tyrosine phosphatase regulated by serine phosphorylation. *EMBO J,* 13**,** 3763-71.

GHOSH, A., SHUMAN, S. & LIMA, C. D. 2008. The structure of Fcp1, an essential RNA polymerase II CTD phosphatase. *Mol Cell,* 32**,** 478-90.

GIANNI, D., BOHL, B., COURTNEIDGE, S. A. & BOKOCH, G. M. 2008. The involvement of the tyrosine kinase c-Src in the regulation of reactive oxygen species generation mediated by NADPH oxidase-1. *Mol Biol Cell,* 19**,** 2984-94.

GODINHO, L. M. & DE SA-NOGUEIRA, I. 2011. Characterization and regulation of a bacterial sugar phosphatase of the haloalkanoate dehalogenase superfamily, AraL, from Bacillus subtilis. *FEBS J,* 278**,** 2511-24.

GOHLA, A., BIRKENFELD, J. & BOKOCH, G. M. 2005. Chronophin, a novel HAD-type serine protein phosphatase, regulates cofilin-dependent actin dynamics. *Nat Cell Biol,* 7**,** 21-9.

GOLDBERG, J., HUANG, H. B., KWON, Y. G., GREENGARD, P., NAIRN, A. C. & KURIYAN, J. 1995. Three-dimensional structure of the catalytic subunit of protein serine/threonine phosphatase-1. *Nature,* 376**,** 745-53.

GRINTHAL, A., ADAMOVIC, I., WEINER, B., KARPLUS, M. & KLECKNER, N. 2010. PR65, the HEAT-repeat scaffold of phosphatase PP2A, is an elastic connector that links force and catalysis. *Proc Natl Acad Sci U S A,* 107**,** 2467-72.

GU, M. & MAJERUS, P. W. 1996. The properties of the protein tyrosine phosphatase PTPMEG. *J Biol Chem,* 271**,** 27751-9.

GUO, F., STANEVICH, V., WLODARCHAK, N., SENGUPTA, R., JIANG, L., SATYSHUR, K. A. & XING, Y. 2014. Structural basis of PP2A activation by PTPA, an ATP-dependent activation chaperone. *Cell Res,* 24**,** 190-203.

GUO, X., ENGEL, J. L., XIAO, J., TAGLIABRACCI, V. S., WANG, X., HUANG, L. & DIXON, J. E. 2011. UBLCP1 is a 26S proteasome phosphatase that regulates nuclear proteasome activity. *Proc Natl Acad Sci U S A,* 108**,** 18649-54.

HAN, G. S., WU, W. I. & CARMAN, G. M. 2006. The Saccharomyces cerevisiae Lipin homolog is a Mg2+-dependent phosphatidate phosphatase enzyme. *J Biol Chem,* 281**,** 9210-8.

HENDRICKX, A., BEULLENS, M., CEULEMANS, H., DEN ABT, T., VAN EYNDE, A., NICOLAESCU, E., LESAGE, B. & BOLLEN, M. 2009. Docking motif-guided mapping of the interactome of protein phosphatase-1. *Chem Biol,* 16**,** 365-71.

HIWADA, K. & WACHSMUTH, E. D. 1974. Catalytic properties of alkaline phosphatase from pig kidney. *Biochem J,* 141**,** 283-91.

HUANG, T. Y., MINAMIDE, L. S., BAMBURG, J. R. & BOKOCH, G. M. 2008. Chronophin mediates an ATP-sensing mechanism for cofilin dephosphorylation and neuronal cofilin-actin rod formation. *Dev Cell,* 15**,** 691-703.

HUANG, Y. F. & GOLDING, G. B. 2012. Inferring sequence regions under functional divergence in duplicate genes. *Bioinformatics,* 28**,** 176-83.

HUNTER, T. 2007. The age of crosstalk: phosphorylation, ubiquitination, and beyond. *Mol Cell,* 28**,** 730-8.

HUYER, G., LIU, S., KELLY, J., MOFFAT, J., PAYETTE, P., KENNEDY, B., TSAPRAILIS, G., GRESSER, M. J. & RAMACHANDRAN, C. 1997. Mechanism of inhibition of protein-tyrosine phosphatases by vanadate and pervanadate. *J Biol Chem,* 272**,** 843-51.

IMAMURA, H., NHAT, K. P., TOGAWA, H., SAITO, K., IINO, R., KATO-YAMADA, Y., NAGAI, T. & NOJI, H. 2009. Visualization of ATP levels inside single living cells with fluorescence resonance energy transfer-based genetically encoded indicators. *Proc Natl Acad Sci U S A,* 106**,** 15651-6.

ISHIHARA, H., MARTIN, B. L., BRAUTIGAN, D. L., KARAKI, H., OZAKI, H., KATO, Y., FUSETANI, N., WATABE, S., HASHIMOTO, K., UEMURA, D. & ET AL. 1989. Calyculin A and okadaic acid: inhibitors of protein phosphatase activity. *Biochem Biophys Res Commun,* 159**,** 871-7.

IVASHCHENKO, O., VAN VELDHOVEN, P. P., BREES, C., HO, Y. S., TERLECKY, S. R. & FRANSEN, M. 2011. Intraperoxisomal redox balance in mammalian cells: oxidative stress and interorganellar cross-talk. *Mol Biol Cell,* 22**,** 1440-51.

JACKSON, M. D., FJELD, C. C. & DENU, J. M. 2003. Probing the function of conserved residues in the serine/threonine phosphatase PP2Calpha. *Biochemistry,* 42**,** 8513-21.

JACOB, C., HOLME, A. L. & FRY, F. H. 2004. The sulfinic acid switch in proteins. *Org Biomol Chem,* 2**,** 1953-6.

JANG, Y. M., KIM, D. W., KANG, T. C., WON, M. H., BAEK, N. I., MOON, B. J., CHOI, S. Y. & KWON, O. S. 2003. Human pyridoxal phosphatase. Molecular cloning, functional expression, and tissue distribution. *J Biol Chem,* 278**,** 50040-6.

JUNG, S. K., JEONG, D. G., CHUNG, S. J., KIM, J. H., PARK, B. C., TONKS, N. K., RYU, S. E. & KIM, S. J. 2010. Crystal structure of ED-Eya2: insight into dual roles as a protein tyrosine phosphatase and a transcription factor. *FASEB J,* 24**,** 560-9.

KABSCH, W. & SANDER, C. 1983. Dictionary of protein secondary structure: pattern recognition of hydrogen-bonded and geometrical features. *Biopolymers,* 22**,** 2577-637.

KAMENSKI, T., HEILMEIER, S., MEINHART, A. & CRAMER, P. 2004. Structure and mechanism of RNA polymerase II CTD phosphatases. *Mol Cell,* 15**,** 399-407.

KARISCH, R. & NEEL, B. G. 2013. Methods to monitor classical protein-tyrosine phosphatase oxidation. *FEBS J,* 280**,** 459-75.

KATANE, M. & HOMMA, H. 2010. D-aspartate oxidase: the sole catabolic enzyme acting on free D-aspartate in mammals. *Chem Biodivers,* 7**,** 1435-49.

KESTLER, C., KNOBLOCH, G., TESSMER, I., JEANCLOS, E., SCHINDELIN, H. & GOHLA, A. 2014. Chronophin dimerization is required for proper positioning of its substrate specificity loop. *J Biol Chem,* 289**,** 3094-103.

KIM, H. Y., HEO, Y. S., KIM, J. H., PARK, M. H., MOON, J., KIM, E., KWON, D., YOON, J., SHIN, D., JEONG, E. J., PARK, S. Y., LEE, T. G., JEON, Y. H., RO, S., CHO, J. M. & HWANG, K. Y. 2002. Molecular basis for the local conformational rearrangement of human phosphoserine phosphatase. *J Biol Chem,* 277**,** 46651-8.

KIM, J. E., KIM, D. W., KWAK, S. E., KWON, O. S., CHOI, S. Y. & KANG, T. C. 2008. Potential role of pyridoxal-5'-phosphate phosphatase/chronopin in epilepsy. *Exp Neurol,* 211**,** 128-40.

KIM, Y., GENTRY, M. S., HARRIS, T. E., WILEY, S. E., LAWRENCE, J. C., JR. & DIXON, J. E. 2007. A conserved phosphatase cascade that regulates nuclear membrane biogenesis. *Proc Natl Acad Sci U S A,* 104**,** 6596-601.

KIM, Y., YAKUNIN, A. F., KUZNETSOVA, E., XU, X., PENNYCOOKE, M., GU, J., CHEUNG, F., PROUDFOOT, M., ARROWSMITH, C. H., JOACHIMIAK, A., EDWARDS, A. M. & CHRISTENDAT, D. 2004. Structure- and function-based characterization of a new

phosphoglycolate phosphatase from Thermoplasma acidophilum. *J Biol Chem,* 279**,** 517-26.

KITA, A., MATSUNAGA, S., TAKAI, A., KATAIWA, H., WAKIMOTO, T., FUSETANI, N., ISOBE, M. & MIKI, K. 2002. Crystal structure of the complex between calyculin A and the catalytic subunit of protein phosphatase 1. *Structure,* 10**,** 715-24.

KLEE, C. B., CROUCH, T. H. & KRINKS, M. H. 1979. Calcineurin: a calcium- and calmodulin-binding protein of the nervous system. *Proc Natl Acad Sci U S A,* 76**,** 6270-3.

KOONIN, E. V. & TATUSOV, R. L. 1994. Computer analysis of bacterial haloacid dehalogenases defines a large superfamily of hydrolases with diverse specificity. Application of an iterative approach to database search. *J Mol Biol,* 244**,** 125-32.

KREBS, E. G. & BEAVO, J. A. 1979. Phosphorylation-dephosphorylation of enzymes. *Annu Rev Biochem,* 48**,** 923-59.

KURIHARA, NOBUYOSHI & KENJI 2000. Bacterial 2-haloacid dehalogenases: structures and reaction mechanisms. *Journal of Molecular Catalysis B: Enzymatic,* 10**,** 57-65.

KURIHARA, T. & ESAKI, N. 2008. Bacterial hydrolytic dehalogenases and related enzymes: occurrences, reaction mechanisms, and applications. *Chem Rec,* 8**,** 67-74.

KWON, J., LEE, S. R., YANG, K. S., AHN, Y., KIM, Y. J., STADTMAN, E. R. & RHEE, S. G. 2004. Reversible oxidation and inactivation of the tumor suppressor PTEN in cells stimulated with peptide growth factors. *Proc Natl Acad Sci U S A,* 101**,** 16419-24.

KWON, J., QU, C. K., MAENG, J. S., FALAHATI, R., LEE, C. & WILLIAMS, M. S. 2005. Receptor-stimulated oxidation of SHP-2 promotes T-cell adhesion through SLP-76-ADAP. *EMBO J,* 24**,** 2331-41.

LAEMMLI, U. K. 1970. Cleavage of structural proteins during the assembly of the head of bacteriophage T4. *Nature,* 227**,** 680-5.

LAHIRI, S. D., ZHANG, G., DAI, J., DUNAWAY-MARIANO, D. & ALLEN, K. N. 2004. Analysis of the substrate specificity loop of the HAD superfamily cap domain. *Biochemistry,* 43**,** 2812-20.

LAHIRI, S. D., ZHANG, G., DUNAWAY-MARIANO, D. & ALLEN, K. N. 2002a. Caught in the act: the structure of phosphorylated beta-phosphoglucomutase from Lactococcus lactis. *Biochemistry,* 41**,** 8351-9.

LAHIRI, S. D., ZHANG, G., DUNAWAY-MARIANO, D. & ALLEN, K. N. 2003. The pentacovalent phosphorus intermediate of a phosphoryl transfer reaction. *Science,* 299**,** 2067-71.

LAHIRI, S. D., ZHANG, G., DUNAWAY-MARIANO, D. & ALLEN, K. N. 2006. Diversification of function in the haloacid dehalogenase enzyme superfamily: The role of the cap domain in hydrolytic phosphoruscarbon bond cleavage. *Bioorg Chem,* 34**,** 394-409.

LAHIRI, S. D., ZHANG, G., RADSTROM, P., DUNAWAY-MARIANO, D. & ALLEN, K. N. 2002b. Crystallization and preliminary X-ray diffraction studies of beta-phosphoglucomutase from Lactococcus lactus. *Acta Crystallogr D Biol Crystallogr,* 58**,** 324-6.

LARROUY-MAUMUS, G., BISWAS, T., HUNT, D. M., KELLY, G., TSODIKOV, O. V. & DE CARVALHO, L. P. 2013. Discovery of a glycerol 3-phosphate phosphatase reveals glycerophospholipid polar head recycling in Mycobacterium tuberculosis. *Proc Natl Acad Sci U S A,* 110**,** 11320-5.

LEE, S., FAUX, C., NIXON, J., ALETE, D., CHILTON, J., HAWADLE, M. & STOKER, A. W. 2007. Dimerization of protein tyrosine phosphatase sigma governs both ligand binding and isoform specificity. *Mol Cell Biol,* 27**,** 1795-808.

LEE, S. R., KWON, K. S., KIM, S. R. & RHEE, S. G. 1998. Reversible inactivation of protein-tyrosine phosphatase 1B in A431 cells stimulated with epidermal growth factor. *J Biol Chem,* 273**,** 15366-72.

LEE, S. Y., CHO, H. S., PELTON, J. G., YAN, D., BERRY, E. A. & WEMMER, D. E. 2001. Crystal structure of activated CheY. Comparison with other activated receiver domains. *J Biol Chem,* 276**,** 16425-31.

LESLIE, N. R., BENNETT, D., LINDSAY, Y. E., STEWART, H., GRAY, A. & DOWNES, C. P. 2003. Redox regulation of PI 3-kinase signalling via inactivation of PTEN. *EMBO J,* 22**,** 5501-10.

LEVINTHAL, D. J. & DEFRANCO, D. B. 2005. Reversible oxidation of ERK-directed protein phosphatases drives oxidative toxicity in neurons. *J Biol Chem,* 280**,** 5875-83.

LI, C., LIANG, Y. Y., FENG, X. H., TSAI, S. Y., TSAI, M. J. & O'MALLEY, B. W. 2008. Essential phosphatases and a phospho-degron are critical for regulation of SRC-3/AIB1 coactivator function and turnover. *Mol Cell,* 31**,** 835-49.

LINK, T. A., HATZFELD, O. M., UNALKAT, P., SHERGILL, J. K., CAMMACK, R. & MASON, J. R. 1996. Comparison of the "Rieske" [2Fe-2S] center in the bc1 complex and in bacterial dioxygenases by circular dichroism spectroscopy and cyclic voltammetry. *Biochemistry,* 35**,** 7546-52.

LIU, J. Q., KURIHARA, T., MIYAGI, M., ESAKI, N. & SODA, K. 1995. Reaction mechanism of L-2-haloacid dehalogenase of Pseudomonas sp. YL. Identification of Asp10 as the active site nucleophile by 18O incorporation experiments. *J Biol Chem,* 270**,** 18309-12.

LIZAMA-MANIBUSAN, B. & MCLAUGHLIN, B. 2013. Redox modification of proteins as essential mediators of CNS autophagy and mitophagy. *FEBS Lett,* 587**,** 2291-8.

LOH, K., DENG, H., FUKUSHIMA, A., CAI, X., BOIVIN, B., GALIC, S., BRUCE, C., SHIELDS, B. J., SKIBA, B., OOMS, L. M., STEPTO, N., WU, B., MITCHELL, C. A., TONKS, N. K., WATT, M. J., FEBBRAIO, M. A., CRACK, P. J., ANDRIKOPOULOS, S. & TIGANIS, T. 2009. Reactive oxygen species enhance insulin sensitivity. *Cell Metab,* 10**,** 260-72.

LU, Z., DUNAWAY-MARIANO, D. & ALLEN, K. N. 2005. HAD superfamily phosphotransferase substrate diversification: structure and function analysis of HAD subclass IIB sugar phosphatase BT4131. *Biochemistry,* 44**,** 8684-96.

LU, Z., DUNAWAY-MARIANO, D. & ALLEN, K. N. 2011. The X-ray crystallographic structure and specificity profile of HAD superfamily phosphohydrolase BT1666: comparison of paralogous functions in B. thetaiotaomicron. *Proteins,* 79**,** 3099-107.

LU, Z., WANG, L., DUNAWAY-MARIANO, D. & ALLEN, K. N. 2009. Structure-function analysis of 2-keto-3-deoxy-D-glycero-D-galactonononate-9-phosphate phosphatase defines specificity elements in type C0 haloalkanoate dehalogenase family members. *J Biol Chem,* 284**,** 1224-33.

LYNCH, M. & CONERY, J. S. 2000. The evolutionary fate and consequences of duplicate genes. *Science,* 290**,** 1151-5.

MACEK, B., GNAD, F., SOUFI, B., KUMAR, C., OLSEN, J. V., MIJAKOVIC, I. & MANN, M. 2008. Phosphoproteome analysis of E. coli reveals evolutionary conservation of bacterial Ser/Thr/Tyr phosphorylation. *Mol Cell Proteomics,* 7**,** 299-307.

MACEK, B., MIJAKOVIC, I., OLSEN, J. V., GNAD, F., KUMAR, C., JENSEN, P. R. & MANN, M. 2007. The serine/threonine/tyrosine phosphoproteome of the model bacterium Bacillus subtilis. *Mol Cell Proteomics,* 6**,** 697-707.

MAEHAMA, T. & DIXON, J. E. 1998. The tumor suppressor, PTEN/MMAC1, dephosphorylates the lipid second messenger, phosphatidylinositol 3,4,5-trisphosphate. *J Biol Chem,* 273**,** 13375-8.

MAHADEV, K., ZILBERING, A., ZHU, L. & GOLDSTEIN, B. J. 2001. Insulin-stimulated hydrogen peroxide reversibly inhibits protein-tyrosine phosphatase 1b in vivo and enhances the early insulin action cascade. *J Biol Chem,* 276**,** 21938-42.

MAJETI, R., BILWES, A. M., NOEL, J. P., HUNTER, T. & WEISS, A. 1998. Dimerization-induced inhibition of receptor protein tyrosine phosphatase function through an inhibitory wedge. *Science,* 279**,** 88-91.

MANNIK, M. & STAGE, D. E. 1971. Antibody-agarose immunoadsorbents: complete removal of classes of immunoglobulins from serum. *J Immunol,* 106**,** 1670-2.

MANNING, G., PLOWMAN, G. D., HUNTER, T. & SUDARSANAM, S. 2002. Evolution of protein kinase signaling from yeast to man. *Trends Biochem Sci,* 27**,** 514-20.

MARIANAYAGAM, N. J., SUNDE, M. & MATTHEWS, J. M. 2004. The power of two: protein dimerization in biology. *Trends Biochem Sci,* 29**,** 618-25.

MATTHIJS, G., SCHOLLEN, E., PARDON, E., VEIGA-DA-CUNHA, M., JAEKEN, J., CASSIMAN, J. J. & VAN SCHAFTINGEN, E. 1997. Mutations in PMM2, a phosphomannomutase gene on chromosome 16p13, in carbohydrate-deficient glycoprotein type I syndrome (Jaeken syndrome). *Nat Genet,* 16**,** 88-92.

MAYNES, J. T., BATEMAN, K. S., CHERNEY, M. M., DAS, A. K., LUU, H. A., HOLMES, C. F. & JAMES, M. N. 2001. Crystal structure of the tumor-promoter okadaic acid bound to protein phosphatase-1. *J Biol Chem,* 276**,** 44078-82.

MAZIN, P. V., GELFAND, M. S., MIRONOV, A. A., RAKHMANINOVA, A. B., RUBINOV, A. R., RUSSELL, R. B. & KALININA, O. V. 2010. An automated stochastic approach to the identification of the protein specificity determinants and functional subfamilies. *Algorithms Mol Biol,* 5**,** 29.

MCCOY, A. J., GROSSE-KUNSTLEVE, R. W., ADAMS, P. D., WINN, M. D., STORONI, L. C. & READ, R. J. 2007. Phaser crystallographic software. *J Appl Crystallogr,* 40**,** 658-674.

MENG, E. C. & BABBITT, P. C. 2011. Topological variation in the evolution of new reactions in functionally diverse enzyme superfamilies. *Curr Opin Struct Biol,* 21**,** 391-7.

MENG, T. C., BUCKLEY, D. A., GALIC, S., TIGANIS, T. & TONKS, N. K. 2004. Regulation of insulin signaling through reversible oxidation of the protein-tyrosine phosphatases TC45 and PTP1B. *J Biol Chem,* 279**,** 37716-25.

MENG, T. C., FUKADA, T. & TONKS, N. K. 2002. Reversible oxidation and inactivation of protein tyrosine phosphatases in vivo. *Mol Cell,* 9**,** 387-99.

MERTZ, P., YU, L., SIKKINK, R. & RUSNAK, F. 1997. Kinetic and spectroscopic analyses of mutants of a conserved histidine in the metallophosphatases calcineurin and lambda protein phosphatase. *J Biol Chem,* 272**,** 21296-302.

MOHI, M. G. & NEEL, B. G. 2007. The role of Shp2 (PTPN11) in cancer. *Curr Opin Genet Dev,* 17**,** 23-30.

MOORHEAD, G. B., DE WEVER, V., TEMPLETON, G. & KERK, D. 2009. Evolution of protein phosphatases in plants and animals. *Biochem J,* 417**,** 401-9.

MOTOSUGI, K., ESAKI, N. & SODA, K. 1982. Purification and properties of a new enzyme, DL-2-haloacid dehalogenase, from Pseudomonas sp. *J Bacteriol,* 150**,** 522-7.

MULLEY, J. C., BARTON, N. & CALLEN, D. F. 1990. Localisation of human PGP and HAGH genes to 16p13.3. *Cytogenet Cell Genet,* 53**,** 175-6.

MYERS, M. P., STOLAROV, J. P., ENG, C., LI, J., WANG, S. I., WIGLER, M. H., PARSONS, R. & TONKS, N. K. 1997. P-TEN, the tumor suppressor from human chromosome 10q23, is a dual-specificity phosphatase. *Proc Natl Acad Sci U S A,* 94**,** 9052-7.

NEET, K. E. & TIMM, D. E. 1994. Conformational stability of dimeric proteins: quantitative studies by equilibrium denaturation. *Protein Sci,* 3**,** 2167-74.

NEFF, C. D., ABKEVICH, V., PACKER, J. C., CHEN, Y., POTTER, J., RILEY, R., DAVENPORT, C., DEGRADO WARREN, J., JAMMULAPATI, S., BHATHENA, A., CHOI, W. S., KROEGER, P. E., METZGER, R. E., GUTIN, A., SKOLNICK, M. H., SHATTUCK, D. & KATZ, D. A. 2009. Evidence for HTR1A and LHPP as interacting genetic risk factors in major depression. *Mol Psychiatry,* 14**,** 621-30.

NEWMAN, J. W., MORISSEAU, C., HARRIS, T. R. & HAMMOCK, B. D. 2003. The soluble epoxide hydrolase encoded by EPXH2 is a bifunctional enzyme with novel lipid phosphate phosphatase activity. *Proc Natl Acad Sci U S A,* 100**,** 1558-63.

NIU, T., LIANG, X., YANG, J., ZHAO, Z. & ZHOU, G. W. 1999. Kinetic comparison of the catalytic domains of SHP-1 and SHP-2. *J Cell Biochem,* 72**,** 145-50.

OLSEN, J. V., BLAGOEV, B., GNAD, F., MACEK, B., KUMAR, C., MORTENSEN, P. & MANN, M. 2006. Global, in vivo, and site-specific phosphorylation dynamics in signaling networks. *Cell,* 127**,** 635-48.

OSTMAN, A., FRIJHOFF, J., SANDIN, A. & BOHMER, F. D. 2011. Regulation of protein tyrosine phosphatases by reversible oxidation. *J Biochem,* 150**,** 345-56.

PANDYA, C., BROWN, S., PIEPER, U., SALI, A., DUNAWAY-MARIANO, D., BABBITT, P. C., XIA, Y. & ALLEN, K. N. 2013. Consequences of domain insertion on sequence-structure divergence in a superfold. *Proc Natl Acad Sci U S A,* 110**,** E3381-7.

PANDYA, C., DUNAWAY-MARIANO, D., XIA, Y. & ALLEN, K. N. 2014. Structure-guided approach for detecting large domain inserts in protein sequences as illustrated using the haloacid dehalogenase superfamily. *Proteins*.

PARSONS, Z. D. & GATES, K. S. 2013. Thiol-dependent recovery of catalytic activity from oxidized protein tyrosine phosphatases. *Biochemistry,* 52**,** 6412-23.

PEERAER, Y., RABIJNS, A., COLLET, J. F., VAN SCHAFTINGEN, E. & DE RANTER, C. 2004. How calcium inhibits the magnesium-dependent enzyme human phosphoserine phosphatase. *Eur J Biochem,* 271**,** 3421-7.

PEERAER, Y., RABIJNS, A., VERBOVEN, C., COLLET, J. F., VAN SCHAFTINGEN, E. & DE RANTER, C. 2003. High-resolution structure of human phosphoserine phosphatase in open conformation. *Acta Crystallogr D Biol Crystallogr,* 59**,** 971-7.

PEISACH, E., SELENGUT, J. D., DUNAWAY-MARIANO, D. & ALLEN, K. N. 2004. X-ray crystal structure of the hypothetical phosphotyrosine phosphatase MDP-1 of the haloacid dehalogenase superfamily. *Biochemistry,* 43**,** 12770-9.

PEREIRA, S. R., VASCONCELOS, V. M. & ANTUNES, A. 2011. The phosphoprotein phosphatase family of Ser/Thr phosphatases as principal targets of naturally occurring toxins. *Crit Rev Toxicol,* 41**,** 83-110.

PETERFY, M., PHAN, J., XU, P. & REUE, K. 2001. Lipodystrophy in the fld mouse results from mutation of a new gene encoding a nuclear protein, lipin. *Nat Genet,* 27**,** 121-4.

PILS, B. & SCHULTZ, J. 2004. Evolution of the multifunctional protein tyrosine phosphatase family. *Mol Biol Evol,* 21**,** 625-31.

PIRARD, M., ACHOURI, Y., COLLET, J. F., SCHOLLEN, E., MATTHIJS, G. & VAN SCHAFTINGEN, E. 1999. Kinetic properties and tissular distribution of mammalian phosphomannomutase isozymes. *Biochem J,* 339 (Pt 1)**,** 201-7.

POSSEMATO, R., MARKS, K. M., SHAUL, Y. D., PACOLD, M. E., KIM, D., BIRSOY, K., SETHUMADHAVAN, S., WOO, H. K., JANG, H. G., JHA, A. K., CHEN, W. W., BARRETT, F. G., STRANSKY, N., TSUN, Z. Y., COWLEY, G. S., BARRETINA, J., KALAANY, N. Y., HSU, P. P., OTTINA, K., CHAN, A. M., YUAN, B., GARRAWAY, L. A., ROOT, D. E., MINO-KENUDSON, M., BRACHTEL, E. F., DRIGGERS, E. M. & SABATINI, D. M. 2011. Functional genomics reveal that the serine synthesis pathway is essential in breast cancer. *Nature,* 476**,** 346-50.

POT, D. A., WOODFORD, T. A., REMBOUTSIKA, E., HAUN, R. S. & DIXON, J. E. 1991. Cloning, bacterial expression, purification, and characterization of the cytoplasmic domain of rat LAR, a receptor-like protein tyrosine phosphatase. *J Biol Chem,* 266**,** 19688-96.

PULIDO, R., ZUNIGA, A. & ULLRICH, A. 1998. PTP-SL and STEP protein tyrosine phosphatases regulate the activation of the extracellular signal-regulated kinases ERK1 and ERK2 by association through a kinase interaction motif. *EMBO J,* 17**,** 7337-50.

PUNTA, M., COGGILL, P. C., EBERHARDT, R. Y., MISTRY, J., TATE, J., BOURSNELL, C., PANG, N., FORSLUND, K., CERIC, G., CLEMENTS, J., HEGER, A., HOLM, L., SONNHAMMER, E. L., EDDY, S. R., BATEMAN, A. & FINN, R. D. 2012. The Pfam protein families database. *Nucleic Acids Res,* 40**,** D290-301.

QUENTAL, R., MOLEIRINHO, A., AZEVEDO, L. & AMORIM, A. 2010. Evolutionary history and functional diversification of phosphomannomutase genes. *J Mol Evol,* 71**,** 119-27.

RAYAPUREDDI, J. P., KATTAMURI, C., STEINMETZ, B. D., FRANKFORT, B. J., OSTRIN, E. J., MARDON, G. & HEGDE, R. S. 2003. Eyes absent represents a class of protein tyrosine phosphatases. *Nature,* 426**,** 295-8.

REBAY, I., SILVER, S. J. & TOOTLE, T. L. 2005. New vision from Eyes absent: transcription factors as enzymes. *Trends Genet,* 21**,** 163-71.

REN, L., CHEN, X., LUECHAPANICHKUL, R., SELNER, N. G., MEYER, T. M., WAVREILLE, A. S., CHAN, R., IORIO, C., ZHOU, X., NEEL, B. G. & PEI, D. 2011. Substrate specificity of protein tyrosine phosphatases 1B, RPTPalpha, SHP-1, and SHP-2. *Biochemistry,* 50**,** 2339-56.

RIDDER, I. S. & DIJKSTRA, B. W. 1999. Identification of the Mg2+-binding site in the P-type ATPase and phosphatase members of the HAD (haloacid dehalogenase) superfamily by structural similarity to the response regulator protein CheY. *Biochem J,* 339 (Pt 2)**,** 223-6.

RINALDO-MATTHIS, A., RAMPAZZO, C., REICHARD, P., BIANCHI, V. & NORDLUND, P. 2002. Crystal structure of a human mitochondrial deoxyribonucleotidase. *Nat Struct Biol,* 9**,** 779-87.

RINALDUCCI, S., MURGIANO, L. & ZOLLA, L. 2008. Redox proteomics: basic principles and future perspectives for the detection of protein oxidation in plants. *J Exp Bot,* 59**,** 3781-801.

ROSSMANN, M. G., MORAS, D. & OLSEN, K. W. 1974. Chemical and biological evolution of nucleotide-binding protein. *Nature,* 250**,** 194-9.

SALMEEN, A., ANDERSEN, J. N., MYERS, M. P., MENG, T. C., HINKS, J. A., TONKS, N. K. & BARFORD, D. 2003. Redox regulation of protein tyrosine phosphatase 1B involves a sulphenyl-amide intermediate. *Nature,* 423**,** 769-73.

SALMEEN, A. & BARFORD, D. 2005. Functions and mechanisms of redox regulation of cysteine-based phosphatases. *Antioxid Redox Signal,* 7**,** 560-77.

SANDIN, A., DAGNELL, M., GONON, A., PERNOW, J., STANGL, V., ASPENSTROM, P., KAPPERT, K. & OSTMAN, A. 2011. Hypoxia followed by re-oxygenation induces oxidation of tyrosine phosphatases. *Cell Signal,* 23**,** 820-6.

SATTLER, M., VERMA, S., SHRIKHANDE, G., BYRNE, C. H., PRIDE, Y. B., WINKLER, T., GREENFIELD, E. A., SALGIA, R. & GRIFFIN, J. D. 2000. The BCR/ABL tyrosine kinase induces production of reactive oxygen species in hematopoietic cells. *J Biol Chem,* 275**,** 24273-8.

SCHNEIDER, C. A., RASBAND, W. S. & ELICEIRI, K. W. 2012. NIH Image to ImageJ: 25 years of image analysis. *Nat Methods,* 9**,** 671-5.

SCHUCK, P. 2000. Size-distribution analysis of macromolecules by sedimentation velocity ultracentrifugation and lamm equation modeling. *Biophys J,* 78**,** 1606-19.

SEIFRIED, A., KNOBLOCH, G., DURAPHE, P. S., SEGERER, G., MANHARD, J., SCHINDELIN, H., SCHULTZ, J. & GOHLA, A. 2014. Evolutionary and Structural Analyses of Mammalian Haloacid Dehalogenase-type Phosphatases AUM and Chronophin Provide Insight into the Basis of Their Different Substrate Specificities. *J Biol Chem,* 289**,** 3416-31.

SEIFRIED, A., SCHULTZ, J. & GOHLA, A. 2013. Human HAD phosphatases: structure, mechanism, and roles in health and disease. *FEBS J,* 280**,** 549-71.

SHI, Y. 2009. Serine/threonine phosphatases: mechanism through structure. *Cell,* 139**,** 468-84.

SILVAGGI, N. R., ZHANG, C., LU, Z., DAI, J., DUNAWAY-MARIANO, D. & ALLEN, K. N. 2006. The X-ray crystal structures of human alpha-phosphomannomutase 1 reveal the structural basis of congenital disorder of glycosylation type 1a. *J Biol Chem,* 281**,** 14918-26.

SINGH, D. K., KUMAR, D., SIDDIQUI, Z., BASU, S. K., KUMAR, V. & RAO, K. V. 2005. The strength of receptor signaling is centrally controlled through a cooperative loop between Ca2+ and an oxidant signal. *Cell,* 121**,** 281-93.

SORESCU, D., WEISS, D., LASSEGUE, B., CLEMPUS, R. E., SZOCS, K., SORESCU, G. P., VALPPU, L., QUINN, M. T., LAMBETH, J. D., VEGA, J. D., TAYLOR, W. R. & GRIENDLING, K. K. 2002. Superoxide production and expression of nox family proteins in human atherosclerosis. *Circulation,* 105**,** 1429-35.

SOUFI, B., GNAD, F., JENSEN, P. R., PETRANOVIC, D., MANN, M., MIJAKOVIC, I. & MACEK, B. 2008. The Ser/Thr/Tyr phosphoproteome of Lactococcus lactis IL1403 reveals multiply phosphorylated proteins. *Proteomics,* 8**,** 3486-93.

STIVALA, A., WYBROW, M., WIRTH, A., WHISSTOCK, J. C. & STUCKEY, P. J. 2011. Automatic generation of protein structure cartoons with Pro-origami. *Bioinformatics,* 27**,** 3315-6.

SUN, C. X., MAGALHAES, M. A. & GLOGAUER, M. 2007. Rac1 and Rac2 differentially regulate actin free barbed end formation downstream of the fMLP receptor. *J Cell Biol,* 179**,** 239-45.

SWANSON, S. K., BORN, T., ZYDOWSKY, L. D., CHO, H., CHANG, H. Y., WALSH, C. T. & RUSNAK, F. 1992. Cyclosporin-mediated inhibition of bovine calcineurin by cyclophilins A and B. *Proc Natl Acad Sci U S A,* 89**,** 3741-5.

SWINGLE, M. R., HONKANEN, R. E. & CISZAK, E. M. 2004. Structural basis for the catalytic activity of human serine/threonine protein phosphatase-5. *J Biol Chem,* 279**,** 33992-9.

TAKAYAMA, Y., WERBECK, N. D., KOMORI, H., MORITA, K., OZAWA, K., HIGUCHI, Y. & AKUTSU, H. 2008. Strategic roles of axial histidines in structure formation and redox regulation of tetraheme cytochrome c3. *Biochemistry,* 47**,** 9405-15.

TALAVERA, G. & CASTRESANA, J. 2007. Improvement of phylogenies after removing divergent and ambiguously aligned blocks from protein sequence alignments. *Syst Biol,* 56**,** 564-77.

TERESA PELLICER, M., FELISA NUNEZ, M., AGUILAR, J., BADIA, J. & BALDOMA, L. 2003. Role of 2-phosphoglycolate phosphatase of Escherichia coli in metabolism of the 2-phosphoglycolate formed in DNA repair. *J Bacteriol,* 185**,** 5815-21.

TERRAK, M., KERFF, F., LANGSETMO, K., TAO, T. & DOMINGUEZ, R. 2004. Structural basis of protein phosphatase 1 regulation. *Nature,* 429**,** 780-4.

TIGANIS, T. & BENNETT, A. M. 2007. Protein tyrosine phosphatase function: the substrate perspective. *Biochem J,* 402**,** 1-15.

TONKS, N. K. 2013. Protein tyrosine phosphatases--from housekeeping enzymes to master regulators of signal transduction. *FEBS J,* 280**,** 346-78.

TOOTLE, T. L., SILVER, S. J., DAVIES, E. L., NEWMAN, V., LATEK, R. R., MILLS, I. A., SELENGUT, J. D., PARLIKAR, B. E. & REBAY, I. 2003. The transcription factor Eyes absent is a protein tyrosine phosphatase. *Nature,* 426**,** 299-302.

TREMBLAY, L. W., DUNAWAY-MARIANO, D. & ALLEN, K. N. 2006. Structure and activity analyses of Escherichia coli K-12 NagD provide insight into the evolution of biochemical function in the haloalkanoic acid dehalogenase superfamily. *Biochemistry,* 45**,** 1183-93.

TREMBLAY, L. W., ZHANG, G., DAI, J., DUNAWAY-MARIANO, D. & ALLEN, K. N. 2005. Chemical confirmation of a pentavalent phosphorane in complex with beta-phosphoglucomutase. *J Am Chem Soc,* 127**,** 5298-9.

VAN MONTFORT, R. L., CONGREVE, M., TISI, D., CARR, R. & JHOTI, H. 2003. Oxidation state of the active-site cysteine in protein tyrosine phosphatase 1B. *Nature,* 423**,** 773-7.

VEIGA-DA-CUNHA, M., VLEUGELS, W., MALIEKAL, P., MATTHIJS, G. & VAN SCHAFTINGEN, E. 2008. Mammalian phosphomannomutase PMM1 is the brain IMP-sensitive glucose-1,6-bisphosphatase. *J Biol Chem,* 283**,** 33988-93.

VIRSHUP, D. M. & SHENOLIKAR, S. 2009. From promiscuity to precision: protein phosphatases get a makeover. *Mol Cell,* 33**,** 537-45.

WALLDEN, K., RINALDO-MATTHIS, A., RUZZENENTE, B., RAMPAZZO, C., BIANCHI, V. & NORDLUND, P. 2007. Crystal structures of human and murine deoxyribonucleotidases: insights into recognition of substrates and nucleotide analogues. *Biochemistry,* 46**,** 13809-18.

WANG, W., KIM, R., JANCARIK, J., YOKOTA, H. & KIM, S. H. 2001. Crystal structure of phosphoserine phosphatase from Methanococcus jannaschii, a hyperthermophile, at 1.8 A resolution. *Structure,* 9**,** 65-71.

WASS, M. & BUTTERWORTH, P. J. 1971. Nucleoside pyrophosphatase activity associated with pig kidney alkaline phosphatase. *Biochem J,* 124**,** 891-6.

WEINFELD, M., MANI, R. S., ABDOU, I., ACEYTUNO, R. D. & GLOVER, J. N. 2011. Tidying up loose ends: the role of polynucleotide kinase/phosphatase in DNA strand break repair. *Trends Biochem Sci,* 36**,** 262-71.

WOOD, Z. A., POOLE, L. B., HANTGAN, R. R. & KARPLUS, P. A. 2002. Dimers to doughnuts: redox-sensitive oligomerization of 2-cysteine peroxiredoxins. *Biochemistry,* 41**,** 5493-504.

WU, R. F., XU, Y. C., MA, Z., NWARIAKU, F. E., SAROSI, G. A., JR. & TERADA, L. S. 2005. Subcellular targeting of oxidants during endothelial cell migration. *J Cell Biol,* 171**,** 893-904.

YAN, D., CHO, H. S., HASTINGS, C. A., IGO, M. M., LEE, S. Y., PELTON, J. G., STEWART, V., WEMMER, D. E. & KUSTU, S. 1999. Beryllofluoride mimics phosphorylation of NtrC and other bacterial response regulators. *Proc Natl Acad Sci U S A,* 96**,** 14789-94.

YAN, S. R. & BERTON, G. 1996. Regulation of Src family tyrosine kinase activities in adherent human neutrophils. Evidence that reactive oxygen intermediates produced

by adherent neutrophils increase the activity of the p58c-fgr and p53/56lyn tyrosine kinases. *J Biol Chem,* 271**,** 23464-71.

YANG, J., LIANG, X., NIU, T., MENG, W., ZHAO, Z. & ZHOU, G. W. 1998. Crystal structure of the catalytic domain of protein-tyrosine phosphatase SHP-1. *J Biol Chem,* 273**,** 28199-207.

YANG, Z. 2007. PAML 4: phylogenetic analysis by maximum likelihood. *Mol Biol Evol,* 24**,** 1586-91.

YEO, M., LEE, S. K., LEE, B., RUIZ, E. C., PFAFF, S. L. & GILL, G. N. 2005. Small CTD phosphatases function in silencing neuronal gene expression. *Science,* 307**,** 596-600.

ZHANG, A. J., BAI, G., DEANS-ZIRATTU, S., BROWNER, M. F. & LEE, E. Y. 1992. Expression of the catalytic subunit of phosphorylase phosphatase (protein phosphatase-1) in Escherichia coli. *J Biol Chem,* 267**,** 1484-90.

ZHANG, M., LIU, J., KIM, Y., DIXON, J. E., PFAFF, S. L., GILL, G. N., NOEL, J. P. & ZHANG, Y. 2010. Structural and functional analysis of the phosphoryl transfer reaction mediated by the human small C-terminal domain phosphatase, Scp1. *Protein Sci,* 19**,** 974-86.

ZHANG, Y., KIM, Y., GENOUD, N., GAO, J., KELLY, J. W., PFAFF, S. L., GILL, G. N., DIXON, J. E. & NOEL, J. P. 2006. Determinants for dephosphorylation of the RNA polymerase II C-terminal domain by Scp1. *Mol Cell,* 24**,** 759-70.

ZHANG, Z. Y., MACLEAN, D., MCNAMARA, D. J., SAWYER, T. K. & DIXON, J. E. 1994a. Protein tyrosine phosphatase substrate specificity: size and phosphotyrosine positioning requirements in peptide substrates. *Biochemistry,* 33**,** 2285-90.

ZHANG, Z. Y., WANG, Y. & DIXON, J. E. 1994b. Dissecting the catalytic mechanism of protein-tyrosine phosphatases. *Proc Natl Acad Sci U S A,* 91**,** 1624-7.

ZHUKOVA, L., ZHUKOV, I., BAL, W. & WYSLOUCH-CIESZYNSKA, A. 2004. Redox modifications of the C-terminal cysteine residue cause structural changes in S100A1 and S100B proteins. *Biochim Biophys Acta,* 1742**,** 191-201.

ZOUDILOVA, M., KUMAR, P., GE, L., WANG, P., BOKOCH, G. M. & DEFEA, K. A. 2007. Beta-arrestin-dependent regulation of the cofilin pathway downstream of protease-activated receptor-2. *J Biol Chem,* 282**,** 20634-46.

7 Appendix

7.1 Supplementary figures

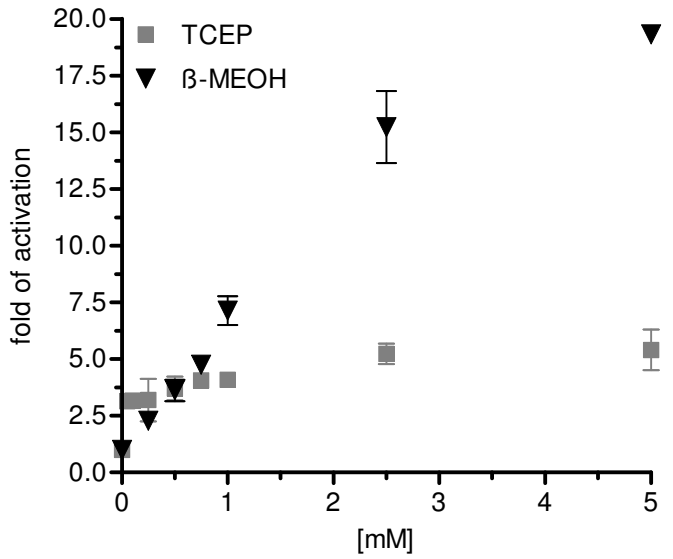

Figure 45: **AUM activity is stimulated upon treatment with the reducing agents TCEP and β-MEOH:** Kinetic measurements of the phosphatase activity of the murine AUM with increasing amounts of TCEP or β-MEOH. Purified AUM^{WT} (0.8 µg) was pre-incubated with 0.001-5 mM of reducing agent for 30 minutes and the phosphatase activity towards *p*NPP was measured. Shown are normalized values, and the phosphatase activity in the absence of reducing agent was set to 1. Results are mean values ± SEM of three independent experiments performed in triplicates with three independently purified protein batches.

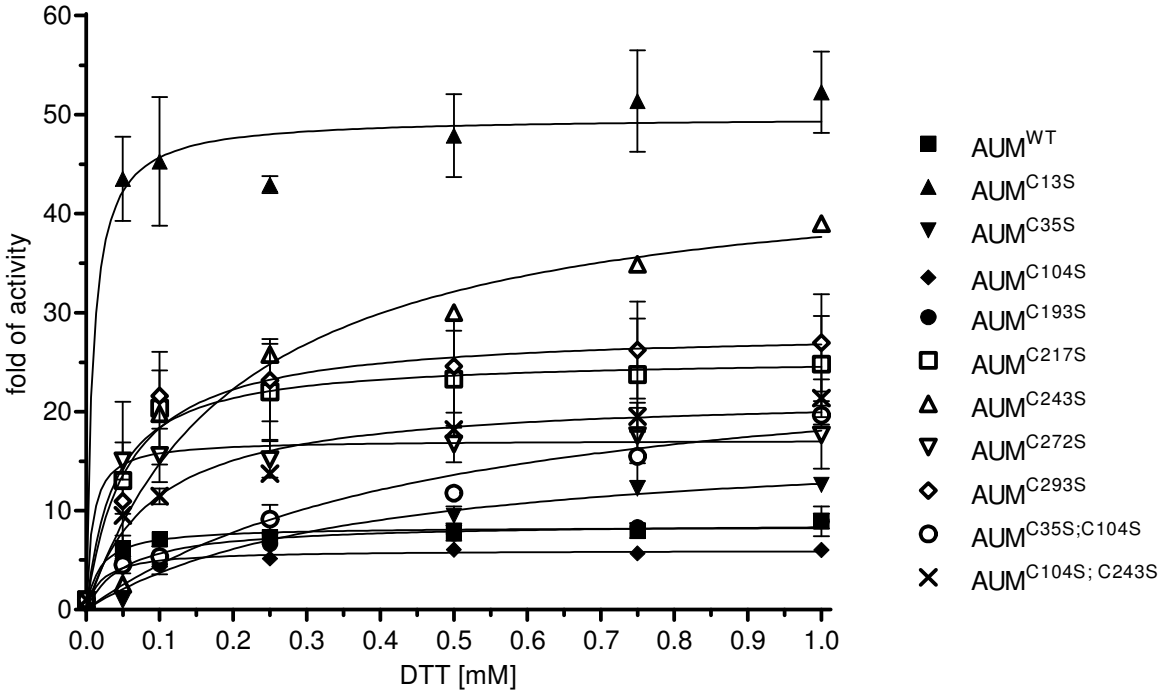

Figure 46: Activation of AUM/CS mutant activity upon DTT treatment. Fold of activation of the phosphatase activity of AUM and the CS mutants in the presence of 0.05-1 mM of DTT after 30 minutes. Results are mean values ± SEM of three independent experiments performed in triplicates with two independently purified protein batches.

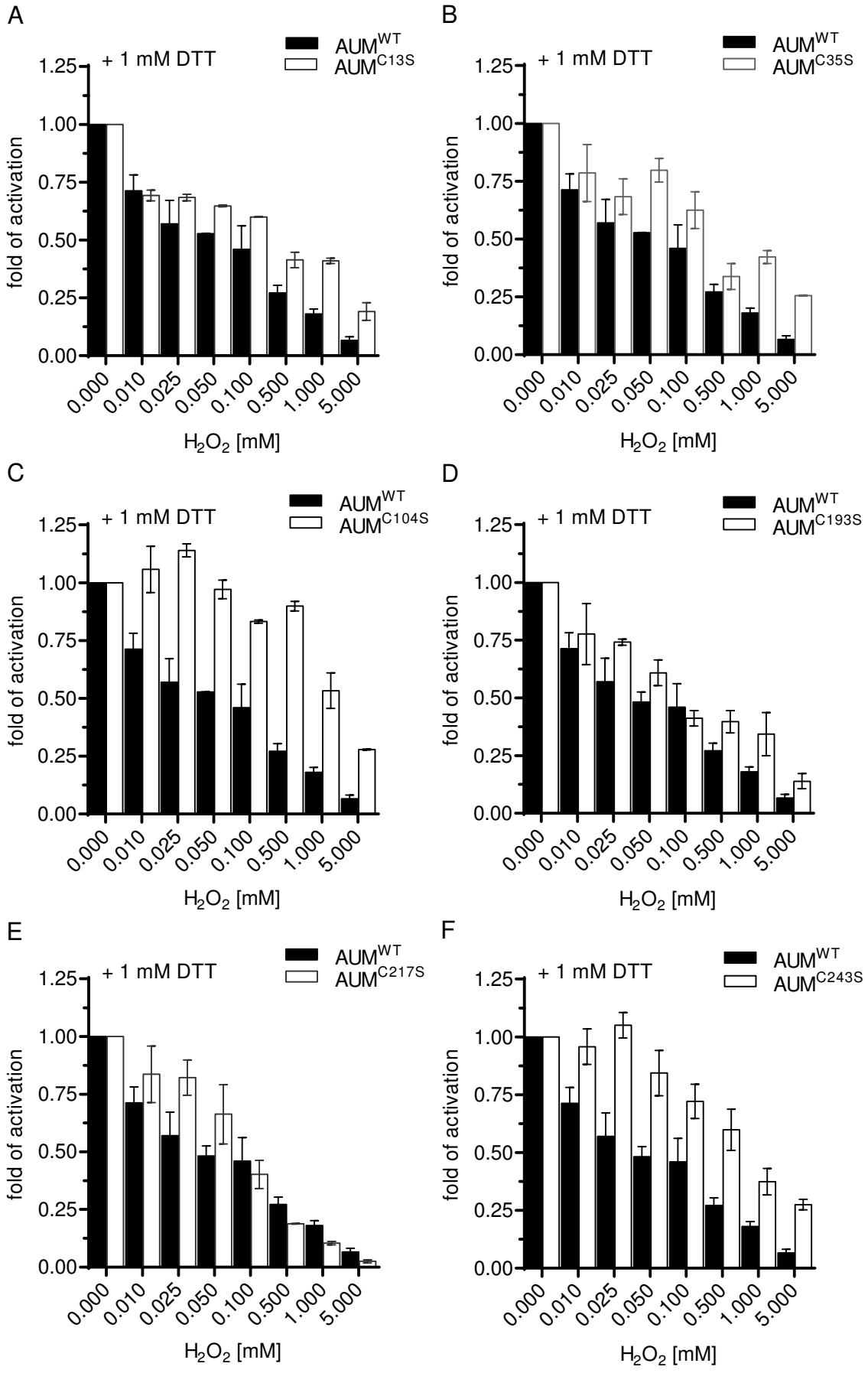
A
+ 1 mM DTT
AUM^WT
AUM^C13S
fold of activation
1.25
1.00
0.75
0.50
0.25
0.00
0.000
0.010
0.025
0.050
0.100
0.500
1.000
5.000
H2O2 [mM]
B
+ 1 mM DTT
AUM^WT
AUM^C35S
fold of activation
H2O2 [mM]
C
+ 1 mM DTT
AUM^WT
AUM^C104S
fold of activation
H2O2 [mM]
D
+ 1 mM DTT
AUM^WT
AUM^C193S
fold of activation
H2O2 [mM]
E
+ 1 mM DTT
AUM^WT
AUM^C217S
fold of activation
H2O2 [mM]
F
+ 1 mM DTT
AUM^WT
AUM^C243S
fold of activation
H2O2 [mM]

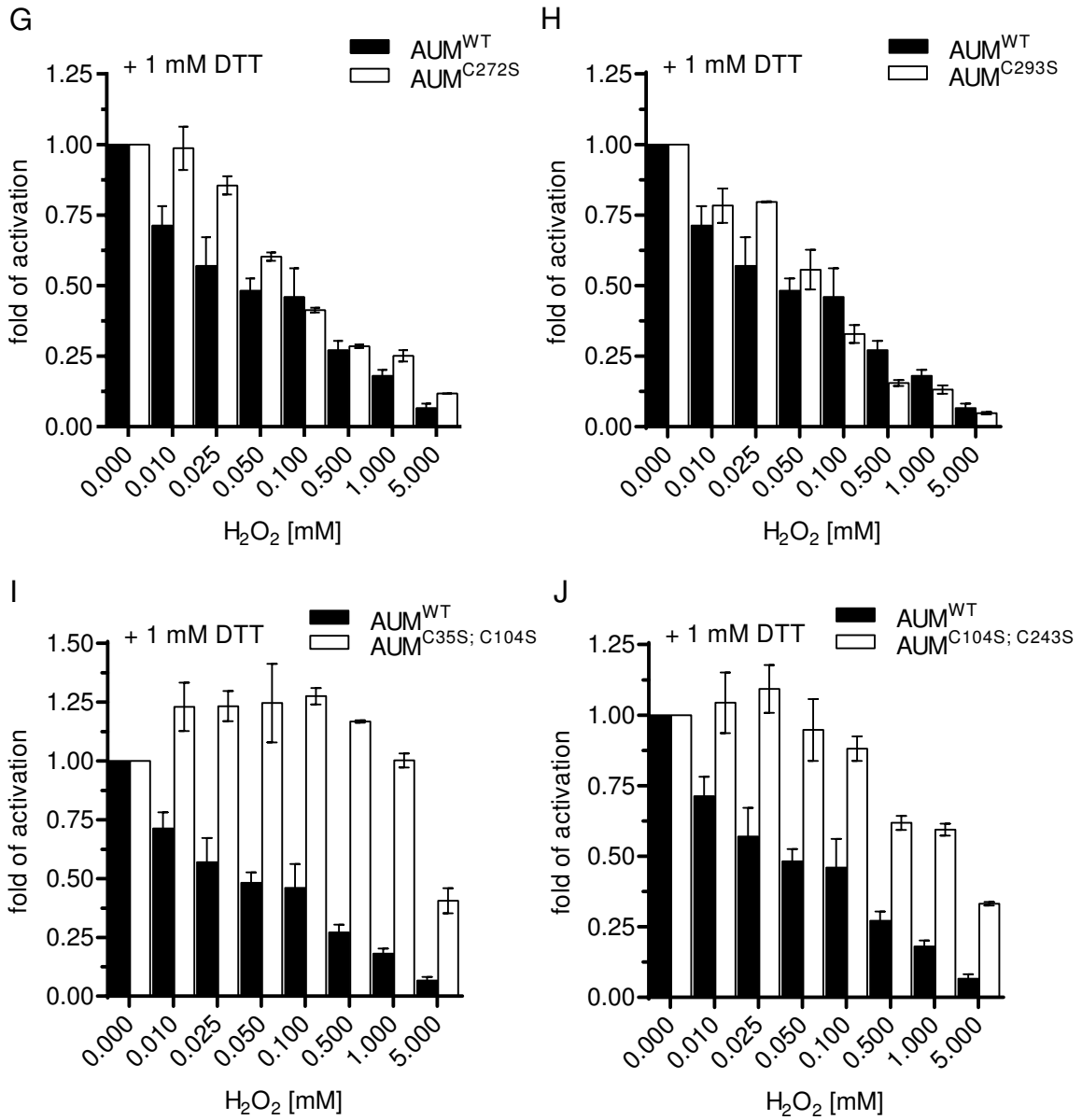

Figure 47: Reversible oxidation of the CS mutants. AUM^{WT} and the CS mutants were pre-incubated with 0.01-5 mM of H_2O_2 for 30 minutes. Phosphatase activity was detected over 30 minutes, followed by an addition of 1 mM of DTT. The activation upon DTT treatment after inhibition is shown for AUM^{WT} (black), AUM^{C13S} **(A)**, AUM^{C35S} **(B)**, AUM^{C104S} **(C)**, AUM^{C193S} **(D)**, AUM^{C217S} **(E)**, AUM^{C243S} **(F)**, AUM^{C272S} **(G)**, AUM^{C293S} **(H)**, $AUM^{C35S;\ C104S}$ **(I)**, $AUM^{C104S;\ C243S}$ **(J)**. Shown are normalized values, activity without inhibitor was set to 1. Results are mean values ± SEM of three independent experiments performed in triplicates with two independently purified protein batches

7.1. Curriculum vitae

7.2 Publication list

Human HAD phosphatases: structure, mechanism, and role in health and disease.
Seifried A, Schultz J, Gohla A.
FEBS J. 2013 Jan280(2):549-71. doi: 10.1111/j.1742-4658.2012.08633.x.
(John Wiley and Sons license: 3281280797987)

Evolutionary and Structural Analyses of Mammalian Haloacid Dehalogenase-type Phosphatases AUM and Chronophin Provide Insight into the Basis of Their Different Substrate Specificities.
Seifried A, Knobloch G, Duraphe PS, Segerer G, Manhard J, Schindelin H, Schultz J, Gohla A.
J Biol Chem. 2014 Feb 7;289(6):3416-31. doi: 10.1074/jbc.M113.503359.

Parts of the presented research were originally published in the two listed publications with permission of the journal.

7.3 Affidavit

I hereby confirm that my thesis entitled *Mechanistic insights into specificity determinants and catalytic properties of the haloacid dehalogenase-type phosphatase AUM* is the result of my own work. I did not receive any help or support from commercial consultants. All sources and / or materials applied are listed and specified in the thesis.

Furthermore, I confirm that this thesis has not been submitted as part of another examination process neither in identical nor in similar form.

Würzburg,

Date Signature

7.4 Acknowledgment

In the first place I would like to thank Professor Antje Gohla for the guidance and her trustful supervision during my work on the PhD thesis.

I would like to thank Professor Hermann Schindelin for supervision and helpful advises. He helped and taught me a lot in the field of X-ray crystallography. With Professor Jörg Schultz I shared fruitful discussions and I am grateful for his contribution to the publications. I thank Professor Martin J. Lohse for helpful discussions and good advice during the committee meetings.

I share the credit of my work with many people, who contributed to the project. I want to thank the members of the Gohla group for the good working environment and the professional technical support. I am especially grateful to Elisabeth for her help through all the years. I would like to thank the colleagues of the institute of pharmacology and the members of the Schindelin/Kisker group for their input and support.

In the end I would like to thank my family and friends, for all the support and understanding throughout the last years.